Development of Joint Deterioration and Energy Management Strategies for a Multi-stack PEM Fuel Cell System

Jian Zuo

THÈSE

pour obtenir le grade de

Docteur de l'Université Grenoble Alpes

Spécialité : **Automatique - Productique**

Arrêté ministériel : 01 Octobre 2019

Présentée par

Jian ZUO

Thèse dirigée par **Catherine CADET** et
codirigée par **Christophe BÉRENGUER**

préparée au sein du **Laboratoire Grenoble Images Parole Signal Automatique (GIPSA-lab)**
dans **l'école doctorale Electronique, Electrotechnique, Automatique, Traitement du Signal (EEATS)**

Development of Joint Deterioration and Energy Management Strategies for a Multi-stack PEM Fuel Cell System

Thèse soutenue publiquement le **19 Octobre 2022**,
devant le jury composé de:

Madame Mitra FOULADIRAD, Présidente
Professeur des Universités, Aix-Marseille Université
Madame Nadia YOUSFI-STEINER, Rapportrice
Professeur des Universités, Université de Franche-Comté
Monsieur Antoine PICOT, Rapporteur
Maître de Conférences, LAPLACE-Institut National Polytechnique de Toulouse
Monsieur Olivier SENAME, Examinateur
Professeur des Universités, Université Grenoble Alpes
Madame Catherine CADET, Directrice de thèse
Maître de Conférences, Université Grenoble Alpes
Monsieur Christophe BÉRENGUER, Co-directeur de thèse
Professeur des Universités, Grenoble INP
Monsieur Zhongliang LI, Co-encadrant de thèse
Maître de Conférences, Aix-Marseille Université
Monsieur Rachid OUTBIB, Co-encadrant de thèse
Professeur des Universités, Aix-Marseille Université

Acknowledgment

This thesis was done while the author was with GIPSA-lab in University Grenoble Alpes and LIS laboratory in Aix-Marseille University. Firstly, I would like to give the most sincere thanks to Prof. Dr. Catherine CADET and Prof. Dr. Christophe BÉRENGUER, who are my advisors in GIPSA-lab, and Prof. Dr. Zhongliang LI and Prof. Dr. Rachid OUTBIB, who are my advisors in LIS laboratory. I am truly grateful for their continued support and teachings during my Ph.D., both in work and personal life. And a special thank you for their efforts on preparing this thesis.

I would also express my great thanks Prof. Dr. Nadia STEINER and Prof. Dr. Antoine PICOT for accepting to review my this thesis. I would also express my gratitude to Prof. Dr. Mitra FOULADIRAD and Prof. Dr. Olivier SENAME for being the examiner for this thesis.

I would also like to express my great thanks to Dr. Zilong ZHAO, Lina GUAN, Dr. Fadoua TAIA-ALAOUI, Dr. Khaled HAJAR, Dr. Reza RAZI, and all other colleagues and friends for their help and support during my life in Grenoble.

Finally, I would like to express my great appreciation to my parents, my parents-in-law, and my wife for their constant support of my studies. And I want to give a special thanks to my wife Xiaoying WANG, for being on my side and always supporting me during my doctoral studies.

Résumé

Les systèmes de piles à combustible offrent une solution durable à la production d'énergie électrique dans le secteur des transports, même s'ils rencontrent encore des problèmes de fiabilité et de durabilité. Le recours à des systèmes multi-piles à combustible (MFC) au lieu de piles à combustible uniques est une solution prometteuse pour surmonter ces limitations en répartissant de manière optimale la demande de puissance entre les différentes piles tout en tenant compte de leur état de santé, au moyen d'une stratégie de gestion de l'énergie (EMS) efficace. Dans ce travail, différentes stratégies ont été développées pour des applications automobiles, avec l'objectif d'optimiser la durée de vie du système de piles à combustible.

Le premier défi est de développer un modèle reliant la détérioration de chaque pile avec la puissance délivrée, de manière à être en mesure de prédire l'effet d'une allocation de charge sur la détérioration de chaque pile, et ainsi prendre une décision post-pronostic pertinente. Plusieurs modèles stochastiques de détérioration, allant du modèle classique de processus Gamma à des modèles plus complexes avec des effets aléatoires, sont développés et adaptés aux spécificités des piles à combustible. Sur la base de ces modèles, plusieurs stratégies de décision post-pronostic pour une MFC sont proposées et, pour chacune d'entre elles, le problème d'optimisation associé est formulé.

Tout d'abord, sous un profil de charge constant, en prenant en compte dans le processus de décision à la fois la consommation totale de combustible et la détérioration attendue, une stratégie de gestion de l'énergie tenant compte de la détérioration est proposée pour un système constitué de trois piles à combustible. Le problème d'optimisation multi-objectif associé à cette stratégie est résolu à l'aide d'un algorithme évolutionnaire, ce qui permet d'obtenir les allocations de charge optimisées pour chacune des piles du système. La durée de vie moyenne obtenue dans le cadre de la stratégie proposée s'avère plus longue que celle résultant de stratégies classiques (Average Load, Daisy Chain).

De plus, sous un profil de charge dynamique aléatoire, et en prenant en compte les phénomènes de détérioration dus à la fois au niveau et aux variations de la charge, une stratégie de prise de décision est proposée pour un système de deux piles à combustible. La prise de décision est réalisée à chaque événement de modification de la demande, et les allocations de charge optimales sont obtenues en minimisant la fonction objectif qui est estimée sur la base de la prévision de la détérioration future du système. Une étude de l'influence des charges dynamiques aléatoires sur les performances de la stratégie proposée montre que la durée de vie moyenne obtenue dans le cas d'une durée inconnue entre deux modifications de demande est proche de celle obtenue avec une durée d'événement connue, ce qui prouve la robustesse de la stratégie proposée. De plus, il est montré que la durée de vie moyenne du système est augmentée par rapport au cas avec une stratégie de charge moyenne, sur plusieurs modèles de détérioration stochastique différents.

Enfin, une étude plus exploratoire ouvre des perspectives de recherche dans le cas où le système multi-piles est composé de trois piles, dont deux seulement fonctionnent en même

temps. Pour optimiser la durée de vie des piles, tout en répondant à la demande de charge, le système de gestion de l'énergie doit également optimiser le démarrage et l'arrêt des différentes piles. En fait, l'optimisation du remplacement des piles est également nécessaire pour une tâche d'exploitation à long terme. Par conséquent, cette étude ouvre la voie à des approches de maintenance pour les systèmes multi-piles.

Mots clés : Piles à combustible à empilement multiple, stratégie de gestion de l'énergie, décision post-prognostic, détérioration stochastique, profil de charge dynamique aléatoire, optimisation multi-objectifs

Abstract

Fuel cell systems offer a sustainable solution to electrical power generation in the transportation sector, even if they still encounter reliability and durability issues. Resorting to Multi-stack Fuel Cell (MFC) systems instead of single fuel cells is a promising solution to overcome these limitations by optimally distributing the power demand among the different stacks while taking into account their state of health, by means of an efficient Energy Management Strategy (EMS). In this work, different strategies have been developed for static and dynamic application scenarios, with the objective of optimizing the fuel cell system lifetime.

The first challenge is to develop a model linking the deterioration trend of each stack with the power delivered by the stack, so as to predict the effect of a load allocation on each stack deterioration, and thus make a relevant post-prognostics decision. For this, several stochastic deterioration models, from the classical Gamma process model to more complex models with random effects are developed and tailored to the fuel cell specificities. Based on these models, several post-prognostics decision-making strategies for an MFC are proposed and, for each of them, the associated optimization problem is formulated.

First, under a constant load profile, taking into consideration both the expected whole fuel consumption and the expected deterioration in the decision-making process, a deterioration-aware energy management strategy is proposed for a three-stack fuel cell system. The multi-objective optimization problem associated to this strategy is solved using an evolutionary algorithm, given the optimized load allocations among stacks. The average lifetime obtained under the proposed strategy is demonstrated to be larger than those resulting from the classical Average Load and Daisy Chain strategies.

Furthermore, under a random dynamic load profile, taking into consideration the deterioration phenomena due to both the load magnitude and the load variations, an event-based decision-making strategy is built for a two-stack fuel cell system. The optimal load allocations are obtained by minimizing the objective function which is estimated based on the prevision of the future system deterioration. An investigation on the influence of the random dynamic loads on the proposed strategy performance shows that the average lifetime obtained with unknown event duration is close to that with known event duration, which proves the robustness of the proposed strategy. Moreover, it is shown that the average system lifetime is increased when compared to the case with an Average Load strategy, on several different stochastic deterioration models.

Lastly, a more exploratory study opening research perspectives in the case where the multi-stack system is composed of three stacks, only two of which are operating at the same time. To optimize the lifetime of the stacks, while meeting the load demand, the EMS must also optimize the start and stop of the different stacks. Moreover, the optimization of stack replacement is also required for a long-term operation task. Therefore, this study opens the way to maintenance approaches to multi-stack systems.

Keywords: Multi-stack fuel cell, energy management strategy, post-prognostics decision, stochastic deterioration, random dynamic load profile, multi-objective optimization

Acronyms

MFC	Multi-stack Fuel Cell.
EMS	Energy Management Strategy.
SDP	Stochastic Dynamic Programming.
FFRLS	Forgetting Factor recursive least Square.
SSM-SVM	Spherical-shaped Multiple-class Support Vector Machine.
FDA	Fisher Discrimination Analysis.
PHM	Prognostics and Health Management.
DOE	U.S Department of Energy.
PEM	Proton Exchange Membrane.
FC	Fuel Cell.
PAFC	Phosphoric Acid Fuel Cell.
PA	Phosphoric Acid.
SOFC	Solid Oxide Fuel Cell.
MCFC	Molten Carbonate Fuel Cell.
AFC	Alkaline Fuel Cell.
MEA	Membrane Electrode Assembly.
ORR	Oxygen Reduction Reaction.
PFSA	Perflurosulfonic Acid.
CLs	Catalyst Layers.
GDLs	Gas Diffusion Layers.
MPLs	Microporous Layers.
BPs	Bipolar Plates.
EIS	Electrochemical Impedance Spectroscopy.
DC	Direct Current.
CPE	Constant Element Phase.
BEVs	Battery Electrical Vehicles.
FCEVs	Fuel Cell Electric Vehicles.
FCEBs	Fuel Cuel Cell Buses.
BOP	Balance-of-Plant.
CHP	Combined-Heat-and-Power.
EOL	End of Life.
RUL	Remaining Useful Lifetime.
AST	Accelerated Stress Test.
RH	Relative Humidity.
OCV	Open-Circuit Voltage.
ECSA	Electrochemical Surface Area.
NEDC	New European Driving Cycle.
FC-DLC	fuel cell dynamic load Cycle.
WLTC	World Harmonized Light Vehicles Test Cycles.
WTVC	World Transition Vehicles Cycle.

SOH	State of Health.
PCA	Principle Component Analysis.
SVM	Support Vector Machine.
KNN	k-Nearest Neighbors.
LSTM	Long Short-term Memory.
CNN	Convolution Neural Network.
HMM	Hidden Markov Chain Model.
ML	Machine Learning.
PF	Particle Filter.
NARNN	Nonlinear Autoregressive Neural Network.
RNN	Recurrent Neural Network.
HI	Health Indicator.
RMSE	Root Mean Square Error.
ESN	Echo State Neural Network.
ARMA	Autoregressive and Moving Average.
TDNN	Time Delay Neural Network.
MPC	Model Predictive Control.
SOC	State of Charge.
ECM	Equivalent Fuel Consumption Minimization.
FCPP	Fuel Cell Power Plant.
PM	Preventive Maintenance.
SQP	Sequential Quadratic Programming.
PMP	Pontryagin's Minimum Principle.
MP	Maximum Power.
ME	Maximum Efficiency.
MIP	Mix Integer Programming.
GP	Gamma process.
RE	Random Effect.
FT	Failure Threshold.
CDF	Cumulative Distribution Function.
PDFs	Probability Distribution Functions.
MC	Markov Chain.
GP-RM	Gamma Process-Random Mean.
GP-RV	Gamma Process-Random Variance.
GP-RE	Gamma Process Random Effect.
MoM	Method of Moments.
DT	Decision Threshold.
ASF	Achievement Scalarizing Function.
MOO	Multi-objective Optimization.
GA	Genetic Algorithm.
MOEA	Multi-objective Evolution Algorithm.
NSGA-II	Non-dominated Sorting Genetic Algorithm.
ND	Non-dominated.
IGD	Inverted Generational Distance.

SLSQP	Sequential Least-squares Programming.
DC-ave	Daisy Chain-based Average Load.
DDC-ave	Deterioration-aware Daisy Chain-based Average Load.

List of Symbols

Sign	Description	Unit
L	Fuel cell load	$\mathrm{Wcm^{-2}}$
D	Fuel cell resistance deterioration rate due to load amplitude	$\Omega\mathrm{cm^2h^{-1}}$
R	Fuel cell overall resistance	$\Omega\mathrm{cm^2}$
n	Number of fuel cell stacks	
n_{cell}	Number of cell within a stack	
E_{cell}	Fuel cell cell voltage	V
E_s	Fuel cell stack voltage	V
$X(t)$	A Gamma process random variable	
Ga	Gamma process	
α	Shape parameter of Gamma distribution	
β	Scale parameter of Gamma distribution	
Γ	Gamma function	
v	Coefficient of the shape function α	
ν	Perturbed shape function of the random effect model	
P	Probability operation	
T_R	Fuel cell lifetime	h
$\overline{T}_R$	Mean (average) fuel cell stack lifetime	h
$T_{R,med}$	Median fuel cell stack lifetime	h
N	Number of Monte Carlo simulation histories	
β_s	Scale parameter of the random effect model	
ω_{1f}	Weight of fuel cell failure probability	
ω_{2f}	Weight of variance of the expected deterioration levels of the different stacks	
$Ratio$	Fuel cell consumed fuel over lifetime ratio	
$\overline{Ratio'}$	Mean fuel cell lifetime over fuel consumption ratio	
$\Delta T_{R,pct}$	Average lifetime improvement percentage	%
$T^{+}_{R,pct}$	The percentage of the lifetimes obtained by the load allocation decision is larger than that of the Average Load	%
$T^{DC}_{R,pct}$	Percentage of the Monte Carlo simulation lifetimes obtained by DC-ave strategy that are large than the average lifetime of DC-ave strategy	%
$T^{DDC}_{R,pct}$	Percentage of the Monte Carlo simulation lifetimes obtained by DDC-ave strategy that are large than the average lifetime of DC-ave strategy	%
$T^{dec}_{R,pct}$	Percentage of the Monte Carlo simulation lifetimes obtained by our strategy that are large than the average lifetime of DC-ave strategy	%

Sign	Description	Unit
ℓ	Constant for defining Gamma process simulation parameters used in the original Gamma process deterioration model	
h	Constant for Gamma process parameters used in the random effect model	
P_d	Fuel cell conditional failure probability	
τ	Decision time interval	h
R_0	Initial fuel cell resistance	Ωcm^2
R^{d,t_0}	Initial deterioration level at the decision time t_0	Ωcm^2
f_{H_2}	Fuel cell stack hydrogen consumption rate function	gs^{-1}
F_{H_2}	Fuel cell stack hydrogen consumption mass	g
F_{det}	Fuel cell deterioration objective function	
τ_s	Simulation time step	h
$\overline{\tau}_e$	Expected load change event time interval	h
Ω	Weights between fuel cell deterioration and hydrogen consumption	
N^+_{ave}	Number of lifetimes where the lifetime obtained by the average split is larger than the average lifetime of average split method	
N^+_{dec}	Number of lifetimes where the lifetime obtained by the proposed strategy is larger than the average lifetime of average split method	
ΔR	Overall fuel cell resistance increment	Ωcm^2
K	Coefficient of calculating resistance deterioration due to load varying	$\Omega\text{cm}^2/\text{Wcm}^{-2}$
$\mathbf{P_{tr}}$	Transition probability matrix	
L_{ds}	All possible load demand states	
τ_e^j	Time length of load change event j	h
J	Optimization index	
γ_i^j	Load allocation ratio for FC_i at decision j	
$\text{M}_{fc,3}$	Three-stack fuel cell system	
k_{ss}	Weight term for fuel cell start-stop deterioration	

Subscript

min	Fuel cell minimal operation load.
nom	Fuel cell nominal operation load.
max	Fuel cell maximal operation load.
d	Fuel cell load demand.
fci	Fuel cell stack i.
ave	Average load split.
dec	Proposed decision-making strategy.
pct	Percentage.
sw	switching on/off stacks.
s	Simulation.
L	Load amplitude factor.
ΔL	Load variation factor.
ss	Start-stop factor.
m	Number of future load change events.

Superscript

DC	Daisy chain-average load split.
DDC	Deterioration-aware Daisy chain-average load split.
$+$	Larger than.
ini	Initial.

Contents

List of Figures

List of Tables

General Introduction

Around the world, actions are taken to fight against climate warming and air pollution. Furthermore, the European "Green Deal" [1] set out a climate change action plan to reduce greenhouse gas emissions by at least 55 % by 2030 to achieve climate neutrality by 2050. To achieve this goal, the wide application of renewable and clean energy is recognized as one of the key solutions. Among solutions, PEM fuel cell which uses hydrogen and oxygen as reactant gases and whose only product is water, is regard as a promising substitute for traditional power sources. PEM fuel cell has a high power density (up to 65 - 72 %) and suitable work temperature (-40°C to 100 °C). Current PEM fuel cells have been deployed in transportation and stationary applications. In transportation fields, the typical fuel cell applications include Fuel Cell Electric Vehicles (FCEVs), Fuel Cuel Cell Buses (FCEBs), and Fuel Cell Trucks, etc. FCEVs are already fabricated for market selling in Korea. In China, FCEBs are widely used in the public transportation to help to reduce CO_2 emission as well as to avoid traffic congestion. Combine-Heat-and-Power is a typical stationary application of fuel cells. It is mainly installed for residential usage.

Despite being widely used in various applications, the problem of fuel cell durability and cost remains as the main obstacle to their commercialization. The durability target of fuel cell in FCEVs is 8,000 hrs according to the U.S Department of Energy (DOE) [2]. Current max fleet average onboard system lifetime is around 4,100 hrs. Another challenge is the high manufacturing and application cost. The DOE cost target is $30 /KW for FCEVs. However, the current fuel cell equipment cost is nearly six times higher than the target cost.

To overcome these barriers, i.e. durability and cost, using a Multi-stack Fuel Cell (MFC) instead of single fuel cells is a promising solution for high-power applications [3]. The flexible modular architecture offers more redundancy than a single fuel cell which is beneficial for improving system durability and reliability. However, using MFC introduces the freedom of allocating different loads among the stacks. Thus, an optimization of the load allocation is needed, which can be addressed by an appropriate EMS. By designing an appropriate EMS, the system lifetime can also be improved at the condition that it takes into account the deterioration of the individual stacks. It is thus mandatory to build a deterioration model that integrates the dynamic behavior of MFC according to the operation conditions, i.e. a deterioration-aware EMS. As fuel cell performance deteriorations are difficult to model as they are linked to complex electrochemical, mechanical, and thermal mechanisms, this thesis first tackles the development of deterioration model adapted for energy management of MFC.

Then, the energy management problems are investigated for MFC system under two typical application load profiles, namely, the constant and the dynamic loads. The first problem to be

[1] https://www.consilium.europa.eu/en/policies/green-deal/

[2] "Fuel Cell Technologies Office Multi-Year Research, Development, and Demonstration Plan - Section 3.4 Fuel Cells." U.S. DOE Fuel Cell Technologies Office

[3] Zhou, Su, et al. "Scenario-oriented stacks allocation optimization for multi-stack fuel cell systems." Applied Energy 308 (2022): 118328.

addressed investigates how improving system lifetime and reducing system fuel consumption under constant load profiles. However, as the purpose is to develop an EMS for vehicle applications, the previous methodology is extended to the energy management of MFC systems under dynamic load profiles. When considering dynamic load profiles, the randomness in the load demand levels as well as their duration need to be considered. A second addressed issue is then proposed to build the EMS under a dynamic load profile. In the previous problems, the start and stop of different stacks were not considered so as to simplify their operation modes. The last problem proposes an exploratory study for including the start and stop of different stacks.

This work has been developed within the framework of a collaboration between GIPSA-lab [4] and LIS Laboratory [5]. In order to address the above problems, this thesis is organized into four parts, as follows:

- First, the backgrounds of fuel cells (Chapter 1) and fuel cell system EMS state-of-the-art (Chapter 2) are introduced. The deterioration of fuel cell and durability challenges are introduced in Chapter 1. The application of fuel cell hybrid system is introduced for the transport and stationary applications. Fuel cell PHM basics are introduced, and the decision-making phase is identified as one of the key research gaps in PHM studies. Chapter 2 presents the start-of-the-art of EMSs in fuel cell hybrid systems and MFC systems. Then the problem statement for joint deterioration and energy management strategy is presented according to the current research gaps of fuel cell deterioration modeling and deterioration-aware energy management.
- Then, the deterioration modeling of MFC systems is studied in Chapter 3. A load-dependent stochastic deterioration model is developed for the studied fuel cell system. The deterioration behavior of these proposed model is investigated by an automotive load profile.
- After that, the EMSs are developed for the studied MFC system under the constant and dynamic load profiles. Chapter 4 focuses on constant load profiles. The fuel cell deterioration model considered here is the basic Gamma process model. The load allocation decisions are optimized in an event-based framework. Then based on the results of Chapter 4, Chapter 5 further studies the MFC EMS problem for dynamic load profiles. The load allocation decisions are optimized for dynamic loads on different types of deterioration models, including a random-effect model.
- Lastly, the management of a three-stack operation problem including start and stop of different stacks is studied in Chapter 6. This last chapter proposes a more exploratory study opening research perspectives for the case where the multi-stack system is composed by a part of in-service stacks and some suspended ones. To optimize the lifetime of the stacks, while ensuring the load demand, the EMS must also optimize the start and stop of the different stacks. In fact, the optimization of stack replacement is also

[4] Gipsa-lab is internationally recognized for the research achieved in Automatic Control, Signal and Images processing, Speech and Cognition. http://www.gipsa-lab.fr/

[5] LIS is a research lab (UMR) focused on the fundamental and applied activities in the fields of Computer Science, Automation, Signal, and Image. https://www.lis-lab.fr/

required for a long-term operation task. Therefore, this study opens the way to maintenance approaches to multi-stack systems.

In the end, the manuscript gives a general conclusion summarizing the highlights in this thesis and provides the perspectives for future investigation.

Chapter 1

Backgrounds on Fuel Cells

This chapter reviews the state-of-the-art of PEM fuel cells. We first introduce fuel cell basics. Owing to their advantages of high efficiency, energy density and limited impact on environmental resources, PEM fuel cells have been deployed in various applications such as transportation and stationary. However, the durability and cost challenges remain the main barriers hindering their commercialization. Fuel cell deterioration studies help to understand its deterioration mechanisms as well as to build deterioration models. Then a possible solution to tackle fuel cell durability and cost challenge can be found out based on these deterioration models. Fuel cell deterioration mechanisms are mainly observed experimentally and are usually not well-formulated with explicit formulas. This arises the need for fuel cell deterioration models to reproduce its deterioration behavior. Related modeling works are presented in the fuel cell deterioration modeling methods section.

PHM techniques are introduced as one solution to solve fuel cell durability and cost challenges. PHM is a systematic approach that can deal with system assessment, prognostics, and decision-making support. The core PHM steps and their research states are introduced first. Among all procedures of PHM, the decision-making aspect is vital for taking control action to improve system lifetime yet is less studied. It is due to the fact that knowing fuel cell deterioration for the decision procedure is challenging. The possible health indicators for monitoring fuel cell state of health and deterioration modeling studies are introduced in the end.

Contents

1.1 Proton exchange membrane fuel cell basics

A Fuel Cell (FC) is an electrochemical device that uses hydrogen and oxygen as reactant fuel and produces electrons, protons, water, and heat. According to the types of electrolyte membrane being used, the fuel cells can be categorized into PEM fuel cell, Phosphoric Acid Fuel Cell (PAFC), Solid Oxide Fuel Cell (SOFC), Molten Carbonate Fuel Cell (MCFC), and Alkaline Fuel Cell (AFC) [1]. Figure 1.1 summarizes the power generation range of main fuel cell types. Fuel cells can provide a wide range of power, from 1 Watt to 100 MWs [2]. PEM fuel cells can provide a wide range of power (range from 10 W to 1 MW) thanks to flexible modularity configuration. It is widely installed in various applications.

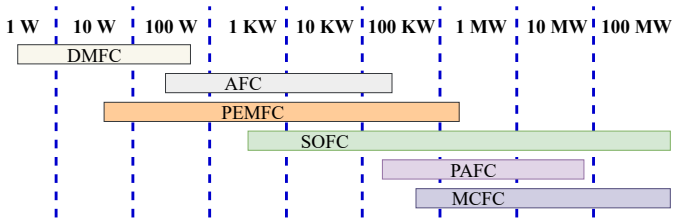

Figure 1.1: Power application range of main types of fuel cells.

Table 1.1 summarized major types of fuel cells and their basics. Among all those fuel cells, PEM fuel cells are currently the most promising in terms of high efficiency (up to 65 - 72%), low operation temperature, and safe to handle. Moreover, PEM fuel cell has a high power density and fast start-up time which makes them easy to use. For instance, SOFC operates under a high temperature (above 500 $°C$), and the ceramic materials used as electrolyte are difficult to handle. These pitfalls limit their further application. Thus, PEM fuel cells are studied in this thesis. The term fuel cell refers to PEM fuel cell in this thesis if not specifically stated.

Table 1.1: Main types of fuel cells [3].

	PEMFC	PAFC	SOFC	MCFC	AFC
Electrolyte	Polymer	Phosphoric acid	Ceramics	Molten carbonate	Potassium hydroxide
Primary fuel	H_2, reformed H_2	H_2, reformed H_2	H_2, biogas, methane	H_2, biogas, methane	H_2, cracked ammonia
Mobile ion	H^+	H^+	O^{2-}	CO_3^{2-}	OH^-
Temperature ($°C$)	-40 - 120	150 - 200	500 - 1000	600 - 700	50 - 200
Efficiency (%)	up to 65 - 72	up to 45	up to 65	up to 60	up to 70

1.1.1 Fuel cell working principle

The overall electrochemical reaction formula is summarized as:

$$\begin{aligned} &Anode: && H_2 \rightarrow H^+ + 2e^- \\ &Cathode: && 1/2O_2 + 2H^+ + 2e^- \rightarrow H_2O \\ &Overall: && \tfrac{1}{2}O_2 + H_2 \rightarrow H_2O \end{aligned} \tag{1.1}$$

The overall reaction in the fuel cell produces only water and heat, therefore it is a totally clean energy device.

PEM fuel cell uses polymer electrolyte membrane (Nafion, PEM) to conduct H^+ protons and separate hydrogen and oxygen reactants. The basic structure of the fuel cell electrode is shown in Figure 1.2. Note that the fuel cell electrode is porous and flat. This is to enable the maximum possible contact between the electrode, the electrolyte, and the reactants. The cathode-electrolyte-anode unit is generally known as a Membrane Electrode Assembly (MEA). Figure further 1.3 depicts the operating principle of a PEM fuel cell. The hydrogen is fed into the anode side of a fuel cell. Then it ionizes through an oxidation reaction, releasing electrons and H^+ ions (also known as protons). At the cathode, oxygen reacts with electrons taken from the electrode, and protons from the electrolyte, to form water. This process is called an Oxygen Reduction Reaction (ORR). The main steps related to fuel cell operation are as follows:

1. Reactants delivery into the fuel cell
2. Electrochemical reaction: ORR and H_2 reduction.
3. Ionic conduction through the electrolyte and electronic conduction through the eternal circuit
4. Product removal from the fuel cell

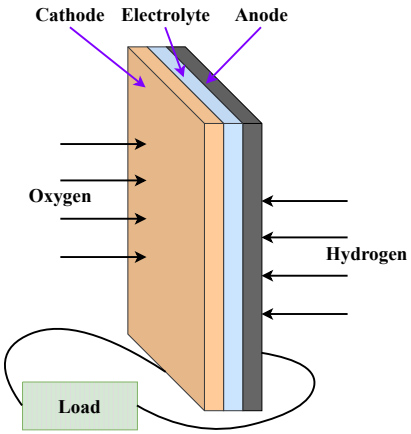

Figure 1.2: MEA schematic diagram

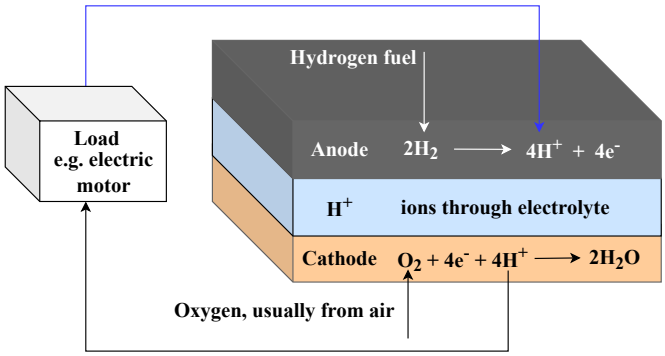

Figure 1.3: Electrode reactions and charge flow for an acid electrolyte fuel cell.

1.1.2 Main components of a single fuel cell stack

Since a single fuel cell can only produce a very small amount of energy (voltage below 1 V), fuel cells are usually electrically connected in series as a stack (i.e., fuel cell stack) to provide power. Figure 1.4 shows the basic structure of a fuel cell stack and details the structure of a MEA. The four main components of a MEA are membrane, catalyst layers, microporous and gas diffusion layers (Figure 1.4).

Generally, the membrane offers three functionalities: (i) it supports the anode and cathode catalyst layers, and (ii) it acts as a separator between anode and cathode reactants (Hydrogen and oxygen) and electrons, and (iii) it conducts protons from the anode to cathode. Thus, the requirements for membranes are manifold and stringent. The membrane is required to have high proton conductivity, thermal and chemical stability. On the other hand, membrane must be impermeable to reactants gases and electrically insulating. Perflurosulfonic Acid (PFSA) is a typically used PEM material for PEM fuel cells.

Catalyst Layers (CLs) are composed of electrocatalyst (i.e., Pt catalyst), carbon support layer, ionomer, and void space. CLs provide the reaction site for electrochemical chemical reactions. Cls offer pathways for various reactant species, including a path for proton transport, a path for gaseous reactant supply and water removal, and a path to link CL and current collector (electron conduction). Therefore, the fabrication of CL is one of the key factors affecting fuel cell performance and durability. A properly designed CL will enable sufficient electrochemical reaction, thus improving the overall performance. The invention of optimized CL ink preparation has greatly progressed the fuel cell technologies [4]. This finding brings out an important concept for fuel cells, i.e., the triple-phase boundaries of ionomer, Pt/C, and void space. Thanks to this structure, all reactants can access the reactions, which greatly improves the fuel cell performance. The ionomer helps to bind together the Pt/C particles. And it is also a conductor for protons. Imbalanced ionomer loading increases the ohmic loss or transport loss. A small amount of ionomer reduces the proton conductivity, and a large amount will increase the gaseous reactants' transport resistance. Electrocatalysts directly influence the ORR inside a fuel cell. Currently, Pt is the widely adopted choice for electrocatalyst. This is mainly due to its high activity. Though ideal for fuel cell performance, Pt

belongs to precious metals, and it is one of the main costs of fuel cell applications.

Gas Diffusion Layers (GDLs) together with Microporous Layers (MPLs), composed the diffusion media of a fuel cell. GDLs are placed between a bipolar plate and the CL. The porous structure is specially designed to transfer gaseous reactants, and water remove. Moreover, GDL also provides a pathway for electron conduction between CL and bipolar plate. The carbon-based material is used in the commercial GDLs and MPLs [5].

The three main components of a typical fuel cell stack are MEA, two bipolar plates, and the sealants. Bipolar Plates (BPs) serve as mechanical support for MEA. They are also responsible for collecting the electric current, removing produced heat and accumulated water. The gas flow channel designed in the inner surface of BP helps to distribute the reactants to electrodes. Sealants are used to combine single-cell in series. And finally, two endplates help to seal together all components, forming a fuel cell stack.

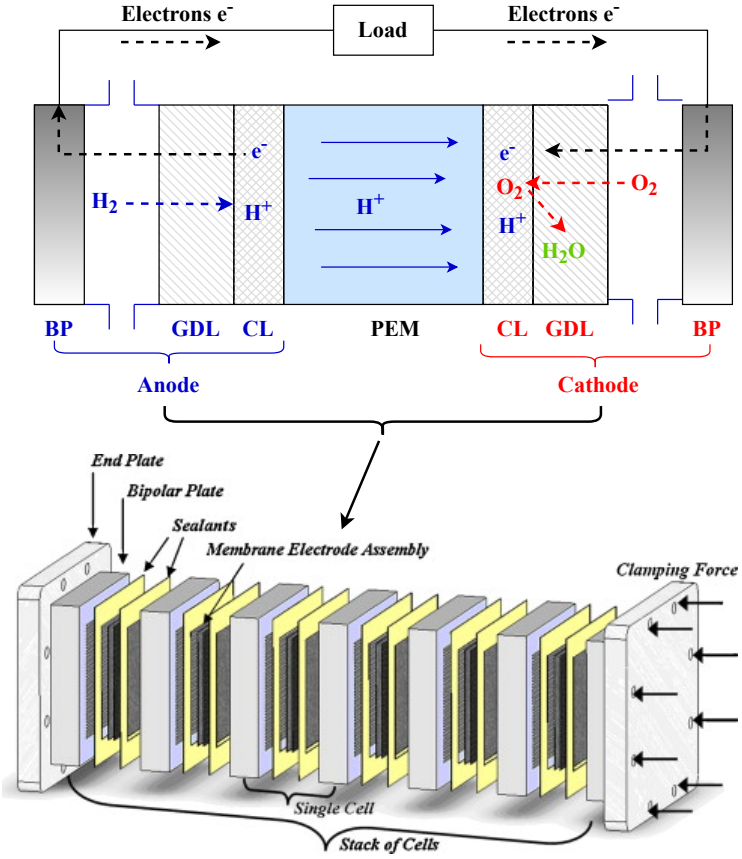

Figure 1.4: Schematic structure diagram of a fuel cell stack and of a MEA [6].

1.1.3 Polarization curve

Fuel cell output voltage and output power are the two commonly used performance indicators. Performance-related studies are at the core of fuel cell research, e.g. fuel cell durability challenges are being studied to decrease fuel cell performance decay. An useful tool to characterize fuel cell output voltage is the polarization curve, which illustrates the cell voltage with respect to the current density (i.e., the i-V curve). Figure 1.5 shows an example of a typical i-V curve for a PEM fuel cell. Note that the current in the x-axis has been normalized by the area of the fuel cell, given a current density (in a unit of $A\ cm^{-2}$). In fuel cells, the energy conversion process is calculated through the concept of Gibbs free energy. Gibbs free energy is defined as the energy liberated or absorbed in a reversible process at constant pressure and constant temperature [7]. For a chemical reaction, the change in free energy ΔG refers to the difference between the Gibbs free energies of the reactants and products which is calculated by Gibbs equation [7]:

$$\Delta G = \Delta H - T\Delta S \tag{1.2}$$

where ΔH is the change in enthalpy, ΔS is the change in entropy between reactants and products. T is the absolute temperature. The electricity is generated through the change in the Gibbs free energy (ΔG_f), namely:

$$\Delta G_f = G_f(products) - G_f(reactants) \tag{1.3}$$

Theoretically, if the Gibbs free energy generated in the reaction could be directly converted into electricity without any loss, the fuel cell would be an ideal voltage generator. This ideal voltage is called reversible voltage, denoted as E_{rev} (also known as thermodynamically predicted output voltage). The reversible voltage (also known as open-circuit voltage) is the cell voltage at an electric current of zero. According to the expression of the Gibbs free energy (Equation (1.2)), fuel cell reversible voltage under constant pressure can be calculated as [8]:

$$E_{rev} = E_0 + \frac{\Delta S}{n_e F}(T - T^0) \tag{1.4}$$

where $E_0 = +1.23$ V is the reversible voltage under the standard-state conditions (room temperature, atmospheric pressure, unit activities of all species). n_e is the number of moles of electrons transferred and F is Faraday's constant. $n_e F$ expresses the quantified transfer of electrons, in the form of an electrical current between reacting chemical species. $T^0 = 298.15$ K is standard room temperature.

In practice, several irreversible losses lower the output voltage. Activation, ohmic, and concentration losses are considered the three major irreversible losses. For low current density, fuel cell voltage drop is dominated by activation losses (E_{act}). These losses are mainly caused by charge-transfer kinetics that fix the oxygen reduction and hydrogen oxidation rate at the electrode surface. Then, at the middle range of current density, the ohmic voltage losses (E_{ohm}), correspond to the internal resistance of fuel cells, that are mainly electrolyte membrane resistance, but also catalyst layer and contact resistances at high current density, concentration losses (E_{conc}) become dominant. It is due to that fact that the higher the cell current density

is, the faster the electrochemical reaction rate on the electrode surface is. But the limited mass transport of H_2 and O_2, due to the relatively slow mass transfer rate, leads to concentration losses and thus to voltage drop. Finally, the actual output voltage of a fuel cell equals to the reversible voltage minus three polarization losses (i.e., activation loss, ohmic losses, and concentration losses), which writes:

$$E_{cell} = E_{rev} - E_{act} - E_{ohm} - E_{conc} \tag{1.5}$$

The stack voltage (E_s) is obtained by multiplying the cell voltage with the number of cells (n_{cell}):

$$E_s = n_{cell} V_{cell} \tag{1.6}$$

Current density is defined as the current per unit area and is usually expressed in terms of A cm^{-2}. Fuel cell output voltage is measured under a specific current. The values of current density multiply the output voltage and number of fuel cells gives the power per unit area, i.e., stack power density (W cm^{-2}).

Limited by the complexities of fuel cell composition and various electrochemical reactions, an empirical formula is chosen over the exact physical laws to calculate the output performance of a fuel cell. The empirical formula for the activation, ohmic, and concentration losses are introduced thereafter.

In this section, an empirical formula for the three major voltage losses (i.e. activation loss, ohmic loss, and concentration loss) is introduced. The Butler-Volmer equation creates a link between the reaction rate and the electrode voltage. In fuel cells, the main electrochemical reactions are hydrogen oxidation reaction and ORR which involves multi-electron transfers. The Butler-Volmer equation for fuel cell reaction is expressed as:

$$i = i_0 \left(exp(-\frac{\alpha_t n_\alpha F E_{cell}}{RT}) - exp(-\frac{(1-\alpha_t) n_\alpha F E_{cell}}{RT}) \right) \tag{1.7}$$

where i_0 is the exchange current density. α_t is the transfer coefficient, n_α is the apparent electron number involved in the electrochemical reaction. Combining the mass transfer effects at high current density, the relationship between the cell voltage and the current density can be written as (fuel cell polarization is larger than 60 mV) [9]:

$$\begin{aligned} E_{cell} \quad &= E_{rev} + \frac{RT}{0.001678 T n_{\alpha O} F} log(i_0^{O_2}) + \frac{RT}{0.5 n_{\alpha H} F} log(i_0^{H_2}) \\ &- \frac{RT}{0.001678 T n_{\alpha O} F} log(\frac{I \cdot I_{dc}^f}{I_{dc}^f - I}) - \frac{RT}{0.5 n_{\alpha H} F} log(\frac{I \cdot I_{da}^f}{I_{da}^f - I}) - RI \end{aligned} \tag{1.8}$$

where $i_0^{O_2}$ is the exchange current density for oxygen ORR on a pure Pt surface, $n_{\alpha O}$ is the electron number which should be taken as 1 (not 2). I_{dc} and I_{da} are the diffusion limiting current density of cathode and anode, respectively. $i_0^{H_2}$ is the electron number of the anode reaction. $0.001678T$ is used to calculate the temperature-dependent transfer coefficient for ORR. R is the overall resistance.

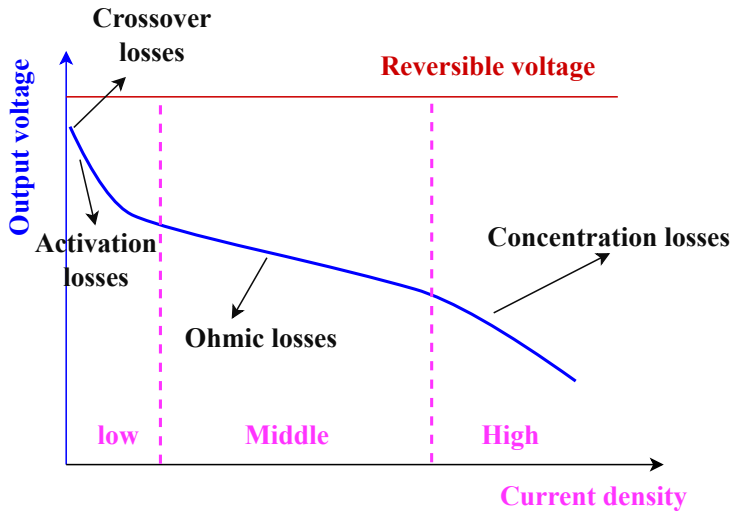

Figure 1.5: Fuel cell polarization curve with voltage losses.

A simplified empirical polarization equation is given as [10]:

$$E_s = n_{cell}\left(E_{rev} - RI - A\log(I) - m_1\exp\left(m_2 I\right)\right) \tag{1.9}$$

where I is fuel cell current density. The activation losses are expressed by $A\log(I)$, A is the Tafel parameter for oxygen reduction. The concentration (mass transfer) losses are calculated by $m_1\exp(m_2 I)$. m_1 and m_2 are transfer coefficient related parameters.

1.1.4 Electrochemical impedance spectroscopy

Electrochemical Impedance Spectroscopy (EIS) is an effective technique to study electrochemical characteristics within a fuel cell. In EIS characterization, a small AC amplitude perturbation is added to a constant Direct Current (DC) signal. By scanning a large frequency range, the impedance can be plotted as a Nyquist plot (Figure 1.6). A typical PEM fuel cell EIS curve has three key characteristics:

- Long-tale at high frequency. Inductive behavior due to the various FC connection elements and electric writes [11].
- Two semi-circles. The circles intercept the real axis at the high frequency is an ohmic activation loss, i.e. the ohmic resistance mainly caused by ionic resistance of the membrane. The diameters of two cycles are anode and cathode activation losses (related to charge transfer phenomena) [12].
- Small arc below real axis at low frequency. Due to the inductive behavior.

Each process described above can be considered as a simple electric circuit. Fuel cell electric circuit is an abstraction of the whole reaction process and is widely used for fuel cell

electrochemical characteristic studies. A typical electric circuit of PEM fuel cell consists of electrolyte resistance, charge-transfer resistance (electrode/electrolyte interface), mass transfer resistance, and double-layer capacitance [9] (Figure 1.7). In the proposed circuit, the semi-circle is modeled with a parallel connection of a Constant Element Phase (CPE) and a resistor [13]. The depression in the semi-circle is handled by adding a CPE. Two indicators are used to describe the inductive behaviors at high and low frequencies. The components presented in the electric circuit can be obtained by fitting measured EIS curve data to the electric circuit model.

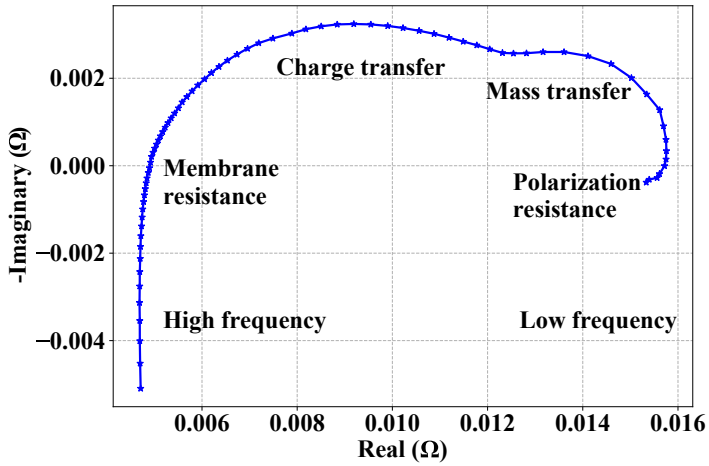

Figure 1.6: Typical Nyquist plots for a fuel cell (EIS spectra).

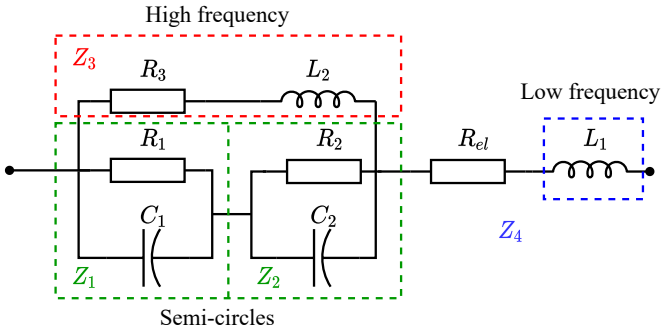

Figure 1.7: A general Electric equivalent circuit model (ECM) of the MEA.

1.1.5 Fuel cell hybrid system

The transportation industry is one of the main fields for deploying clean energy technologies. This is mainly due to the fact that they are responsible for 17% of the global greenhouse emissions every year [14]. The overwhelming advantages of PEM fuel cells like zero-emission, high efficiency, and high power density make them suitable for transportation applications. The

Battery Electrical Vehicles (BEVs) and FCEVs are both zero-emission exhaust gas compared to traditional gasoline vehicles. However, the FCEVs provide a longer drive range, shorter refueling time (less than 2 min), better performance under extreme weather (e.g. cold environment), and are lightweight compared to BEVs. As a result, the FCEV market is growing bigger rapidly worldwide. Figure 1.8 shows FCEVs and hydrogen refueling station market by region (2020). It is seen that Korea takes a lead in deploying FCEVs. Hyundai Nexo is their representative auto brand which contributes to a big part of FCEVs. Followed by the US, China, and Japan as the major countries for deploying FCEVs. Hydrogen refueling station is the main infrastructure for deploying FCEVs.

Figure 1.9 summarizes the main FCEVs types deployed in the world market. Fuel cell passenger light-duty electrical vehicles, FCEBs, and Fuel cell heavy-duty trucks are the main types of FCEVs being deployed. Fuel cell passenger light-duty vehicles take the major application market thanks to the advancement of fuel cell technologies. Figure 1.9 shows that China is dominant in deploying FCEBs, and Fuel cell trucks. FCEBs are widely used in public transportation to help reduce air pollution as well as to avoid urban traffic congestion. Recently, after the fulfillment of deploying vehicles and hydrogen stations for the 2022 Winter Olympics, China has decided to keep progressing in the development of FCEVs and hydrogen infrastructures. For example, the FCEB project started in Zhangjiakou is a good practice [15]. Based on the analysis of the life cycle inventory method, the economic feasibility of deploying FCEB in the northern part of China is verified. Fuel cell trucks are also growing fast in the FCEV market.

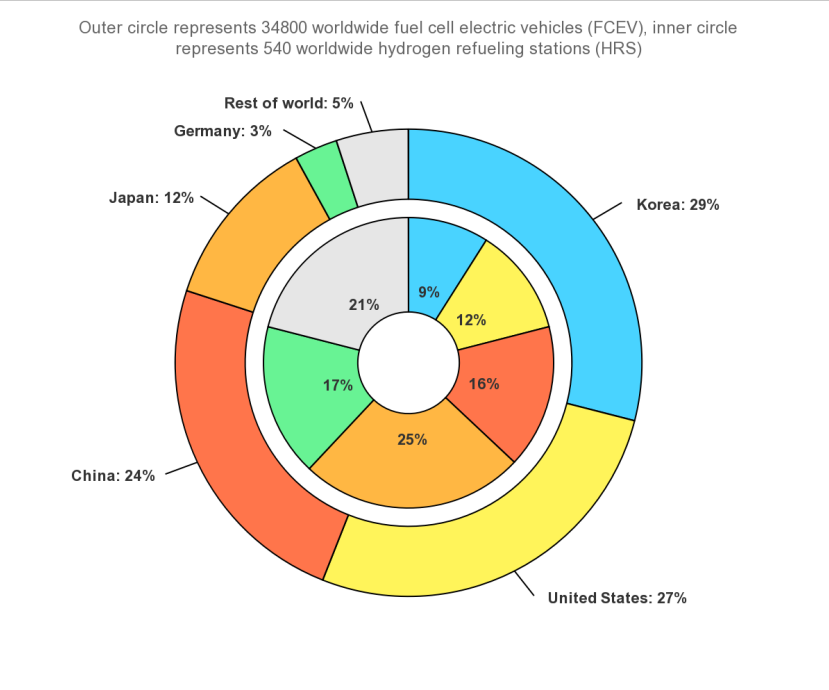

Figure 1.8: FCEVs and hydrogen refueling station market by region [16].

The fuel cell system installed in FCEVs includes fuel cell stacks, fuel cell cooling system,

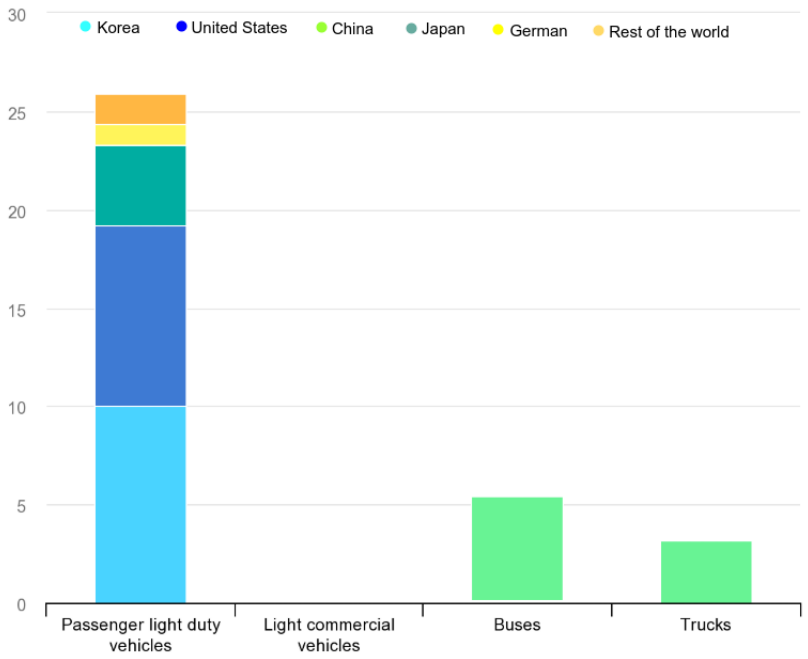

Figure 1.9: Fuel cell electric vehicles market by region and types [16].

high-pressure hydrogen storage tanks, electric motor, main power control unit, high-voltage batteries/super capacitor (response to transient power surges), air and hydrogen supply systems, and other auxiliary Balance-of-Plant (BOP) components. It is noted that fuel cells are seldom used alone due to the delay of transient response. Therefore, the fuel cells are usually installed together with other power sources, e.g. Li-battery, photovoltaic, super capacitor, etc. to construct a hybrid system for automotive applications. In this hybrid system, the fuel cell is used as the main power source and the other devices are deployed as backup energy source.

In stationary applications, PEM fuel cells are mainly used by the residential, commercial, and industrial stationary power generation sectors. The stationary applications generally consider PEM fuel cells as primary power, backup power, and Combined-Heat-and-Power (CHP). For primary power, PEM fuel cells are connected to the grid to provide electricity demand. Usually, the electricity demand greatly varies from on- to off-peak hours. PEM fuel cells are equipped with flexibility in output power adjustment which makes them a preferable primary power source. Li *et al.* [17] reviewed the opportunities of applying fuel cells in microgrids. The conclusion showed that fuel cells can help to improve the performance of microgrids and promote the usage of hydrogen energy. In backup power applications, PEM fuel cells are mainly used for emergency power supply (in remote areas) e.g., for the power supply of cars, buses, and ships and for the emergency power supply of aircraft [18]. PEM fuel cell systems inherently produce both electricity and heat which makes them suitable for meeting the daily needs of the building sector. Moreover, the PEM fuel cell guarantees high efficiency and supplies the peak power needs during the day and energy needed during the night. Thus, it is a mature technology for building and CHP applications. The micro-CHP system is mainly designed for

residential usage and Europe and Japan are leading the market [2]. A residential CHP can be used to provide electricity, space heating, and domestic water heating demands. Europe has installed more than 4100 fuel cell units for CHP applications [2]. The European project DEMCOPEM-2MW has installed a 2 MW PEM fuel cell power plant in Yingkou, China as the current world's largest PEM fuel cell power plant [19]. Japan has installed 360,000 CHP units in 2020, around 62% of them are PEM fuel cells [20]. These applications highlight the need for very high power demand. For example, mining trucks use several megawatts of electrical power. Thus, the study of improving fuel cell production capacity is highly needed to achieve the commercialization of fuel cells.

1.1.6 Fuel cell durability and cost definitions and challenges

Despite the widespread industrial application introduced above, the current MFC system still suffers from two major challenges, namely durability, and cost. PEM fuel cell output power decreases as the system operates, making it challenging to meet the durability target. The U.S. DOE released several durability targets for a specific application. For example, the DOE ultimate target durability of the fuel cell system in a FCEV is 8,000 hours [21]. The current max fleet average onboard system lifetime was only 4,100 hours [21]. For heavy-duty trucks, and FCEBs, the fuel cell system durability target is 25,000 hours. 40,000 hours durability target has been set for stationary applications. Fuel cell costs mainly originate from production material and operating costs. PEM fuel cell uses the costly platinum as an electrocatalyst. The development of a more efficient electrocatalyst with less platinum while maintaining high performance remains a key method to reducing fuel cell production costs. Fuel cell operation costs include hydrogen fuel consumption costs and system maintenance costs. Although hydrogen is the most abundant element in the universe, it is stored in water, hydrocarbons, and other organic matter, making the hydrogen fuel difficult and costly to produce [22]. The maintenance or replacement of the fuel cell system is also a major part of the overall operation cost. The ultimate DOE cost target is \$30/ KW for FCEVs and $\$600,000$ for each FCEB (2020 target) [3]. Data from several key fuel cell developers suggests that the equipment cost is around 6 times higher than the target of \$1000/ KW [23].

As a clean electrochemical power source, fuel cell takes hydrogen and oxygen as two reactants and then converts their chemical energies into electricity, heat, and water. Figure 1.10 shows the main energy flow of a fuel cell. In a fuel cell, the power or power density is a key operating parameter that reflects the production capacity of a fuel cell. The energy provided by the fuel cell is measured by its output power over a certain period of time. Fuel cell system efficiency is related to the energy conversion as depicted in Figure 1.10. It is defined as the electrical energy delivered by the fuel cell system compared with the energy supplied as fuel. A fuel cell system that operates with high efficiency will cost less fuel thus reducing system fuel consumption. For a long-term operating task, fuel cell replacement and repair are needed which invokes the maintenance cost. Resuming above, the cost is an important parameter to consider, but that can be defined in several manners.

The other crucial parameter is lifetime, that has to be dramatically increased. In practice,

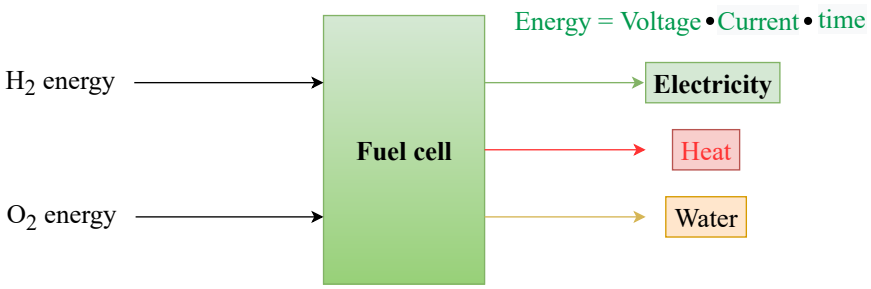

Figure 1.10: Inputs and outputs energy flow of a fuel cell.

the performance (i.e. power) of a fuel cell gradually deteriorates as the operating time increases. Thus, the definition of fuel cell lifetime is usually linked to its performance decay. For example, the DOE lifetime target for fuel cells is defined as the time it takes for their power rating to drop by more than 10% [24]. Based on the experimental data of fuel cell electrical vehicles, Pei *et al.* [25] define the lifetime as the duration time from initial operation till the output voltage drops by 10% under the rated power conditions. When fuel cell performance decay reaches a predefined threshold, the unit is considered as reaching the End of Life (EOL). It should be noted that fuel cell lifetime and performance decay are related to following three key concepts [26]:

1. *Reliability*: Fuel cell's ability to perform as required in a stated operating context and for a stated period of time. It involves fuel cell failure modes that may lead to catastrophic failure.
2. *Durability*: Fuel cell's ability to resist permanent performance decay during the operation period. Note that durability decay usually refers to fuel cell performance decrease which is not recoverable, but not a catastrophic failure. It is related to fuel cell aging.
3. *Stability* Fuel cell's ability to recover performance decay during system operation. It is related to fuel cell operation conditions and reversible changes in its components (materials).

Then, the overall fuel cell performance decay rate which is measured during fuel cell continuous operation is the summation of stability and durability decay rates [26]. For fuel cells, it is verified that when their performance decay exceeds a certain threshold, a significant performance drop is observed. The fast decreasing in performance yields poor fuel economy and a high probability of occurring catastrophe failure in fuel cell components. Then the fuel cell system is considered to reach EOL.

1.2 Fuel cell deterioration

Fuel cell deterioration studies dedicate to understanding fuel cell deterioration behavior, proposing deterioration mechanisms, and finally developing deterioration models. A proper

deterioration model enables to reproduce fuel cell performance decay. Fuel cell deterioration is unavoidable in practice, but the deterioration rate can be minimized based on fuel cell deterioration models. Therefore, performing fuel cell durability test and understanding the various mechanisms of deterioration modes is critical to the development of long-lasting and cost-sensitive fuel cells.

1.2.1 Degradation under constant load

Some experimental deterioration studies have first been carried out for constant load profile. The IEEE Reliability Society, FCLAB research federation (FR CNRS 3539, France), FEMTO-ST Institute, and the Laboratory of excellence ACTION lunched a data challenge for fuel cell performance prognostics, i.e., IEEE PHM 2014 Data Challenge [27]. Two five-cell PEM fuel cell stacks are tested under a fuel cell test bench in FCLAB. Each cell has an active area of 100 cm^2. The nominal and maximal current density of the cells are 0.7 and 1 $A\ cm^{-2}$ respectively. Two long-term durability tests were carried out:

- The first stack (FC stack 1) was operated in a constant load (roughly nominal operating conditions).
- The second stack (FC stack 2) was operated under nominal load with high-frequency current ripples.

During fuel cell operation, characterization tests, i.e., Polarization curve test and EIS test, were performed on fuel cell stack once per week (around every 160 hours). The main measurements results are plotted in Figures 1.11, 1.12. Figure 1.13 shows the overall stack voltage decay curves recorded during test. Fuel cell performance degradation is reflected in the polarization curves and EIS measurements. In polarization curves, the FC stack output voltage is decreasing from 3.048 V to 2.864 V at I_{max} (i.e. maximal current density) for FC stack 1. Similarly in FC stack 2, the output voltage drops from 2.954 V to 2.715 V.

The dynamic behavior of fuel cell stacks can be analyzed through the EIS curves. According to the ECM as shown in the Figure 1.7, the equivalent impedance (Z_{eq}) of the PEM fuel cell is expressed as:

$$Z_{eq} = \frac{(Z_1 + Z_2) \cdot Z_3}{Z_1 + Z_2 + Z_3} + Z_4 \tag{1.10}$$

The polarization resistance is calculated as:

$$R_{pol} = \frac{(R_1 + R_2) \cdot R_3}{R_1 + R_2 + R_3} + R_{el} \tag{1.11}$$

Then the polarization resistance can be estimated based on the EIS measurements. The results prove that the resistance is generally increase in time which enables the feasibility of using fuel cell resistance as a degradation indicator [28].

To better understand the link between degradation mechanisms and performance decrease, specific tests, called Accelerated Stress Test (AST) have been experimented [26], [29]. AST

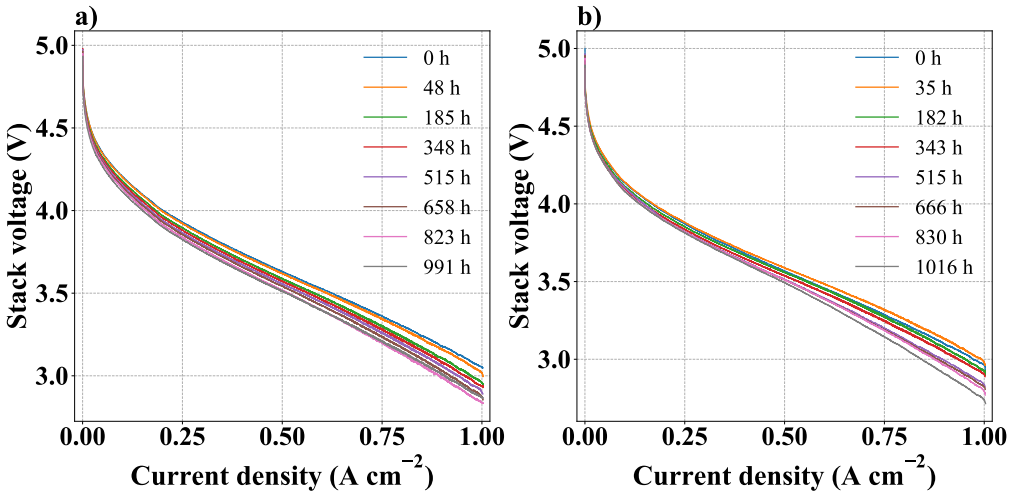

Figure 1.11: Polarization curves [27] measured for a) FC stack 1; b) FC stack 2.

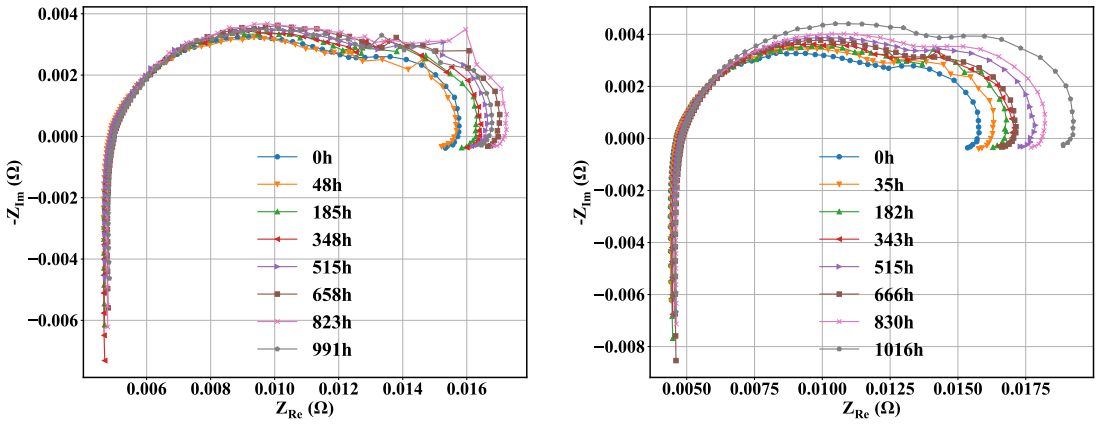

(a) FC stack 1

(b) FC stack 2

Figure 1.12: Measured EIS curves during durability test.

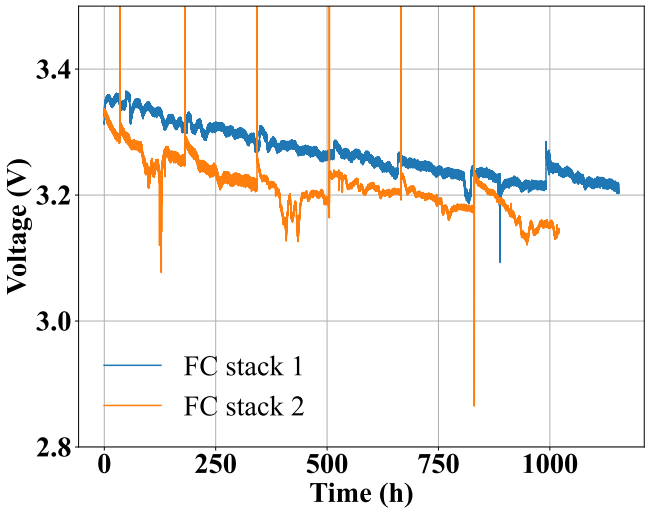

Figure 1.13: FC stacks voltage decay curves.

utilizes so-called Accelerated test protocols which push fuel cells to operate under undesirable conditions to accelerate their performance decreasing. These undesirable conditions are linked to key fuel cell operation parameters which include temperature, load cycling, Relative Humidity (RH), pressure, etc. These tests able to link some model parameters to degradation phenomena.

The idling operation is defined as the fuel cell system running without power output. During idling, the fuel system is operating with a small current density to produce the power for the auxiliary systems (e.g. fuel cell gas supply system, cooling system) to maintain its normal function. A small current density makes a high cell voltage (0.85-1.0 V), which is closed to the Open-Circuit Voltage (OCV). Pei *et al.* [25] performed a durability test on automotive fuel cells to check the fuel cell performance degradation. It is reported that in the idling operation condition, the water produced inside the fuel cell is small, causing MEA easy to be dry. Franck-Lacaze *et al.* [30] studied fuel cell aging under different current density level, i.e. 120 and 20 mA cm^{-2}. It is reported that the nominal voltage decreasing rate under lower current density (20 mA cm^{-2}) is around eight times the aging rate of the higher current conditions. The characterization analysis confirms the aging of Pt dissolution and loss of sulfur and fluorine from the membrane.

The AST studies show that the major aging components in the fuel cell are the membrane and catalyst layer when exposed to the open-circuit/idling operation. The high cathode potential and gas crossover are the main factors for membrane degradation. Chemical degradation is the core mechanism of fuel cell membrane degradation under open-circuit/idling operation. Chemical deterioration of the PFSA membrane is mainly caused by the attack of free radicals generated during fuel cell OCV operation, e.g. hydroxyl radical (·OH) [31], hydrogen radical (·H), and the hydroperoxyl radical (·OOH) [32]. These free radicals caused membrane thinning, cracks, and pinholes [26]. In addition to the deterioration of the fuel cell membrane, the

CL decays greatly due to the high cell voltage. The experimental studies confirmed that the Pt catalyst in the fuel cell cathode side experiences severer deterioration [33], [34]. Zhang *et al.* [34] reported a 51.9 % decay in Electrochemical Surface Area (ECSA) after 256 h OCV test. Figure 1.14 summarized the main deterioration mechanisms of Pt catalyst under OCV conditions. Figure 1.14(a) and Figure 1.14(b) show the growth in Pt particles caused by Electrochemical Ostwald ripening and coalescence. Pt dissolution can be described by the following electrochemical reactions due to high cell voltage [35], [36]:

$$\begin{aligned} &\text{Pt dissolution :} && Pt - 2e^- \rightarrow Pt^{2+} \\ &\text{Pt oxide formulation :} && Pt + H_2O - 2e^- \rightarrow PtO + 2H^+ \\ &\text{Pt oxide dissolution :} && PtO + 2H^+ \rightarrow Pt^{2+} + H_2O \end{aligned} \tag{1.12}$$

The precipitation of Pt^{2+} in the fuel cell membrane is shown in Figure 1.14(c). Figure 1.14(d) shows Pt detachment due to the loss of carbon support. These behaviors caused the decay of Pt catalyst thus causing fuel cell deterioration.

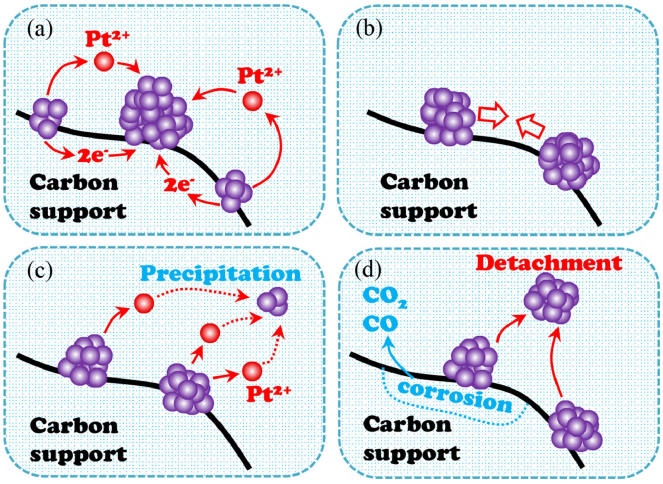

Figure 1.14: Deterioration mechanisms of Pt catalyst [37]: (a) Electrochemical Ostwald ripening, (b) coalescence, (c) migration of Pt catalyst, and (d) detachment of Pt catalyst.

1.2.2 Deterioration under driving cycles

In real life, fuel cell stacks are operating in dynamical conditions. To simulate operating profiles that are the most representative as possible of reality, some load profile driving cycles have been proposed.

New European Driving Cycle (NEDC) is a typical light-duty vehicle driving cycle with features periods of acceleration, deceleration and constant speed modes [38]. Figure 1.15 depicts a detailed NEDC cycle with varying driving speeds. It consists of four repetitions of a low-speed urban cycle of 780 seconds in total, followed by a highway driving (extra-urban driving cycle) of 400 seconds duration. An NEDC cycle is equivalent to a theoretical distance of 11 km driven in around 20 minutes. To apply the NEDC in Figure 1.15 to FCEVs, the

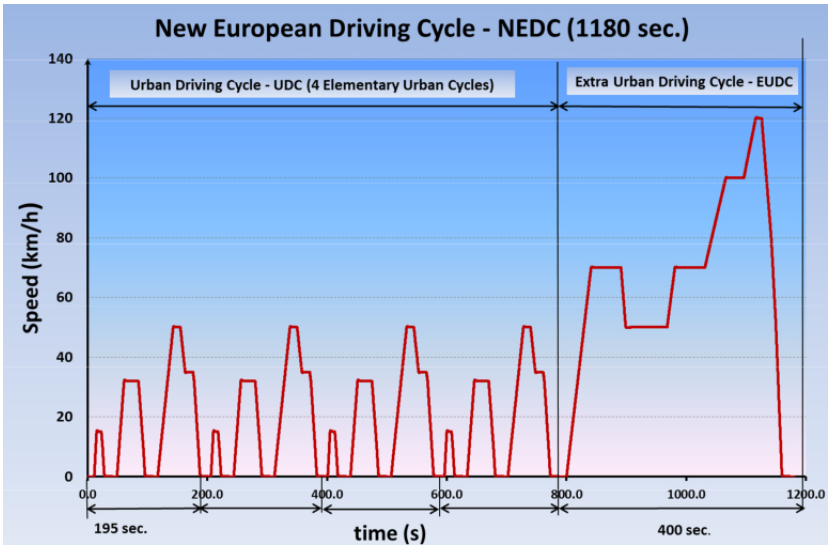

Figure 1.15: NEDC profile [38].

speed of the driving cycle needs to be transferred into current load ratio. This is done by:

$$\int_0^{1180} I_{NEDC} dt = \int_0^{1180} I_{Squared} dt \tag{1.13}$$

where I is the cell current. The transferred squared cycle (see Figure 1.16) can be applied to fuel cell test benches. Figure 1.17 is the fuel cell dynamic load cycle (FC-DLC) implemented in the real fuel cell test bench.

Another standard driving cycle being used is the World Harmonized Light Vehicles Test Cycles (WLTC) [40]. The WLTC stands for a harmonized driving cycle from "real world" driving data in various regions around the world. Similar to the NEDC cycle, the WLTC consists of urban, rural, and highway. The usual duration of one WLTC cycle is 1800 seconds. The initial velocity profile of WLTC is shown in the Figure 1.18.

According to the above typical fuel cell driving cycles, the load operation conditions of an automotive used fuel cell can be categorized into open-circuit/idling, dynamic load, start-stop, and high power load conditions [25]. These operation modes are the main source of fuel cell performance decay. Various operation modes triggered during fuel cell system operation directly caused damage to fuel cell core components. Thus causing an overall fuel cell performance decay.

Fuel cell deterioration is closely linked to its operating parameters. The operation parameters refer to fuel cell physical operation conditions, such as the temperature, RH, pressure, and the operation mode of a fuel cell. This section dedicates to introducing fuel cell deterioration mechanisms under typical dynamic load profiles.

Dynamic load (load variation) is another typical operation mode for PEM fuel cells. PEM fuel cells need to adjust their output power to meet the varying power demand of vehicles. Load varying caused a transient process with fluctuations of fuel cell output voltage, reac-

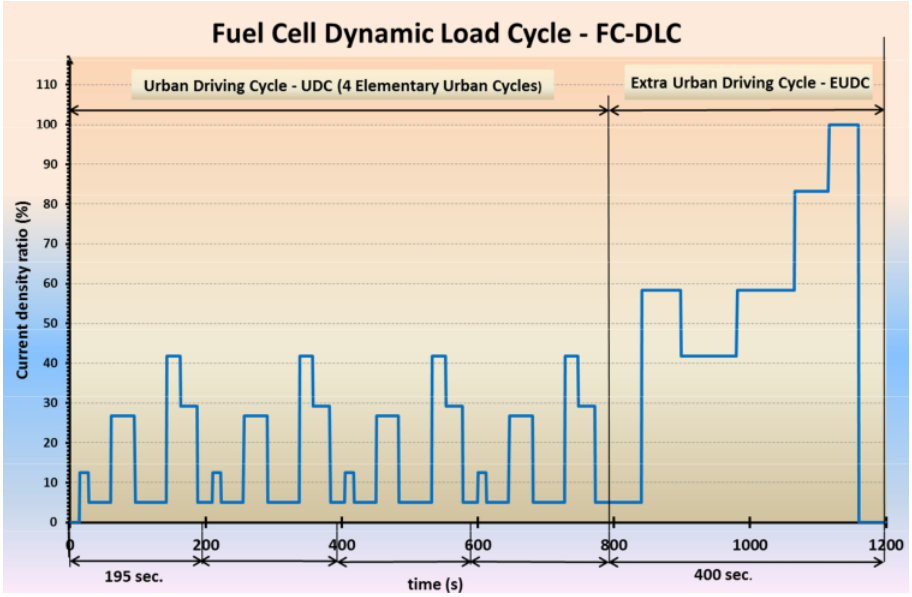

Figure 1.16: Transferred NEDC profile [38].

tant gas stoichiometric ratio, operation temperature, pressure, etc. Thus accelerating fuel cell deterioration. Meng *et al.* [42] experimentally studied the load varying effects on fuel cell deterioration characteristics. They conclude that gas starvation caused by the transient process is the main cause of fuel cell deterioration. During load variation, the load can be switched in milliseconds. However, the reactant gas is supplied by a controller and passes through a long tube to reach the fuel cell. This caused the reactant gas starvation. Hydrogen starvation in the anode caused carbon corrosion and catalyst layer deterioration become more severe when operating with a larger load-varying rate. It is reported that the voltage drop due to high load varying can reach three times that under a smaller load varying rate. Load varying causes a thermal/humidity cycling with fuel cells which is harmful to fuel cell performance. Liu *et al.* [43] studied the effect of humidity cycling on fuel cell deterioration. Microstructure changes in fuel cell CL are observed when operating under dynamic load. The output voltage drops around 6.56% for deteriorated fuel cell in comparison with the fresh one.

The formation of hydrogen-air interface inside a fuel cell is the main cause of fuel cell deterioration by start-stop operation [44]. The presence of hydrogen-air interface leads to oxidation in the fuel cell anode. This introduced a high voltage in the cathode which caused the oxidation corrosion of the cathode carbon support layer. Consequently, fuel cell ECSA and output power are decreased due to Pt particles detached from the catalyst surface.

High power load operation pushes fuel cells operating under undesirable conditions and accelerated their deterioration. The experimental study reported in [45] showed that a high load cycle operation leads to electrode flooding and the decrease of proton conductivity. Membrane deterioration due to Phosphoric Acid (PA) loss is another important cause of fuel cell deterioration in high power load conditions. Thomas *et al.* [46] reported that PA loss is observed in a deteriorated fuel cell. Besides, the membrane resistance is increased due to PA

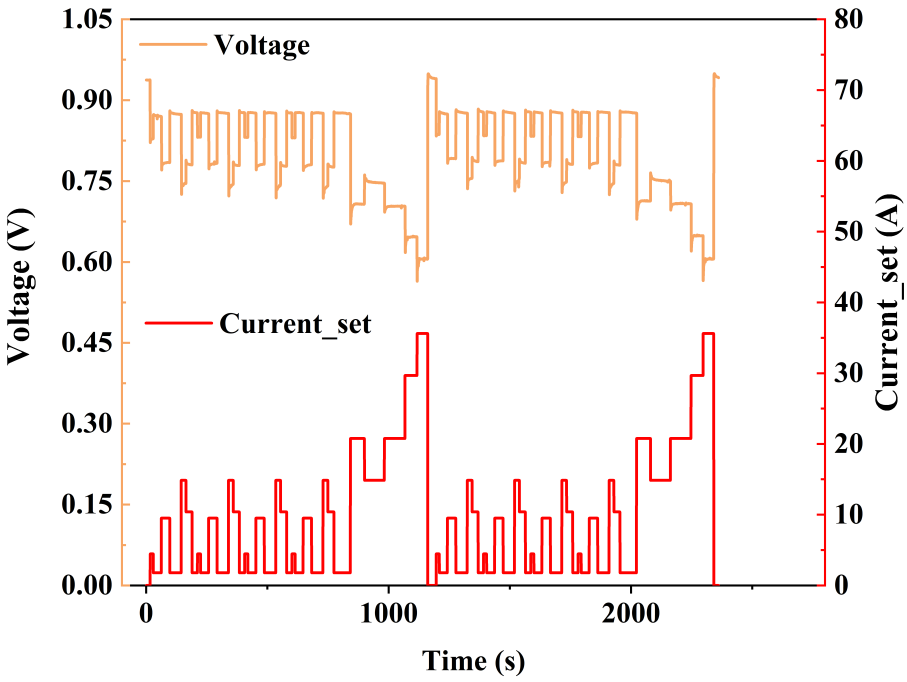

Figure 1.17: NEDC profile in real fuel cell test [39].

loss. The EIS measurements verified that the PA loss is proportional to resistance increments.

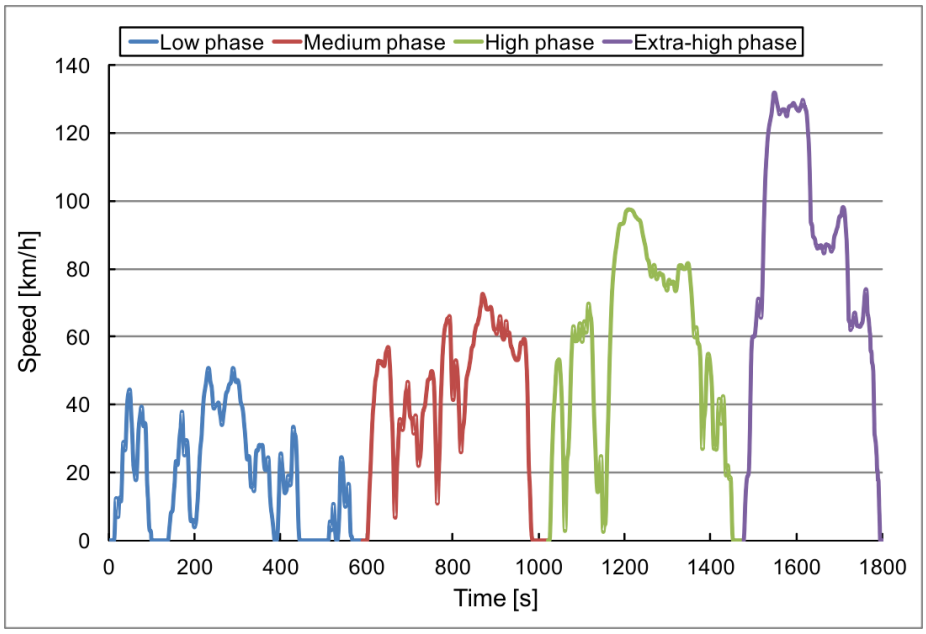

Figure 1.18: Initial velocity profile of WLTC cycle [41].

1.3 Fuel cell prognostics and health management studies

Facing the limited durability and high-cost challenges, a synthetic energy management strategy is needed to pave the path to the commercialization of MFC technologies. The role of the EMS is to combine the study of fuel cell deterioration mechanisms, and deterioration modeling to produce optimized operation strategies for fuel cell systems. These operation strategies are expected to extend fuel cell lifetime and operation cost (maintenance related). For example, in FCEVs, the fuel cells are put together with batteries forming a network system. In such a system, the battery used is small with limited battery power. As a result, the fuel cell has to be operated dynamically across a wide load range. This arises the need for fuel cell operation mode control [47]. The decision-making process (operation strategy) addressed by an EMS is considered to be a crucial step to complete the PHM cycle. Thus, the PHM for fuel cells will be introduced first as a general approach background. Then the works on two key studies of fuel cell EMS are introduced, i.e. the Deterioration-aware EMS and Maintenance-based EMS.

1.3.1 Prognostics and health management

PHM is a diverse, interdisciplinary field which covers the concept of diagnostics, prognostics, and condition-based monitoring [48]. PHM provides a wide range of tools for system health assessment and reliability improvement which involves a number of subareas in different aspects. PHM integrates various modeling computation approaches to process physical knowledge, information and data of systems and components operation and maintenance, to enable detecting anomalies, diagnosing degradation states and faults, predicting the evolution of degradation to failure and estimating the Remaining Useful Lifetime (RUL) of a system

[49]. The outcomes of RUL prediction computations can be further used to support the maintenance decisions for improving system operation time and reliability. It is thus a promising approach that could be useful in various industrial applications including fuel cells. PHM approaches in fuel cell systems are mainly focused on improving their durability and operating cost, the main related PHM tasks are presented in Figure 1.19. The main stages of PHM include: data acquisition and processing, State of Health (SOH) estimation and diagnostic, prognostics, and decision-making. The core tasks for each step of PHM are summarized as follows:

- Data acquisition and processing

Data acquisition module consists of digital sensors to monitor the value of the fuel cell system physical variables, e.g. voltage, power, temperature, pressure, etc. Data storage and transition are also installed to provide initial monitoring information data of a fuel cell system. These obtained data are usually noisy and with hidden features, thus proper data processing is needed. The data processing module receives data from the sensor and processes them by using different data processing and analysis techniques and tools, e.g. perform feature extraction by Principle Component Analysis (PCA) and feature selection by clustering technique.

- Model analysis

Model analysis in PHM includes anomaly detection, diagnostics, and prognostics. Anomaly detection is mainly for determining the fuel cell system operation state. Approaches like support vector machine (SVM), and Bayesian neural networks can be applied to classify fuel cell states, i.e. normal or abnormal, sending alarms when anomaly states are detected. Diagnostics is a critical step based on anomaly detection to determine the health status of the fuel cell system (SOH, reflected by fuel cell output voltage, current density distribution, impedance spectra, etc.). Diagnostics analyze the severity levels of system degradation by using supervised machine learning techniques such as random forest, k-Nearest Neighbors (KNN), etc. And the final step is to predict the future degradation of fuel cell performance and estimate its remaining useful lifetime (RUL). Several tools are being used to achieve prognostics of fuel cells such as Long Short-term Memory (LSTM) neural networks, hidden Markov chain Model (HMM), etc.

- Decision

Decision support refers to the management part of PHM. It uses the outputs of diagnostics and prognostics for taking timely, proper maintenance and operation control decisions for optimizing system operation in order to achieve an extended lifetime and reduced cost. It is thus considered as a key part of conducting PHM approaches to improve system operation efficiency. The Energy Management Strategy and maintenance scheduling are two main techniques to offer decision-support for fuel cell systems.

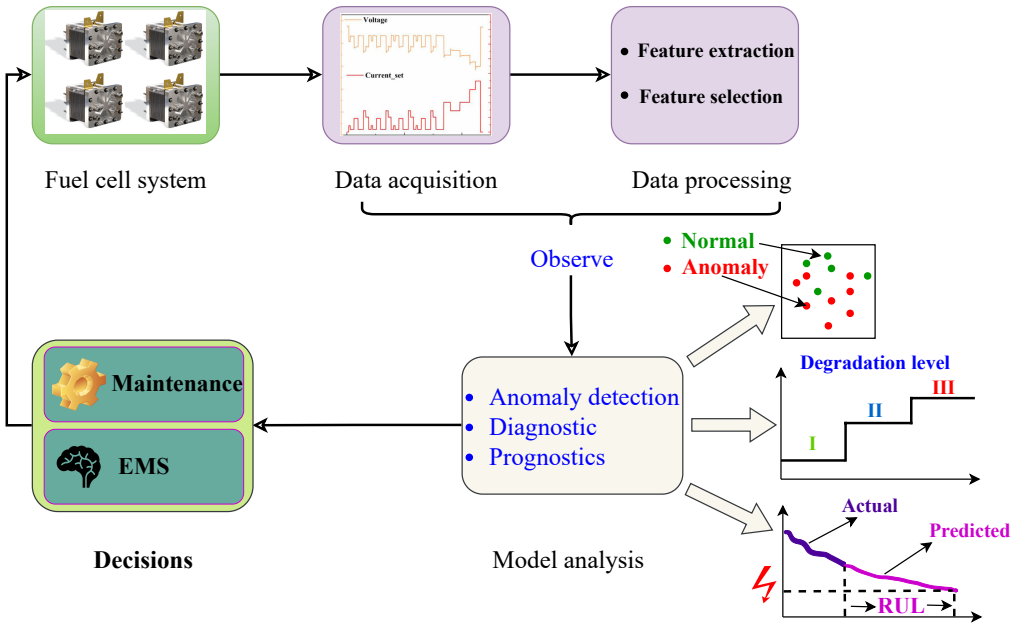

Figure 1.19: PHM architecture.

Currently, fuel cell PHM studies mainly focused on the previous two stages to process fuel cell diagnostics and prognostics. Fuel cell diagnostics is targeted to identify system degradation levels, raise alarms in case of faulty operation modes, and finally analyze the main factors for fuel cell fault operation. Li *et al.* [50] developed a classification fault diagnostic model based on SVM for fuel cell systems. This diagnostic model can effectively classify the four fault degrees based on measured fuel cell voltage signals. Since fuel cell test data contains multiple factors which may causing fuel cell fault operation, the fuel cell diagnostic approach needs to identify the key influence factors. Lin *et al.* [51] proposed an enhanced PCA algorithm to generate key features based on history datasets. The data analysis efficiency of the diagnostic approach is one of the key focuses on fuel cell studies. Process limited input data can provide rapid but limited analysis accuracy. On the other hand, performing comprehensive characterization that provides more accurate analysis will require invasive measurements.

The recent progress in the Machine Learning (ML) approach proves to be a promising approach to overcoming the data analysis challenges. Zhou *et al.* [52] reviewed the main ML techniques that are suitable for fuel cell diagnostics. Generally, ML approaches follow the procedures of model training and diagnostic. The collected historical data are used to train an ML-based diagnostic model. Fuel cell SOH is then diagnosed based on the trained model. Techniques like Fisher Discrimination Analysis (FDA), Spherical-shaped Multiple-class Support Vector Machine (SSM-SVM), and PCA are efficient techniques for feature extraction. The training of diagnostic models can be achieved by using various neural networks, e.g. LSTM, extreme learning machine (ELM), autoencoder, etc. Gu *et al.* [53] performed fuel cell flooding fault diagnostics based on a LSTM model. The analysis showed that the proposed model can effectively diagnose fuel cell flooding, thus help optimizing fuel cell water management. Moreover, the newly developed branch of ML, i.e. deep learning further improves the general-

ization ability of diagnostic models on untrained samples. A stacked sparse autoencoder-based diagnostics model was proposed by Zhang *et al.* [54]. Experiments verified that this model can diagnose fuel cell faults with high accuracy rely on a few training samples. Another way of overcoming the data analysis and computation challenges is to develop physical-based diagnostics tools. That is, to combining fuel cell fault diagnosis with physical models to develop an efficient diagnosis methods. Jullian *et al.* [55] proposed a physical model-based diagnostic tool by taking into account fuel cell voltage and resistance information to produce a reliable and efficient diagnosis for fuel cells.

Prognostics deal with the prediction of fuel cell future deterioration trend and finally obtain the RUL. Based on the SOH estimation, the prognostics phase predicts the system's RUL. Generally, the present prognostics approaches can be concluded as model-based, data-driven and hybrid methods. The model-based method is based on physical models to study the performance decreasing prediction of a fuel cell. As fuel cell deterioration physical laws are not fully known, the current model-based approaches are proposed based on semi-empirical formulas. Jouin *et al.* [56], [57] have studied fuel cell prognostics based on the Particle Filter (PF) framework. The first model combined three empirical voltage drop model with PF to predict fuel cell RUL. They achieved a prediction accuracy of 90 h for a 1000 h lifespan. Then in the second model, the authors proposed a fault tree-based approach to analyze the critical deterioration mechanisms of a fuel cell. And finally construct a prognostic model based on the obtained deterioration model PF method.

The data-driven method overcomes the drawbacks of the physical model by building fuel cell prognostics model purely reply on experimental data. Besides, the advanced ML-based approaches being used usually give a relatively high prediction accuracy. Zuo *et al.* [58] developed a fuel cell prognostic model based on the attention-based Recurrent Neural Network (RNN). The prediction accuracy is validated by a dynamic fuel cell durability test dataset. Hua *et al.* [59] proposed a long-term fuel cell prognostics model based on Echo State Neural Network (ESN). However, These methods belong to black-box paradigm thus they are lacking the interoperability in terms of the obtained prognostics models. The hybrid method offers a compromise between the two methods by combining the advantages of the model-based and data-driven approaches. For instance, Zhou *et al.* [60] proposed a moving window-based hybrid prognostic approach. They combine an empirical polarization model and a data-driven model based on the Nonlinear Autoregressive Neural Network (NARNN). They conclude that the model-based approach can be used to forecast fuel cell long-term deterioration trend, where the data-driven model can accurately predict local nonlinear characteristics of fuel cell voltage drop. Therefore, the combination of these two methods gave an improved prediction accuracy. The hybrid model is relatively complicated and requires a good design of the two approaches.

Compared to fuel cell diagnostics and prognostics studies, the decision aspect of PHM methods is less studied yet vital for deploying PHM in reality. However, the RUL predicted from prognostics remains of limited interest if it is not used to make a decision, and its performance can be sensibly assessed only at the level of the whole processing chain, i.e. from prediction to decision-making.

In summary, PHM deals with three main issues: SOH estimation, RUL prediction, and

system operation decision-making [61]. Within these stages, the decision-making process is receiving increasing attention [62]. Indeed, its development requires prior knowledge of the SOH and the system RUL under study. In the case of fuel cells, the great complexity of fuel cell operation makes these steps difficult to carry out. This explains why the development of a comprehensive PHM approach for fuel cell systems is challenging.

1.3.2 Fuel cell health indicator and deterioration modeling

Deterioration modeling plays a key role in PHM. It links fuel cell system and decision-making strategies, which enables to extend system lifetime based on available deterioration information. This section summarizes the works of defining proper fuel cell degradation indicator and deterioration modeling approaches. In this part, we intentionally limit the methods to those are based on electrical parameters. In this part, we intentionally limit the methods to those that are based on electrical parameters. The fuel cell deterioration model is used to simulate the dynamic deterioration behavior of a fuel cell system. Based on the measured historical data, a deterioration model allows for reproducing, diagnosing, and predicting the dynamic behavior as well as the SOH of fuel cells.

1.3.2.1 Health indicator

A fuel cell health/deterioration indicator (HI) should carry and reflect key deterioration information of a fuel cell. Defining a proper HI is a key process for fuel cell SOH estimation and deterioration modeling. Generally, fuel cell output voltage and power are two widely used HIs as they are relatively easy to measure and calculate. Besides, it is assumed that their deviation is only influenced by the fuel cell deterioration phenomenon. Chen *et al.* [63] designed a Kalman filter to estimate the output voltage of a PEM fuel cell under real operating conditions to access the aging state of fuel cells. The output voltage [58], [64] and power [65] measured from fuel cell durability test are used to characterize the SOH of fuel cells.

However, for more dynamic operation scenarios (e.g. FCEV driving cycles), the output voltage and power are influenced by varying operating parameters and deterioration factors [66]. In these cases they are not suitable used as HI. Zhang *et al.* [67] investigated the deterioration indicators for fuel cells. They identify the difficulties in interpreting the measurements and distinguish various causes of fuel cell performance decay. Based on the EIS measurements, they proposed the HI as a key aging parameter estimated from EIS data.

A fusion or extracted HI is proposed to overcome the limits of purely relying on fuel cell voltage or power. Chen *et al.* [68] proposed an original fusion HI by combining fuel cell inner resistance, stack voltage, and the stack power. This novel HI enables better tracking and prediction of fuel cell deterioration. Dedicated to the development of more accurate and comprehensive HIs, Liu *et al.* [69] proposed a multi-scale hybrid HI for fuel cells. The proposed hybrid HI is selected based on several deterioration indexes such as ECSA, Pt particle radius, and membrane thickness. The fusion criteria was built based on their influences on fuel cell

deterioration. Hua *et al.* [66] reviewed the HI development for fuel cell HI suitable for both static and dynamic operating conditions. The authors conclude that novel HIs like extracted virtual stack voltage [70], average resistance [71] are suitable for dynamic operating conditions. Moreover, they proposed two other HIs, i.e. polarization resistance and power loss to estimate fuel cell SOH. The polarization resistance is calculated based on the EIS measurements and power loss is calculated by:

$$\Delta P = (P - P_0)/P_0 \tag{1.14}$$

where P is the actual power and P_0 is the power at the Beginning of Life (BoL).

A proper HI needs to be defined at first in order to model fuel cell deterioration behavior [72]. Based on the discussion of Section 1.3.2, the HI needs to be able to reflect key deterioration information of fuel cells. Besides, the HI is expected to be applicable under dynamic load profile considering the varying operation modes of various application scenarios (for example in FCEVs). Fuel cell resistance is closely linked to fuel cell deterioration and being used in several studies as HI [65], [66], [71]. The EIS [69] and online estimating algorithms [73], [74] ensure that resistance can be measured or estimated. Hence, the overall fuel cell resistance R can be taken as a global health indicator. Fuel cell deterioration modeling is then focused on fuel cell resistance. Combining the proposed polarization equation (Equation (1.9)), the value of R increases with the deterioration of a fuel cell (output voltage is decreasing). Without a further statement, the fuel cell deterioration is represented by the increment of fuel cell overall resistance.

1.3.2.2 Fuel cell deterioration modeling approaches

Based on the model assumptions and techniques being used, the existing fuel cell deterioration modeling approaches can be categorized into physics-informed, data-driven, and hybrid approaches.

- Physics-informed models. These models are proposed based on the physical laws of fuel cell systems such as thermodynamics, and electrochemistry. They can be white-box models based on exact laws of physics, or be Grey-box models based on semi-empirical mechanisms.
- Data-driven models. These methods are recognized as black-box. Instead of building the mechanical deterioration models for fuel cells, they learn fuel cell deterioration behavior from the measured durability test dataset.
- Hybrid models. They can be considered as a combination of physics-informed and data-driven models. Depending on semi-empirical laws, combing with data-driven approaches to build fuel cell deterioration models.

Fuel cell performance deterioration is linked to complex electrochemical, mechanical, and thermal mechanisms which are difficult to model using a white-box model. Besides, due to the complex configuration, the measurement of some parameters (states) that are required by

the model are challenging to measure, such as fuel cell membrane water content. The Grey-box model overcomes these challenges by using semi-empirical models and measured data to model fuel cell performance decay. In general, the Grey-box approaches use the measured dataset to estimate aging parameters in semi-empirical models. Then based on the obtained model to study fuel cell deterioration behavior. Grey-box models are widely used in fuel cell deterioration modeling studies. Depending on fuel cell empirical polarization equations to propose deterioration models is one of the most popular approaches thanks to the mature basis of fuel cell polarization-related studies. Jouin *et al.* [57] proposed a semi-empirical deterioration model for fuel cell prognostics. According to available fuel cell deterioration mechanisms, several aging-related parameters such as ionic, electronic, and contact resistances are selected from fuel cell polarization equation [75] and modeled with empirical formula. Bressel *et al.* [76] reproduced fuel cell deterioration behavior based on a typical polarization equation:

$$E_s = n(E_0 - Ri - AT\log(\frac{i}{i_0}) - BT\log(1 - \frac{i}{i_L})) \tag{1.15}$$

where E_s is the stack voltage, i is the current density, and n is the number of cells. T is the temperature, A is Tafel constant, and B is a concentration constant. E_0 is fuel OCV for a given temperature and pressure. R is fuel cell overall resistance (membrane, end plates, connectors, etc.). i_0 is the exchange current and i_L is the limiting current. Kalman filter is applied to identified parameters (E_0, R, i_0, and i_L) in Equation (1.15) from measured durability test data. It is reported that R increases by more than 50% and i_L decreases 45% which is chosen as HIs for predicting fuel cell performance decay. For the same purpose of predicting fuel cell performance decay, Zhang *et al.* [77] proposed a similar deterioration model based on a fuel cell polarization equation. To increase the accuracy of estimating fuel cell SOH evolving trends, they proposed a novel identification method that combines fuel cell stack voltage and EIS measurements. The obtained model is validated through real fuel cell test data with improved prediction accuracy compared with traditional prognostics based on a single HI deterioration model.

Different from the physics-informed modeling approach builds the model based on fuel cell semi-empirical formula, data-driven methods purely learn a model from fuel cell durability test data. But this learned model is a black-box one compared to the semi-empirical equation obtained from the physical-informed model. Thanks to the rapid development of ML-based approaches, e.g. Long short-term memory (LSTM) [78], Convolution neural networks (CNN) [79], these data-driven approaches can ensure a high prediction accuracy. Ma *et al.* [80] developed a Grid LSTM (G-LSTM) model for predicting fuel cell voltage. Based on the experimental dataset of 1.2 KW Ballard Nexa fuel cell, 1 KW PEM fuel cell, and 25 KW PEM fuel cell, the G-LSTM model achieves a high prediction accuracy (root-mean-square error of 0.004). Zuo *et al.* [58] proposed an attention-based RNN to learn the fuel cell voltage deterioration model. They provided a long-duration dynamic load durability test dataset [39]. Note that the collection of fuel cell durability test data is costly work both in terms of money and time. In current data-driven approaches, the limited available dataset is also a bigger challenge. The attention-based RNN achieved a high short-term prediction accuracy (Root Mean Square Error (RMSE) of 0.0155). However, the low long-term prediction accuracy remains one of the challenges. Hua *et al.* [59] proposed a multiple-input ESN based deterioration

model. In order to perform prognostics for dynamic load conditions, the authors proposed a novel power loss rate based HI (Equation (1.14)). The experiment results showed a decreasing accuracy for a long prediction horizon. But the proposed HI and ESN model can effectively learn fuel cell performance decay trends compared with other approaches.

Hybrid approaches are designed to leverage the advantages of the previous two modeling approaches to produce a fuel cell deterioration model. Jouin *et al.* [56] proposed a hybrid prognostics method based on a semi-empirical model and joint PF method. PF method is used to include non-observable deterioration states into semi-empirical models. The model's prediction accuracy is of 90 h for a 1000 h lifetime. Zhou *et al.* [81] developed a hybrid model by using autoregressive and moving average (ARMA) and an empirical physical deterioration model of fuel cell. The physical deterioration model is used to remove the non-stationary trend in original fuel cell aging data. Then the ARMA model is used to process the stationary data. And finally the nonlinear pattern is used to train the time delay neural network (TDNN) to provide the final prediction results. It can be seen that hybrid approaches requires a sophisticated structure design to be able to combine the advantages of two types of modeling approaches.

1.4 Conclusion

This chapter reviewed the applications barriers and PHM studies for a single stack PEM fuel cells. The deployment of PEM fuel cell systems are hinder by durability, cost, and reliability challenges. Fuel cell durability test and deterioration modeling studies contribute to understand and the modeling of fuel cell various deterioration phenomena. Key fuel cell deterioration mechanisms are investigated based on the fuel cell durability tests under static and dynamic load profiles. Generally, the operation of a fuel cell system subject to four typical operation modes, i.e., the open-circuit/idling, dynamic load, start-stop, and high power load conditions. Due to the complexity of fuel cell deterioration phenomenon, semi-empirical polarization equation based models are widely used in fuel cell deterioration modeling studies.

PHM method is one of the most promising approaches in dealing with fuel cell durability and cost challenges. It contains multiple functional steps from data collection to final decision-making which contributes to enhance fuel cell lifetime. However, the literature review shows that the decision aspect of current PHM method is relatively lacking which needs to be improved which leads to the fuel cell operation problem in next chapter. Within PHM, fault diagnosis was well studied at first, then prognostics are better handled. Now the challenge is to deploy EMS methodology for fuel cells.

Chapter 2

Multi-stack Fuel Cell System and Energy Management Strategy Problem Statement

Fuel cell stacks can be used in networking systems instead of isolated situations. Among solutions, multi-stack fuel cell systems, composed of multiple stacks, are promising. Indeed, these systems can extend the functionality of a single stack and offer more redundancy, enhanced durability, and flexible modular architecture compared with a single stack fuel cell system. To operate, integrate and interconnect several devices in a generation system, a control system to manage the energy is necessary. A proper energy management strategy enables the system to supply the demand, increase the lifetime of the elements, reduce operating costs and therefore maximize system performance, providing a technically and economically feasible option. The aims of the different management strategies influence the behavior of the system. As most of the works found in the scientific literature present simulated strategies for hybrid systems, the section 2.2 introduces the different aims of EMS and reviews the EMS for hybrid fuel cell systems. Then different MFC architectures and their advantages are introduced. Section 2.3 provides a literature review about different EMSs for multi-stack systems, including basic EMS, deterioration-aware EMS, and maintenance-based EMS. Finally, the problem statement that will be studied in this work is detailed, and the main contributions of the thesis are presented.

Contents

2.1 Multi-stack fuel cell systems architecture and application advantages

It is noticed that fuel cell applications present a growing trend for high power demands. For instance, the growing market of FCEBs and fuel cell trucks. In these applications, a single fuel cell stacks based hybrid system can hardly satisfy the high power demands operation requirement. MFC integrates two or more PEM fuel cell stacks which can supply a lager power. Moreover, the multi-stack modular architecture can be utilized to extend fuel cell system durability. In this section, the basic architecture and various advantages of MFC system are introduced. The EMS studies of MFC systems will be reviewed in the next section.

A multiple fuel cell stack system is not only composed of fuel cell stacks, but also of several auxiliaries, including fluidic, electrical, and thermal systems, that have to be connected [82]. The Fluidic system is the reactant supply system that provides the hydrogen and oxygen reactants to MFC. The electrical system (DC/DC, DC/AC converters) is responsible to adapt the output voltage of all stacks to meet the operating load demand. And the thermal architecture controls fuel cell operation temperature to produce optimal performance.

The two commonly studied configurations for connecting MFC stacks are serial and parallel structures, that are shown in Figure 2.1. In series architecture, the system output voltage is the summation of individual stack voltage ($n_{stack}V_{stack}$). Because fuel cells are operating with low voltage, the series architecture can effectively increase the MFC output voltage. The two switches (M' and M) enable power allocation and stack isolation in case of failure [83]. Similarly, the parallel structure which constructs all stacks in parallel is also used in MFC. The power demand can be allocated between different stacks. And the failed (or malfunctioned) stacks can be isolated through the switches. In parallel architecture, all stacks share the same level of output voltage and the system current density is the summation of current density in each stack. Each fuel cell stack is connected to a DC-DC converter (used to adapt the FC stack output voltage) in a parallel configuration. A power converter is used to enable individual current control and adjust the power demand of each system. Cardozo *et al.* [84] studied MFC system architecture for residential power generation. They compared MFC with parallel and series architectures in terms of their influences on system aging and hydrogen consumption. The results showed that the parallel structure is more efficient in improving system durability and minimizing hydrogen consumption when the ratio of the deterioration per start-stop cycle to the deterioration per hour of use is low. By contrast, series architecture is more effective when the ratio is high. Generally, the parallel structure has higher reliability than the series configuration.

Thanks to the modular architecture, MFC offers a number of strengths compared to the single stack configuration. Firstly, MFC systems offer more redundancy than a single stack and

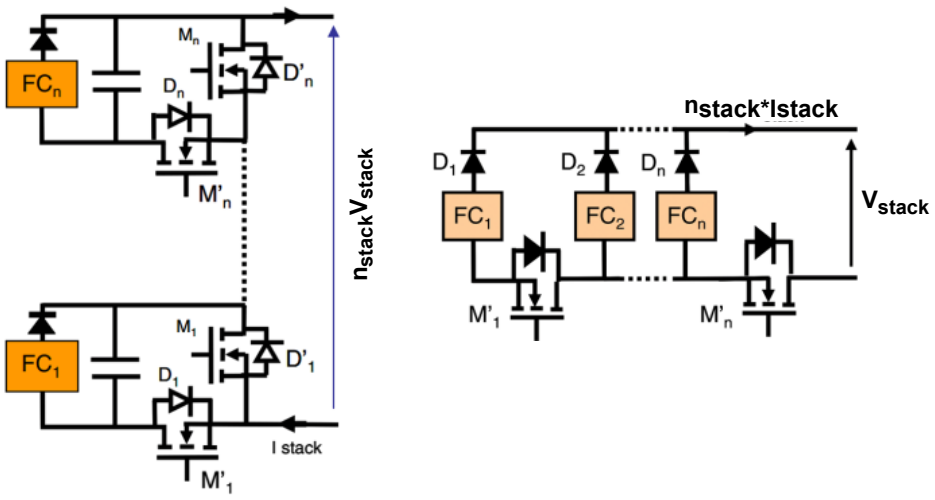

(a) **Series MFC** (b) **Parallel MFC**

Figure 2.1: MFC series and parallel structures [83].

thus the system reliability is improved. Another one is that the durability of MFC systems can be increased by optimally distributing the power demand among different stacks, thus avoiding degradation mode operation. In addition, as MFC can be manufactured in standard size and can be easily combined to meet different power demands, this could help balance the increased cost of modular architecture [85].

Marx *et al.* [86] studied the degraded mode operation of an MFC system. The results of this study showed that the MFC system keeps functioning and is able to fulfill a driving cycle when one stack is failed. Compared with single stack system configuration, the MFC system can adjust its operating mode in terms of various stack sizes which offers more redundancy and improved reliability. In fact, the multi-stack configuration can help improve fuel cell system operation efficiency, extending system lifetime as well as saving fuel costs [82]. In [87], the MFC system has been integrated into an energy microgrid and the simulation results of the Model Predictive Control (MPC) controller prove the advantage of the multi-stack fuel cell configuration. The MPC controller was built for the MFC to reduce fuel cell deterioration and operation costs. Thanks to the modular configuration of MFC, the MPC controller can optimally distribute the power demands into available stacks, achieving high operation efficiency and reducing operation cost. MFC has also been used in transportation applications scenarios to help overcome the operation cost and lifetime challenges. Becherif *et al.* [88] studied the integration of MFC on a vehicle. By applying several lower power stacks instead of one single big stack, the system lifetime is improved thanks to a flexible operation mode that allows selecting the required stacks. The parallel structure of MFC allows replacing a stack separately without stopping the entire system, thus increasing overall system reliability. Zhou *et al.* [89] highlights the application of the MFC system in high-power demands application scenarios. They highlighted that the MFC system is better than a single fuel cell system in terms of system lifetime, efficiency, and hydrogen consumption.

To sum up, the application of MFC systems is promising and studies on MFC systems are still in their early stages. The research challenges are to design the MFC system architecture and power distribution management to optimize system lifetime and efficiency. In this thesis, we will focus on developing an efficient power allocation strategy to improve system lifetime.

2.2 Energy management for hybrid fuel cell systems

Energy management is a collective term for all the systematic practices to control and minimize both the quantity and cost of energy used in providing the requested power [90]. In general, EMS refers to the system level control strategies for allocating the overall power demand towards multiple components of a system [91]. For example, for powertrain systems, the primary aim of the EMS is to distribute power by the components of the powertrain effectively by selecting the optimal operation modes [92]. Consequently, this aim hide actually several objectives, such as (i)improving fuel economy, (ii) reducing emissions, (iii) maintaining drivability and (iv) enhancing lifetime of power source devices [93]. Thus, the different strategies available in the scientific literature, listed by their objectives, are presented in this section. The discussed strategies are classified into basic, deterioration-aware, and maintenance-based EMSs according to their management objectives. Table 2.1 summarizes the discussed EMSs literature for fuel cell hybrid systems.

2.2.1 Strategies in which the objective is to improve system fuel economy or basic EMS

The primary objective of this type of strategy is to improve system fuel economy. Indeed, to minimize system fuel consumption while ensuring the power demand is necessary because the hydrogen fuel used by fuel cells is expensive to produce and store. This type of strategy is also known as the Basic EMS. The concept of fuel economy evaluation in a hybrid fuel cell/battery system has been introduced in [94]. The Energy Management Strategy consisted in optimizing the power allocation between a fuel cell and a battery. The constraint on the SOC of the battery was the initial and the final SOC have to be identical. An empirical formula is adopted to estimate the fuel consumption of a fuel cell.

Ramos-Paja *et al.* [95] built a controller for a hybrid fuel cell/capacitor power system. By controlling the air pump voltage and regulating the fuel cell current, it successfully forces the fuel cell to operate following the minimum fuel consumption operating points. Kim *et al.* [96] developed a pseudo-stochastic dynamic programming controller for improving fuel cell hybrid system efficiency. Moreover, this strategy is combined with the component size optimization to further optimize fuel cell system efficiency. Zhang *et al.* [97] proposed an Equivalent Consumption Minimization Strategy (ECMS) to minimize fuel cell hybrid system fuel consumption. As an instantaneous optimization technique, the ECMS decides the equivalent fuel consumption of energy storage system through an equivalent coefficient. Then the overall fuel cell hybrid system fuel consumption can be decided and optimized in real-time. The proposed

EMS helped to save 3.5 % hydrogen consumption.

Fuel cell electrical efficiency is generally defined as the electric output energy divided by the energy emitted from the electrochemical reaction. Thus, to improve fuel cell efficiency is beneficial for improving the fuel economy. Some works have been done to improve overall fuel cell system efficiency. König. *et al.* [98] developed a modular model aided system analysis to evaluate and improve stationary fuel cell system efficiency. Kelouwani *et al.* [99] developed an adaptive airflow control strategy for tracking fuel cell system maximum efficiency. The proposed approach can improve fuel cell efficiency up to 10%. The study on fuel cell system fuel consumption and efficiency are critical for reducing fuel cell operation cost. However, these studies usually did not take into account fuel cell deterioration when developing the EMS. Therefore, the basic EMSs fail to enhance fuel cell system durability which is a major concern of fuel cell systems.

The main advantage of these strategies is the simplicity in the defined objective. In fuel cell hybrid systems, the quantification of system fuel consumption is directly modeled as polynomial function of operating load. Thus, the objective function in these strategies is relatively easy to define. In many cases, the optimal solution of this strategy does not necessarily lead to a favorable operation condition for the studied system since the other factors like deterioration is not considered. This is this aspect that has lead to define new strategies, presented in the next part.

2.2.2 Strategies in which the objectives are including durability improvement or degradation-aware EMS

These strategies, as well as ensuring power demand at all times, take into account technical criteria in order to ensure the proper use of fuel cell systems. The pivotal goal of these strategies is to reduce the degradation of fuel cells during operation of the system. They are also known as deterioration-aware or health-aware EMSs.

Recent studies emphasized the need of developing deterioration-aware EMS due to the fact that ignoring the performance decay of a fuel cell may increase system fuel consumption. Kandidayeni *et al.* [100] showed that the ignorance of health adaption increases the hydrogen consumption by around 6.5%.

This kind of EMS receives fuel cell system deterioration information thanks to a deterioration model. Thus, Kandidayeni *et al.* [101] reviewed the health-aware EMS in FCEVs. They proposed a classification into three categories for dealing with health-aware EMS, i.e., prognostic-based, diagnostic-based, and systemic EMSs. The previous two methods were dedicated to enhance fuel cell system performance by utilizing various deterioration monitoring techniques (e.g., Particle filtering [56], Kalman filter [76]). Systemic EMSs are developed from a more holistic perspective which considers also some local controls or managements such as thermal or water management.

Developing a deterioration-aware EMS is generally treated as an optimization problem.

Zheng *et al.* [102] proposed a Pontryagin's Minimum Principle (PMP) EMS to improve the lifetime of a fuel cell stack in FCEVs. A trade-off between lifetime and fuel consumption is achieved by properly formulating the cost function and the simulation results proved the positive economic influence of the proposed approach. PMP-based strategy can instantaneously provide optimal power distribution decisions between power sources. Its application efficiency is checked by Zheng *et al.* [103], based on the driving characteristics of buses. The deterioration of fuel cell is estimated by the empirical formula proposed in [25], [104]. The two-stage EMS proposed by Geng *et al.* [105] helps to minimize hydrogen consumption and simultaneously protect fuel cell health. The first stage is to design a predictive controller for predicting the optimal global battery SOC trend and local control reference. Then the second stage constructs a tracking controller for producing feasible local control decisions with respect to fuel cell health constraints and other physical limitations. De Pascali *et al.* [106] proposed an aging-aware EMS for the hybrid vehicles based on electrochemical degradation dynamics. An improved system life and fuel economy are achieved by incorporating the electrochemical degradation dynamics into the EMS. To facilitate the development of real-time deterioration-aware EMS, Hu *et al.* [107] proposed a soft-run strategy for a fuel cell/Li-battery hybrid system. The fuel cell aging model is also based on [25], [104]. Speed prediction-based EMS for FCEVs is presented by Zhang *et al.* [108]. The fuel cell economy and power train system durability are modeled through a mathematical model and directly used to formulate the optimization objective functions. The formulated optimization problem is solved by using a Sequential Quadratic Programming (SQP) method.

The above-mentioned studies did not consider updating fuel cell performance in real-time when developing the EMS. For instance the deteriorated fuel cell may influence fuel cell system fuel consumption which need to be considered when optimizing system fuel economy. An adaptive type deterioration-aware EMS is proposed to address this issue. Song *et al.* [109] proposed an unbalanced degradation model of fuel cell at different current densities. This is built based on the observation that fuel cell polarization curve deteriorates differently under different current densities, and that the degradation rates at different current are thus different. A degradation adaptive EMS is then built to deal with fuel cell durability and fuel economy. The proposed approach can update the efficiency curve based on the degradation model which is effective in improving fuel economy. Hahn *et al.* [47] presented a comprehensive study of optimizing the efficiency and degradation rate of an automotive fuel cell system. They derived a physically-based polarization curve model for developing the EMS. They verified that aging of the stack leads to a drift of optimal operation parameters which highlights the needs of deterioration-aware EMS. Yue *et al.* [110] proposed a health-conscious EMS by developing a prognostics-enabled decision-making process. A fuzzy logic controller that receives the prognostics results of fuel cell deterioration level is used by the EMS.

Deterioration-aware EMSs have been attracting a growing research interests. However, in current EMS studies, the access to fuel cell deterioration information is still challenging for developing an efficient deterioration-aware EMS.

2.2.3 Strategies whose objectives include maintenance costs or maintenance-based EMS

Maintenance studies are closely related to system reliability. Reliability is defined as the ability of a system to perform as required in a stated operating context and for a stated period of time [111]. The fuel cell system's ability to supply a prefixed power demand (required by a specific operation task) will depend on altogether the environment conditions the fuel cell is used in, the load demand it is subjected to, and how the fuel cell is maintained. Thus, fuel cell as well as many mechanical systems need to be maintained to preserve high operational reliability during their useful life [111]. The definition of maintenance, according to the standard (IEV 192-06-01), is the combination of all technical and management actions during the life cycle of an item intended to retain the item in, or restore it to, a state in which it can perform as required [111]. To integrate the maintenance actions like fuel cell stack replacement into fuel cell system management strategies is called the Maintenance-based EMS.

Firstly, it is noticed that the current research on PEM fuel cell reliability, maintenance studies are relatively scare compared to the studies of energy management strategies for enhancing system durability. Indeed, the lack of failure dataset is a very important barrier in fuel cell reliability studies. To overcome it, researchers have proposed a stochastic process-based aging model. Tanrioven *et al.* [112] presented a methodology for modeling and calculating the reliability of stand-alone PEM Fuel Cell Power Plant (FCPP). The components aging in the studied system are modeled through a Weibull distribution. A fuzzy logic rule-based system is developed as there is no publicly available data associated with FCPP failures. The results showed that improved reliability is achieved by applying the maintenance procedure. Mangoni *et al.* [113] studied the fuel cell system reliability assessment by a stochastic model. They assumed that the output voltage decay is a gradual decreasing process in which the decreasing rate is accessed through the stochastic aging model (linked with Beta distribution). It is pointed by the authors that the proposed probabilistic approach can take into account the lack of data and the uncertainties of fuel cell design and operating conditions.

The maintenance strategy takes action to enhance the reliability of a fuel cell system. Among various types of maintenance activities, Preventive Maintenance (PM) is one of the most popular approaches in power systems. PM refers to the maintenance conducted at predetermined intervals or according to prescribed criteria to decrease the system failure probability [111]. Maintenance scheduling (preventive maintenance) is receiving a growing attention in recent years among a number of industrial applications. For instance in the energy systems, PM is applied to enhance system operation reliability. Gargari *et al.* [114] proposed a preventive maintenance scheduling strategy for a multi-energy microgrid. The validation on three operation scenarios confirms that the proposed maintenance strategy achieved 30% reliability improvement in average. In hydro-thermal system, a PM strategy is used to optimize hydropower generation [115]. To enhance the electricity supply of remote area, a maintenance strategy was integrated into an off-grid photovoltaic energy system to handle system power generation as well as the environmental constraints (such as flood period variation, consumer locations, etc.).

Table 2.1: Summary of EMSs for fuel cell hybrid systems

Strategy types	Power sources	Optimization objectives	Objective formulation	Optimization algorithms
Basic	Fuel cell/battery [96], [97]	Fuel economy	Fuel by empirical polynomial function of load	Stochastic dynamic programming [96] ECM [97]
	Fuel cell CHP system [98]	Efficiency	Physical-based	Constrained optimization
	Fuel cell/capacitor [95]	Fuel economy	Fuel by empirical polynomial function of load	Tracking minimum fuel point
Deterioration-aware	Fuel cell/battery [102] [103], [107], [108]	Lifetime fuel economy	Deterministic empirical degradation model [25] Fuel by empirical polynomial function of load	PMP [102], [103] Two-stage optimal control [105] Multi-objective optimization [107] SQP [108]
	Battery [106]	Lifetime	Deterministic physical-based degradation model	Multi-objective Constrained nonlinear optimization
	Fuel cell/battery [109]	Lifetime fuel economy	Deterministic empirical degradation model Fuel by empirical polynomial function of load	Multi-objective Constrained nonlinear optimization
	Fuel cell system [47]	Efficiency Lifetime	Semi-empirical correlations for the loss of electrical catalyst activity	Multi-objective Constrained nonlinear optimization
	Fuel cell/battery [110]	Lifetime	Degradation estimated from historical datasets	Fuzzy logic controller
Maintenance-based	Microgrid system [114]	Resiliency of system	Micro-turbine, CHP, and energy storage costs	PM strategy, sequential optimization
	Hydro-power plants [115]	Minimize thermal generation	System generation power	Multi-objective optimization

Maintenance-based EMSs require knowledge from reliability and maintenance studies which belongs to an interdisciplinary field. The objective of such approach is to combine EMS studies in fuel cell systems with reliability and maintenance investigations to produce more durable and reliable fuel cell system. Due to the intrinsic complexity of fuel cell system configuration, the maintenance-based EMS are still in an exploring stage. More efforts are expected to be done in terms of demonstrating the possibilities and advantages of applying maintenance studies in fuel cell systems.

2.3 Energy management for multi-stack fuel cell systems

MFC systems are promising for enhancing the durability and operation efficiency if properly managed by efficient EMSs. This section presents the state-of-the-art of MFC system EMS. Similarly to the EMS study of hybrid fuel cell system, we first review the basic EMS in MFC systems that is developed to improve system fuel economy. Next, the deterioration-aware type EMS is introduced for improving MFC system durability. Followed by the maintenance-based EMS studies. Finally, the possible research gaps are analyzed and identified based on above EMS state-of-the-art studies. The discussed MFC EMS literature studies are summarized in Table 2.2.

Basic EMS Similarly to the EMS studies in hybrid fuel cell systems, the basic EMS has been the most studied in MFC literature. Bortoli *et al.* [116] developed an EMS for the thermal management of the MFC system in FCEVs. Simulation results showed that the proposed EMS can effectively control a proper operating temperature via preheating/cooling process. Several works studied the optimization-based EMS for minimizing MFC fuel consumption. Wang *et al.* [117] proposed a Forgetting Factor recursive least Square (FFRLS) algorithm based EMS

to improve parallel-connected MFC system efficiency and reduce the fuel consumption. The FFRLS algorithm ensures an accurate estimation of MFC system parameters which is suitable for online power allocation. The efficiency of the proposed strategy is validated with a two 300 W PEM fuel cell stacks system. Moghadari *et al.* [118] built an Equivalent Fuel Consumption Minimization (ECM) strategy for an MFC/battery hybrid system. The results showed that the proposed ECM strategy achieved a similar consumption as the Dynamic Programming method, although it is an online optimization strategy. Several sophisticated design of EMSs have been proposed recently. Wang *et al.* [119] have developed a two-level EMS to improve fuel cell system operation efficiency. For the considered hybrid power system (fuel cell and battery), the first level of EMS is designed to manage the operation of MFC and the second level on the coordination of fuel cell and battery. The overall MFC system performance is improved through proposed strategy.

Deterioration-aware EMS To build the deterioration-aware strategy, the fuel cell deterioration information is further used in the objective function of the optimization problem. Thus, Ghaderi *et al.* [120] designed a two layers EMS for an MFC system-based FCEV. The first layer is responsible for estimating system health state, i.e., fuel cell Maximum Power (MP) and Maximum Efficiency (ME) points. Then based on this information, a second layer is developed to build the strategy that optimizes the operation. Usually such strategy refers to the load allocation between different power sources. This two-layer EMS can effectively minimize system fuel consumption and power source deterioration. Based on this two-layer EMS, Fernandez *et al.* [121] further proposed an adaptive state machine based approach for improving MFC system lifetime and fuel economy. The first layer is composed of an empirical fuel cell deterioration model and a Kalman filter which is used to estimate deterioration parameters. The empirical deterioration is modeled by the fuel cell polarization equation. The parameters of this equation are predefined aging parameters and are dependent on fuel cell operating time. Then the second layer make the decision on the allocation of the operating load for each stack. The effect of the proposed strategy is verified by comparison with the Average Load and Daisy Chain strategies.

However, in the above studies fuel cell deterioration is only modeled as a function of time and no direct links between fuel cell deterioration and their influence factors are considered. A few research works have recently emerged to address this issue. Herr *et al.* [122] proposed an empirical deterioration model by linking fuel cell remaining useful lifetime with the operating power. Then a post-prognostic decision strategy is proposed based on this model to improve fuel cell lifetime. The Mix Integer Programming (MIP) is used to solve the decision-making problem, deciding the optimal operation load for each stack. Based on a similar deterioration modeling approach, Zhou *et al.* [123] extended the load allocation strategy by adding the minimization of system fuel consumption. Moreover, a stochastic dynamic load demand profile adapted from the World Transition Vehicles Cycle (WTVC) is used as the application scenario. The optimal load allocations are obtained by solving a bi-level optimization problem with RUL and efficiency as the objective functions.

Stochasticity exists both within fuel cell intrinsic deterioration phenomena and the power

demand profile imposed on the fuel cell system. The above discussed EMSs did not include the consideration of stochasticity. Currently, only a few works have taken into account the existence of stochasticity when build a EMS. A Stochastic Dynamic Programming (SDP)-based EMS is proposed by Fletcher *et al.* [124] to deal with the uncertain deterioration of a fuel cell-based power system. Jiang *et al.* [125] build several random and realistic power profiles based on a Markov chain model. Then proposed an SDP-based EMS to decide the optimal load allocation for a fuel cell/super capacitor hybrid system. These approaches are mainly using stochastic programming methods to handle random demand profile, however, the stochasticity of fuel cell stack deterioration is not considered.

In summary, deterioration-aware EMS can help to enhance MFC system durability by considering available deterioration information. Usually this deterioration information is obtained from a deterioration model. With regard to available deterioration-aware EMSs, most of them are focused on deterministic deterioration models instead of stochastic models. The performance of deterministic deterioration models is limited in the sense that it cannot capture the randomness and variability of the considered deterioration phenomena.

Maintenance-based EMS Fuel cell systems are required to be reliable enough to operate during the expected duration. This is interpreted as the system reliability. For example, consider using fuel cell system to power a data center. Such system requires high operation reliability (99.99%) [126], thus the reliability and availability of the system must be analyzed and understood ensuring a stable operation. Thus, in addition to the requirement of high durability, reliability is also a very important topic in MFC EMS studies. This thesis refers such strategies as maintenance-based EMS.

A few recent works related to fuel cell reliability studies in the context of a network system. Cardoso *et al.* [127] studied the microgrid reliability modeling based on a stochastic linear programming technique. The deterioration of a 1 MW molten carbon fuel cell is modeled through a Markov Chain model. The obtained results confirm that the proposed stochastic scheduling method provides a conservative but cost-effective operation schedule. Colombo *et al.* [128] performed a reliability analysis of a multi-stack SOFC system with strict constant power supply requirements. The system failure probability function is built based on the experimental data and physics-based deterioration model. Reliability analysis of a multi-stack SOFC from a system engineering perspective is presented by Colombo *et al.* [129]. They systematically demonstrate the methodology of combining physical modeling and experimental data to construct system failure probability which is inspiring for fuel cell-based system reliability studies. Based on the results of reliability analysis, maintenance studies are performed to further enhance the reliability and durability of MFC systems. Phommixay *et al.* [130] applied the PM to combine with the power-sharing of different power sources to study the operation of an MFC-based microgrid system. The optimization objective of the microgrid system is composed of finding the lowest total operation cost while meeting the load requirements as well as the physical constraints of power sources. The PM is implemented to prevent system breakdown.

It is seen that a very limited works have been conducted in terms of fuel cell reliability

Table 2.2: Summary of EMSs for MFC systems

Strategy types	Power sources	Optimization objectives	Objective formulation	Optimization algorithms
Basic	MFC/battery [116], [119]	Efficiency	Thermal condition	Rule-based control [116] Two level optimization [119]
	MFC [117], [118]	Fuel economy	Empirical formula	FFRLS algorithm [117] ECMS [118]
Deterioration-aware	MFC/battery [120], [121] [123]	Lifetime fuel economy	Deterministic physical-based degradation model[120], [121] Deterministic empirical formula model [123] Fuel by empirical polynomial function of load	Quadratic programming [120] Adaptive state machine [121] constrained optimization [123]
	MFC [122]	Lifetime	Deterministic empirical formula model	Post-prognostic MIP
Maintenance-based	Microgrid (MCFC) system [127]	System reliability	Stochastic degradation model	Stochastic programming
	Multi-stack SOFC [128], [129]	Reliability	Degradation estimated by experimental data	Reliability analysis
	MFC [130]	fuel economy	Maintenance cost	PM

and maintenance (almost no related works on multi-stack PEM fuel cells). Moreover, the combination of maintenance and EMS studies, i.e., maintenance-based EMS is a brand-new field for fuel cell EMS studies. It enables to combine the reliability studies and fuel cell EMS, thus helping enhance fuel cell system reliability and durability.

2.4 Problem statement for joint deterioration and energy management strategy

The state-of-the-art presented first the EMS for hybrid systems. However, these strategies have to be adapted to the specificity of multi-stack systems. So far, the majority of load profiles used to develop energy management strategies are based on deterministic load profiles, and no stochastic dynamic load profiles has been developed. It is on this new basis that the EMS approaches have been developed.

2.4.1 Multi-stack PEM fuel cell system

In this section, the multi-stack system that has been taken for this study is defined. The studied multi-stack PEM fuel cell system consists of n identical parallel-connected stacks. For the operation of this system, a query demand required by the user is denoted as system load demand L_d. In order to allocate optimally each load, the system load demand is known at each time. In addition, the state of deterioration of each stack has also to be known. To achieve this, a representative HI has to be chosen. This health index has to be representative of the stack deterioration, must be measurable, and it must be possible to deduce the stack voltage. Based on literature, the chosen indicator is the fuel cell overall resistance (R) and the fuel cell polarization equation (Equation (1.9)) is used to calculate the corresponding stack voltage.

The following assumptions are made on the MFC system:

- The fuel cell stacks are physically connected in parallel, but are in series from the reliability point of view;
- The fuel cell stacks in the network system are identical, and the output power density of each stack ranges from the minimal output power density L_{min} to the maximum output power density L_{max};
- The values of the fuel cell overall resistances are considered to be measurable whenever necessary, in the sense that a monitoring system and algorithm (e.g. a Kalman filter [76], [131]) are assumed to be available to deliver the estimated values of the resistances.

2.4.2 Challenges to be addressed for multi-stack PEM fuel cells

Several challenges are addressed in this thesis to build the management strategies for MFC systems, beginning with a classical simple problem, and progressively making it more complex to get closer to reality.

Especially, the studies on multi-stack systems have shown some gaps in the field of deterioration modeling, such as, (i) the deterioration model must be load-dependent so that the cause of the deterioration is related to the load demand and (ii) the individual deterioration variability of the stacks make the use of a stochastic approach relevant. Then, such a degradation model has to be developed.

The first problem to be addressed investigates to improve overall system lifetime and reduce system fuel consumption. This problem, depicted in Figure 2.2, is limited to the case for which the load demand L_d is constant, and the individual fuel cell degradation rates D_{fci} (for stack $i = 1, ..., n$) are a function of the load demand. The EMS algorithm has to provide optimized the individual fuel cell powers (L_{fci}). The problem is thus focused on the management of individual stack power production under a constant load demand.

As the purpose is to develop an EMS for vehicle applications, the previous energy management problem is extended to the energy management of MFC systems under dynamic load profiles. Figure 2.3 summarizes the overall problem diagram of the EMS studies under dynamic load profiles. The first problem is to study fuel cell deterioration modeling under dynamic load scenario. Compared to the static type demand, the dynamic loads involve more complicated operation modes like load varying. Moreover, the randomness of the dynamic loads may exist and further influences the management of the studied system. Herein, how to develop an effective management strategy for extending the lifetime of MFC system under dynamic load profiles is considered. To the author's knowledge, the energy management for MFC system with stochastic deteriorating subjected to a dynamic (also stochastic) load profile is brand new.

The last chapter proposes a more exploratory study opening research perspectives in the case where the multi-stack system is composed of three stacks, only two of which are operating at the same time. To optimize the lifetime of the stacks, while ensuring the load demand, the EMS must also optimize the start and stop of the different stacks (see Figure 2.4). This

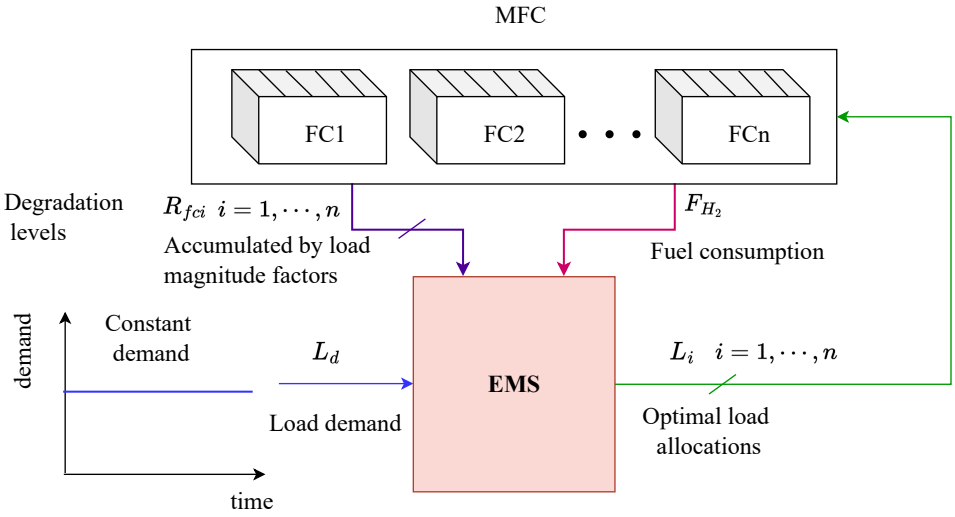

Figure 2.2: Diagram of load allocation-based EMS problem under constant load profile.

start-stop operation mode must be included in the deterioration function.

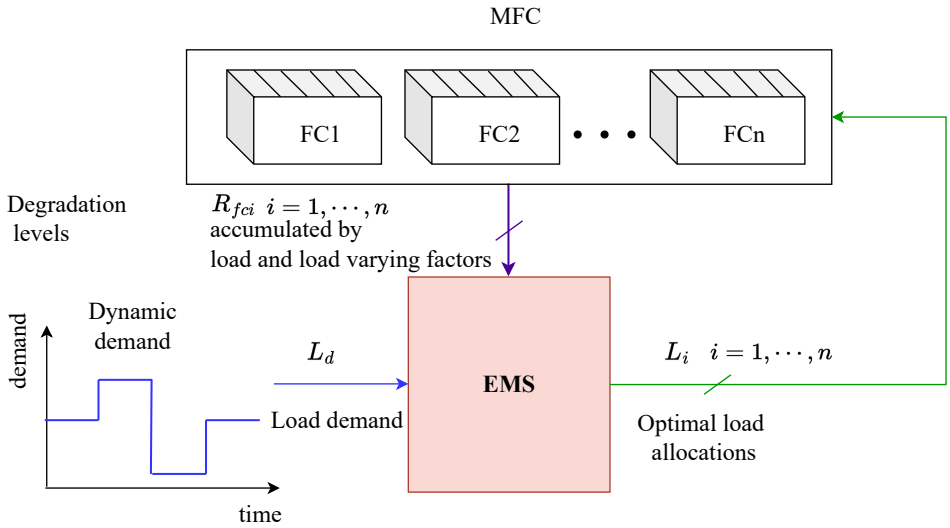

Figure 2.3: Diagram of load allocation-based EMS problem under dynamic load profile.

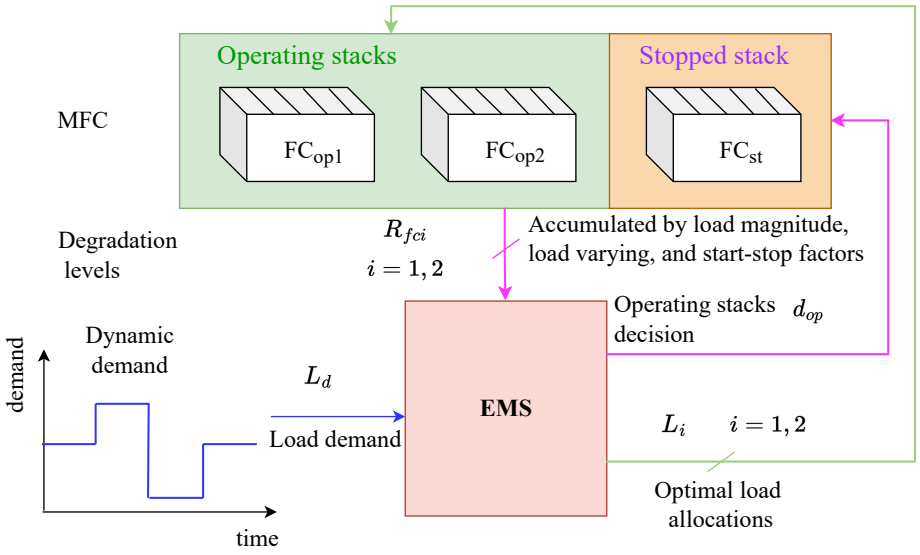

Figure 2.4: Diagram of three-stack fuel cell system operation problem.

2.5 Contributions of the thesis

The main work of this thesis focuses on developing deterioration-aware EMSs for MFC systems under different application scenarios. According to the literature review, the application of MFC systems has been recognized as a practical solution for the growing power demand in fuel cell applications. Multi-stack fuel cell system outperforms single-stack fuel cell systems in terms of reliability, durability, and operation cost. However, an appropriate EMS is needed to optimally distribute the load demand by different stacks such that the system's durability and efficiency can be improved. This leads to the three challenges listed in the above section 2.4.2. Each challenge is formulated as an operation management problem under different load cycles.

This thesis contributes to the energy management studies of MFC systems in terms of MFC deterioration modeling, EMS development under random dynamic load profiles, and the exploration of combining maintenance scheduling and energy management strategy to produce a synthetic management strategy for MFC systems. The fuel cell deterioration modeling problem remains an open challenge in current fuel cell research. This problem becomes more challenging for an MFC system. A stochastic deterioration modeling for energy management in an MFC system is studied in Chapter 3 for tackling the fuel cell deterioration modeling challenge. The following challenge is to build a deterioration-aware EMS that is on the basis of the proposed deterioration model for enhancing system durability. The current literature showed that the study of fuel cell management under random dynamic load demands is relatively lacking. Thus, we then studied two EMS development problems under constant and dynamic load profiles, respectively. The influence of the random dynamic load on EMS development is explored in the formulated problem. And lastly, we presented a three-stack operation problem which includes the optimization of the start and stop of the different stacks. For the application of long-term operation tasks, the stacks in the MFC system may need to be replaced, in this way, the maintenance approaches can be considered to enhance system reliability and minimize stack replacement costs.

The main contributions of this thesis are the following:

1. Building an empirical deterioration rate formula-based stochastic deterioration model to simulate the deterioration of an MFC system. This model includes the load-dependent and stochasticity deterioration features of an MFC system which can be used to simulate fuel cell deterioration under different operation modes, namely, load magnitude, load varying, and start-stops (Chapter 3). Moreover, the proposed deterioration model is used in the energy management strategy to support load allocation decisions.
2. Developing an original post-prognostics load allocation strategy for the stochastically deteriorating MFC under static demands. The objectives of minimizing system deterioration and fuel consumption are formulated as a multi-objective problem. Importance weights are assigned to account for the trade-off between the considered objectives (Chapter 4).
3. Based on the strategy developed under static loads, the MFC system management problem are further extended to a dynamic load demand. An event-based deterioration

aware strategy is proposed while taking into account the load varying deterioration mode and individual stack deterioration heterogeneity. The proposed strategy achieves an improved system life comparing with the classic average load method (Chapter 5).

4. A more general operation modes is considered by allowing the start-stop action among stacks under a stochastic dynamic load profile. For the proposed three-stack system operation problem, a two-layer management strategy is proposed to enhance system life by adding an extra optimization for managing fuel cell stack start-stop caused deterioration. Inspired by the studied three-stack operation problem, a maintenance scheduling problem is formulated for enhancing the MFC system lifetime and minimizing system maintenance costs in a more general operation scenario (Chapter 6).

These contributions are presented in detail in the following chapters.

List of publications and meetings

During the thesis, several papers have been published to present these contributions:

Publications

- Zuo, J., Cadet, C., Li, Z., Bérenguer, C., & Outbib, R. (2022). Fuel cell stochastic deterioration modeling for energy management in a multi-stack system. To be appeared in 2022 13th International Conference on Reliability, Maintainability, and Safety (ICRMS). IEEE, 2022.
- Zuo, J., Cadet, C., Li, Z., Bérenguer, C., & Outbib, R. (2022). A load allocation strategy for stochastically deteriorating multi-stack PEM fuel cells. To be appeared in Proceedings of the 32th European Safety and Reliability Conference (ESREL).
- Zuo, J., Cadet, C., Li, Z., Bérenguer, C., & Outbib, R. (2022). Post-prognostics decision-making strategy for load allocation on a stochastically deteriorating multi-stack fuel cell system. Proceedings of the Institution of Mechanical Engineers, Part O: Journal of Risk and Reliability, 1748006X221086381.
- Zuo, J., Cadet, C., Li, Z., Bérenguer, C., & Outbib, R. (2021, May). Post-Prognostics Decision Making Strategy to Manage the Economic Lifetime of a Two-Stack PEMFC System. In 2021 Annual Reliability and Maintainability Symposium (RAMS) (pp. 1-7). IEEE.
- Zuo, J., Cadet, C., Li, Z., Bérenguer, C., & Outbib, R. (2020, July). Post-prognostics decision making for a two-stacks fuel cell system based on a load-dependent deterioration model. In PHME 2020-European Conference of the Prognostics and Health management (PHM) Society (Vol. 5, No. 1, p. 9).

During the thesis, the following talks are given in the French group meetings:

French group meetings

- Fuel cell stochastic deterioration modeling for energy management in a multi-stack system 2ème REUNION PLENIERES de la Fédération HYDROGENE (FRH2) du CNRS (2022), Aussois, France
- Fuel cell stochastic deterioration modeling for energy management in a multi-stack system European Network for Business and Industrial Statistics (ENBIS 2022), Grenoble, France
- Post-prognostics decision-making strategy for a multi-stack fuel cell system 1ème REUNION PLENIERES de la Fédération HYDROGENE (FRH2) du CNRS (2022), Online
- Post-prognostics decision strategy of a proton exchange membrane fuel cell system, Automatic Control National Day(2020), Online.

Chapter 3

Fuel Cell Stochastic Deterioration Modeling for Energy Management in a Multi-stack System

Fuel cell deterioration modeling aims to develop a proper deterioration model which enables to reproduce fuel cell degradation processes. Besides the commonly studied operating parameters like temperature and air pressure, fuel cell deterioration behavior is also characterized by two main features: (i) it is load-dependent, (ii) it is stochastic and exhibits a stack-to-stack variability. The modeling problem in this chapter is investigated keeping these two points in mind. The load-dependent characteristics link the fuel cell deterioration to its operation load modes, which is closely related to the EMS problem dealing with load allocation among multiple sources. The stochastic and stack-to-stack deterioration variability are closely linked to fuel cell system reliability which is critical for potential applications, and necessitates special consideration in the design of EMS.

After defining the deterioration modeling problem, we then present the proposed modeling methods. First, the overall resistance is chosen as the degradation indicator, as it carries the key deterioration information of a fuel cell stack. Then, a stochastic non-homogeneous Gamma process (GP) is used to model the deterioration of the fuel cell, i.e., the increase in the fuel cell resistance. The shape parameter of the considered GP is further modeled by an empirical function of the fuel cell operation load in order to make the resistance deterioration load-dependent. Finally, to model the individual deterioration heterogeneity, a random effect is added to the GP on its scale parameter, taken as a random variable following a probability distribution (a Gamma law is chosen in this work). Resistance degradation paths can then be simulated based on the proposed deterioration model, based on which the first hitting time distribution of a failure threshold (or equivalently a remaining useful life distribution) can be estimated and the reliability of the system can be analyzed. The results of this chapter are presented in the 13^{th} International Conference on Reliability, Maintainability, and Safety (ICRMS), 21-24 August 2022, Hong-Kong, China (Best Conference Paper Award).

Contents

3.1 Fuel cell deterioration modeling problem formulation

According to the discussion in Chapter 1, Section 1.3.2, fuel cell overall resistance R is chosen as the HI which is to be modeled through a deterioration model. This section presents the fuel cell deterioration model problem under an automotive load profile. Load dependency and stochasticity are considered as the key deterioration features of fuel cells. The problem is then presented as building a deterioration model by taking into account the two deterioration features which will be further applied to build the management strategy for an MFC system.

3.1.1 Fuel cell deterioration behavior characteristics

Identifying the core deterioration features to be covered in deterioration model is a prerequisite of fuel cell deterioration modeling. The deterioration of a PEM fuel cell strongly depends on operating conditions. Principal among these are load, temperature, and humidity. Fuel cell operation load is considered as the primary operating parameters which influences fuel cell degradation. In fuel cells, the operation load depends on specific applications, usually called the demand profile. For instance, the performance of a fuel cell may decrease much fast under dynamic demand profile than the constant profile. As a matter of fact, various sources of randomness exist in fuel cell operating process. For example, the operating environment changes (e.g., temperature, pressure variations) of a fuel cell system will cause varying deterioration behavior.

According to the above discussions, we conclude that fuel cell deterioration presents two fundamental features:

- It is load-dependent. The deterioration is affected by the operation load applied to the stack.
- It is stochastic and exhibits a stack-to-stack variability.

Fuel cell deterioration is directly influenced by the load condition in operation. Different operation loads may create different internal conditions as well as different deterioration mechanisms for fuel cells. Various load profiles are used as the demand for a fuel cell system (Chapter 1 Section 1.2). For instance, in FCEV application, the open-circuit/idling, load varying, start-stop, and high power load are four typical operation modes. Each operation mode will cause a typical deterioration on fuel cell main components. For example, the start-stop is extremely harmful to fuel cell membrane and catalyst. Besides, the damage severity varies in different operation modes and load levels. Pei *et al.* [25] concludes that the load varying cycling and the start-stop are the main deterioration factors for automobile applications. Experimental result shows that the start-stop cycles account for 33.3% of overall fuel cell deterioration, and load varying cycling account for 55.6% of the overall deterioration. Thus, we conclude that the degradation is not only driven by natural aging, but also the way the fuel cell is operated contributes to make the deterioration rate vary, i.e., fuel cell deterioration presents load-dependent characteristic.

Another specificity of fuel cells is their individual deterioration variability, which can be due to stochasticity in the intrinsic fuel cell deterioration phenomena. Generally, the deterioration heterogeneity of MFC mainly comes from two sources: i) the manufacturing procedure; ii) the design of fuel cell systems. The stochastic differences between different cells/elements forming the stack can exit during the manufacturing procedure. For example, the hydrophobicity of bipolar plate surface, membrane electrical properties, and mechanical properties of seals. It is very unlikely to make them perfectly identical for different stacks. Fuel cell stack is much more complicated than the single fuel cell due to the stacked structure. When the reactants pass through the single inlet to the inside cells, it is hard to make them evenly distributed. Same problems exist for cooling and heating of a stack. These phenomena will affect fuel cell performance which caused deterioration variability. MFC system is composed of several stacks, thus, the deterioration heterogeneity still exists.

Chatillon *et al.* [132] experimentally studied the deterioration variability of a fuel cell stack. For a stack composed of three single cells, it is found that the back cell, i.e. located far from the inlet and outlet, tend to deteriorate faster than the other cells. Besides, the experiment verified the pre-aged cell will deteriorate faster compared to the other normal cells. Figure 1.13 (Chapter 1) shows a long-term fuel cell stack durability test data (output voltage) [27]. It is observed that the voltage decreasing trend presents variations rather than a smooth decreasing line. Another example is the different efficiency curves shift trend measured for an MFC (Figure 3.1). The four efficiency curves which corresponding to different stacks are shifting to different level under same operating task. Those observations prove that the individual deterioration heterogeneity exists and need to be considered when building a fuel cell deterioration model. Macias *et al.* [133] studied the stack-to-stack deterioration variability. MFC system presents a variable performance due to deterioration characteristic, material, and external factors. They showed that by controlling all stacks degrading at nearly same level helped to improve system fuel economy.

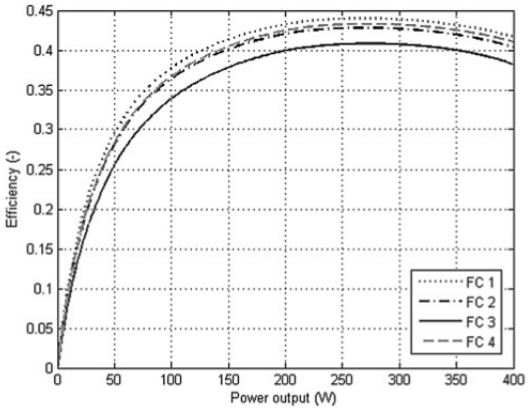

Figure 3.1: Efficiency curves of an MFC system (four stacks) [86].

3.1.2 Dynamic power load profile

FCEVs are currently one principal application for fuel cells. The driving cycle of a FCEV is composed of various operation modes and is considered to be a challenging factor for current fuel cells' durability improvement. Thus, an automotive fuel cell operating load profile is used to study fuel cell deterioration behavior.

Figure 3.2 depicts the FC-DLC used for the studied stack. The overall system operation is to repeat this FC-DLC cycle as shown in the figure (cycle 2 is a repetition of cycle 1). The original FC-DLC cycle is taken from [38] as discussed in Chapter 1 section 1.2.2. It is seen that the FC-DLC driving cycle contains load maintaining, load varying, and start-stop operation modes. The specific power loads are adapted based on the studied fuel cell stack parameters as listed in Table 3.1.

Table 3.1: Initial electrical performances for the studied fuel cell stack.

Operating load level	Min	Nom	Max
Current density ($A\ cm^{-2}$)	0.04	0.7	2
Voltage for one cell (V)	0.875	0.6803	0.418
Stack power density (W cm^{-2})	0.175	2.381	4.181

3.1.3 First hitting time of a fuel cell

A fuel cell is said to fail when its deterioration level $R(t)$ exceeds a fixed threshold, which is called the failure threshold FT. In fuel cells, this threshold is usually given (defined) based on conventional fuel cell lifetime definition. For example, if we define the EoL of a fuel cell as their voltage decrease to 10% of the initial performance. Then an equivalent threshold in resistance can be defined based on fuel cell polarization equation. The failure time corresponds to the first hitting-time of level FT by $R(t)$. Then the fuel cell lifetime denoted T_R, is defined as the time duration from the time the stack is put into use ($t = 0$) to the time of stack failure, and

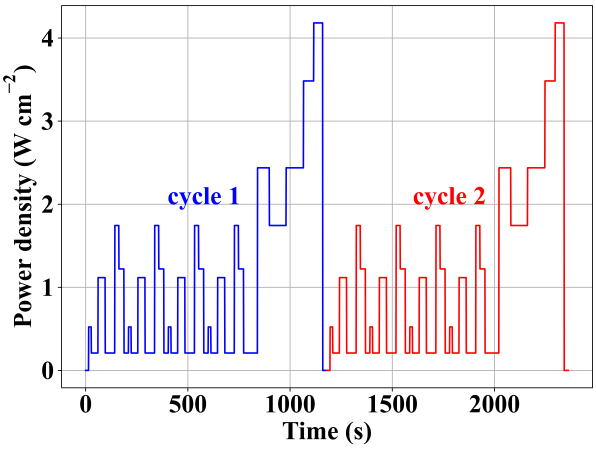

Figure 3.2: FC-DLC load profile for studied fuel cell stack.

is written:

$$T_R = \min_t(R(t) > FT) \tag{3.1}$$

In summary, a dynamic load profile $L_d(t), t \in [t_0, t_f]$ which includes the typical operation modes like load maintaining, load varying, are proposed for the studied fuel cell system. Under such dynamic load profile, the problem deterioration modeling needs to represent different deteriorations of various operation modes. Then, the overall system deterioration is calculated as the summation of all mode-dependent deteriorations. Another part of the modeling problem is how to interpret the two deterioration features into a deterioration model such that it can well reproduce fuel cell system deterioration. Finally, the first hitting time is defined for determining fuel cell lifetime. The following section will present the proposed MFC deterioration model based on the formulated problem.

3.2 Fuel cell deterioration model

3.2.1 Fuel cell stochastic deterioration modeling tool

In the thesis work, stochastic processes are used to build stochastic deterioration models for fuel cell. More precisely, Gamma process is considered as a relevant tool for modeling fuel cell resistance deterioration for the following reasons:

- It is suitable to model monotonic continuous increasing deterioration that accumulates over time through many tiny increments. Fuel cell resistance deterioration follows a similar trend. It is gradually increasing during fuel cell operation.
- Gamma distributed increments of different time duration still obeys a Gamma law which makes Gamma process suitable for modeling various deterioration processes. (deduced from Gamma preservation property).

Thus, the Gamma process is used to build the stochastic deterioration model of a fuel cell.

3.2.1.1 Gamma process definition

A Gamma process (GP) is a stochastic process with independent, positive increments that obey a Gamma distribution $Ga(\alpha, \beta)$ characterized by two key parameters: its shape parameter α and scale parameter β. Gamma processes are suitable for continuous and monotonous deterioration modeling [134]. By definition, the increment of a Gamma process $X(t)$ between time t_1 and t_2 ($t_2 > t_1 \geqslant 0$) is given by (see Figure 3.3):

$$\Delta X(t_1, t_2) \sim Ga((\alpha(t_2) - \alpha(t_1)), \beta) \tag{3.2}$$

where $\Delta X(t_1, t_2) \triangleq X(t_2) - X(t_1)$. For a stationary Gamma process with constant scale parameter β, i.e., $\alpha(t_2) - \alpha(t_1) = \alpha(t_2 - t_1)$, $Ga(\alpha(t_2 - t_1), \beta)$ represents the probability density function of the Gamma law with shape function $\alpha(t)$ and scale parameter β:

$$f_{Ga}(x, \alpha(t_2 - t_1), \beta) = \frac{x^{\alpha(t_2-t_1)-1} e^{-x/\beta}}{\beta^{\alpha(t_2-t_1)} \Gamma(\alpha(t_2 - t_1))} \tag{3.3}$$

where $\Gamma(\alpha) = \int_0^{+\infty} x^{\alpha-1} e^{-x} dx$ is the Gamma function. Let $X_1, \cdots, X_n$ be independent Gamma distributed with respect to parameters $(\alpha_1, \beta), \cdots, (\alpha_n, \beta)$ respectively (assuming same scale parameter). Then,

$$\sum_{i=1}^{n} X_i \sim Ga(\sum_{i=1}^{n} \alpha_i, \beta) \tag{3.4}$$

Considering $t_3 > t_2 > t_1 \geqslant 0$, according to Gamma preservation property (Equation (3.4)) we can deduce that

$$X_{t_3} - X_{t_1} = (X_{t_3} - X_{t_2}) + (X_{t_2} - X_{t_1})$$

is Gamma distributed with shape parameter

$$(\alpha(t_3) - \alpha(t_2)) + (\alpha(t_2) - \alpha(t_1)) = \alpha(t_3) - \alpha(t_1)$$

Thus the definition of Gamma process is coherent with the Gamma preservation property.

The mean and variance of the deterioration increment in the time interval (t_1, t_2) are given by:

$$\text{Mean}(\Delta X(t_1, t_2)) = \alpha(t_2 - t_1) \cdot \beta \tag{3.5}$$

$$\text{Var}(\Delta X(t_1, t21)) = \alpha(t_2 - t_1) \cdot \beta^2 \tag{3.6}$$

Then, the mean deterioration increment in a time interval of length Δt is calculated as $\alpha(\Delta t)\beta$, which is independent of when the interval begins. The variance of the process increases with the time horizon between t_1 and t_2. Besides, the variance of the process can be tuned independently of the mean.

The Gamma process is suitable to model gradual degradation monotonically accumulating over time in a sequence of small increments [134]. For instance, Cholette *et al.* [135] applied

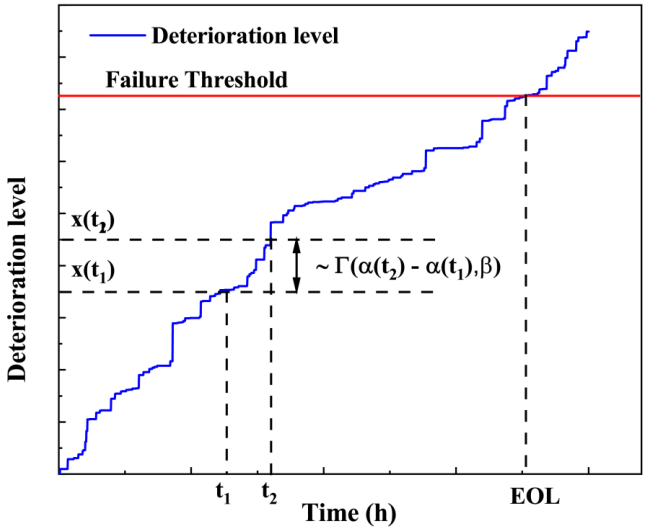

Figure 3.3: Deterioration path of a Gamma process.

the Gamma process to build a degradation model for modeling boiler heater exchange erosion. [136] applied stochastic process to estimate the lifetime of photovoltaic modules. The analysis results proved that the Gamma process model presented a relatively good estimation of lifetime. A two-phase Gamma process with fixed change-point is used to model lithium battery voltage decay. This deterioration model can be further used to estimate battery lifetime, state of charge, etc. which contributes to energy management of lithium batteries [137]. Gamma process is a well-formulated stochastic process that makes it convenient for mathematical analysis. Following section 3.2.1.2 will present the details of deterioration trajectories simulation. Failure analysis, in terms of first-hitting time distribution, will be conducted based on the simulated trajectories.

3.2.1.2 Lifetime calculation

In this section, we explore the deterioration behaviors of a homogeneous Gamma process where the coefficient of the shape function is denoted as v, namely

$$\alpha(t) = vt \tag{3.7}$$

for all $t \geq 0$ with $v > 0$.

Using Gamma processes, various deterioration behaviors can be simulated by resorting to different v and β values. Assuming that $X(t)$ represents the deterioration level of a component at time t satisfying $X(0) = 0$ and $X(t_2) \geq X(t_1)$ with $t_2 > t_1$. The component is said to fail when $X(t)$ exceeds a fixed threshold, which is called failure threshold FT. The failure time corresponds to the first-hitting time of level FT by the stochastic process $X(t)$, and it defines the lifetime of the component (denoted as T_x). The mean Lifetime $\overline{T}_x$ can be calculated by:

$$\overline{T}_x = \frac{FT}{v \cdot \beta} \tag{3.8}$$

In practice, with a known Gamma process model, $\overline{T}_x$ can be estimated based on a set of simulated lifetimes $\{T_{i,x}|i = 1, 2, \ldots, N_t\}$. $T_{i,x}$ is the lifetime acquired in the ith simulation. N_t is the number of simulated lifetimes (based on Monte Carlo simulation). According to the law of large numbers, the mean of the values in set $\{T_{i,x}\}$ will approach $\overline{T}_{i,x}$ when N_t is bigger enough.

The lifetime distribution of $X(t)$ (cumulative distribution function) can then be written as [134]:

$$\begin{aligned} F(t) = P\left(T_x \leq t\right) &= P\left(X(t) > FT\right) \\ &= \frac{Ga\left(v \cdot t, \left(FT - X^0\right) \cdot \beta\right)}{\Gamma(v \cdot t)} \end{aligned} \tag{3.9}$$

where P denotes the cumulative probability. The survivor function $S(t)$ of $X(t)$ is defined by

$$\begin{aligned} S(t) = 1 - F(t) = P\left(T_x > t\right) \\ = 1 - \frac{Ga\left(v \cdot t, \left(FT - X^0\right) \cdot \beta\right)}{\Gamma(v \cdot t)} \end{aligned} \tag{3.10}$$

The survival function is the probability that the component does not fail in time interval $(0, t)$. It is also called reliability function to characterize component/system reliability [111].

3.2.1.3 Numerical experiments

To illustrate the characteristics of a Gamma process, simulations with different parameters are conducted here. The main parameters used to simulate $X(t)$ deterioration trajectories are listed in Table 3.2. The variance of $X(t)$ are mainly decided by scale parameter according to Equation (3.6). The variance of $X(t)$ is modified by introducing a coefficient ℓ which writes:

$$v' = v/\ell, \beta' = \beta \cdot \ell \tag{3.11}$$

where v', β' are perturbed parameters which are used as the shape and scale parameters used in the simulations.

Table 3.2: Main parameters used in simulating $X(t)$.

Parameters	$X(0)$	FT	v	β	N_t
Values	0.0	100	0.02	5	2000

Figure 3.4 presents three examples of $X(t)$ deterioration trajectories with different tuned variance: 1) Figure 3.4(a) low variance; 2) Figure 3.4(b) medium variance; 3) Figure 3.4(c) high variance. We computed the mean increments of all simulated trajectories (shown as blue dotted lines) to compare with the average increments calculated by Equation (3.5) (shown as red dots). It is seen that the two results are very close. Since we keep mean increment $v'\beta'$ as a constant though Equation (3.11), the estimated $\overline{T}_x$ (average lifetime) is nearly the same for the three cases, but the lifetime distribution is different.

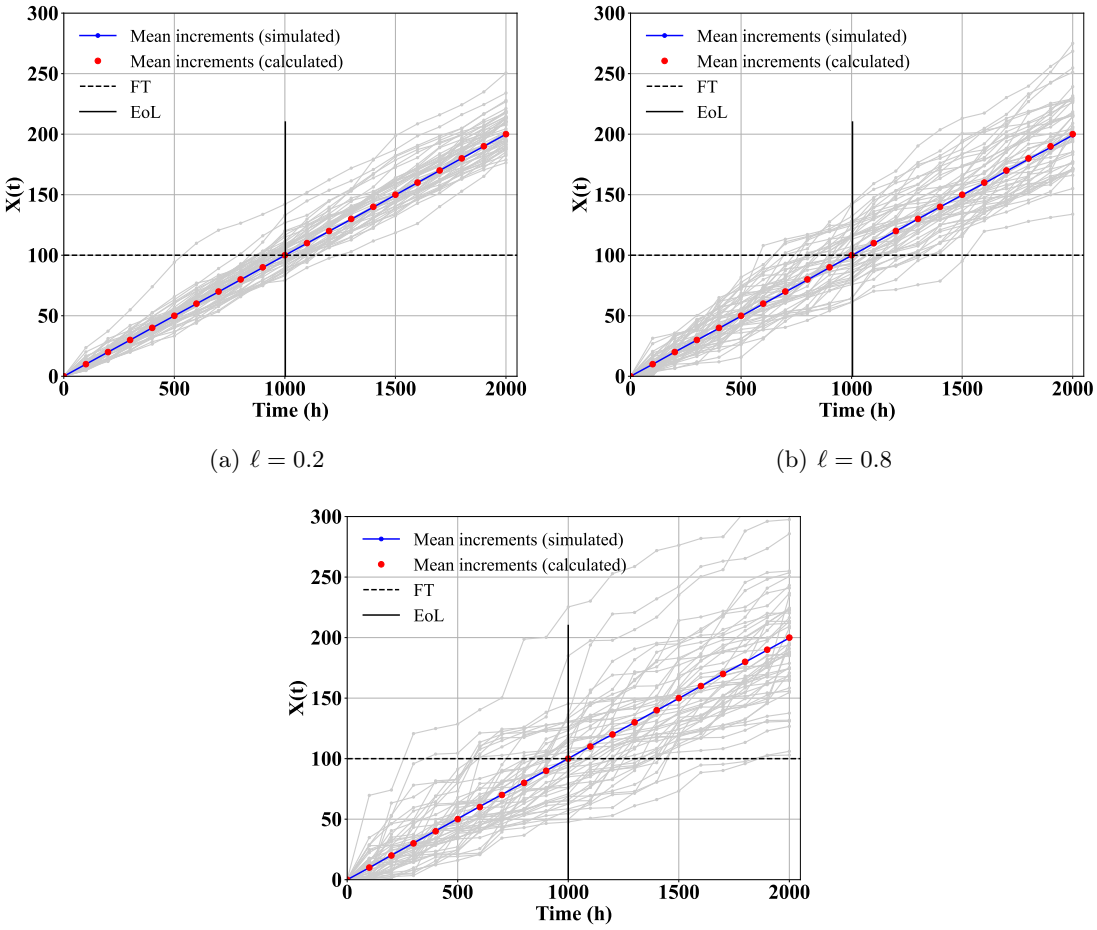

(a) $\ell = 0.2$

(b) $\ell = 0.8$

(c) $\ell = 2$

Figure 3.4: Deterioration trajectories of $X(t)$ simulated with three levels of variance.

The lifetime distribution of parameter $\ell = 0.8$ is investigated using the Monte Carlo simulation and compared with the analytical approach as shown in Equation (3.9). The results are presented in Figure 3.5(b). Figure 3.4(a) shows the empirical cumulative distribution function based on the simulation results. Figure 3.4(b) shows the lifetime cumulative probability distributions and survival function. It is confirmed that when the number of simulated trajectories (i.e., N) is big enough, the results of Monte Carlo simulation are very close to the analytical calculations.

Now that we have built the Gamma process-based deterioration modeling tools and investigated the basic deterioration behavior of a basic GP model. The next step is to build the deterioration model based on GP.

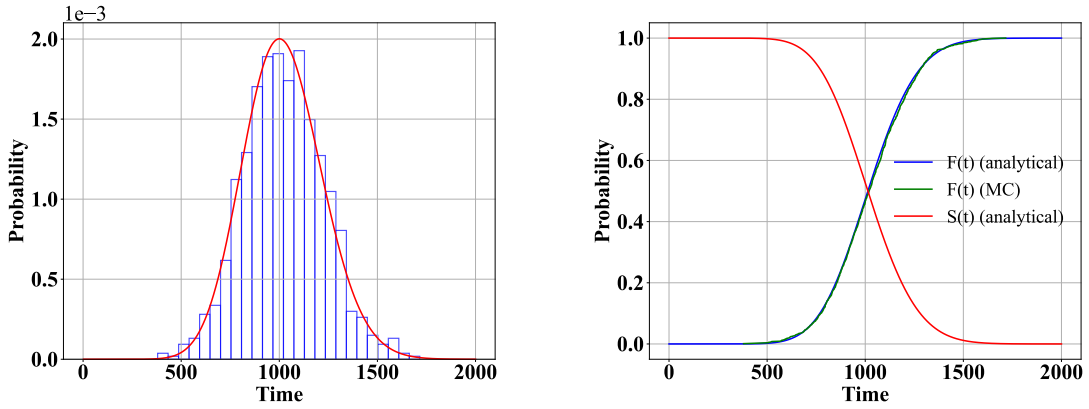

(a) Lifetime histogram (MC)

(b) Lifetime distribution and Survival function

Figure 3.5: Lifetime distribution function and Survival function ($\ell = 0.8$).

3.2.2 Fuel cell stochastic load-dependent deterioration model

As presented in Chapter 1, it is difficult to model fuel cell deterioration with a "white-box" approach. Therefore, this work focused on the empirical deterioration modeling approach.

Pei *et al.* [25] proposed an empirical fuel cell lifetime formula based on the analysis of automotive fuel cell operation dataset, which writes:

$$T_f = \frac{\Delta L}{k_p(r_1^{'} n_1 + r_2^{'} n_2 + r_3^{'} t_1 + r_4^{'} t_2)} \tag{3.12}$$

where k_P is a constant coefficient. ΔL is fuel cell output power decay. $r_1^{'}, r_2^{'}, r_3^{'}$, and $r_4^{'}$ are the performance decay rates of load varying, start-stop, idle condition and high power load condition, respectively. The n_1, n_2, t_1 and t_2 are load varying change cycle times, start-stop cycle times, idle time, and high power load time per hour.

In this work, the load amplitude, load varying, and start-stop are considered to build the load-dependent deterioration model. The fuel cell resistance deterioration model of this work is expressed as:

$$\Delta R = \Delta R_L + \Delta R_{\Delta L} + \Delta R_{ss} \tag{3.13}$$

where ΔR is the overall resistance increment with respect to the initial value as the fuel cell is put into use. ΔR_L is the contribution dependent on the load level, $\Delta R_{\Delta L}$ is the load variation contribution to the resistance increment, and ΔR_{ss} is the resistance increment resulting from the start-stop effect. $\Delta R_{\Delta L}$ and ΔR_{ss} are issued from literature [25]. The expression of ΔR_L is detailed below.

The deterioration due to the load amplitude is modeled as a Gamma process, which means that the increment of the deterioration level due to the load level between time t_1 and t_2

$(t_2 \geq t_1)$can be modeled as:

$$\Delta R_L(t_1, t_2) = R_L(t_2) - R_L(t_1) \sim Ga(v \cdot (t_2 - t_1), \beta) \tag{3.14}$$

To link fuel cell deterioration with operating conditions, an empirical function is proposed. To build this function, the nominal power load is considered to lead to the best-operating conditions that deteriorate the least the fuel cells. On the contrary, operating conditions due to lower or higher power load cause higher deterioration rates. Experimental works in [138], [139] showed that a high power load will cause irreversible degradation in many parts of the stack, as for example, the electrolyte or the carbon support in the catalyst layer. Similarly, [25], [104] proved that a higher deterioration rate is occurring during fuel cell operation at high power load demand. On the other hand, fuel cell damages are even worse when the fuel cell operates at low power [140]. To handle these properties, a parabola deterioration function which represents the different deterioration rates of the fuel cell with respect to power load demand is built (Figure 3.6). As can be seen in this figure, the three typical operating conditions are directly depicted. The minimal power, for which the deterioration rate is the highest, the nominal power, which presents the lowest deterioration rate, and the maximal power for which the deterioration rate is high but less than the minimal power. The deterioration rate function, denoted as $D(L)$, is thus expressed as a function of the operating power density L, which writes:

$$\begin{aligned} D(L) &= \alpha(L)\beta \\ &= A(L - L_{nom})^2 + B \end{aligned} \tag{3.15}$$

where constant A is expressed by two parts with respect to the load range, i.e., $A = A_1$, $L_{min} \leq L < L_{nom}$, and $A = A_2$, $L_{nom} \leq L < L_{max}$. B is also a constant term to be fitted from experimental data. Note that for a standard GP model, the scale parameter β is set as a constant. L_{min}, L_{nom}, and L_{max} are the operating load of minimal, nominal, and maximal load conditions, respectively. Note that here the shape function is defined as a function of fuel cell operation load, i.e. $\alpha(L)$.

Based on Equation (3.12), the resistance deterioration due to load variation (ΔL) is computed by:

$$\Delta R_{\Delta L} = K \Delta L \tag{3.16}$$

where the constant $K = \frac{K_{\Delta R} D_{R,\Delta R}}{L_{max} - L_{min}}$ (Ωcm^2/ $\mathrm{W}cm^{-2}$), $D_{R,\Delta R}$ (Ωcm^2 / $\mathrm{W}cm^{-2}$) is a reference deterioration rate by load varying adapted from Pei *et al.* [25], and $K_{\Delta R}$ is a constant to tune different deterioration rate for $\Delta R_{\Delta L}$.

The resistance deterioration of each start-stop cycle is assumed to be a constant which is adapted from an average deterioration rate [25] (Equation (3.12)):

$$\Delta R_{ss} = R_0 D_{ss} \tag{3.17}$$

where R_0 is the initial resistance of a fuel cell. D_{ss} stands for resistance deterioration rate due to start-stop.

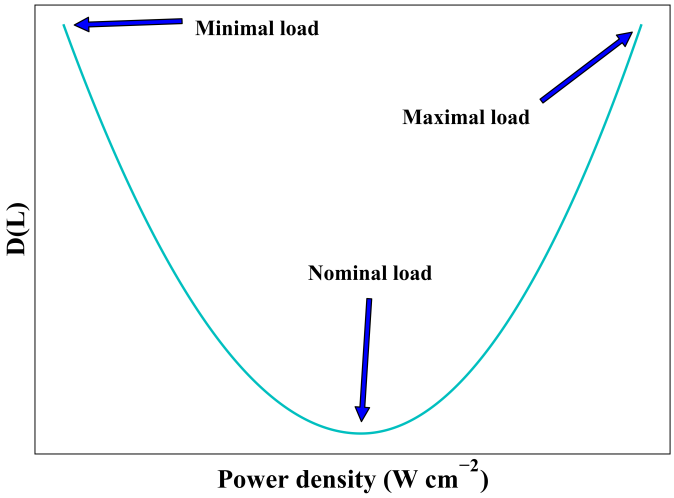

Figure 3.6: Dependence of fuel cell deterioration rate (overall resistance) on power load demand

3.2.3 Gamma process with random effects

According to the deterioration behavior analysis in Section 3.1.1, the deterioration in different fuel cell stacks has a large variation due to some hidden effects. That is, fuel cell stack deterioration is not only influenced by operating load, but also due to some random effects which will cause deterioration variability among different stacks. And the standard GP model is unable to fully capture such variations, i.e., individual deterioration heterogeneity. This can be translated through the introduction of a random parameter in the GP model where each individual corresponds to one realization of the random parameter.

On this basis, we propose a GP model with random effects for modeling MFC system deterioration. A random effect is imposed on the GP on its scale parameter, taken itself as a random variable following a Gamma distribution. More precisely, three different types of random effects-based models are investigated, namely, Gamma process random-effect model, Gamma process random mean model, and Gamma process random variance model.

Gamma process random effect model Consider the GP model ($Ga(\alpha,\, \beta)$) as proposed for modeling the fuel cell resistance increment over time $t_2 - t_1, t_2 > t_1$, namely $\Delta R_L(t_1, t_2)$. The first random effect model is expressed as:

$$\begin{aligned} \Delta R_L(t_1, t_2) &\sim Ga(v \cdot (t_2 - t_1), \beta_s) \\ \beta_s &\sim Ga(\delta, \phi) \end{aligned} \tag{3.18}$$

where δ, ϕ are the shape and scale parameter that formulates the gamma distribution for β in the standard GP model. The new shape parameter sampled from $Ga(\delta, \phi)$ is denoted as β_s.

This model is called Gamma Process Random Effect (GP-RE) model. The mean and

variance of the GP-RE model in the time interval $(t_1, t_2), t_2 > t_1 \geq 0$ is calculated as:

$$\begin{aligned} \text{Mean}(\Delta R_L(t_1, t_2)) &= v \cdot (t_2 - t_1) \cdot \beta_s \\ \text{Var}(\Delta R_L(t_1, t_2)) &= v \cdot (t_2 - t_1) \cdot \beta_s^2 \end{aligned} \tag{3.19}$$

Gamma process random mean model In Equation (3.19), the value of β_s is sampled from $Ga(\delta, \phi)$ and varies from one stack to the other. Thus, both the values of mean and variance in GP-RE model are changed, i.e., influenced by the random effect. However, other possibilities of modeling random effects exist in practice. For instance, the studied MFC system deterioration only presents a large dispersion of the deterioration rates, or only a large variation of the variance of the deterioration observations for each stack. In this regard, the random effect only affects the mean or the variance of the deterioration process (GP model) which introduces the Gamma Process-Random Mean (GP-RM) and Gamma Process-Random Variance (GP-RV) models [141].

GP-RM model is formulated by parameterizing the shape parameter of the GP model into ν to keep a constant variance, which writes:

$$\begin{aligned} \Delta R_L(t_1, t_2) &\sim Ga(\nu, \beta_s) \\ \nu = v \cdot (t_2 - t_1)(\tfrac{\beta}{\beta_s})^2, \beta_s &\sim Ga(\delta, \phi) \end{aligned} \tag{3.20}$$

The variance of the Gamma process defined in Equation (3.20) keeps as a constant $v \cdot (t_2 - t_1)\beta^2$.

Gamma process random variance model For GP-RV model, the shape parameter is parameterized to keep a constant mean, which writes:

$$\begin{aligned} \Delta R_L(t_1, t_2) &\sim Ga(\nu, \beta_s) \\ \nu = v \cdot (t_2 - t_1)(\tfrac{\beta}{\beta_s}), \beta_s &\sim Ga(\delta, \phi) \end{aligned} \tag{3.21}$$

The increment of the Gamma process defined in Equation (3.21) over time interval (t_1, t_2) keeps as a constant $v \cdot (t_2 - t_1)\beta$.

Since the random effects for all models are added through Gamma law, one basic principle here is to keep the mean value ($\delta\phi$) equal to the original scale parameter β (denoted as β_0). In the above three random-effect models, the scale parameter of standard GP follows a Gamma distribution, and it is unit-specific, such that it can capture the individual deterioration variability.

3.3 Gamma process-based deterioration behavior investigation

The deterioration behaviors of proposed models, i.e., GP, GP-RE, GP-RM, and GP-RV models are checked for fuel cells through numerical simulations. GP-based stochastic load dependent models have been proposed and developed to model fuel cell deterioration. In this section, we will use the developed models to study the fuel cell deterioration behaviors.

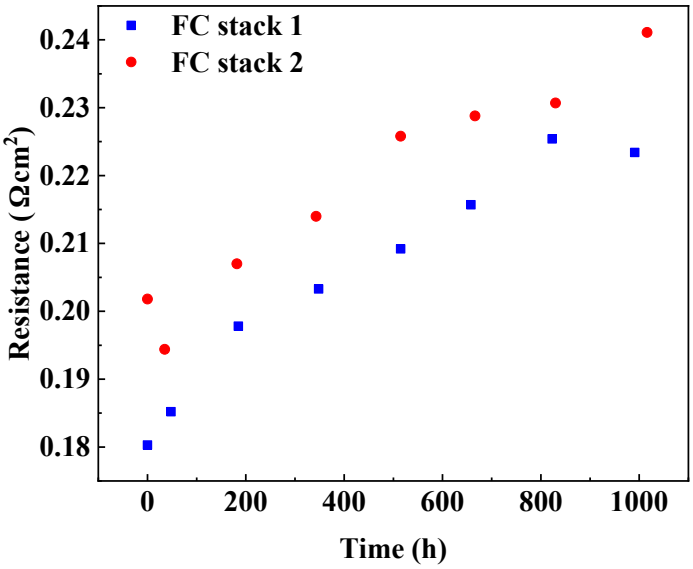

Figure 3.7: Overall resistance estimated from measured polarization curves, see Figure 1.11, Chapter 1.

3.3.1 Gamma process model parameter estimation

The identification of the scale (β) and shape coefficient (v) of the Gamma process for the deterioration modeling is based on the dataset published in IEEE PHM 2014 data challenge [27]. The dataset provides the data acquired in two typical durability tests on two fuel cell stacks. The resistance values were fitted based on the measured polarization curves within the aging data. The parameters are estimated by using the non-linear least square approach to fit the polarization equation (Chapter 1 Equation (1.9)) to all measured polarization curves.

The resistance estimations as shown in Figure 3.7 are used to estimate the shape coefficient and the scale parameters (v and β) of the stochastic deterioration Gamma process. To that aim, the Method of Moments (MoM) is applied [142]. From the data, the resistance and time increments are defined as:

$$\begin{aligned} \Delta t_i &= t_i - t_{i-1}, \\ \Delta R_i &= R_i - R_{i-1} \end{aligned} \tag{3.22}$$

where $i = 1, 2, \cdots N_s$ is the index of the data sample; N_s is the number of samples. Here the resistance is characterized by the relative value with respect to the initial resistance value. The time t_i is also accounted from the moment when the fuel cell is put into use. That is to say $t_0 = 0$ and $R_0 = 0$.

According to Cinlar *et al.* [142], the MoM estimated values of v and β, written v_0 and β_0,

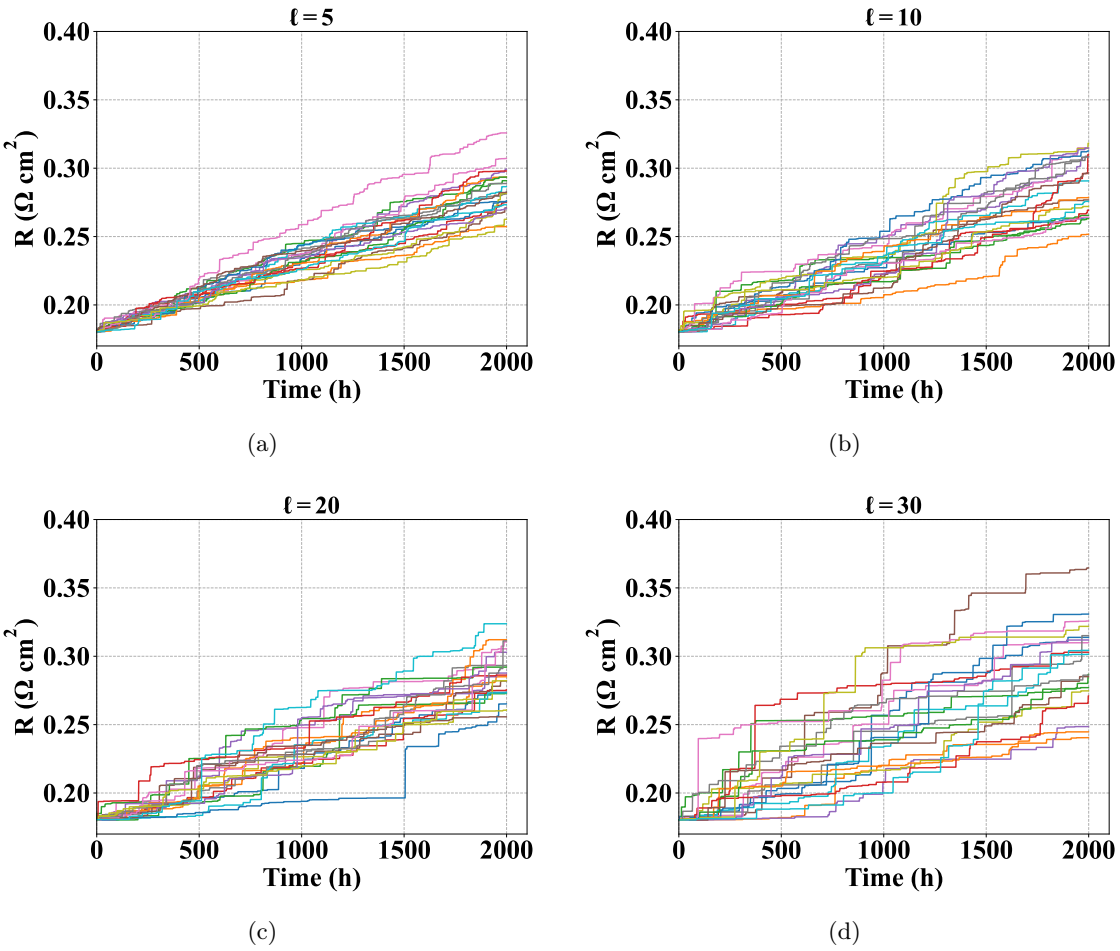

Figure 3.8: Deterioration trajectories with different ℓ values.

can be determined from the solution of the equations:

$$\begin{aligned} v_0\beta_0 &= \frac{\sum_{i=1}^{N_s}\Delta R_i}{\sum_{i=1}^{N_s}\Delta t_i} = \frac{R_{N_s}}{t_{N_s}} \\ R_{N_s}\beta_0\left(1-\frac{\sum_{i=1}^{N_s}\Delta t_i^2}{\left[\sum_{i=1}^{N_s}\Delta t_i\right]^2}\right) &= \sum_{i=1}^{N_s}\left(\Delta R_i - \frac{R_{N_s}}{t_{N_s}}\Delta t_i\right)^2 \end{aligned} \tag{3.23}$$

The estimated parameter values for FC stack 1 are: $v_0 = 0.1245$, $\beta_0 = 4.34 \times 10^{-4}$. For FC stack 2, the results are: $v_0 = 0.1768$, $\beta_0 = 4.36 \times 10^{-4}$. Figure 3.9 presents the fitted resistance increments for FC stack 1 and FC stack 2. These results verify that the GP model with the estimated parameters can capture the increasing trend of fuel cell stack resistance. It can be seen that the GP model mean and variance of these two parameter settings are similar. The parameters used in this work referred to FC stack 1.

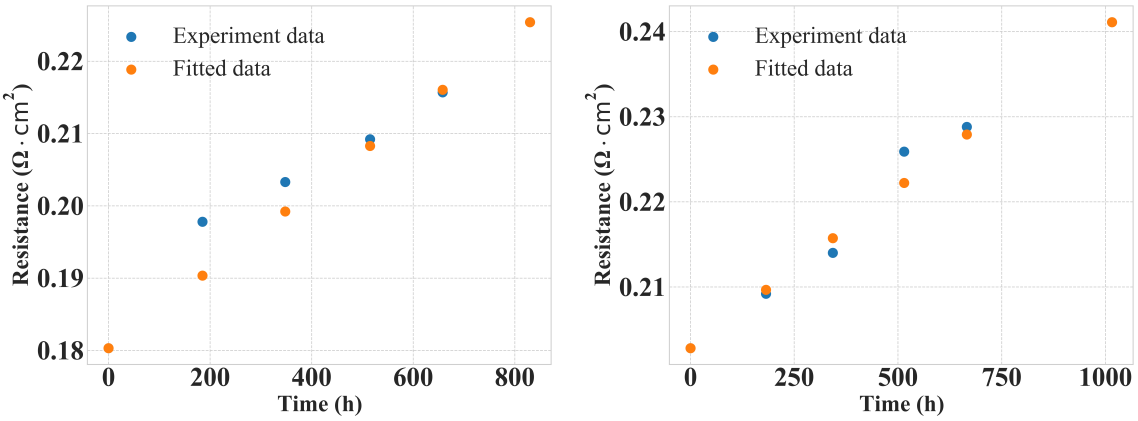

(a) Fuel cell stack 1 (b) Fuel cell stack 2

Figure 3.9: Parameter estimation results using MoM method.

3.3.2 Main simulation parameters

The main simulation parameters of the studied fuel cell stack are listed in Table 3.3. The minimal, nominal, and maximal output power are set based on IEEE PHM 2014 data challenge. The fuel cell stack life under nominal load is set as 1788 hrs based on the experimental data. The average lifetimes ($\overline{T}_R$) under minimal and maximal loads are designed based on fuel cell deterioration characteristics (both are set as 500 hrs) due to the lack of experimental data. The failure threshold FT are calculated by

$$FT = v_{0,nom} \cdot \beta_0 \cdot \overline{T}_{R,nom} \tag{3.24}$$

where $v_{0,nom}, \overline{T}_{R,nom}$ are the shape coefficient and lifetime values under nominal loads.

Then the average deterioration rate $D(L)$ is computes by

$$D(L) = \alpha(L)\beta = \frac{FT - R_0}{\overline{T}_{R,nom}} \tag{3.25}$$

where R_0 is the initial fuel cell stack resistance which is set as 0.1803 Ω cm^2. The empirical deterioration rate function (Equation (3.15)) are fitted based on known data points $(L_{min}, D(L_{min}))$, $(L_{nom}, D(L_{nom}))$, and $(L_{max}, D(L_{max}))$. The obtained deterioration rate curve is shown in Figure 3.10.

The variance of the deterioration trajectories has to be neither too large, because the lifetime would not be controllable, nor too small, because the system would not be stochastic. This variance is tuned based on Equation (3.11). Based on the simulated trajectories (Figure 3.8), the $\ell = 5, 10, 20, 30$ gradually increase the trajectory variance. $\ell = 20$ is used in the simulation. To construct the random effect model, three extra parameters need to be defined, that is, δ, ϕ, and h. The δ and ϕ define the Gamma distribution used in the proposed random effect models, which are computed by:

$$\delta = \frac{1}{h}, \phi = \beta_0 \ell h \tag{3.26}$$

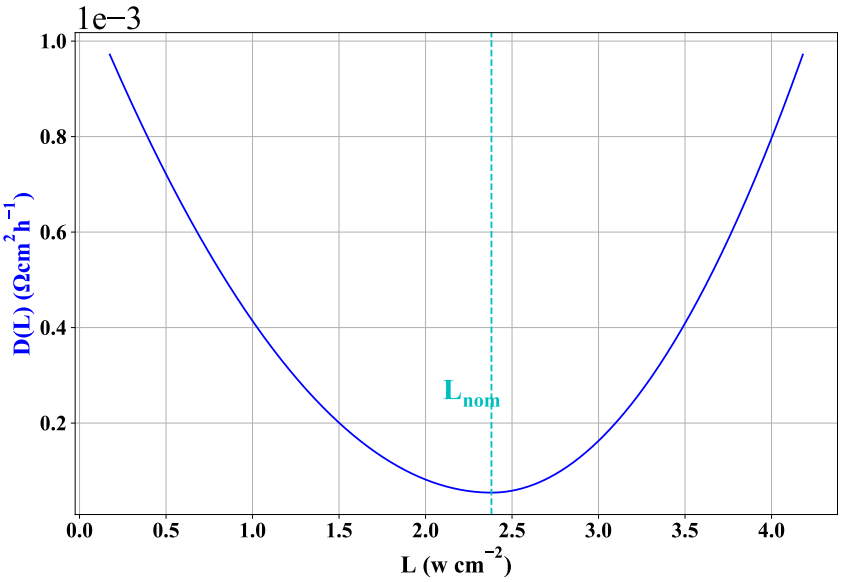

Figure 3.10: Proposed load-dependent deterioration rate curves.

Table 3.3: Fuel cell stack parameters.

Load conditions	L (W cm^{-2})	$\overline{T}_R$ (h)	v_0	β_0	FT (Ωcm^2)
Minimal	0.175	500	0.4454		
Nominal	2.381	1788	0.1245	4.34×10^{-4}	0.2775
Maximal	4.181	500	0.4454		

where h is a constant to tune the variance of used Gamma distribution, taken as 1.5 in the simulations.

3.3.3 Fuel cell deterioration trajectory result

Figure 3.11 presents resistance deterioration trajectories during one dynamic cycle. The accumulated resistance values include the deterioration of load, load varying, and start-stop effects. Figure 3.12 shows the simulated deterioration trajectories of the GP, GP-RE, GP-RM, and GP-RV models. By comparing the RE models with GP model, it is observed that the deterioration behavior is affected by different random effects.

For instance, in the GP-RM model, the resistance deterioration rates are modified for different trajectories, obtaining relatively lower lifetimes compared with the GP model. In GP-RE model, both the deterioration rate and variance of the trajectories are influenced by RE. A relatively wide range of lifetimes is obtained. For GP-RV model, the deterioration rate is not influenced by the RE, only the variance is altered. Thus, the simulated lifetimes

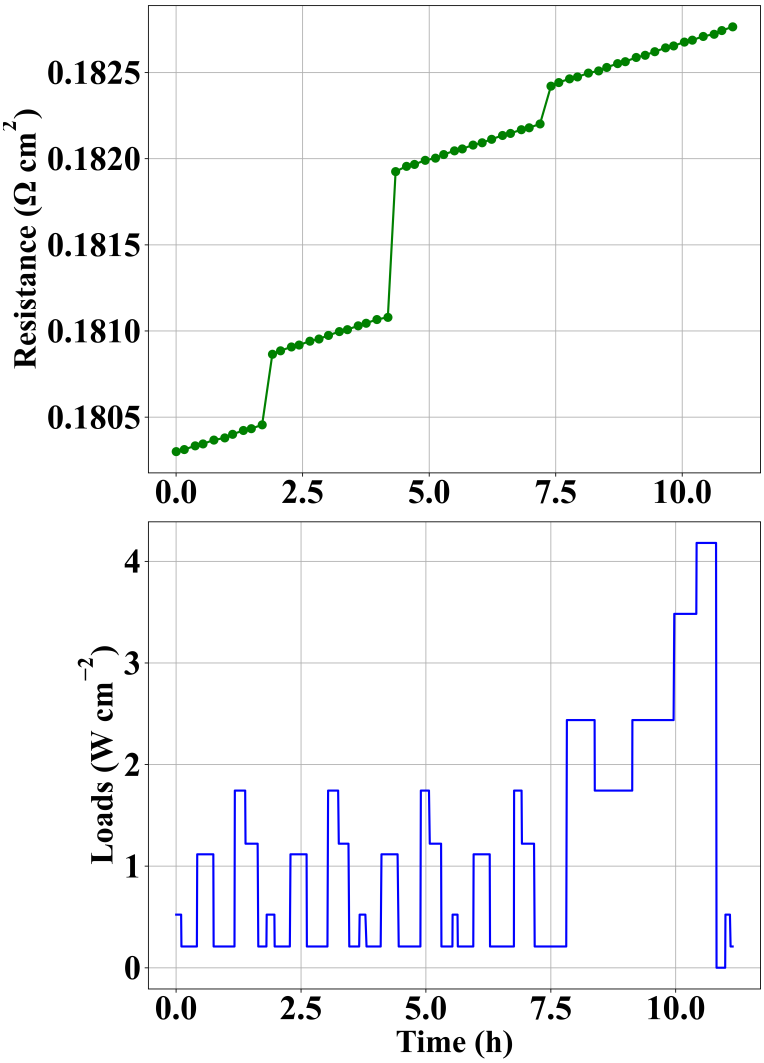

Figure 3.11: Example resistance trajectory of GP model.

generally lie in a similar range as GP.

Figure 3.13 plotted the lifetime histograms of 300 runs (Monte Carlo simulations) for all models. It is observed that the lifetimes of GP-RE and GP-RM models lie in a wider range compared to the GP model. But in GP-RV model, the distribution is similar to GP. These results are further confirmed in the Cumulative Distribution Function (CDF) results as shown in Figure 3.14. The CDF curves of GP, GP-RV models are nearly overlapped, whereas the GP-RE and GP-RM models extend the CDF curve to a wide range.

Table 3.4 summarized the statistical results of simulated lifetimes. The GP-RE model produced the longest lifetime. The GP-RM model modified the system lifetime to a lower value. In GP-RV, the lifetime is similar to GP. In terms of standard deviation results, the RE-based models are relatively larger than the GP model. This work mainly focused on the random effect-based stochastic deterioration modeling of fuel cells. The next step of work will

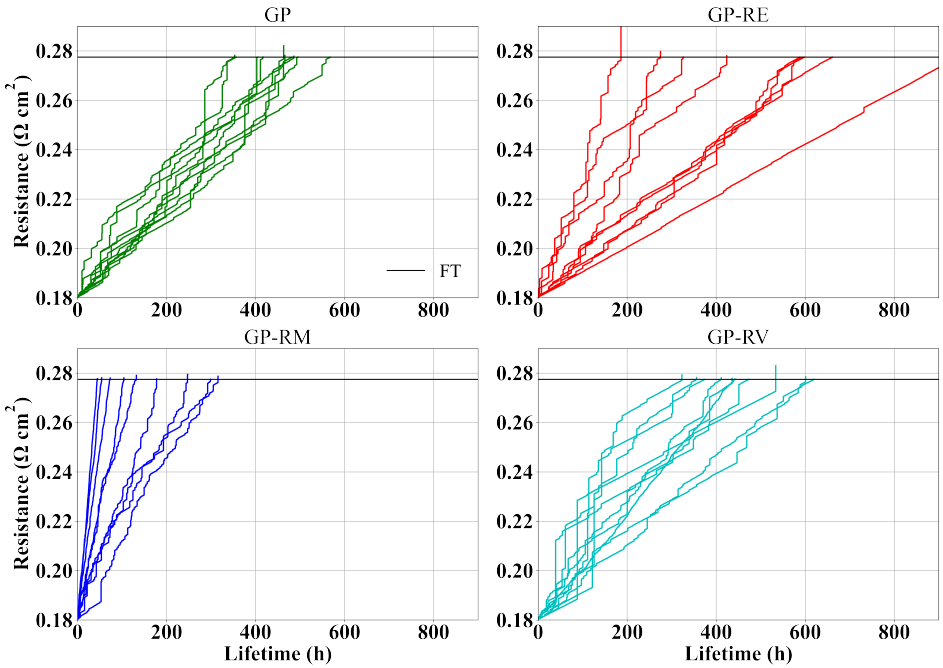

Figure 3.12: Resistance deterioration trajectories of proposed four models (10 trajectories for each model).

Table 3.4: Simulated lifetimes' statistic results

Models	$\overline{T}_R$ (h)	$T_{R,med}$ (h)	stand deviation
GP	447.4	447.6	75
GP-RE	600.9	575.8	284
GP-RM	337.5	312.1	262
GP-RV	444.1	438.9	80

be focused on the statistical inference studies using the proposed deterioration models.

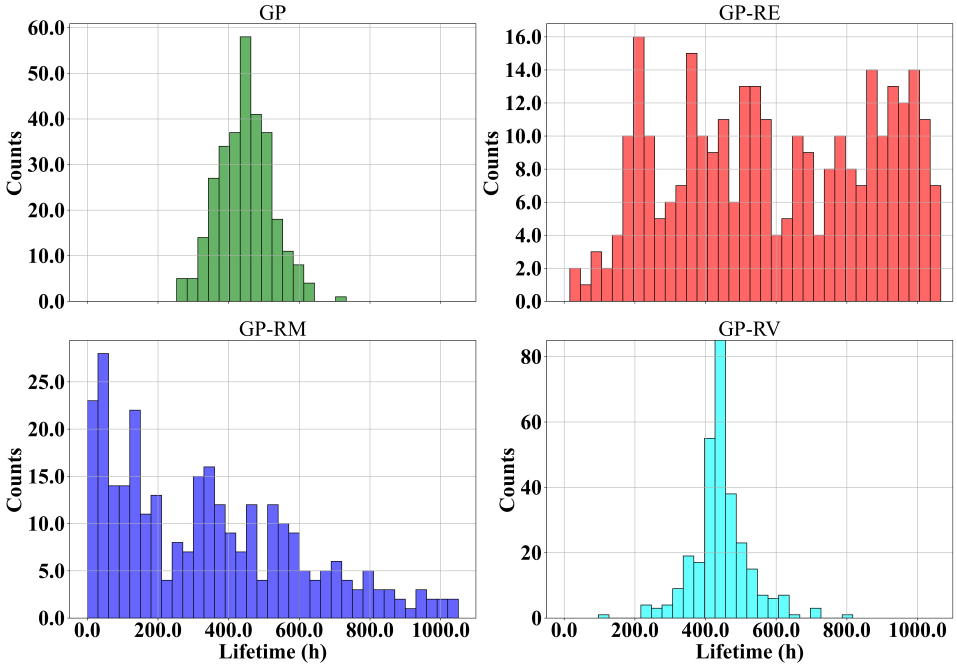

Figure 3.13: Lifetime histograms of GP, GP-RE, GP-RM, and GP-RV models.

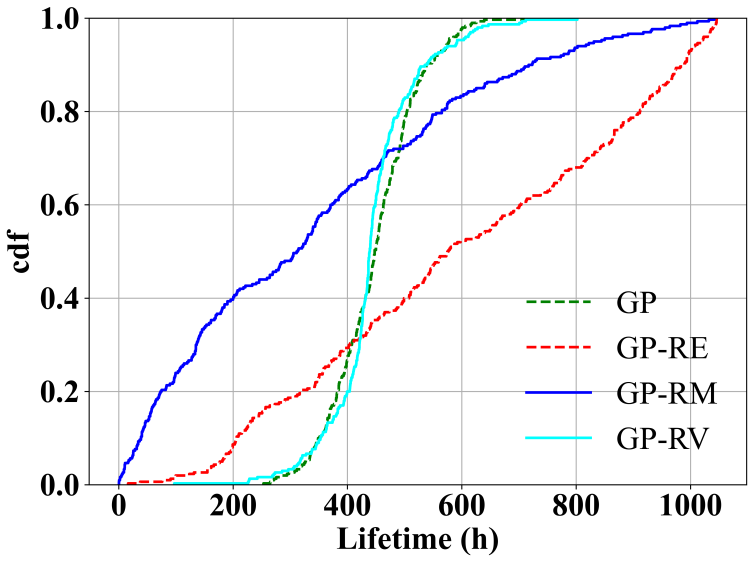

Figure 3.14: CDF functions of the four deterioration model.

3.4 Conclusion

This chapter studied the deterioration modeling of an MFC system. The goal is to develop a deterioration model with two typical features, that is, load-dependent, stochastic with individual stack deterioration heterogeneity. A Gamma process-based load-dependent deterioration model is proposed for the studied fuel cell system. The shape parameter of GP model is further modeled as a function of fuel cell operating load. An empirical function is used to build this function, i.e., $\alpha(L)$. Despite being suitable for stochastic deterioration modeling of a gradual degradation process, GP model is unable to model the deterioration variability among different stacks. Thus, a random effect is introduced to the GP model on its scale parameter β, taken as a random variable following a Gamma distribution. Moreover, three different effects on the GP model studied. GP-RE model is a general random effect model in which the influences on both the mean and variance are considered. In GP-RM, only the influence of the deterioration rate is considered. In GP-RV, only the influence on the deterioration variance is modeled.

An automotive-used dynamic load cycle is applied to test the deterioration behavior of the proposed models. The lifetime statistical results are used to analyze the deterioration characteristics of the GP, GP-RE, GP-RM, and GP-RV models. These models will be further used in an EMS to study the optimal load allocation problem of an MFC system in the following chapters.

Chapter 4

Multi-Stack Fuel Cells Energy Management Strategy Studies under Static Loads

In this chapter, a multi-stack fuel cell energy management strategy is developed under static load profiles. The objective of such a strategy is to improve the overall system lifetime and to reduce system fuel consumption. The deterioration of the studied fuel cell stack is modeled using the classic Gamma process model presented in Chapter 3. First, the management of a two-stack fuel cell system is investigated. From a single objective of minimizing system deterioration to a multi-objective of minimizing system deterioration as well as improving fuel economy, the associated optimization problems are formulated by setting different objectives, namely, objective functions. Based on the conclusions of the above strategies, the energy management of three-stack fuel cells is studied with the objectives of minimizing system deterioration and fuel consumption. The obtained lifetime results are compared with two classical management methods, i.e., Average Load and Daisy Chain strategies. The results of this chapter are based on the work presented in the European Conference of the PHM Society - PHME20, 1-3 July 2020, Turin, Italy (virtual) [143] and Annual Reliability and Maintainability Symposium (RAMS), 24-27, May 2021, Orlando, United States (virtual) [144]. The last parts of the work are published in Proceedings of the Institution of Mechanical Engineers, Part O: Journal of Risk and Reliability [145].

Contents

4.1 Energy management for a two-stack fuel cell system

Two energy management problems are studied for a two-stack PEM fuel cell system. The first problem is designed to investigate the degradation behavior of a two-stack MFC system using the proposed fuel cell deterioration model. After that, the second problem is proposed to build the energy management strategy by considering both fuel cell system degradation and fuel consumption. This section presents the formulation of these two problems and the proposed decision-making strategies.

4.1.1 Objectives definition for the fuel cell system

Maximizing MFC system lifetime and minimizing system fuel consumption are the two objectives studied in the proposed EMS problem. MFC system lifetime is linked to its deterioration process, thus the first objective of maximizing system lifetime can be achieved with the assistance of a fuel cell stack deterioration model. The fuel cell resistance deterioration model used in this chapter is based on the modeling work discussed in Chapter 3. A GP model ($\Delta R_L(t_1, t_2) \sim Ga(v(t_2 - t_1), \beta)$) is used to model the deterioration of fuel cell resistance caused by load effect.

Fuel cell hydrogen consumption objective Fuel cell stack fuel consumption rate is derived based on the fuel cell electrochemical reactions. According to Equation (1.1), the amounts of hydrogen and oxygen consumed by the fuel cell are described as a function of operating current. The expression of the required hydrogen consumption rate f_{H_2} (g/s) with respect to the stack current can be qualified by Faraday's law [75]:

$$f_{H_2} = \frac{n_{cell} \cdot M_{H_2}}{z \cdot F} \cdot I_{stack} \cdot \lambda \tag{4.1}$$

where I_{stack}, M_{H_2}, z are stack current in A, molar mass of hydrogen, and number of electrons acting in the reaction, respectively. F is the Faraday's constant with a unit of $C\ mol^{-1}$. λ stands for hydrogen stoichiometric ratio.

In fuel cell, the term stoichiometric can be defined as just the right amount [7]. In Equation 1.1, exactly two moles of hydrogen would be provided to react with one mole of oxygen and produced $4F$ of charge. Usually, both reactants are provided at greater than the stoichiometric rate to ensure the performance of fuel cells. Thus, if the rate of usage of hydrogen in reaction is $\dot{x}$ models per second, then the according to the defined stoichiometric ratio λ, the rate of supply is $\lambda\dot{x}\ mol\ s^{-1}$.

Thus, the hydrogen consumption rate is proportional to the stack current. Besides, hydrogen consumption is also caused by the auxiliary components in fuel cell systems, such as air compressors, and humidifiers for example. Several experimental or simulation-based research works proved that a quadratic polynomial equation can be applied to represent the hydrogen consumption rate with respect to the useful power [117], [146], [147]. Based on these studies,

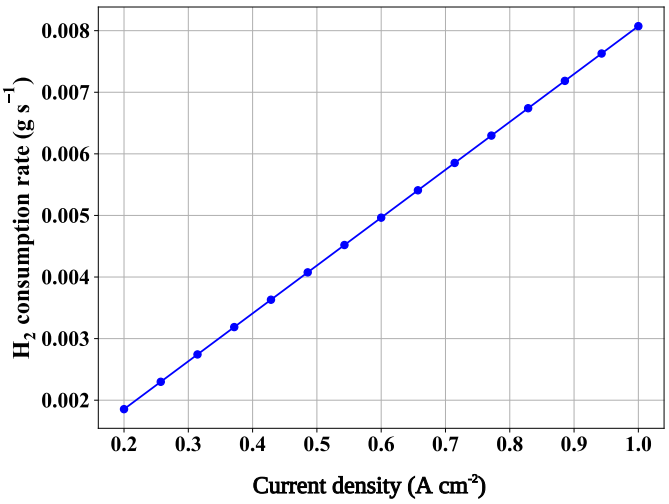

Figure 4.1: Fuel cell stack hydrogen consumption rate and current density curve.

the hydrogen consumption rate of a fuel cell stack is expressed as follows:

$$f_{H_2}(L) = aL^2 + bL + c \tag{4.2}$$

where L is the power density load of a fuel cell, a, b, c are parameters to be fitted. The overall fuel consumption over a period of time t_0 is calculated by $F_{H_2}(t_0)$:

$$F_{H_2}(t_0) = \int_0^{t_0} f_{H_2}(L(t))dt \tag{4.3}$$

where $L(t)$ is the load power at t.

Fuel cell deterioration objective Assuming that the initial resistance R_0 and the failure threshold FT are known for the studied stack, the lifetime distribution can then be written as:

$$\begin{aligned} F(t) = P\left(T_R \leq t\right) &= P\left(R(t) > FT\right) \\ &= \frac{\Gamma\left(\alpha(L) \cdot t, (FT - R_0) \cdot \beta\right)}{\Gamma(\alpha(L) \cdot t)} \end{aligned} \tag{4.4}$$

where $\Gamma(a, x) = \int_x^{\infty} z^{a-1} e^{-z}\, dz$ is the incomplete Gamma function for $x \geq 0$ and $a > 0$. This work applies P to denote the cumulative probability.

Since the actual deterioration of the fuel cell depends on the operating conditions, the residual life, i.e. the difference between the expected life and the actual age, needs to be updated regularly. This can be carried out by using the measured resistance value R_{obs} at time t_{obs}, indicator of the actual deterioration level of the fuel cell. Therefore, a conditional failure probability $P_d(t)$ at time t after t_{obs} can be defined as the probability for $R(t)$ to exceed a predefined failure threshold before time t, given an observed level R_{obs} at t_{obs}. Thus, based on the previous Equation (4.4), $P_d(t)$ is written as follows [134]:

$$\begin{aligned} P_d(t) &= F\left(t|R_{obs}(t_{obs})\right) \\ &= P\left(T_R \leq t|R_{obs}(t_{obs})\right) \\ &= P\left(R(t) > FT|R_{obs}(t_{obs})\right) \\ &= \frac{\Gamma\left(\alpha(L)\cdot(t-t_{obs}),(FT-R_{obs}(t_{obs}))\,\beta\right)}{\Gamma\left(\alpha(L)\cdot(t-t_{obs})\right)} \end{aligned} \tag{4.5}$$

where T_R is the first hitting-time of level FT, L is fuel cell operating power load, $\alpha(L)$ is the corresponding shape parameter and R_{obs} represents the observed resistance deterioration value at the current time step.

The proposed post-prognostic decision-making strategy is developed to make a trade-off between slowing the PEM fuel cell deterioration and reducing the fuel consumption. The next part is to introduce the principle of proposed decision-making strategy.

4.1.2 Post-prognostics decision-making principle

Decision-making considering fuel cell deterioration In the first decision problem, the developed model is used for the post-prognostics decision-making phase to decide the optimal load split between two PEM fuel cell stacks so that the maximum system service life can be achieved. This decision-making procedure is made periodically, at a fixed decision time interval τ.

For each decision period, the decision probability is noted as P_d and the decision threshold DT. As shown in Figure 4.2, a system with two PEM fuel cells has been running for t_0. FC1 and FC2 are two PEM fuel cell stacks in the system. For the studied fuel cell system, the failure occurs due to an excess of deterioration threshold, and the probability distribution law of the failure time T for one single stack can be calculated analytically as [148]:

$$F(t) = P(T \leq t\Big|R_{obs}) = \frac{\Gamma(vt,(DT-R_{obs})\cdot\beta)}{\Gamma(vt)} \tag{4.6}$$

where T is the first hitting time of the level DT by the stochastic process $x(t)$. R_{obs} represents the measured resistance at the current decision step.

According to the previous discussion, the threshold used for the decision-making at each decision step can be set as:

$$DT = v\cdot\beta\cdot\tau + R^{d,t_0} \tag{4.7}$$

where R^{d,t_0} represents the initial deterioration level at the decision time t_0; The value of R^{d,t_0} is set as the maximum value of stacks resistances at the decision time, namely, $R^{d,t_0} = max\{R^{t_0}_{FC1}, R^{t_0}_{FC2}\}$.

This approach is sketched in Figure 4.2: the red and black solid curves above the decision threshold represent the predicted lifetime distribution for FC1 and FC2 that are calculated at time t_0. P_{d1} is the probability that the deterioration level of FC1 exceeds the decision threshold before $(t_0+\tau)$ hours; similarly, the decision probability of FC2 is P_2. In this work,

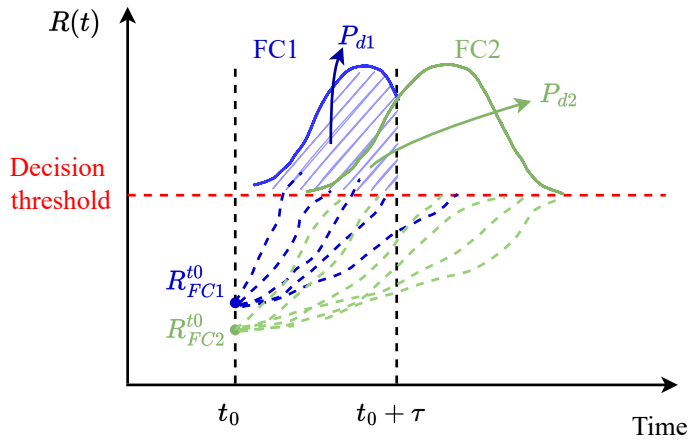

Figure 4.2: Principle of the post-prognostics decision-making strategy at time t_0.

the decision criterion is then defined as $(1 - P_{d1}) \cdot (1 - P_{d2})$, and we seek to maximize the criterion to obtain the longest system lifetime. This is realized by searching the optimal load split between the two stacks. The solid line below DT is the corresponding deterioration trajectories simulated for FC1 and FC2 after the decision.

Decision-making considering fuel cell deterioration and hydrogen consumption In the second decision problem, an extra objective (system fuel consumption) is considered during the decision process. Then a similar sequential decision-making process is scheduled during system operation. The conditional failure probability and fuel consumption are used to define the mixed criterion:

$$C_{dec}(L_1, L_2) = \max\{\Omega \cdot (1 - P_{d1}) \cdot (1 - P_{d2}) + (1 - \Omega) \cdot (\frac{1}{F_{H_2,1} + F_{H_2,2}})\} \tag{4.8}$$

where P_{di} is the conditional failure probability for fuel cell stack i (FCi) calculated by Equations (4.5, 4.6). $F_{H_2,i}$ is fuel consumption of FCi that calculated through the integration of Equation (4.3). A normalization operation is applied to this criterion so that a trade-off between system aging and fuel consumption can be achieved by defining different weights Ω. The decision variables are operating loads of different stacks, namely, L_1, L_2.

4.1.3 Numerical simulations

Monte Carlo simulation is used to investigate the efficiency of the proposed strategy. The results are compared with the classic Average Load Split strategy. The Average Load Split strategy attributes the overall system load demand evenly among all stacks [149]. The MFC system with two stacks is chosen in this section to study the load allocation problem.

Table 4.1: Main simulation parameters for the proposed Gamma process deterioration model.

Load conditions	L (A cm^{-2})	$\overline{T}_R$ (h)	$D(L)$ ($\times 10^{-4}$) ($\Omega\ cm^2 h^{-1}$)	FT ($\Omega\ cm^2$)
Minimal	0.214	200	0.4454	
Nominal	0.7	2800	0.1245	0.32
Maximal	1.6	300	0.4454	

4.1.3.1 Simulations considering fuel cell deterioration

Simulation settings The main simulation parameters used in this section are summarized in Table 4.1 and the detailed calculation of related parameters refer to Chapter 3, Section 3. The initial fuel cell stack resistance R_0 is set based on the polarization equation (1.9) and the measured polarization curves taken from [27] ($R_0 = 0.1797\ \Omega\ cm^2$). The initial fuel cell stack resistance value of the studied two stacks is set to be equal to R_0, namely, $R_{FC1}^{init} = R_{FC2}^{init} = R_0$. Due to the lacking of enough experimental data, the average stack lifetimes $\overline{T}_R$ for the minimal, nominal, maximal conditions are decided based on fuel cell deterioration characteristics (Chapter 3, Section 3.2.2). The scale parameter β is defined as constant value 0.32. According to the proposed GP deterioration model, the shape parameter α is modeled as a function of operation load (Chapter 3, Section 3.2.2).

The periodic decision time interval τ is set as 150 h. Based on Equation (4.7), the decision threshold DT corresponding to the maximum deterioration rate $D(L_{min})$ which is used in this work is calculated for each decision step. The scheduled simulation horizon is set as 3900 hrs to ensure the deterioration levels reach the failure threshold (FT) for all Monte Carlo simulation histories such that system lifetime T_R can be collected for further analysis. The decision steps of a one-run trajectory are calculated as 26. The conditional failure probability (Equation (4.6)) for all possible combinations of current loads of FC1 and FC2 are then calculated at each decision step. Then the optimal operating loads are the decision variable pair that produces the lowest failure probability P_d.

The current load demand in this section is defined as a constant value, $L_d = 1.8\ A\ cm^{-2}$. This load demand level is set to push at least one of the stack to work at a load level larger than L_{nom}. The number of Monte Carlo histories is chosen as 100 so that the convergence of the performance indicators is guaranteed.

Performance estimation indicators In order to justify the efficiency of the proposed decision-making strategy, the lifetime of two stacks system are calculated based on the simulated trajectories. For system lifetime observed on a single deterioration trajectory, the simulation was denoted as one-run simulation; for system lifetime estimated on N deterioration trajectories (average system lifetime and distribution), the simulation was denoted as N-run simulation. The lifetime of one-run simulation (T_R) is determined as:

$$T_R = min\{T_{1,R}, T_{2,R}\} \tag{4.9}$$

Table 4.2: Examples of EoL results for a single simulation and for 100 simulations.

Strategies	$T_{R,med}$ (h)	$\overline{T}_R$ (h)
Our strategy	3019	2909
Average Load	2662	2615

where $T_{1,R}$ represents the lifetime of FC1, $T_{2,R}$ is the lifetime of FC2.

The lifetime of the system can then be estimated by averaging the results over the N simulations ($\overline{T}_R$):

$$\overline{T}_R = \frac{1}{N}\sum_{i=1}^{N}(T_{Ri}) \tag{4.10}$$

where T_{Ri} stands for the simulated lifetime of the $i-th$ deterioration trajectory.

Main simulation results First, the lifetime histogram results ($N = 100$) of the proposed load allocation strategy and the Average Load Split method are presented in Figure 4.3. For description convenience, the simulation results obtained from the proposed load allocation strategy are noted as results with decision and the results obtained from the Average Load method are noted as results without decision. By comparing Figure 4.3(a) and Figure 4.3(b), the system lifetime results with decision are mostly distributed in the range $(2500, 4000)$ hrs, with a median lifetime of 3018.5 hrs. The lifetimes without decision are mainly distributed in $(1500, 3000)$ hrs with a median lifetime ($T_{R,med}$) value equal to only 2662 hrs (Table 4.2).

Then the deterioration trajectories are further discussed for checking the detailed resistance deterioration behavior under two operation strategies, i.e., the proposed load allocation strategy and the Average Load method. Figure 4.4 shows the average deterioration trajectories estimated from the 100-run trajectories. $\overline{R}_{1,dec}$ and $\overline{R}_{2,dec}$ are the average resistance deterioration trajectories obtained from the proposed load allocation strategy. $\overline{R}_{1,ave}$ and $\overline{R}_{2,ave}$ are the trajectories obtained from the Average Load strategy. It is observed that the trajectories of $\overline{R}_{1,dec}$ and $\overline{R}_{2,dec}$ tend to be more grouped together compared with the trajectory results of $\overline{R}_{1,ave}$ and $\overline{R}_{2,ave}$. Thus, the load allocation decisions tend to reduce the variance of stacks resistance deterioration values: they are synchronized which increases the system lifetime and a fast deterioration behavior of one stack is compensated and balanced with the deterioration of the other stack. Without the decision-making strategy, the deterioration paths remain desynchronized and there is high risk that one of the two FC stacks fails early, hence reducing the lifetime of the studied system. Moreover, the specific deterioration trajectories from a set of 10 simulations are presented in Figure 4.5 that further verifies the above analysis. The overall results in Figure 4.5 show that the trajectories that developed with decision are more grouped together with a lower variance than those without decision.

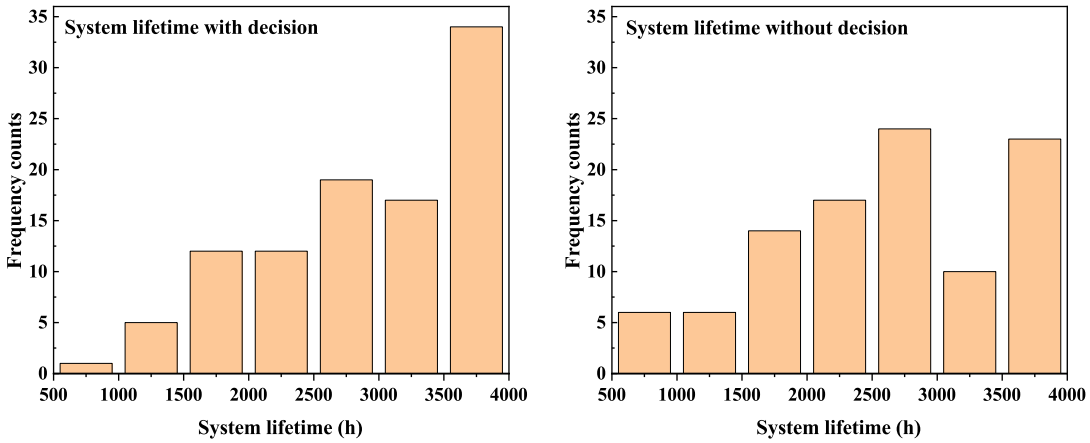

(a) (b)

Figure 4.3: Histograms of the observed system lifetimes for N =100 simulations

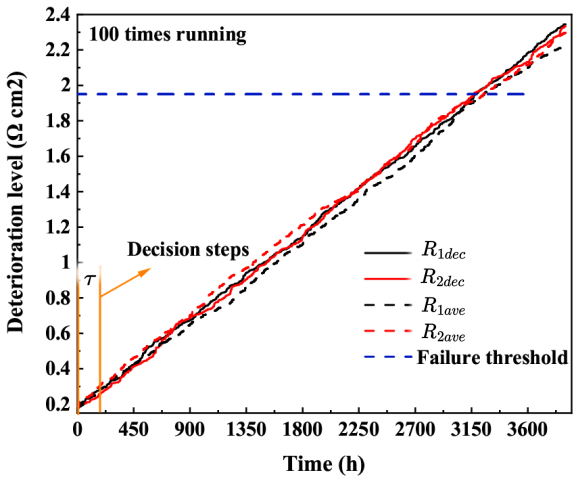

Figure 4.4: Average deterioration trajectories results ($N = 100$)

4.1.3.2 Simulations considering both fuel cell deterioration and fuel consumption

Simulation settings The basic simulation parameters are summarized in Table 4.3. The initial fuel cell stack resistance value of the studied two stacks is set to be equal to R_0 ($R_{FC1}^{init} = R_{FC2}^{init} = R_0$). Both constant and a piece-wise constant type load profiles are studied. As shown in Figure 4.6, the piece-wise constant type demands contain three load levels, i.e., $I_{load1} = 12.4, I_{load2} = 13, I_{load3} = 15\ A\ cm^{-2}$. For the constant type demands, the demand level is set as 13 $A\ cm^{-2}$. Note that here the fuel cell deterioration is modeled purely by the load effect (ΔR_L), thus the dynamic load profile considered here will not influence the load allocation decisions. The influence of a dynamic load profile (e.g., the load demand change event duration, the load demand level) will be further investigated in following chapters.

The scale parameter of the GP deterioration model (β) is set as 0.36. In the simulation

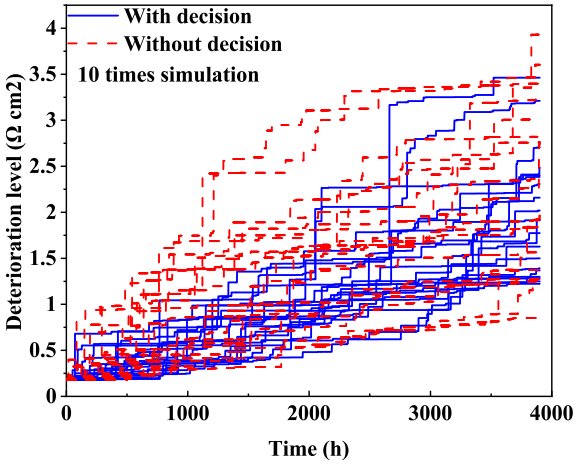

Figure 4.5: Deterioration trajectories results (10 runs)

Table 4.3: Main simulation parameters (one stack).

Load conditions	L (A cm^{-2})	$\overline{T}_R$ (h)	D(L) ($\times 10^{-4}$) ($\Omega\ cm^2 h^{-1}$)	FT ($\Omega\ cm^2$)
Minimal	2	200	0.4454	
Nominal	8	2800	0.1245	3
Maximal	10	300	0.4454	

process, the overall simulation length is defined as 2700 h, and the periodical decision time step (τ) is 150 h. Here, the simulation horizon is set based on the deterioration rate and failure threshold values to ensure the hitting of failure threshold such that fuel cell system lifetime can be estimated with Monte Carlo simulations. The number of Monte Carlo histories $N = 100$ is used so that the convergence of the estimation of the performance indicators is guaranteed. Four different weights Ω values were used in the proposed decision-making strategy, i.e. $\Omega = 0.3, 0.5, 0.7, 0.9$. It is noticed that the Ω defined in Equation (4.8) stands for the importance weight between fuel cell deterioration and fuel consumption. A larger Ω means putting more importance on minimizing deterioration. The simulation problem studied here is designed as a first attempt to design a management strategy that considering two objectives. Thus, the simulation parameters are exaggerated such that a relatively large system lifetime improvements can be observed for the proposed management strategy.

Performance estimation indicators System lifetime is defined as the first estimation indicator to assess the efficiency of proposed decision strategy. Since the defined problem considers both fuel cell deterioration and fuel consumption, an estimation index including the fuel consumption is used (*Ratio*), which writes:

$$Ratio = \frac{F_{H_2}}{T_R} \tag{4.11}$$

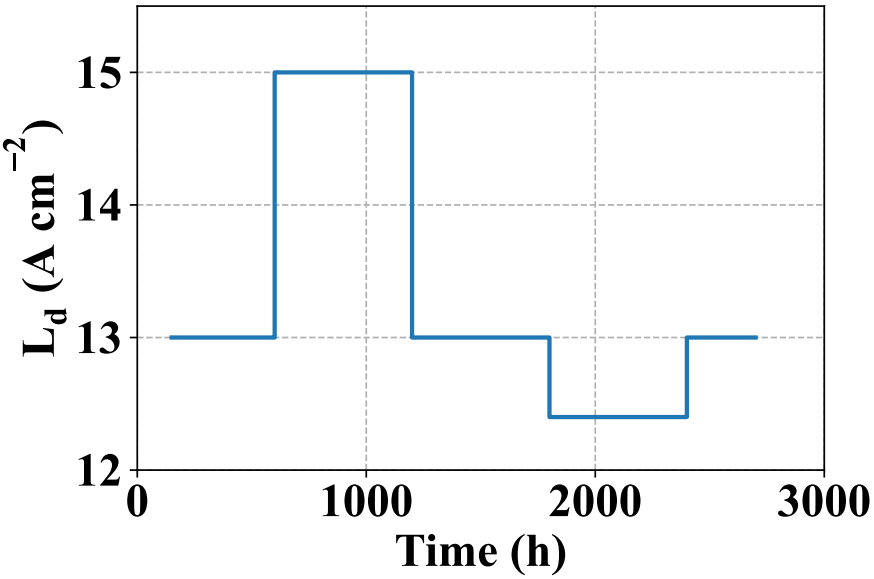

Figure 4.6: Piece-wise constant load demand.

where T_R (Equation (4.9)) is simulated system lifetime and F_{H_2} is fuel cell hydrogen consumption function (Equation (4.3)).

Main simulation results The proposed load allocation strategy is compared with the average load split method in terms of the defined indicators. Firstly, the histograms under constant load demand are shown in Figure 4.7 and Figure 4.8. It can be seen that 68% of the system lifetimes of average load strategy are distributed between 1200 and 1800 hours. For the proposed load allocation strategy (Figure 4.8), 65% of the system lifetimes are distributed between 1400 and 2800 hours for $\Omega = 0.3$. This percentage value are increased to 86% and 97% for $\Omega = 0.7$ and 0.9. This shows that when increasing the value of Ω, i.e., put more weights on minimizing fuel cell deterioration, our strategy can help to improve overall system lifetime. Moreover, the proposed strategy achieves an improved lifetime compared to the average load method. For our strategy, the practitioners can choose the value of Ω based on their own interests to achieve the trade-off between fuel cell deterioration and fuel consumption.

For the fuel consumption and system life ratio indicator *Ratio* (see Figure 4.9), the value of average load strategy is the lowest which equals to 40.88 $g\ s^{-1}$. The indicator values for $\Omega = 0.3, 0.5, 0.7$, and 0.9 are 41.04, 41.5, 47.67, and 58.16 $g\ s^{-1}$, respectively. When increasing the value of Ω, the proposed strategy tends to force fuel cell operates at higher load range which consumes more hydrogen. Thus, the *Ratio* of $\Omega = 0.9$ is the highest.

Then the two indicator results are calculated and discussed for the piece-wise dynamic load demand scenario. The system lifetime histograms of our strategy are shown in Figure 4.10. Compared with the average load strategy (Figure 4.7 b), 81% of the system lifetimes are distributed between 1400 and 2800 hours for $\Omega = 0.3$. For $\Omega = 0.5, 0.7$, and 0.9, the percentages

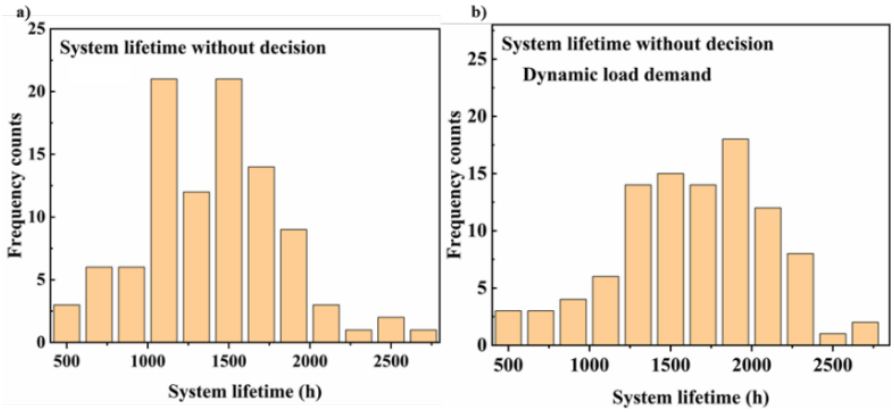

Figure 4.7: System lifetime histograms in the case of the average load split policy.

of the same lifetime range are 89%, 93%, and 98%, respectively. Therefore, for the dynamic load demand, the proposed decision-making strategy still works well. The second indicator *Ratio* shows a similar trend as in the constant loads. *Ratio* reaches the highest value at $\Omega = 0.9$ ($58.62\ g\ s^{-1}$). The similarity in the simulations results of the two types of load demands verifies that the piece-wise constant loads studied here is equivalent to a constant load in terms of influence on the management strategy.

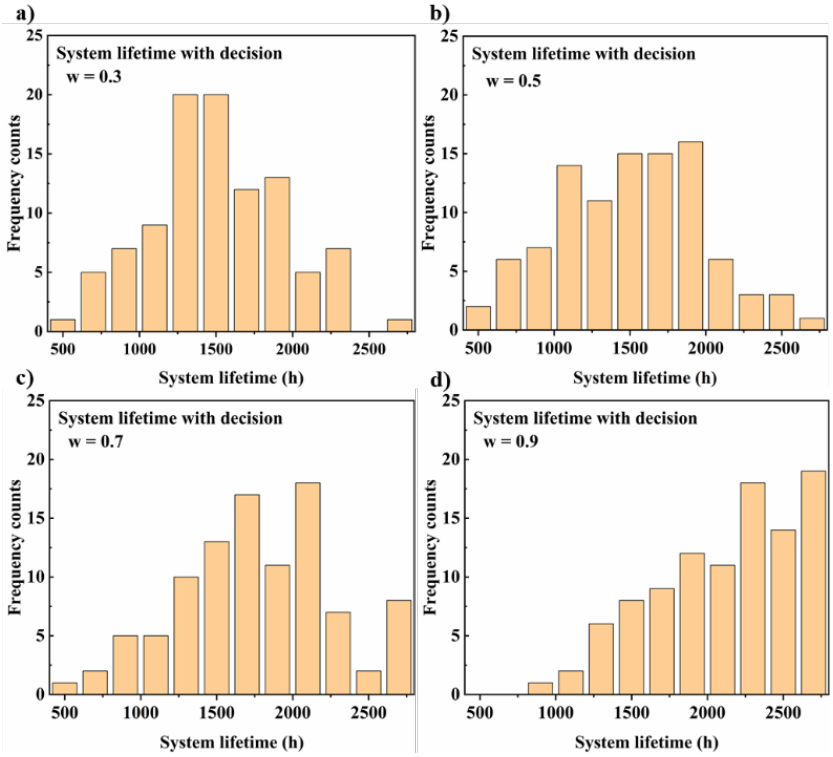

Figure 4.8: System lifetime histograms in the case of our proposed strategy (constant loads).

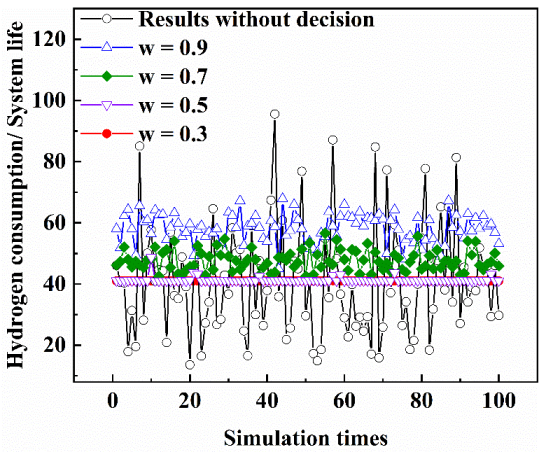

Figure 4.9: *Ratio* indicator results (constant loads).

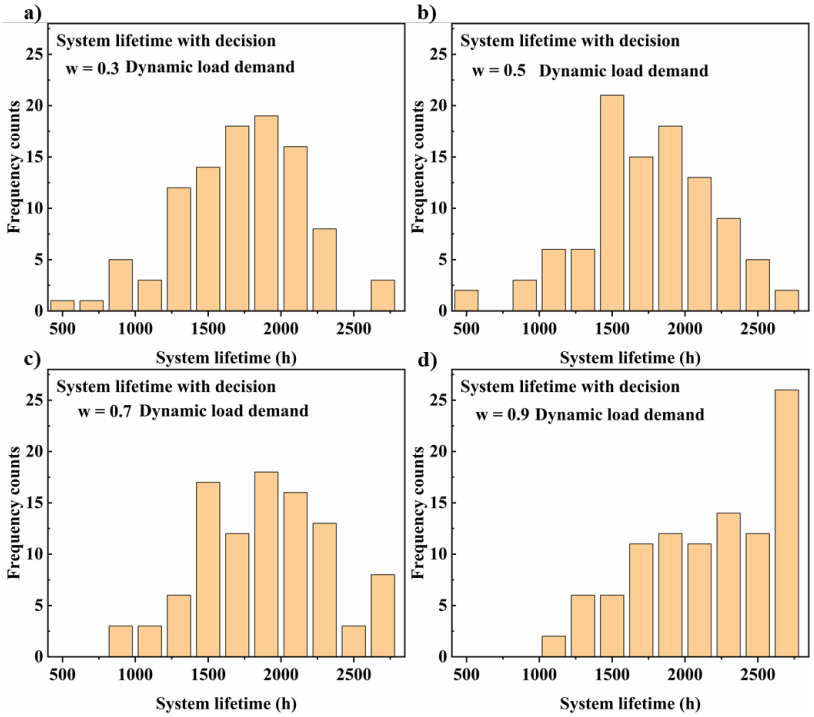

Figure 4.10: System lifetime histograms in the case of our proposed strategy (dynamic loads).

4.2 Energy management strategy for a three-stack fuel cell system

The previous discussed EMS issues are the first attempt to develop a load allocation strategy. Simulation results proved that the proposed strategy can help to enhance fuel cell system lifetime and optimize hydrogen consumption. However, several limits can be identified in the previous two studies:

- Parameters. The key parameters (e.g. shape and scale parameters of the Gamma process model) were chosen to clearly show the behavior of our proposed strategy, but they do not necessarily correspond to fully realistic situations for PEM fuel cells.
- System configuration. Only two stacks are considered in the EMS problems which may limits the generality of the proposed approach.
- Optimization method. The optimization approaches used in the previous EMS problems are based on basic exhaustive search and more efficient optimization approaches are needed if one seeks real-time implementation.

Therefore, an EMS problem of three-stack fuel cell system is investigated in this section that corresponds to the problem diagram presented in Figure 2.2 (Chapter 2). The general problem is to maintain the operation of a three-stack fuel cell system subject to a constant load profile. The detailed energy management strategy will be presented in the following section.

4.2.1 Post-prognostic decision-making

4.2.1.1 Decision-making principle and policy structure

In order to decide and to adapt the load dynamically to the state of health of the different stacks, a sequential decision policy is carried out. A periodic policy in which the decision is made every time interval of τ hrs is considered. At each periodic decision time $k\tau$ (k is an integer which denotes the decision numbers), the information on the deterioration level, i.e. the overall resistance of each stack is assumed to be available, and the power load allocation is made according both to the deterioration of each stack and to the overall fuel consumption of the multi-stack system.

At each decision time $k\tau$, based on the measured resistance level for each stack $R_{i,obs}^{(k)}$, the conditional probability $P_{i,d}^{(k)}(L_i)$ for this stack to reach a given deterioration level threshold $DT^{(k)}$ at the end of the next period, under a given load L_i, is computed as (similar to Equation (4.5)), see also Figure 4.11):

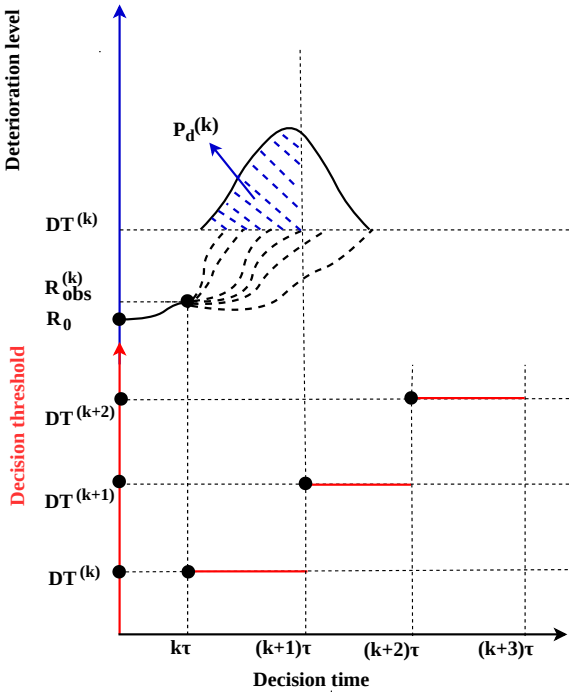

Figure 4.11: Principle of the determination of the conditional probability distribution for the decision threshold hitting time at each decision time

$$\begin{aligned} P_{i,d}^{(k)}(L_i) &= P\left(T_{DT^{(k)}} \leq (k+1)\tau \middle| R_{i,obs}^{(k)}\right) \\ &= P\left(R_i(k\tau) > DT^{(k)} \middle| R_{i,obs}^{(k)}\right) \\ &= \frac{\Gamma\left(\alpha(L_i)\tau, \left(DT^{(k)} - R_{i,obs}^{(k)}\right) \cdot \beta\right)}{\Gamma(\alpha(L_i)\tau)} \end{aligned} \tag{4.12}$$

Note that DT in Equation (4.12) is not a failure threshold for the stack (contrary to Equation (4.5)), but rather a decision threshold used in the decision-making procedure to assess the future deterioration evolution of the considered stack under a given power load L_i, based on its actual deterioration level at the decision time $k\tau$. In order to follow the deterioration evolution of the stack, the value of this decision threshold DT is updated at each decision time step, using the following empirical updating formula:

$$DT^{(k)} = max\left(R_{1,obs}^{(k)}, R_{2,obs}^{(k)}, \cdots, R_{n,obs}^{(k)}\right) + \alpha\beta\tau \tag{4.13}$$

with α is taken in minimal conditions:

$$\alpha = \alpha(L_{min})$$

Using this heuristic formula, the threshold DT is computed as the sum of the maximum of the current deterioration values and the average deterioration increment over the next period

(for the more degrading power load, here L_{min}), which guarantees a value for DT allowing a sensible comparison of the quantities $P_{i,d}^{(k)}(L_i)$.

The decision variables for this decision-making policy are the loads allocated at each stack $L_1, L_2, \cdots, L_n$, adapted at each decision period. We now have to build the objective functions to optimize these decision variables. Based on these deterioration measurements $R_{i,obs}^{(k)}$ and on the estimated $P_{i,d}^{(k)}(L_i)$, two objective functions, function of the decision variables L_i, are evaluated and eventually optimized:

- The first F_{det} is related to the objective of controlling the deterioration by a proper choice of the load allocation among the stacks;
- The second one F_{H_2} corresponds to the objective of controlling the fuel consumption.

At each decision time $k\tau$, the load allocation $\{L_i\}_{i=1,\cdots,n}$ is decided by the optimization of these two objective functions that are detailed in the following subsection. The periodic decision process is repeated until the system failure. Recall that the multi-stack system is said to be failed as soon as one of the stacks failed (or several stacks failed at the same time). In other words, if the greatest resistance of the system stacks exceeds the failure threshold FT, the whole system failed, thus, the condition of system failure is:

$$max(R_{1,obs}^{(k)}, R_{2,obs}^{(k)}, \cdots, R_{n,obs}^{(k)}) > FT \tag{4.14}$$

4.2.1.2 Multi-objective optimization formulation

At each decision time $k\tau$, the problem is stated as a multi-objective optimization problem which consists of the simultaneous optimization of several objective functions, subject to several constraints that determine the feasible set of solutions. Ultimately, the goal is to find a solution on which the decision can evolve with time, as for instance to give priority to one objective function and after some time to give priority to another objective function.

In this work, the objective is to design a decision-making strategy to minimize the life-cycle operation cost of the multi-stack fuel cell system, by acting on two cost key drivers, i.e. prolonging its lifetime (or reducing its degradation) and minimizing its fuel consumption. Two criteria are thus jointly considered - fuel consumption minimization and resistance deterioration minimization, and the Multi-objective Optimization (MOO) problem consists of two conflict objective functions, namely, F_{det} and F_{H_2}. At each decision time, the two objective functions are evaluated for all the combinations of load allocation that are explored by the optimization algorithm and that fits the power load demand (L_d). The fuel cell system deterioration objective function F_{det} is calculated so as to avoid high failure probability and high deterioration level altogether. Additionally, as shown in a previous work [143], it is interesting to maintain the deterioration trajectories grouped so as to avoid early failures. The multi-optimization algorithm returns a set of non-dominated solutions, and the power load allocation to be applied is chosen thanks to a weighted scalarizing function. Thus, one of the objective functions, that is consumption or deterioration, can be favored over the other.

Thus, the MOO problem of an n-stack fuel cell system can be formulated as:

$$\begin{aligned} \underset{L_i}{\text{minimize}} \quad & (F_{det}(L_i), F_{H_2}(L_i)) \\ \text{subject to} \quad & \sum_{i=1}^{n} L_i \geq L_d \\ & L_{\min} \leq L_i \leq L_{\max}\,, (i = 1, \cdots, n) \end{aligned} \tag{4.15}$$

where L_d is the system power load demand, L_{min} and L_{max} are fuel cell stack minimal and maximal output power density loads.

According to Equation (4.2), the overall system fuel consumption F_{H_2} is a function of the considered load allocation $\{L_i\}_{i=1,\cdots,n}$ (i.e., the policy decision variables) and is calculated by:

$$F_{H_2} = \sum_{i=1}^{n} \int f_{H_2}(L_i)\, dt \tag{4.16}$$

The fuel cell system deterioration objective function F_{det} is formulated as a weighted sum of two terms. The first term is a sum of the conditional probabilities $P_{i,d}(L_i)$, see Equation (4.12)). The weights are given by the ratio of the resistance deterioration $R_{i,obs}$ on the total resistance, which allows to put a strong weight to the stacks that have a high deterioration level, and thus avoid failure as much as possible. The second term is the variance of the resistance deterioration levels, so as to avoid early failure of a stack that would deteriorate much faster than the others. The fuel cell system deterioration objective function F_{det} is a function of the considered load power allocation $\{L_i\}_{i=1,\cdots,n}$ (i.e. the policy decision variables) and of the measured resistance levels $\{R_{i,obs}\}_{i=1,\cdots,n}$ (i.e. the deterioration monitoring information) and it is expressed as:

$$F_{det} = \omega_{1f} \frac{\sum_{i=1}^{n} (R_{i,obs} \cdot P_{i,d}(L_i))}{\sum_{i=1}^{n} R_{i,obs}} + \omega_{2f} \sqrt{\frac{1}{n-1} \sum_{i=1}^{n} \left(R_{i,est} - \bar{R}_{\text{est}}\right)^2} \tag{4.17}$$

where $R_{i,obs}$ represents the measured resistance deterioration level for the fuel cell stack i, the corresponding conditional probability is denoted as $P_{i,d}(L_i)$. ω_{1f} accounts for the weight of fuel cell failure probability, ω_{2f} determines the weight of variance of the expected deterioration levels of the different stacks. $R_{i,est}$ is the expected deterioration at next decision time step $(k+1)\tau$:

$$R_{i,est} = R_{i,obs} + \alpha(L_i)\beta \cdot \tau \tag{4.18}$$

The average expected deterioration for n stacks is:

$$\bar{R}_{est} = \frac{1}{n} \sum_{i=1}^{n} R_{i,est} \tag{4.19}$$

Now that the objective functions of the defined MOO problem are defined, the next step is to search for a resolution algorithm to solve the optimization problem.

4.2.1.3 Multi-objective optimization algorithm

To solve the multi-objective problem defined in Equation (4.15), a traditional optimization approach, in which a single objective is optimized subject to a given set of constraints, might not be the most appropriate choice. Instead of finding a solution that optimizes all the objectives at the same time, a Pareto optimal set of solutions can be established, in which an improvement of one objective leads to a deterioration in at least one of the others. The framework of MOO allows handling the trade-off among several conflicting objectives, even with different units. One of the most popular Pareto-based evolutionary multi-objective optimization algorithms, a non-dominated sorting-based Multi-objective Evolution Algorithm (MOEA) called Non-dominated Sorting Genetic Algorithm (NSGA-II), has been successfully applied to many real-life multi-objective optimization problems [150].

Originally inspired by nature selection, the NSGA-II algorithm can be summarized by the following steps:

(1) Generate the initial population of individuals randomly.

(2) Evaluate the fitness of each individual generated in the population.

(3) Repeat the following operations until the termination condition is satisfied.

   a) Select the best-fit individuals for reproduction;
   b) Create new individuals through selection, crossover, and mutation operations;
   c) Reevaluate the individual fitness of new individuals, replace least-fit population with new individuals.

As depicted in Figure 4.12, the algorithm skeleton of NSGA-II stems from classic Genetic algorithm (GA). NSGA-II proposed a modified version of mating and survival selection. A non-dominated sorting and crowding distance are used to determine fitness of individuals, the individuals with better fitness should be retained after selection. Figure 4.12 actually describes the t-th generation of NSGA-II. First, a hybrid population of parent population P_t and offspring population Q_t is formed. Then, the population of R_t is sorted according to non-domination, with a size of $2N_p$. During the the selection process, the elitism is ensured. F_1 collects the solutions of best non-dominated set, emphasized as the best solution (denoted with darker green color in the figure). Keep filling the parent population P_{t+1} with sorted best solutions until it reaches population size N_p. During this process, the crowding distance of non-dominated set F is calculated as criterion to select the best solutions for P_{t+1}. The newly selected parent population P_{t+1} is used to create a new population Q_{t+1} through selection, crossover, and mutation operations. The optimization procedure is stopped when the termination condition is satisfied.

An Achievement Scalarizing Function (ASF) based decomposition method is used to choose the final optimal decision within the obtained Pareto Front [151]. According to the principle of ASF, the minimum ASF values calculated from all solutions are chosen as the final optimal decision.

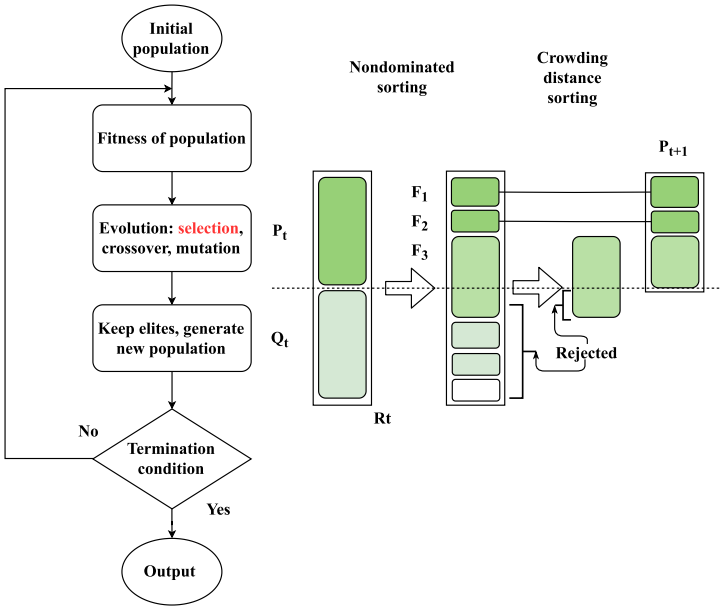

Figure 4.12: Schematic diagram of NSGA-II.

The final implementation of ASF-based decision-making is based on the pymoo library [152]. The ASF function is defined by [153]:

$$ASF(f(x), \Omega, \hat{z}^*) = \max_{j=1}^{M=2} \frac{f_j(x) - \hat{z_j}^*}{\Omega_j} \tag{4.20}$$

where j is either 1 (for F_{det}) or 2 (for F_{H_2}); $f(x)$ is the objective function values; $\hat{z_j}^*$ stands for the utopia ("ideal") point of objective j and Ω_j is the assigned (by the user) weight factor for objective j.

Figure 4.13 shows the Pareto front, i.e. a set of non-dominated solutions is obtained thanks to the NSGA-II algorithm. The values have been normalized between 0 and 1 for two objective functions, F_{det} and F_{H_2}. Finally, the ASF function-based decomposition approach is applied to find the final optimal decision with respect to defined ASF weights Ω. The weights Ω are chosen by the user, according to his preferences and priorities, so that the preferred objective function has the smallest weight. For fuel cells, usually the main preference is to prioritize the control of the system deterioration (i.e. a smaller Ω_1), but two weights vectors representing different preferences among the defined objectives are considered in this study. In Figure 4.13, two different weights are shown. For $\Omega = (0.5, 0.5)$, an equal importance of F_{det} and F_{H_2} is applied to perform decision-making process. To improve fuel cell durability, $\Omega = (0.2, 0.8)$ will be preferred.

4.2.1.4 Post-prognostics decision-making algorithm implementation

The algorithm of the post-prognostics decision-making strategy is presented in Algorithm 1. An internal loop estimates the power load allocation for each stack until the failure threshold

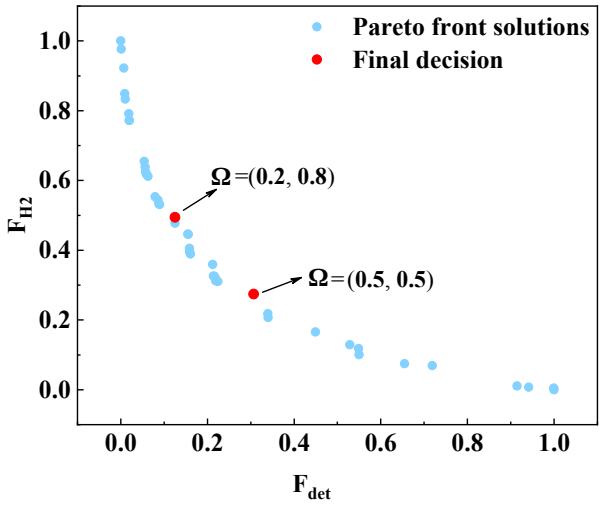

Figure 4.13: Principle of Pareto front and of final decision-making

is reached for one of the stacks. The sequential decision policy adapts the load dynamically to the state of health of the different stacks.

Algorithm 2 shows the evaluation of multi-objective optimization objective function. All values that are needed to calculate F_{det} and F_{H_2} are presented with their calculation equations. Algorithm 2 is called by Algorithm 1 to solve the optimal load allocation decision.

4.2.2 Performance evaluation

Fuel cell system lifetime is defined as in Equation (4.9). For a n-stack fuel cell system, the system lifetime for one run simulation (T_R) is:

$$T_R = min(T_{1,R}, T_{2,R}, \cdots, T_{n,R}) \tag{4.21}$$

where $T_{i,R}$ is the end of lifetime of stack i (first hitting time of FT).

Additionally, a second performance index with respect to fuel consumption should be proposed. However, fuel consumption alone is not suitable, as when the system life is extended, it automatically consumes more fuel. Therefore, a ratio representing the operating time per unit quantity of consumed fuel is used, noted as $Ratio'$. Thus, the greater is the index, the lower is fuel consumption. The mean value of the index is determined with :

$$\overline{Ratio'} = \frac{1}{\overline{Ratio}} = \frac{1}{N}\sum_{i=1}^{N}\{(T_{R,i})/F_{H_2,i}\} \tag{4.22}$$

where the unit is h kg^{-1}. $Ratio$ is the indicator defined in Equation (4.11). $\overline{Ratio'}$ is the average value of this indicator over N simulation trajectories. The same calculation approach is applied for the median system lifetime ($T_{R,med}$) and Median Ratio ($Ratio'_{med}$).

Algorithm 1: Main decision-making loop

Data: FT, DT_0, τ, α, β

Initialization $k = 0$, $DT = DT_0$;

repeat

  % *At each decision time* $k\tau$;

  Measure the resistance deterioration levels $\left(R_{1,obs}^{(k)}, R_{2,obs}^{(k)}, \cdots, R_{n,obs}^{(k)}\right)$;

  Solve the MOO problem through NSGA-II algorithm to return the optimal load allocation $\left(L_1^{(k)}, L_2^{(k)}, \cdots, L_n^{(k)}\right)$;

  % *This optimization step include calls to the evaluation procedure of the objective functions (Algorithm 2) to obtain* $(F_{det}^{(k)}, F_{H_2}^{(k)})$ *for all the combinations of load allocations that are explored by the optimization algorithm*;

  $k = k + 1$;

  % *The system is operated with* $\left(L_1^{(k)}, L_2^{(k)}, \cdots, L_n^{(k)}\right)$ *until next decision step*;

until $max\left(R_{1,obs}^{(k)}, R_{2,obs}^{(k)}, \cdots, R_{n,obs}^{(k)}\right) > FT$ % *System failure*;

4.2.3 Simulation results

4.2.3.1 Simulation settings

The parameters to calculate the objectives (F_{H_2} and F_{det}) are estimated with the 2014 data challenge data [27]. The detailed estimation methods are presented in Chapter 3. Table 4.4 summarized the main parameters used in the simulation. The initial resistance R_0 is 0.1803 $\Omega\ cm^2$.

The resistance deterioration rate is calculated as:

$$D(L) = (C \times (L - 2.3811)^2 + 2.727) \times 10^{-4} \tag{4.23}$$

with

$$C = \begin{cases} 1.6364 & L_{\min} \leq L < L_{nom} \\ 6.77 & L_{nom} \leq L \leq L_{\max} \end{cases}$$

where $D(L)$ represents the deterioration rate of R, L is fuel cell operating power load. L_{min}, L_{nom}, and L_{max} are fuel cell operating power density load for minimal, nominal, and maximal conditions.

With the above simulation parameters, the weights ω_{1f} and ω_{2f} introduced in Equation(4.17) are investigated based on actual simulation effects. According to the grid search-based parameter tuning, $\omega_{1f} = 12$, and $\omega_{2f} = 1.2$ can capture fuel cell deterioration well, enable the decision-making strategy to control the system efficiently. Therefore, these values are used in the post-prognostics decision-making strategy.

Due to the randomness in the proposed Gamma process deterioration model, the policy performance is assessed using Monte Carlo simulation. By the law of large numbers, the

Algorithm 2: Evaluation of the objective functions for multi-objective optimization

Input: Measured deterioration levels $\{R_{i,obs}\}_{i=1,\cdots,n}$; Candidate loads per stack $\{L_i\}_{i=1,\cdots,n}$

Output: $F_{det}(\{R_{i,obs}\}_{i=1,\cdots,n}, \{L_i\}_{i=1,\cdots,n})$, $F_{H_2}(\{L_i\}_{i=1,\cdots,n})$

1 Calculate system fuel consumption objective function: $F_{H_2}(\{L_i\}_{i=1,\cdots,n}) \longleftarrow$ Equation (4.16);

2 Using $\{R_{i,obs}\}_{i=1,\cdots,n}$, calculate the expected deterioration resistances and the average expected deterioration: $R_{i,est} \longleftarrow$ Equation (4.18), $\bar{R}_{\text{est}} \longleftarrow$ Equation (4.19) ;

3 Update decision threshold $DT \longleftarrow$ Equation (4.13);

4 Using $\{R_{i,obs}\}_{i=1,\cdots,n}$ and $\{L_i\}_{i=1,\cdots,n}$, calculate the conditional probabilities $P_{i,d}(L_i)_{i=1,\cdots,n} \longleftarrow$ Equation (4.12);

5 Calculate system deterioration objective function $F_{det}(\{R_{i,obs}\}_{i=1,\cdots,n}, \{L_i\}_{i=1,\cdots,n})$ $\longleftarrow$ Equation (4.16);

6 Return (F_{det}, F_{H_2})

Table 4.4: Key parameters for three-stack system.

Load conditions	L (W cm^{-2})	T_R (h)	v_0	β_0
Minimal	0.804	400	0.028	
Nominal	2.381	1000	0.011	0.024
Maximal	3.084	450	0.025	

sequence of simulated average lifetimes converges to the expected value. For each value of power load demand considered, $L = 6.6$ W cm^{-2} and $L = 7.8$ W cm^{-2}, 8000 independent simulations were performed. Based on these simulated trajectories, an accumulated average system lifetime is calculated. The plots in Figure 4.14 show that when the number of simulation runs is increased to 1500, the average system lifetime estimation converges. Therefore, the following simulation results are analyzed based on 1500 independent simulation runs. Here, the load demand is set based on the basic fuel cell stack parameters in Table 4.4. The demand $L = 6.6$ W cm^{-2} allows three-stacks to both work with lower power than the L_{nom}, whereas $L = 7.8$ W cm^{-2} force at least one of the stacks to work at a power that is larger than L_{nom}.

4.2.3.2 Simulation results for $L_d = 7.8$ W cm^{-2}

Convergence check of NSGA-II algorithm The convergence of the NSGA-II algorithm is analyzed for the designed parameters. A newly proposed running performance metric based on the calculation of Inverted Generational Distance (IGD) is used to estimate the convergence of the NSGA-II algorithm [152], [154]. This running metric shows the difference in the objective space from the initial generation to the current generation. It is suitable for analyzing the optimization process when the true Pareto Front is not known. This running metric is calculated by accumulating the Non-dominated (ND) solutions from initial generation to

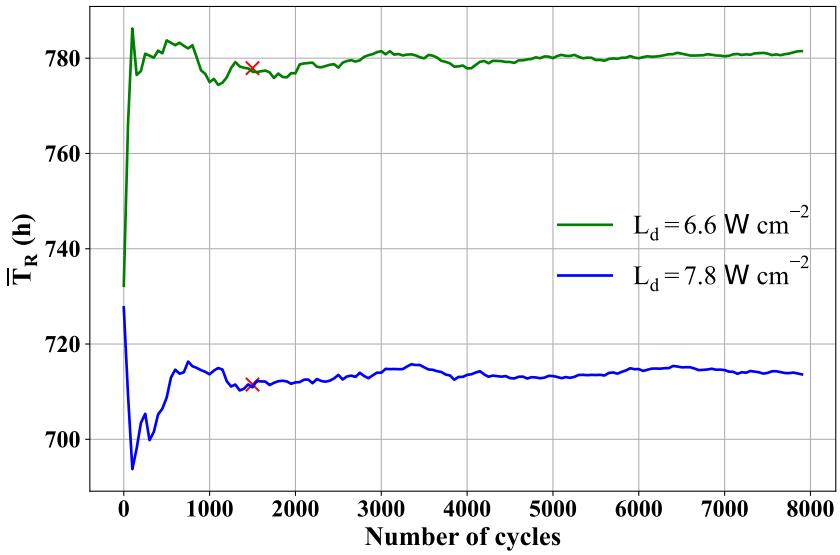

Figure 4.14: Number of Monte Carlo simulation histories

generation (x):

$$\begin{aligned}\Delta f^x &= IGD(\bar{P}^x(t), \bar{P}^x(x)) \\ &= \frac{1}{|\bar{P}^x(x)|} \sum_{i=1}^{|\bar{P}^x(x)|} (\min_{j=1}^{|\bar{P}^x(t)|} \|\bar{P}_i^x(x) - \bar{P}_j^x(t)\|)\end{aligned} \tag{4.24}$$

where x is the accumulated current generation number (here x increment interval is set as 10); $\bar{P}^x(t)$ is the evolving ND set $(0 \leq t \leq x)$ and $\bar{P}^x(x)$ is the ND set of current generation x (normalized). This metric is computed for all past generations.

Figure 4.15 shows the running metric accumulated by a generation step of 10 during one optimization ($L_d = 7.8$ W cm^{-2}, $R_{1,obs} = 0.1903$, $R_{2,obs} = 0.3103$, $R_{3,obs} = 0.2403$ Ω cm^2). A bigger drop in Δf means better improvement for ND solutions. Figure 4.15(a) shows the algorithm gradually improves for past 60 generations. From Figure 4.15(c), it can be seen that the algorithm terminates at the 170-th generation and the Pareto fronts and final decision are plotted in Figure 4.15(d) (the black marked point). The final decisions for weight vector $\Omega = (0.2, 0.8)$ are $(L_1, L_2, L_3) = (2.749, 2.430, 2.621)$ W cm^{-2}.

Main results Now that we have set all required simulation parameters, the next step is to collect the simulated lifetimes from Monte Carlo simulation. Figure 4.16 presents the detailed one-run simulation results for $L_d = 7.8$ W cm^{-2}. Figure 4.16(a) shows the evolution of the overall resistance of each stack and the power load allocation for $\Omega = (0.5, 0.5)$. At time 0 h, the overall resistances of the three stacks are initialized at $R_0 = 0.1803$, and a first post-prognostic decision-making is performed, giving the power load allocation $(L_1, L_2, L_3) = (2.6, 2.6, 2.6)$ W cm^{-2} to be applied. After $\tau = 100$ h of operation, another post-prognostics decision is performed. It can be found out that, though the stacks are assumed to be identical and have the same initial deterioration, their states of health vary. FC2 has the highest

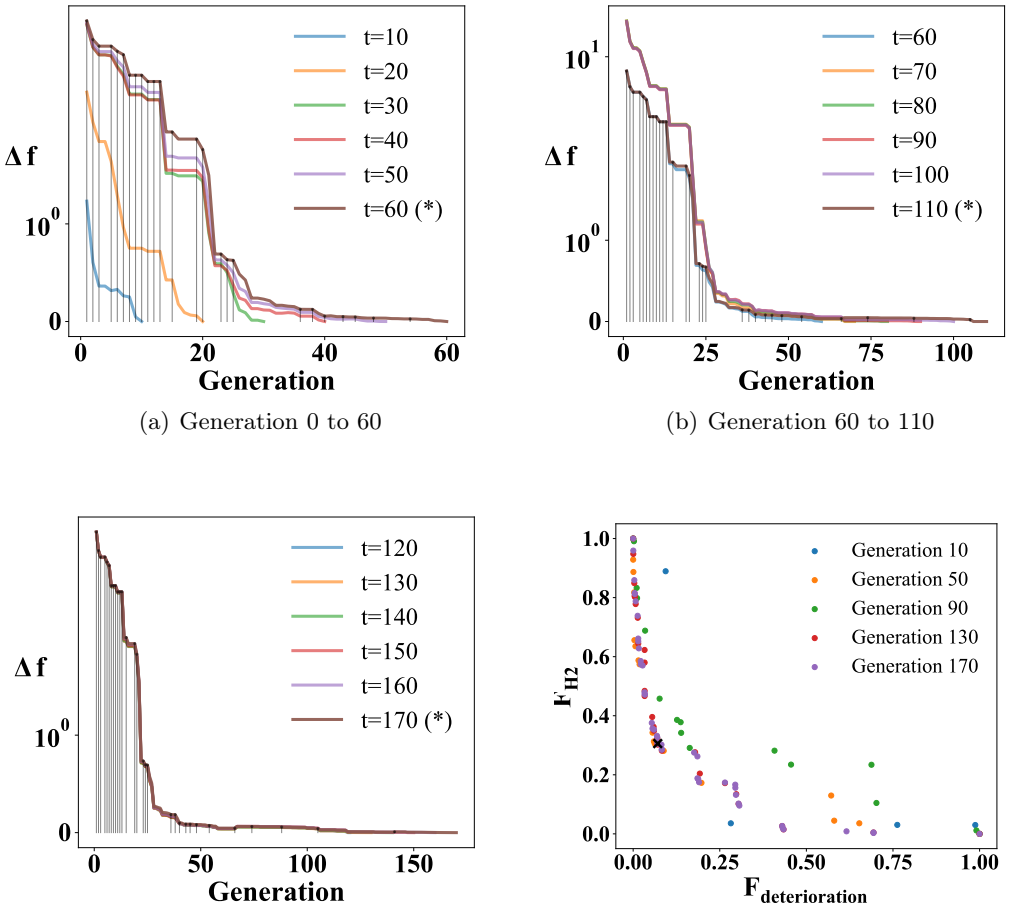

(a) Generation 0 to 60

(b) Generation 60 to 110

(c) Generation 170 to 220

(d) Pareto Front and final decision

Figure 4.15: Convergence of NSGA-II algorithm.

deterioration level, followed by FC3 and FC1. The optimal power loads calculated by proposed post-prognostics decision-making strategy are $(L_1, L_2, L_3) = (2.695, 2.539, 2.565)$ W cm^{-2}. FC1 is assigned to the highest power density to balance the system deterioration and fuel consumption. The third post-prognostic decision is performed at 200 hours. FC3 reaches the highest resistance value. Thanks to the decision-making control, the deterioration rate of FC2 is much slower compared to the previous decision steps. In this case, the measured resistance of FC2 puts a heavy weight on the objective function F_{det} of Equation (4.17), so as to avoid FC2 to deteriorate more. Thus, FC3, which had a lower deterioration at the previous decision step, deteriorates slightly more than FC2. By doing this, the stacks that are more deteriorated can be assigned to a power density load closer to the nominal value, and thus their deterioration slows down. Similar results can be observed for the following decisions. The one-run simulation terminates at 714 h when FC3 reaches FT. From the data in Figure 4.16(b), the control effects are more obviously seen. It is observed that it is not always the same fuel cell that is the most deteriorated though the lifetime is shorter in this case. A bigger

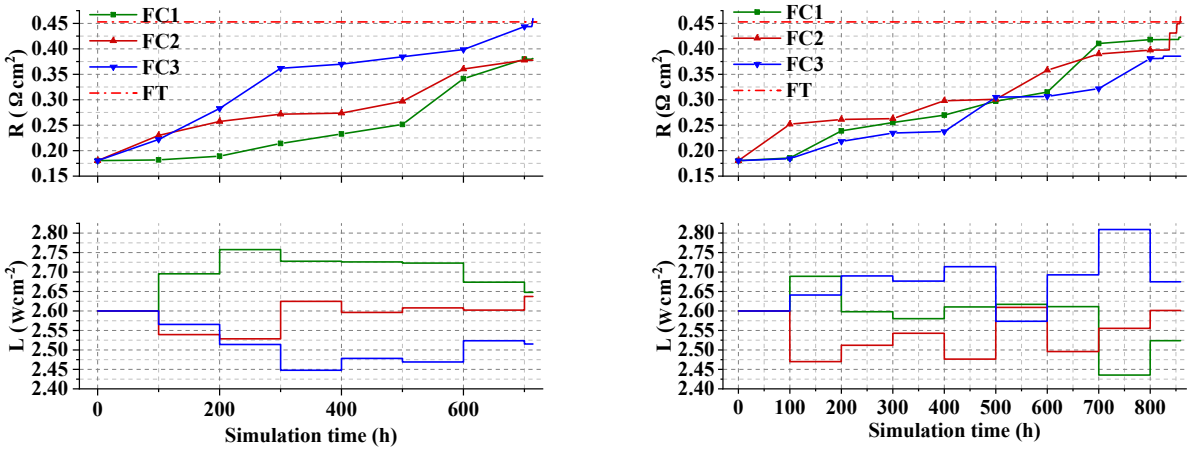

(a) $\Omega = (0.5, 0.5)$ (b) $\Omega = (0.2, 0.8)$

Figure 4.16: One-run optimal load allocation and system deterioration for $L_d = 7.8$ W cm^{-2}.

weight is assigned to control fuel cell deterioration, thereby preventing the most deteriorated fuel cell from further fast deteriorating. This result is consistent with the design of F_{det} as shown in Equation (4.17), and the ASF function.

Figure 4.17 presents histograms of the system lifetime obtained with 1500 runs, for different load allocation strategies. The post-prognostics decision-making with no preference ($\Omega = (0.5, 0.5)$) and with preference for limiting the degradation ($\Omega = (0.2, 0.8)$) are compared with the daisy chain and the average load strategies. The histograms obtained with the post-prognostics decision-making and the average load strategies are mostly distributed in the range [400, 1000] h, whereas the lifetimes for the daisy chain algorithm are mainly distributed in [300, 900] h. For the daisy chain, the poor performance can be explained by the fact that, as two stacks operate at their nominal power density load, the third one adapts to the power load demand and thus operates with conditions that will damage the stack. In addition, one can see in this figure that the distribution for the daisy chain case is more grouped with a peak at 600 h, which is not the case for the other strategies.

Figure 4.18 shows the simulated deterioration trajectories for our strategy and for the average load split strategy with $\Omega = (0.2, 0.8)$. 50-run trajectories are plotted among the 1500 simulated trajectories. It shows that the trajectories simulated with the proposed decision-making strategy tend to be more grouped together and with a lower variance than the one simulated with the average load split strategy. This is the result that was expected with the second term of Equation (4.17), that is the sum of the variance of the resistance deterioration. This helps to avoid situations where one stack in the system deteriorates too fast leading to the failure of the overall system. Such effect is also visible in the previous lifetime histogram.

Further results are given in Table 4.5 which summarizes statistical results for $L_d = 7.8$ W cm^{-2}. In this table, it can be seen that the mean lifetime and the medium lifetime are

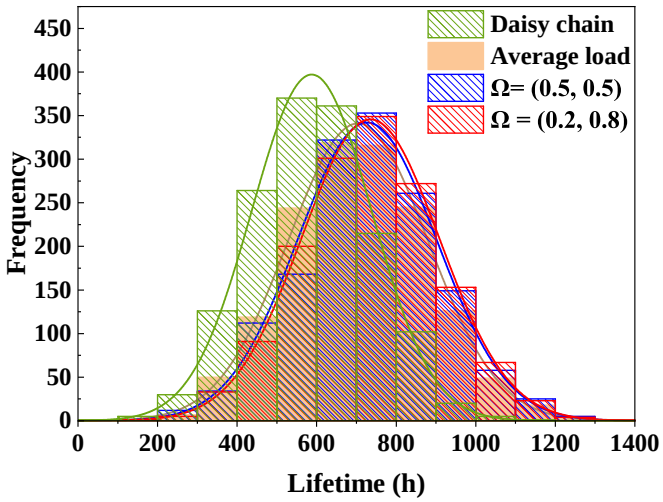

Figure 4.17: Histograms (and fitted Gaussian pdf) of the system lifetime for $L_d = 7.8$ W cm^{-2}, under different load allocation strategies.

better for the proposed strategy, and it confirms that the daisy chain strategy has the worst results. For the proposed strategy, a slight difference can be noticed between the two weights distributions, showing that the $\Omega = (0.2, 0.8)$ allocation leads to a mean lifetime of 735 hours, which is the highest among all simulation cases. The results for the Ratio index, whether it be mean or median, are very close together. The Ratio of the average load split is the highest, that is the largest operating time per quantity of consumed fuel, with both Mean and Median ratio of 21.3603 h kg^{-1}. Then followed by $\Omega = (0.5, 0.5)$, with Mean and Median ratio of 21.3525 h kg^{-1} and 21.3545 h kg^{-1}. These results show that increasing the fuel cell lifetime does not mean that the fuel consumption is exploding accordingly.

Simulations were also conducted for a relatively lower system demand case, $L_d = 6.6$ W cm^{-2}, to check the control effects of the proposed strategy.

Table 4.5: 1500 runs simulation statistic results for $L_d = 7.8$ W cm^{-2}.

Simulations	$\overline{T}_R$ (h)	$T_{R,med}$ (h)	$\overline{Ratio'}$ (h kg^{-1})	$Ratio'_{med}$ (h kg^{-1})
Daisy chain	587	588	21.2522	21.2522
Average load	704	703	21.3603	21.3603
$\Omega = (0.5, 0.5)$	727	727	21.3525	21.3545
$\Omega = (0.2, 0.8)$	735	731	21.3450	21.3501

4.2.3.3 Simulation results for $L_d = 6.6$ W cm^{-2}

This time, a relatively lower demand is set to enable the studied fuel cell be able to work with lower power than the nominal load (L_{nom}). Figure 4.19 provides the detailed one-run results for $L_d = 6.6$ W cm^{-2}. Similarly to $L_d = 7.8$ W cm^{-2}, the overall resistances of the

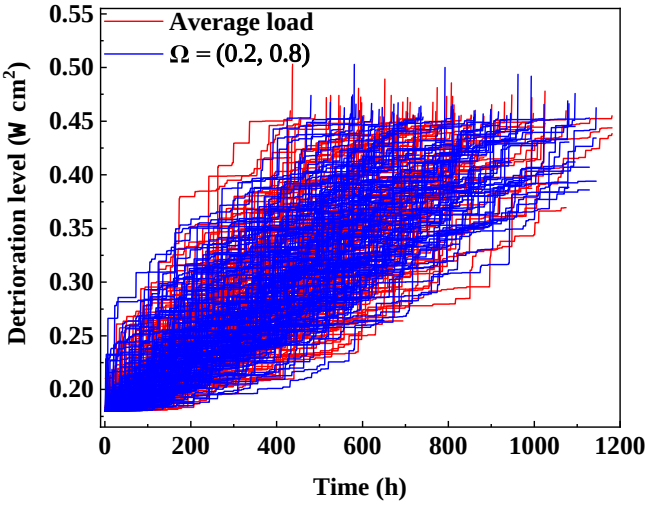

Figure 4.18: System resistance deterioration trajectories (50-run) for $L_d = 7.8$ W cm^{-2}.

stacks are initialized to R_0 at time 0 h. At that time, a post-prognosis decision is carried out, giving the allocation of $(L_1, L_2, L_3) = (2.268, 2.271, 2.269)$ W cm^{-2}. Then at $\tau = 100$ h, a second decision is performed. The most deteriorated fuel cell, FC2, with $R = 0.2746\ \Omega\ cm^2$, is assigned to a power load close to the nominal value to mitigate its deterioration. The optimal allocation is then $(L_1, L_2, L_3) = (2.218, 2.353, 2.197)$ W cm^{-2}. As shown in Figure 4.19(a), FC2 tends to have the highest deterioration during all the operation period. The decision-making strategy lets FC2 operates at a near nominal condition to mitigate its deterioration. While for the stacks with a relatively lower deterioration, the decision-making strategy will assign less desirable operating loads to satisfy the system power demand. However, it can be seen from the deterioration path of FC2 that even though a favorable power is provided, it still deteriorates more rapidly than others because of the randomness. Figure 4.19(b) shows the simulation results when the priority is assigned to deterioration mitigation with $\Omega = (0.2, 0.8)$. It is observed that from 0 to 200 h, the deterioration levels of the three stacks are closed to each other. At 300 h, FC3 has the highest deterioration level, followed by FC1 and FC2. However, from 300 to 600 h, the deterioration rate of FC3 is gradually decreasing and tends to be the lowest. And the deterioration rate of FC2, initially less deteriorated, is increasing. By comparing the results of different Ω values, it is observed that it is not always the same fuel cell that is the most deteriorated though the lifetime is shorter with $\Omega = (0.2, 0.8)$. These results are consistent with those that have been reported in Section 4.2.3.2.

Figure 4.20 shows the histogram of the system lifetime for different strategies both with post-prognostics decision-making or not. This time the histogram allocation of the Daisy chain is similar to the other ones, and the lifetimes are mostly distributed in the range $(400; 1100)$ h. However, the average load split strategy achieves a slightly longer lifetime than the Daisy chain, and the proposed decision-making strategy is even better. Indeed, for $\Omega = (0.2, 0.8)$ and $\Omega = (0.5, 0.5)$, their system lifetimes are more frequently in the range $(800; 1400)$ h than the Daisy chain and average load strategies.

Figure 4.21 presents 50-run deterioration trajectories for $\Omega = (0.2, 0.8)$ and average load

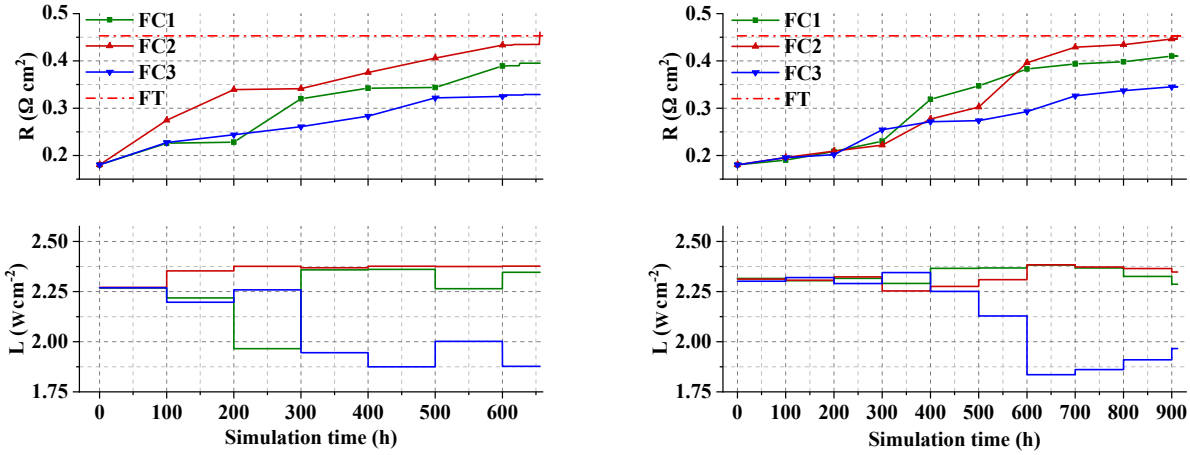

(a) $\Omega = (0.5, 0.5)$ (b) $\Omega = (0.2, 0.8)$

Figure 4.19: One-run optimal load allocation and system deterioration for $L_d = 6.6$ W cm^{-2}.

split strategies. Similar to the results reported in Figure 4.18, the deterioration trajectories with decision-making control appear to be more grouped together than the comparison strategy. The statistical results for $L_d = 6.6$ W cm^{-2} are summarized in Table 4.6. As can be seen, a longer lifetime is achieved for simulations with the decision-making strategy. In addition, the decision strategy that prioritize lifetime with $\Omega = (0.2, 0.8)$ obtains the highest lifetime among the four simulation cases. The Ratio index results are similar to those in section 4.2.3.2, with very close values. These results show that the proposed decision-making strategy can be applied in practice to improve fuel cell system lifetime without consuming far more fuel.

Table 4.6: 1500 runs simulation statistic results for $L_d = 6.6$ W cm^{-2}.

Simulations	$\overline{T}_R$ (h)	$T_{R,med}$ (h)	$\overline{Ratio'}$ (h kg^{-1})	$Ratio'_{med}$ (h kg^{-1})
Daisy chain	759	760	26.3925	26.3925
Average load	774	768	26.5065	26.5065
$\Omega = (0.5, 0.5)$	785	784	25.8183	25.8322
$\Omega = (0.2, 0.8)$	800	804	23.7155	23.8972

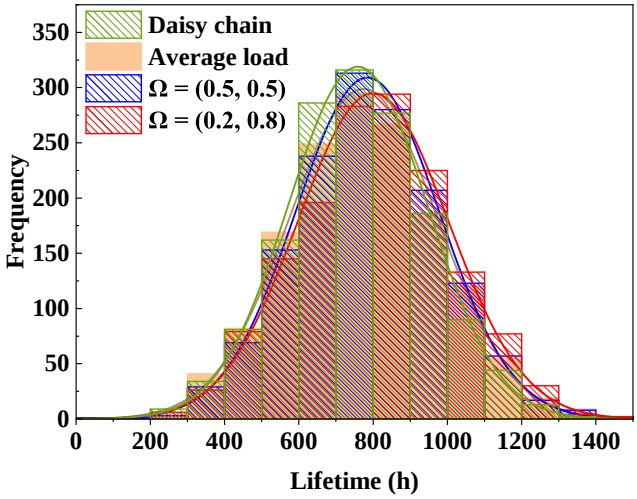

Figure 4.20: Histograms (and fitted Gaussian pdf) of the system lifetime for $L_d = 6.6$ W cm^{-2}, under different load allocation strategies.

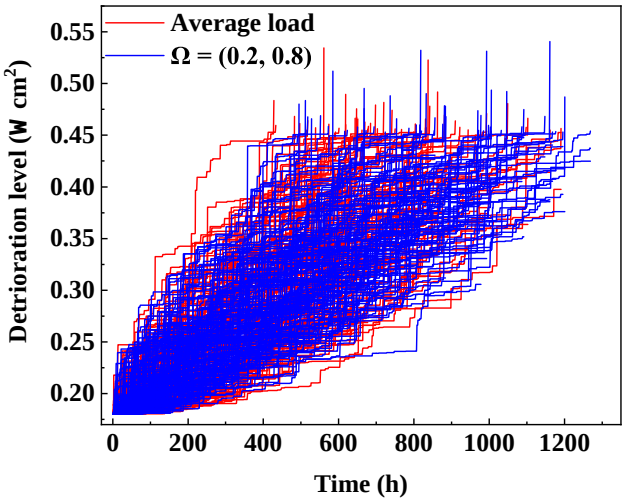

Figure 4.21: System resistance deterioration trajectories comparison for $L_d = 6.6$ W cm^{-2}.

4.3 Conclusion

This chapter investigated the load allocation strategy of an MFC system under constant demand profile. A post-prognostics decision-making strategy is developed for the studied MFC system. The system lifetime is managed through the post-decision control of distributing system power demand among stacks. Both fuel cell deterioration and system fuel consumption are considered in the management strategy. Fuel cell stack resistance is chosen as an HI and its deterioration is modeled through a GP model. A deterioration objective function is then built to access system deterioration during operation, together with fuel consumption objective function. Then, a multi-objective optimization problem is formulated to take the post-prognostic decisions. The simulation results are obtained and analyzed through a 1500-run simulation on a 3-stack fuel cell system. The simulation results of our approach are compared with the results of the daisy chain and average load to validate the control efficiency. As fuel cell are popular in automotive applications which requires a dynamic power demand, the EMS problem of dynamic loads will be studied in the next chapter.

Chapter 5

Multi-Stack Fuel Cells Energy Management Strategy Studies under Dynamic Loads

This chapter focuses on the energy management of MFC systems under dynamic load profiles. Two typical operating management problems are proposed in terms of different load profiles. A deterministic dynamic load profile is defined in the first problem. In this problem, the deterioration of a fuel cell stack is modeled by a GP model. Then, the studied problem is extended by taking into account the randomness in the dynamic load profile and stack-to-stack deterioration variability. Two deterioration-aware EMSs are developed for the proposed problems. This chapter is based on the work presented at the European Safety and Reliability Conference (ESREL), 28 August - 01 September 2022, Dublin Ireland.

Contents

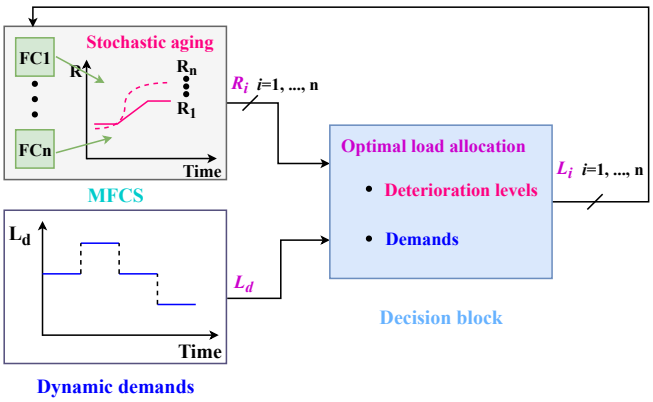

Figure 5.1: Proposed EMS principle.

5.1 Multi-stack fuel cells dynamic load profile energy management problem formulation

The MFC system consists of n parallel connected stacks (Figure 5.1). All the stacks are identical but are providing different load power, denoted $\{L_i\}_{i=1,\cdots,n}$. The global load demand is noted L_d. As the system provides exactly the total amount of power, the contribution of each stack can be written as a part of the global load demand:

$$L_{fci} = \gamma_i L_d, \quad \text{where} \sum_{i=1}^{n} \gamma_i = 1 \tag{5.1}$$

where γ_i is the ratio of allocated load for fuel cell stack i. The input degrees of freedom are the individual stack powers (L_{fci}). The proposed strategy is to decide the optimal load allocation between available stacks such that an extended system lifetime can be achieved.

The external load demand dynamics are considered as a sequence of piece-wise constant values, each value change representing an event after which the optimal load distribution has to be calculated (Figure 5.1).

The problem addressed in this chapter can be divided into two parts. The first part of the problem is to improve a load-dependent model of fuel cell deterioration so as to include dynamical phenomena. Then, the second part is to build an optimal EMS for MFC system based on the proposed deterioration model.

Both load amplitude and load variations are considered in order to build the load-dependent deterioration model (Chapter 3, Equation (3.13)). The fuel cell resistance aging model is expressed as:

$$\Delta R = \Delta R_L + \Delta R_{\Delta L} \tag{5.2}$$

where ΔR is the overall resistance increment. ΔR_L is the load level contribution and $\Delta R_{\Delta L}$ is the load variation contribution to the resistance increment. Note that the deterioration term due to load variation $\Delta R_{\Delta L}$ is expressed with a quadratic form for the optimization convenience.

The Gamma process is used to model the stochastic deterioration of ΔR_L, denoted as:

$$\Delta R_L(t_1, t_2) = R_L(t_2) - R_L(t_1) \sim \text{Ga}(v(t_2 - t_1), \beta) \tag{5.3}$$

The model can be found in the deterioration modeling work reported in Chapter 3 Section 3.2.3.

5.1.1 Dynamic load demand profile

The use of a MFC system is to provide a certain amount of power load over a period of time. As presented in Chapter 1, the FC-DLC is one of the widely used dynamic load profiles for automotive fuel cells. The FC-DLC is used to define our dynamic load profile which is further used in testing various load allocation strategies. Both deterministic and random dynamic load profiles are studied.

Deterministic load profile As shown in Figure 5.3, two types of dynamic loads are used as the global demands for the studied MFC system. Figure 5.3(a) presents the deterministic type power demands. The load profile is obtained by repeating the two load levels with a fixed time interval between two loads as shown in the figure. The two load levels are chosen to represent lower and higher demands applied to fuel cells.

Random load profile A discrete Markov Chain (MC) model is used to construct the random dynamic load profile. To begin, let S denote a (finite) sequence of power demands with c elements $\{x_1, \cdots, x_c\}$. The set S is called the state space, and $x_1, \cdots, x_c$ are the state values. Then an MC X_t (t is discrete) on S is a sequence of random variables on S that have the Markov property, which is expressed as:

$$P\{X_{t+1} = y | X_t\} = P\{X_{t+1} = y | X_t, X_{t-1}, \cdots\} \tag{5.4}$$

where $P(\cdot)$ denotes the probability of the event. The future behavior of the process does not depend on its past but only on its present state. The dynamics of an MC model are fully determined by a set of transition probabilities:

$$P(x, y) = P(X_{t+1} = y | X_t = x)(x, y \in S) \tag{5.5}$$

where $P(x, y)$ is the transition probability of going from state x to state y in one step. $P(x, \cdot)$ is the conditional distribution of X_{t+1} given $X_t = x$. We can view the transition probability between different states as a Markov matrix P_c where

$$P_{i,j} = P(x_i, x_j)\ 1 \leq i, j \leq n \tag{5.6}$$

And P_c satisfies:

- each element of P_c is non-negative, and

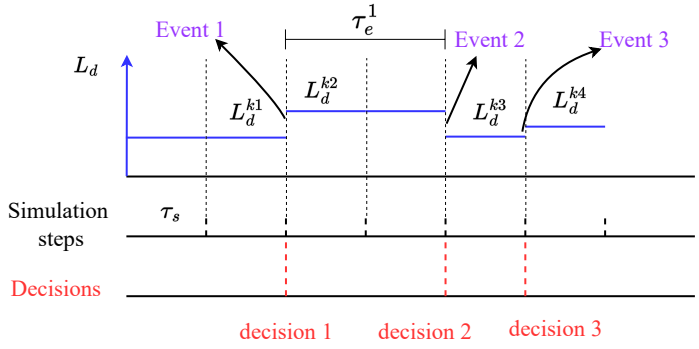

Figure 5.2: Schematic diagram of generating random load profile.

- each row of P_c sums to 1.

Then we can define (generate) a MC X_t as follows:

- Draw an initial state X_0 from specified distribution.
- For each $t = 0, 1, \cdots$, draw X_{t+1} from the transition probability matrix $P(x, y)$.

Assuming that the load profile of a fuel cell system $L_d(t)$ can be described as a MC model with Markov transition matrix P_{tr} and all possible states L_{ds}. Then we can obtain a random dynamic load profiles for MFC systems. A diagram is sketched in Figure 5.2 to demonstrate the generation of such random load profile. At each simulation step τ_s (equivalent to the discrete time step t defined in Equation (5.4)), the next state is drawn from transition probability matrix $P(x, y)$. In the case of a deterministic power demands, the duration of a event (τ_e) is fixed, however this is not the case in random load profile. For random load profile, the load demand level of each simulation step τ_s is generated through a Markov Chain model, thus the load change event duration varies from time to time. This is demonstrated in the figure as the event duration of Event 1 is $2\tau_s$ whereas the duration of the following event equals to τ_s.

Figure 5.3(b) shows a realization of a random type load profile by taking:

$$\mathbf{P_{tr}} = \begin{bmatrix} 0.1 & 0.35 & 0.35 & 0.2 \\ 0.35 & 0.1 & 0.35 & 0.2 \\ 0.2 & 0.35 & 0.1 & 0.35 \\ 0.2 & 0.35 & 0.35 & 0.1 \end{bmatrix}, L_{ds} = [2.9, 4.1, 5.8, 7.0] \tag{5.7}$$

where L_{ds} defines all possible load demands. $\mathbf{P_{tr}}$ stands for the transition probability matrix. This dynamic loads include four levels of demands which are adapted from the FC-DLC cycle. The load percentage of 100%, 83.3%, 58.3%, and 41.7% (with respect to L_{max}) are selected. This load profile contains lower to higher power loads which is used as a typical dynamic load profile.

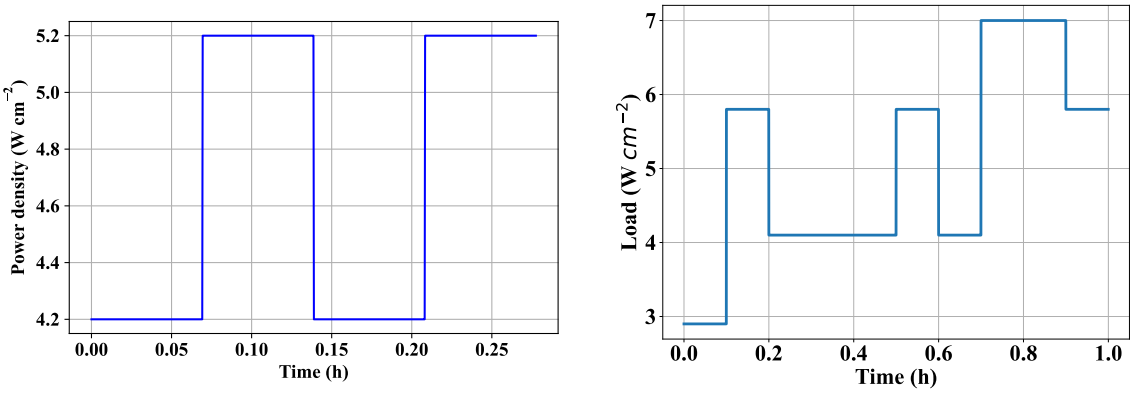

(a) Deterministic load demands

(b) Random load demands

Figure 5.3: Dynamic load profiles

5.1.2 System lifetime and failure definition

For a multi-stack system, the system failure is defined as the end of the system's ability to supply the external global load demands. Thus, the failure of one stack does not necessarily correspond to the MFC system failure, as long as the external power load demand can be provided by the other stacks. In this chapter, the system lifetime is calculated by the Equation (4.9) (Chapter 4).

5.2 Energy management under deterministic dynamic loads

This section focuses on the load allocation strategy of an MFC under deterministic type load demands. The deterioration model of studied MFC system is taken from Equation (5.2). The GP model is used to model fuel cell resistance deterioration due to load magnitude.

5.2.1 Energy management strategy

5.2.1.1 Decision-making principle

The external load demand dynamics is considered as a sequence of piece-wise constant values, each value change corresponding to what will be called hereinafter as an "event". The decision-making process is event-based, i.e. the load allocation is determined at each new event. We assume here that several future events are known in advance.

Figure 5.4 depicts the diagram of the event-based decision-making process with m future known events. The current event E^0_{ind} is the beginning of current decision. The decision horizon ranges from E^0_{ind} to E^m_{ind}. τ^j_e is the time length of event j ($j = 0, \cdots, m-1$). The

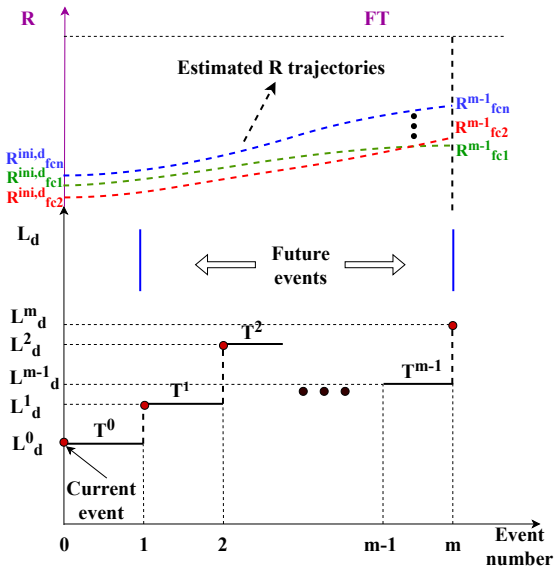

Figure 5.4: Principle of the proposed decision procedure.

system is required to produce exactly the amount of external load demands, and the output power of each stack is constrained within the fuel cell production range, i.e. from L_{min} to L_{max}. The external load demand of event j is denoted as L_d^j. Note that the initial load demand which is equal to the load demand at previous event, denoted as $L_d^{ini,d}$.

$\{R_{fci}^{j-1}\}_{i=1,\cdots,n}$ are the resistance levels of all stacks at the beginning time of event j which is assumed to be measured. Note that the initial resistance value for the first event $m = 0$ is denoted as $R_{fci}^{ini,d}$. The average deterioration levels at decision m are estimated using Equation (5.2). The future global deterioration weighted by the distance of current deterioration to the failure threshold FT is defined as the optimization index J. With all combinations of load allocations $\gamma_i L_d^j$, the optimal decision is decided by minimizing J. The calculation of J will be derived in the following Section 5.2.1.2. In this way, the global system deterioration is balanced among the stacks which helps to improve system lifetime.

5.2.1.2 Objective function formulation

The objective function is formulated so as to minimize the resistance increments along the decision-making horizon. Then the proposed dynamic optimization problem is formulated as:

$$\begin{aligned}
\underset{\{\gamma_i^j\}_{i=1,\cdots,n}}{\text{minimize}} \quad & J(\{\gamma_i^j\}_{i=1,\cdots,n}) = \sum_{i=1}^{n} \omega_i \{(\Delta R^0_{\Delta L,i})^2 + \Delta R^0_{L,i} + \sum_{j=1}^{m-1} (\Delta R^j_{L,i} + (\Delta R^j_{\Delta L,i})^2)\} \\
\text{subject to} \quad & L_{min} \leq \gamma_i^j L_d^j \leq L_{max}, \sum_{i=1}^{n} \gamma_i^j = 1 \\
& \Delta R^j_{L,i} = D(\gamma_i^j L_d^j) \cdot \tau_e^j \\
& \Delta R^0_{\Delta L,i} = K|\gamma_i^0 L_d^0 - \gamma_i^{ini,d} L_d^{ini,d}| \\
& \Delta R^j_{\Delta L,i} = \sum_{j=1}^{m-1} K|\gamma_i^{j+1} L_d^{j+1} - \gamma_i^j L_d^j|, \quad j = 1, \cdots, m-1
\end{aligned} \tag{5.8}$$

where L_d^j defines the external dynamic load demands; γ_i^j is the load allocation ratio for FCi at decision time j, and $\gamma_i^{ini,d}$ is the initial load allocation ratio of stack i at each decision. K is given in Equation (3.16).

The distance of the deterioration level to the preset failure threshold FT is leveraged to formulate the weight factor ω_i:

$$\omega_i = \frac{1/(FT - R_{fci}^{ini,d})}{\sum_{i=1}^{n} 1/(FT - R_{fci}^{ini,d})} \tag{5.9}$$

The defined weight terms (Ω_i) aim to balance the aging of all stacks, i.e., by adjusting the value of weights to force the less deteriorated stacks to operate under less desirable conditions so as to allow the more deteriorated stacks to work at relatively more desirable conditions. More details on the system lifetime control effects will be further discussed in Section 5.2.2.

5.2.2 Results for Gamma process model under deterministic loads

5.2.2.1 Monte Carlo simulations settings

The studied MFC system is assumed to consists of two identical stacks ($n = 2$). Table 5.1 summarizes the key parameters of the stacks. The other chosen parameters are $\beta_0 = 4.4\times10^{-4}$, $FT = 0.2775\ \Omega\ cm^2$, and $R_0 = 0.1803\ \Omega\ cm^2$.

To study the performances of the EMS, deterioration trajectories with different variances but the same average trend are simulated. Hence, the initial shape and scale parameters (α^{ini}, β^{ini}) of the studied Gamma process are modified by introducing a constant ℓ (refer to Equation (3.11), Chapter 3). Here $\ell = 5, 10, 20, 30$ so as to gradually increases the deterioration trajectory variance.

Table 5.1: Fuel cell stack parameters.

Load conditions	L (Wcm^{-2})	Lifetime (h)	α_0
Minimal	0.8035	100	2.227
Nominal	2.3811	1788	0.125
Maximal	3.084	100	2.227

In addition, this thesis also investigates the influence of deterioration imbalance between the stacks. This is done by assigning different initial resistance values (R_{fc1}^{ini} and R_{fc2}^{ini}):

$$R_{fc1}^{ini} = R_0 + \Delta R_0, R_{fc2}^{ini} = R_0 \tag{5.10}$$

The modified increment terms of $\Delta R_0 = 0.0, 0.01, 0.02, 0.03\ \Omega\ cm^2$ are studied.

A two-stack fuel cell system is operated to provide a deterministic type load profile as presented in Figure 5.3(a). To formulate the optimization objectives, one future event is being considered (i.e. $m = 1$) in the objective function. The Sequential Least-squares Programming (SLSQP) algorithm is used to solve the optimization problem. Due to the stochastic behavior of the stack aging, modeled by a Gamma process, the system lifetime is estimated with Monte Carlo simulations. The simulation of the system from the beginning of use till system failure (denoted as one-run) is repeated N times (i.e., a realization of N simulation runs), obtaining N system lifetime samples. Then the average system lifetime ($\overline{T}_{R,dec}$) is estimated by the average of those lifetime samples. According to the simulations, $N = 300$ ensures the convergence of $T_{R,dec}$.

The results are compared with the classic average load split method, which distributes the overall load demand evenly among stacks.

5.2.2.2 Performance indicators

Lifetime-related indicators are established to assess the performance of the proposed strategy. Based on the two basic lifetime indexes introduced in Chapter 4, i.e., the mean system lifetime $\overline{T}_R$ and median system lifetime $T_{R,med}$, this section further introduced three extra lifetime-related indexes.

The first indicator ($\Delta T_{R,pct}$) gives the relative improvement in lifetime compared to the average load split strategy which is computed by:

$$\Delta T_{R,pct} = \frac{\overline{T}_{R,dec} - \overline{T}_{R,ave}}{\overline{T}_{R,ave}} \times 100\% \tag{5.11}$$

where $\overline{T}_{R,dec}$ is the mean simulated lifetime over N trajectories that simulated by proposed load allocation strategy, $\overline{T}_{R,dec} = \frac{\sum_{i=1}^{N} T_{i,R,dec}}{N}$. $T_{i,R}$ is simulated lifetime of trajectory i. $\overline{T}_{R,ave}$ is the mean simulated lifetime of average load method. The second indicator $T_{R,pct}^{+}$ represents,

in percentage terms, the number of the simulated lifetimes that are higher than those of the average split method. Let N^+ denote the number of lifetimes where the lifetime obtained by the load allocation decision ($T_{R,dec}$) is larger than the results of average split ($\overline{T}_R$). Then the proposed indicator is written as:

$$T^+_{R,pct} = N^+/N \times 100\% \tag{5.12}$$

Due to the complexity of obtained system lifetime distribution, it would be necessary to compare obtained lifetimes with mean lifetime in average split methods ($\overline{T}_R$). This may offer extra information in terms of the effectiveness of the proposed strategy. The third performance indicator compares the simulated lifetimes to mean lifetime of average split method, which writes:

$$\begin{aligned} T^{ave}_{R,pct} &= \frac{N^+_{ave}}{N} \times 100\% \\ T^{dec}_{R,pct} &= \frac{N^+_{dec}}{N} \times 100\% \end{aligned} \tag{5.13}$$

where N^+_{ave} stands for the number of lifetimes where the lifetime obtained by the average split is larger than $\overline{T}_{R,ave}$. N^+_{dec} denotes the number of the lifetime obtained by the load allocation strategy that is larger than $\overline{T}_{R,ave}$.

5.2.2.3 Simulation results

Convergence of the SLSQP algorithm The proposed load allocation decision problem is formulated as an nonlinear constrained optimization problem. SLSQP methods solve a constrained nonlinear optimization problem in an iterative manner. The main optimization parameters for SLSQP solver are the maximum number of iterations and the precision goal for the objective function in the stopping criterion.

The SLSQP is selected as the optimization solver for solving the optimization problem (Equation (5.8)). The convergence of SLSQP algorithm is investigated on a single step optimization. In this optimization, the resistance values of two stacks are set as $R_{fc1} = 0.2003\ \Omega\ cm^2$ and $R_{fc2} = 0.1803\ \Omega\ cm^2$. The power demand is defined as 5.2 W cm^{-2}. The maximum number of iterations of SLSQP solver is set as 100, and the precision goal for the objective function is set as 1×10^{-8}. This optimization solver related parameters are set to ensure a reasonable optimization time as well as convergence. The objective function values J_{obj} are plotted in Figure 5.5. It is seen that the SLSQP ensures a quick convergence after 8 evaluations (final objective function values is 0.048). The optimal load allocations are $L_{fc1} = 2.57$ W cm^{-2}, $L_{fc2} = 2.63$ W cm^{-2}.

Analysis of the proposed strategy behavior on a single realization Firstly, the decision strategy behavior is examined on a single simulated deterioration path, according to the predefined parameter settings (Section 5.2.2.1), $\ell = 5, \Delta R_0 = 0.01\ \Omega\ cm^2$ are chosen, denoted as Case 1.

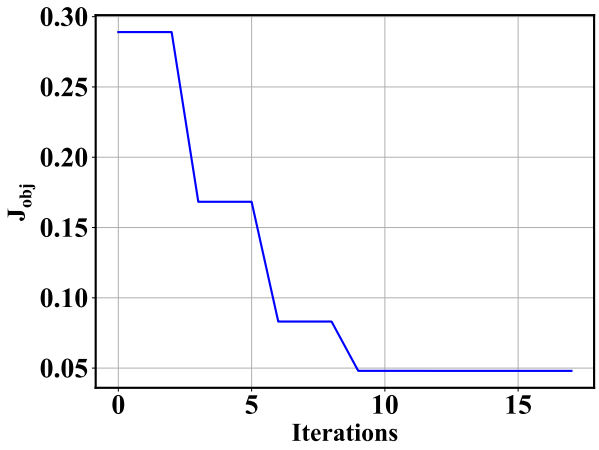

Figure 5.5: Convergence check of the SLSQP algorithm.

Figure 5.6 presents the overall resistance values and the optimal allocation decisions made for four events in Case 1. Consider event number 3, it is noticed that for the previous two decisions, the FC1 is more deteriorated. And the aging trend is reversed for the last two decisions (Figure 5.6 (a)). Combing with the optimal allocations (Figure 5.6 (b)), it is confirmed that our strategy lets the more deteriorated stacks operate at relatively more desirable conditions than the ones that are less deteriorated. According to the recorded deterioration, the sudden increment of R_{fc2} is due to the load effect, i.e. $\Delta R_{fc2,L}$ (increased 4.185×10^{-3} Ω cm^2 from event number 2 to event number 3 while the other increments are nearly zero) which confirms the stochasticity in ΔR_L. This stochasticity is investigated by a stochastic Gamma process with different initial resistance and increment variance to account for individual variability in an MFC system.

Figure 5.7 shows the overall load decisions distribution of our strategy. It can be seen that most of the allocation decisions are distributed between 2 and 2.25 W cm^{-2} on the left side and from 2.5 to 2.75 W cm^{-2} on the right side. Instead of assigning demands with a fixed average split, our strategy optimally decides the load allocations conditionally to the estimated system resistance at the decision stage.

Overall performance analysis Let now examine the results on $N = 300$ simulation histories. Figure 5.8 presents the lifetime histograms and corresponding fitted Gaussian Probability Distribution Functions (PDFs) for $\Delta R_0 = 0.01$ Ω cm^2 and different deterioration variances. In all these figures, the PDF of our strategy presents a higher mean value than the average split strategy, proving thus that an extended lifetime is achieved. Additionally, the PDFs curves widen as the value of ℓ increases, i.e., as the variance of stack aging becomes larger. According to the definition of system lifetime, a greater variance in the R trajectories will widen the interval of the first-hitting-time of FT and thus that of the simulated lifetimes as well. In Figures 5.8 (a), (b), and (c), it is seen that the PDF curve of our strategy is more centered on the mean than the one of the average split method. However, in Figure 5.8 (d), the two PDF curves are similar in terms of the PDF curve width. This is caused by the

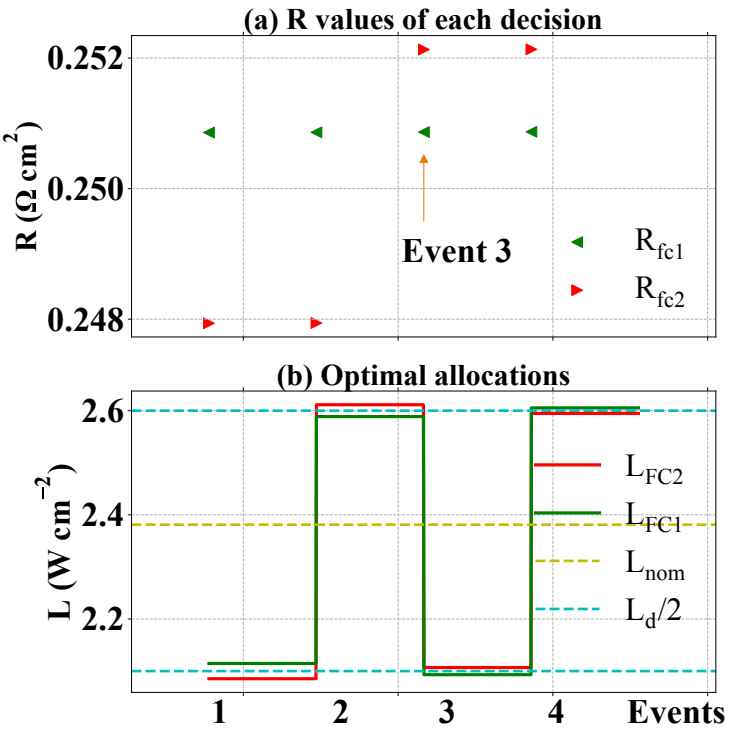

Figure 5.6: Case 1: four events.

growing variance in R trajectories. The calculated standard deviation results further justify the observations. In Figure 5.8 (a), the standard deviation of our strategy is 47.52, whereas that of the average split is 66.37. The standard deviation of our method (137.61) is slightly bigger than the average split (133.67) in Figure 5.8 (d). In the obtained results, the histograms results of $\Delta R_0 = 0.0, 0.02, 0.03$ ($\Omega\ cm^2$) show similar trends.

The two proposed lifetime-related performance indicators are computed and listed in Tables 5.2 and 5.3. In general, the $\Delta T_{R,pct}$ results of the groups with initial increment (i.e. $\Delta R_0 > 0$) are higher than the group with identical initial resistance. This proves the efficiency of the proposed strategy in dealing with imbalanced deterioration in MFC. Moreover, in Table 5.2, the $\Delta T_{R,pct}$ values are monotonically increasing as ℓ increases. In comparison, the value of $\Delta T_{R,pct}$ shows a fluctuation trend. These results show that the R trajectory variance and deterioration level of all stacks have a mutual influence on the lifetime control effects. Setting a bigger variance will vary the resistance values of all stacks. The proposed strategy tries to reverse this imbalanced aging through optimized load allocations, which helps to decrease the overall system deterioration, thus improving the lifetime. But in the cases where ΔR_0 is much bigger or the variance is too high, it will limit the control effects of the proposed strategy. These results encourage us to study the behavior of the proposed strategy under different variance levels and variability situations (e.g. consider the random effects in the Gamma process).

The results of lifetimes comparison percentage $T^{+}_{R,pct}$ in Table 5.3 confirm that generally

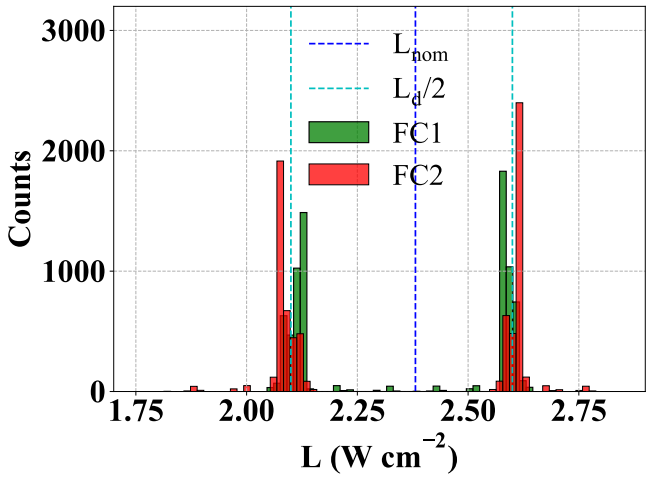

Figure 5.7: Overall load allocation histogram for Case 1.

Table 5.2: Simulation results for $\Delta T_{R,pct}$.

ΔR_0 ($\Omega\ cm^2$)	$\Delta T_{R,pct}$ (%)			
	$\ell = 5$	$\ell = 10$	$\ell = 20$	$\ell = 30$
0.0	5.8	6.3	6.7	15.1
0.01	6.5	8.9	12.8	13.9
0.02	9.6	12.4	10.3	13.7
0.03	17.6	18.7	10.7	14.8

over 60% lifetimes simulated with allocation decision are better than the average split method. In some cases, $T^{+}_{R,pct}$ even reaches 85%.

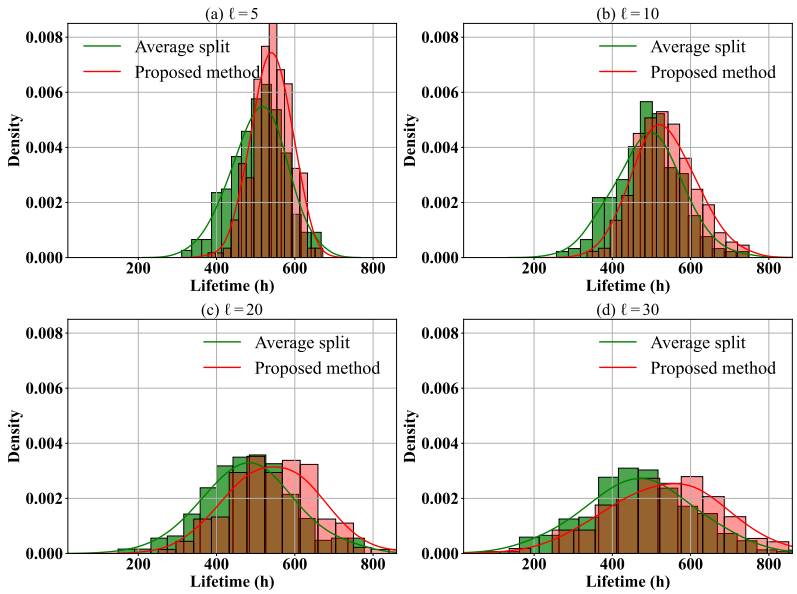

Figure 5.8: Lifetime histograms (and fitted Gaussian pdf) for $\Delta R_0 = 0.01\ \Omega\ cm^2$.

Table 5.3: Simulation results for $T^+_{R,pct}$.

$\Delta R_0\ (\Omega\ cm^2)$	$T^+_{R,pct}\ (\%)$			
	$\ell = 5$	$\ell = 10$	$\ell = 20$	$\ell = 30$
0.0	66.7	63.5	59.3	67.3
0.01	66.0	66.7	62.3	66.7
0.02	74.0	69.0	61.7	64.3
0.03	85.7	75.7	61.0	61.3

5.3 Energy management under random dynamic loads

In the above discussed problem, we have developed an EMS under a deterministic dynamic load profile. A GP-based deterioration model is adapted to model the deterioration of the studied MFC system. In this section, we further extend the developed EMS to a random dynamic load scenario, and the stack-to-stack deterioration variability is included and the random-effect models (Chapter 3) are tested. The random load profile remains the same as depicted in Section 5.1.1.

First, the influence of the random loads on the proposed management strategy is investigated. Different from the deterministic type loads, the event duration for the random loads may vary for different events. And this event duration is considered as information that may be known or unknown at each decision. The study of qualifying the value of known load profile information is thus studied. Another related problem is to check the possibilities of improving the performance of the event-based decision-making strategy. For the event-based decision-making strategy, each load allocation decision is triggered by a load change event. Then, one question on improving this event-based decision is: Would it be beneficial for overall system life if a decision is scheduled before a load change event if current event duration is relatively long? Finally, the EMS is tested for GP with three random effects-based GP models under a random dynamic load profile. The efficiency of the proposed strategies are compared with the classic average load split method.

5.3.1 Energy management strategy

The EMS (load allocation strategy) is developed based on an event-based decision procedure as demonstrated in above Section 5.2.1. The main difference is that a random dynamic load profile is used as the system power demands. The basic event-based decision-making procedure is depicted in Figure 5.2. The load allocation decision is scheduled whenever a load change event is detected. For instance, at decision 1, a load demand change is detected, i.e., loads changed from L_d^{k1} to L_d^{k2} (both values are assumed to be known).

In fact, the event duration is considered as the information of a random load profile. It can either be known (request from fuel cell operator or qualified with high-cost estimation techniques) or be unknown at the decision stage. When the event duration is unknown, an expected event duration ($\overline{\tau}_e$) estimated from the MC model is used in the decision-making process. Assuming we are at decision k, and we know exactly the load demand level $L_d^k, L_d^k \in L_{ds}$. Then the expected duration of current event $\overline{\tau}_e$ is computed by:

$$\begin{aligned} \overline{\tau}_e &= \sum_{i=0}^{\infty} \tau_s (i+1) P^i (1-P) \\ &= \tau_s \tfrac{1}{1-P} \end{aligned} \tag{5.14}$$

where τ_s is the discrete simulation time step used in Markov Chain model. P is the probability of staying at L_d^k which is defined in P_{tr}.

Table 5.4: Main fuel cell parameters used in the simulation.

Load conditions	L (W cm^{-2})	$\overline{T}_R$ (h)	v_0	β_0	FT (Ω cm^2)	R_0 (Ω cm^2)
Minimal	0.42	200	1.114			
Nominal	2.381	1788	0.125	4.4×10^{-4}	0.278	0.1803
Maximal	3.869	200	1.114			

5.3.2 Simulation settings

Table 5.4 summaries the main parameters of the investigated MFC system. The MFC system consists of two identical fuel cell stacks (R_{fc1}^{ini}=R_{fc2}^{ini}=R_0). The basic Monte Carlo simulations confirm that 600 samples can obtain a convergence on the average system lifetime. Thus, the number of simulation trajectories N_{trj} is set to 600 in the following simulations.

The random load profile as shown in Figure 5.3(b) is generated through a Markov Chain model as defined in Equation (5.7). The simulation time step (τ_s) is set as a constant value of 360 s.

5.3.3 Simulation results

5.3.3.1 Investigation on load information and decision schedule

Information on load profile First, the random load profile presented in Figure 5.3 is used to define the overall load demands. The expected event duration is calculated based on the MC model for all possible load levels. Based on Equation (5.14) and the MC model define in Equation (5.7), the expected event duration for four possible load demands is all equal to 400 s. Then, a comparison study of using the expected event duration and the true event duration in proposed strategy is performed by Monte Carlo simulations. The GP and GP-RE models are selected to model fuel cell resistance deterioration (both the classic Gamma process model and random-effect model are considered). According to previous simulation results, $\ell = 10$ is chosen in the GP and GP-RE model for tuning the variance of resistance deterioration trajectories. The lifetime results are summarized in Table 5.5. The lifetime improvement percentage ($\Delta T_{R,pct}$) in the table is calculated by:

$$\Delta T_{R,pct} = \frac{\overline{T}_{R,exact\ duration} - \overline{T}_{R,expect\ duration}}{\overline{T}_{R,expect\ duration}} \times 100\% \tag{5.15}$$

where $T_{R,exact\ duration}$ represents the average lifetime simulated with known event duration, $T_{R,expect\ duration}$ is the average lifetime simulated without known exact event duration. $\Delta T_{R,pct}$ qualifies the value of having load profile information in terms of system lifetime improvement. A higher $\Delta T_{R,pct}$ represents a high value in knowing the event duration.

It is seen from the $\Delta T_{R,pct}$ results that for both GP and GP-RE models the lifetime

improvements are relatively small. This result shows that the proposed strategy is robust to load profile information. Not knowing the exact event duration is not causing significant loss of the EMS strategy performance.

Checking the influence of scheduling extra decision The next step is to explore the possibilities of improving system lifetime results by scheduling an extra decision before the occurrence of the next load change event. A relatively less dynamic load profile (denoted as load cycle 2) is defined for comparing with the original load profile (Equation (5.7), load cycle 1). The new load profile is generated by:

$$\mathbf{P_{tr}} = \begin{bmatrix} 0.7 & 0.1 & 0.15 & 0.05 \\ 0.05 & 0.8 & 0.05 & 0.1 \\ 0.05 & 0.05 & 0.85 & 0.05 \\ 0.05 & 0.15 & 0.2 & 0.6 \end{bmatrix}, L_{ds} = [2.9, 4.1, 5.8, 7.0] \tag{5.16}$$

Figure 5.9 shows the shape of two load cycles defined above. It is observed that the load cycle 2 is relatively less dynamic compared with the load cycle 1. This is decided by the transition matrix defined in the MC model. The probability of staying at current state in Equation (5.16) is much larger than those in Equation (5.7). Therefore, load cycle 2 presents a relatively longer event duration.

Here, the comparison strategy is formulated by adding an extra decision for previous event-based decision strategy when the event duration τ_e exceeds a predefined duration threshold $\tau_{e,th}$, namely, $\tau_e \geq \tau_{e,th}$. According to the simulation results, $\tau_{e,th}$ is taken as $10\tau_s$. If the event duration condition is satisfied, a decision will schedule at the middle of the event duration. Notice that here we are assuming that the event duration τ_e is known for current event.

The lifetime comparison results of load cycle 1 and load cycle 2 are summarized in Table 5.6, and Table 5.7, respectively. The lifetime improvement percentage in the table is calculated by:

$$\Delta T_{R,pct} = \frac{\overline{T}_{R,extra\ decision} - \overline{T}_{R,no\ extra\ decision}}{\overline{T}_{R,no\ extra\ decision}} \times 100\% \tag{5.17}$$

where $\overline{T}_{R,extra\ decision}$ stands for the average lifetime obtained from the proposed strategy with extra decision, and $\overline{T}_{R,no\ extra\ decision}$ is the average lifetime obtained from the event-based load allocation strategy where the decisions are scheduled at each load change event.

For the GP deterioration models, no obvious improvement is observed in both load cycles. By contrast, a relatively obvious difference is observed for the random-effect model, i.e. GP-RE. The average lifetime is improved by 3.15% when adding extra decision under load cycle 1. This value is increased to 9.46% for load cycle 2. These results verify the efficiency of our strategy for the random-effect deterioration model. Moreover, for the load profile with relatively long event duration, the extra decision helps to re-allocation the loads among stack to balance overall system deterioration such that an improved system life can be obtained. It is verified in previous Chapter 3, the GP-RE model considers the deterioration variability

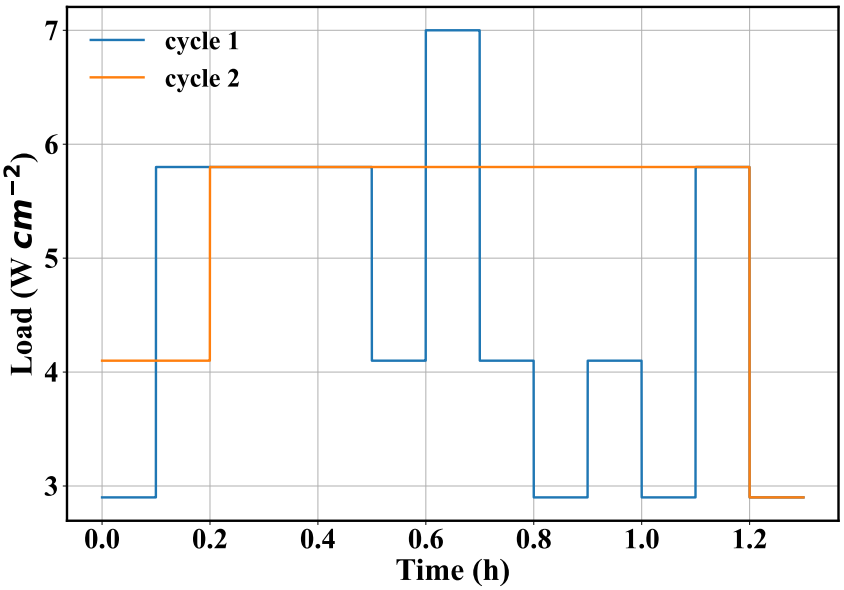

Figure 5.9: Proposed two types of dynamic load cycle.

Table 5.5: Lifetime comparison for with and without event duration information.

Models	Known event duration		Expected event duration		$\Delta T_{R,pct}(\%)$
	$\overline{T}_R$ (h)	$T_{R,med}$ (h)	$\overline{T}_R$ (h)	$T_{R,med}$ (h)	
GP	475	477	472	473	0.45
GP-RE	687	566	675	573	1.74

and their deterioration trajectories show high variability compared to the standard GP model. Thus, an obvious improvement in average system life are observed for the GP-RE model.

5.3.3.2 System lifetime Results of different random effects-based deterioration models

In parallel with the previous studies, this section presents the lifetime (first hitting time of the failure threshold FT) results of the proposed load allocation strategy on four types of stochastic deterioration models, i.e., GP, GP-RE, GP-RM, and GP-RV (see Chapter 3). The main purposes of this part of work are two-fold:

1. To investigate the applications of different types of stochastic deterioration models for MFC system energy management study.
2. To evaluate the performance of our strategy under a random dynamic load profile.

Firstly, the lifetime histograms of the different deterioration models are presented. According to the same settings as in the deterministic load scenario, different ℓ values are in-

Table 5.6: Lifetime comparison for with and without scheduling extra decision - load cycle 1 (Figure 5.9).

Models	With extra decision		Without extra decision		$\Delta T_{R,pct}(\%)$
	$\overline{T}_R$ (h)	$T_{R,med}$ (h)	$\overline{T}_R$ (h)	$T_{R,med}$ (h)	
GP	476	477	475	477	0.2
GP-RE	708	608	687	566	3.15

Table 5.7: Lifetime comparison for with and without scheduling extra decision - load cycle 2 (Figure 5.9).

Models	With extra decision		Without extra decision		$\Delta T_{R,pct}(\%)$
	$\overline{T}_R$ (h)	$T_{R,med}$ (h)	$\overline{T}_R$ (h)	$T_{R,med}$ (h)	
GP	650	651	648	647	0.35
GP-RE	1261	804	1152	742	9.46

troduced in the GP model to investigate the influence of different deterioration variances (Equation (5.10)). Figure 5.10 shows the lifetime histograms with $\ell = 5$. It is noted that in all figures, the "dec" represents decision -making strategy (proposed method), and "ave" stands for the average load split method. Setting $\ell = 5, 10$ enables a relatively small variance in the original GP model. By comparing the GP model results in Figures 5.10, 5.11, 5.12, and 5.13, it is seen that the histograms are getting wider and lower. Regarding the shapes of the different deterioration models, the GP, and GP-RV models are approximately Gaussian (symmetrically) distributed, whereas the GP-RE and GP-RM models are not symmetrically distributed. Another interesting phenomenon is that the histogram shapes of the random effect models are less sensible to the value of ℓ. The random effects dominant the distribution of first-hitting times.

The corresponding cumulative distribution function results are plotted in Figures 5.14, 5.15, 5.16, and 5.16. The failure probability (F_x) taken from Monte Carlo analysis are shown in these CDF curves. In Figure 5.14 GP model, it is seen that the MFC system reaches the value $F_{0.1}$ (i.e. failure probability at 0.1) at approximately 347.2 hrs for the average load strategy. On the other hand, when the system operates with load allocation decision (our strategy), the systems attains $F_{0.1}$ at approximately 379.5 hrs, resulting in a meaningful prolongation of system life. Similar improvements are observed for the three random-effect models. Such improvements are also observed for the comparison results of $\ell = 10, 20, 30$.

The five lifetime-related indicators, i.e., mean system lifetime $\overline{T}_R$, median system lifetime $T_{R,med}$, and four lifetimes comparison percentages ($\Delta T_{R,pct}$, $T^{+}_{R,pct}$, $T^{ave}_{R,pct}$, $T^{dec}_{R,pct}$) are computed from the obtained simulation results. Table 5.8 summarizes the indicators results. For all cases, the lifetimes (both the mean and median) obtained from load allocation decisions are larger than that of the average split strategy. These results are also visible with the average lifetime improvement indicator $\Delta T_{R,pct}$. The values of $T^{+}_{R,pct}$ show that generally over 60%

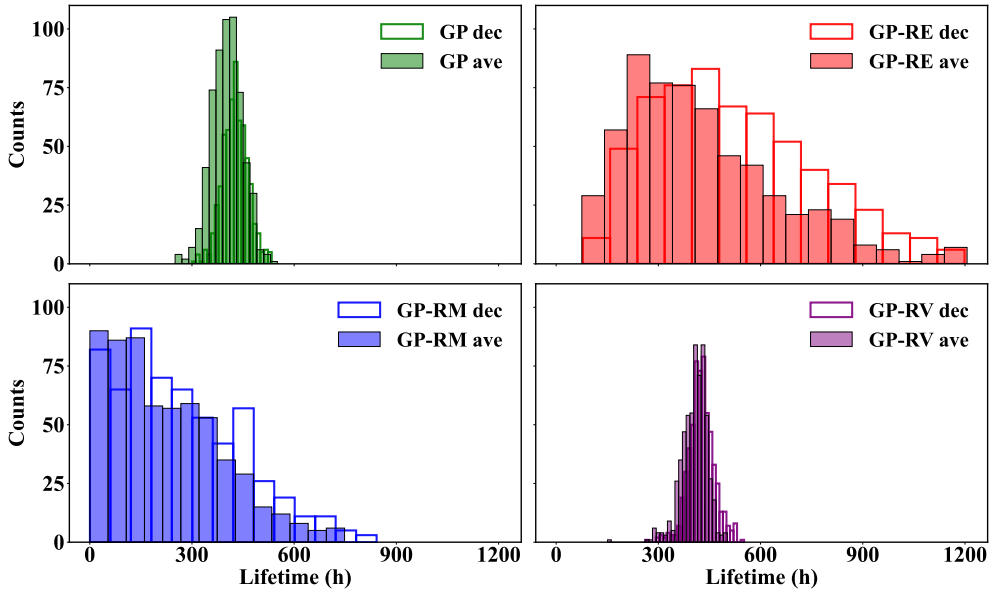

Figure 5.10: Lifetime histograms results with $\ell = 5$.

of the simulated lifetimes are higher than the average split. Moreover, the comparison of the lifetimes of the decision strategy and the average split strategy prove that our strategy can achieve around 20% of improvement.

By comparing the results with the GP model to the random effects models, it is observed that the average lifetime improvement indicator $\Delta T_{R,pct}$ is improved. These results confirm that when considering the stack deterioration heterogeneity, the proposed load allocation strategy can still obtains an improved system lifetime compared with the classical average split strategy. For the random effect-based models, the statistical information of the studied stochastic models are used in the decision-making procedure to decide the optimal load allocations. In GP deterioration model, the deterioration behavior of different stacks tend to be similar on average, and the statistical information may not contribute too much for helping to improve fuel cell lifetime. On the contrary, the variability of individual stack deterioration behavior is highlighted in random effects models, thus it would be useful to include the statistical information when computing the optimal load allocations. These are reflected by the average lifetime improvement indicator $\Delta T_{R,pct}$ where the results of the random effects models are generally better than those of the GP models. However, the random effects increase the variability of first hitting time and the indicators of $T^{+}_{R,pct}$, $T^{ave}_{R,pct}$, and $T^{dec}_{R,pct}$ are slightly lower than those of the GP model. However, the global results with decision-making strategy are better than those for the comparison strategy, i.e., average load method.

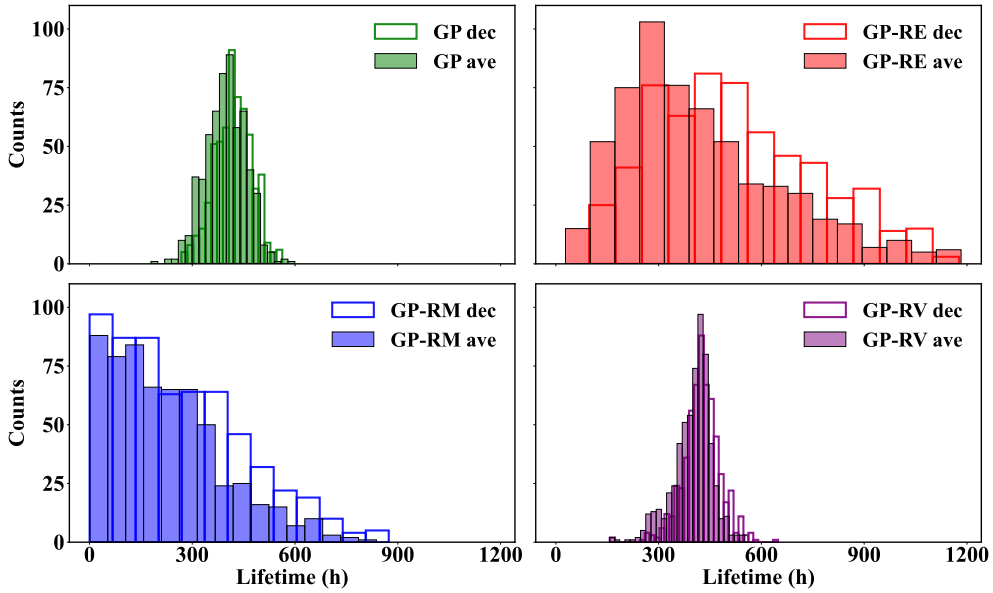

Figure 5.11: Lifetime histograms results with $\ell = 10$.

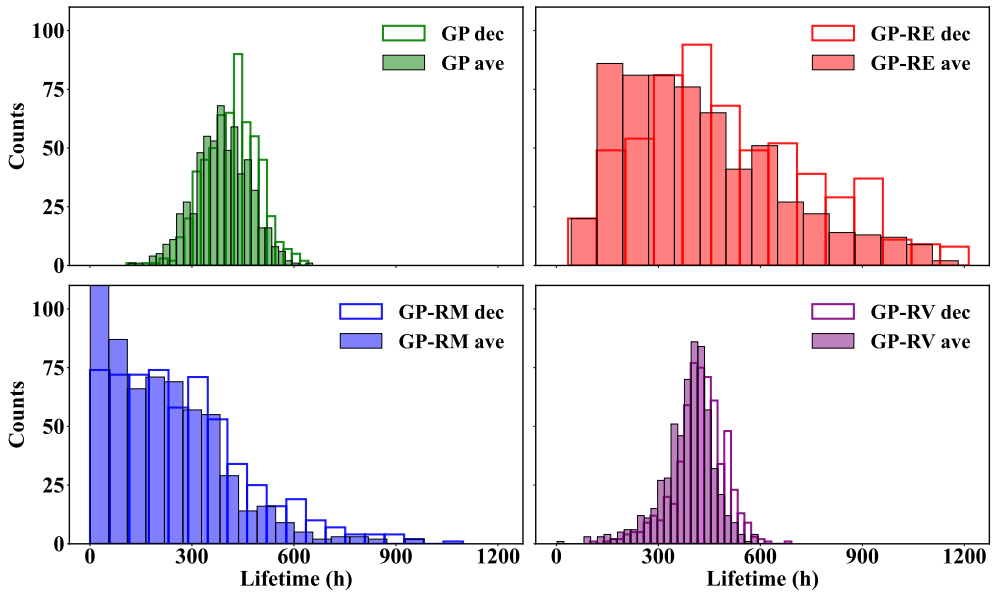

Figure 5.12: Lifetime histograms results with $\ell = 20$.

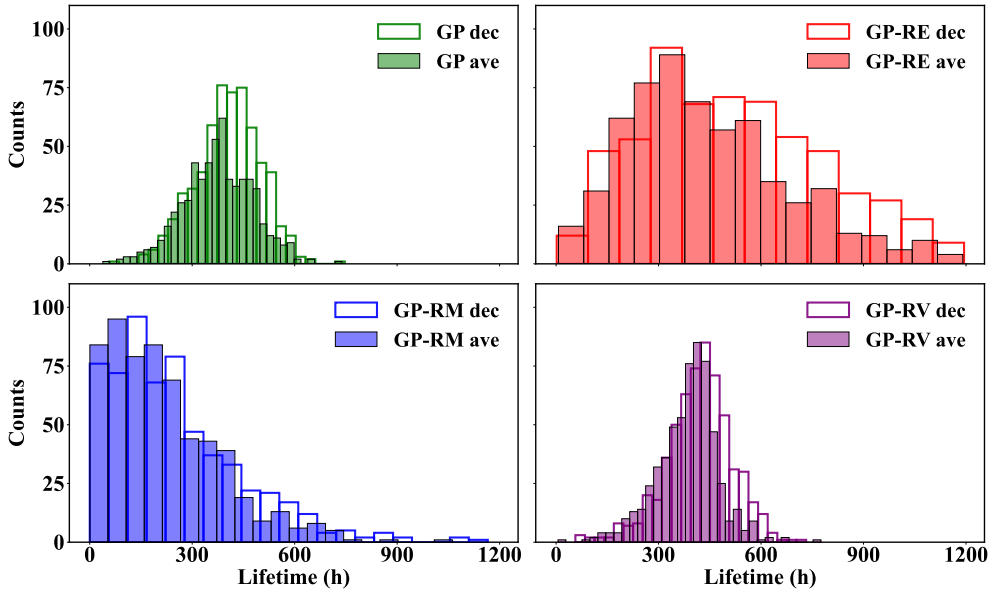

Figure 5.13: Lifetime histograms results with $\ell = 30$.

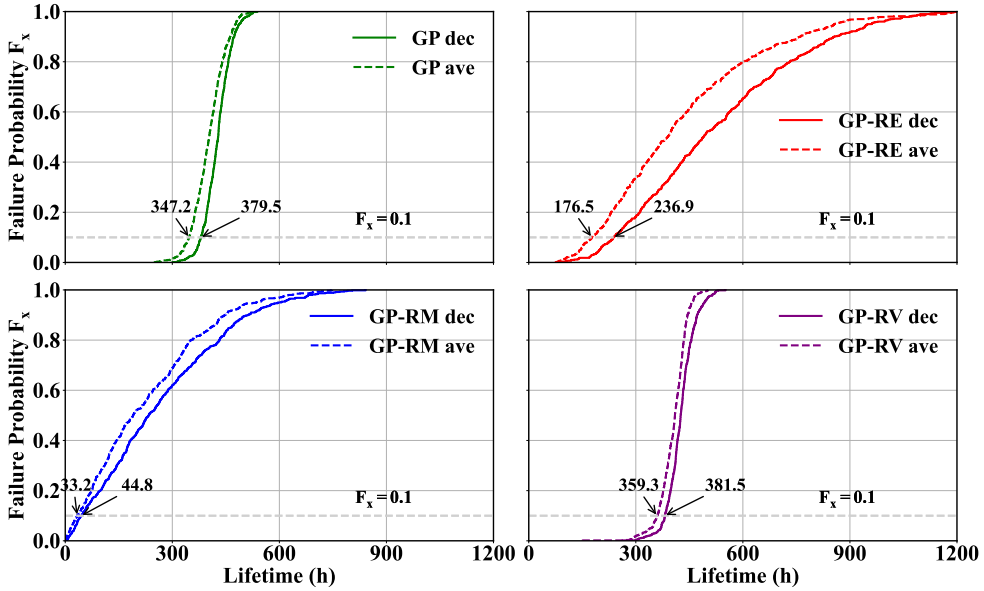

Figure 5.14: CDF results with $\ell = 5$.

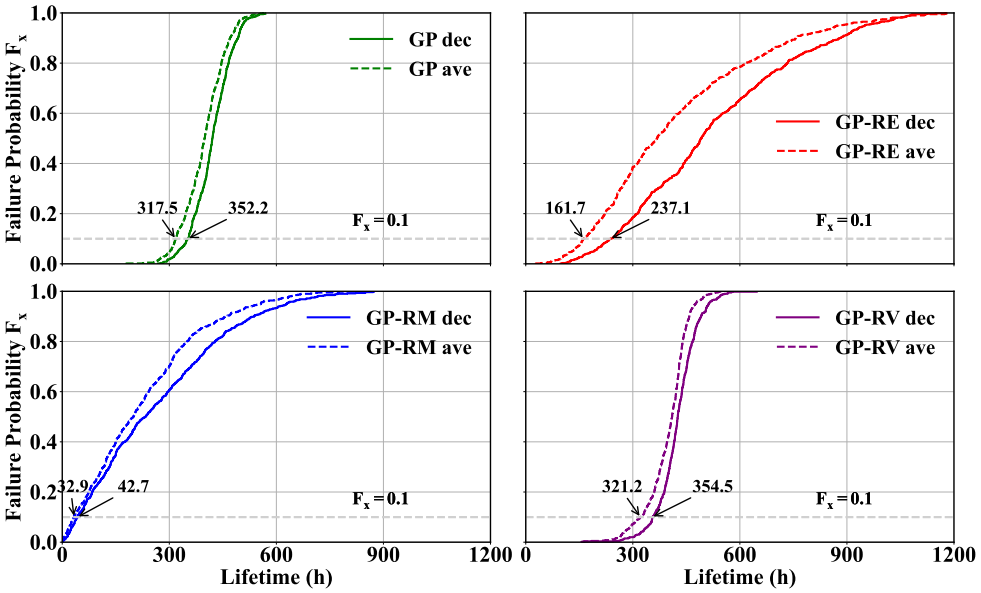

Figure 5.15: CDF results with $\ell = 10$.

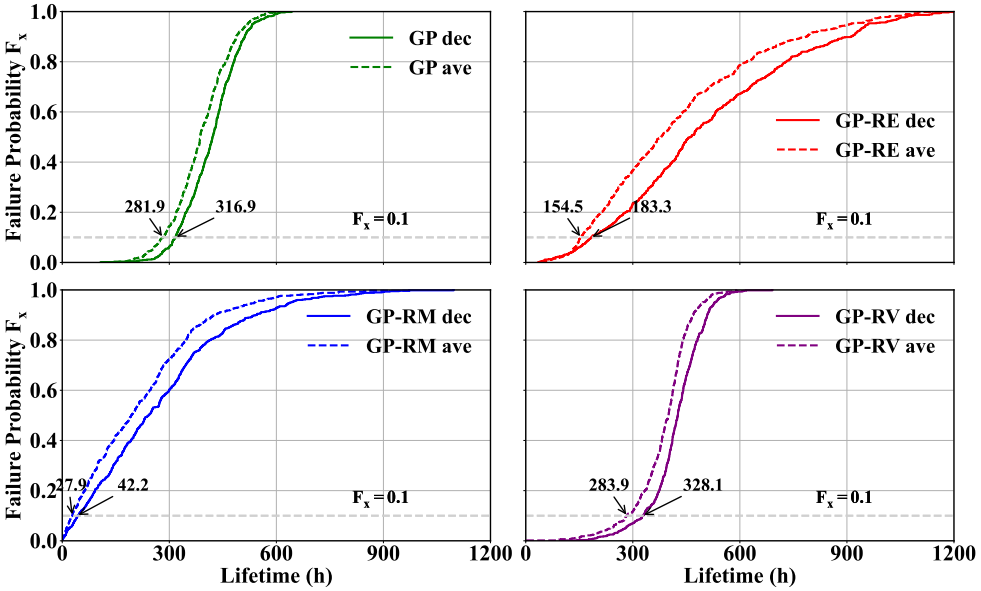

Figure 5.16: CDF results with $\ell = 20$.

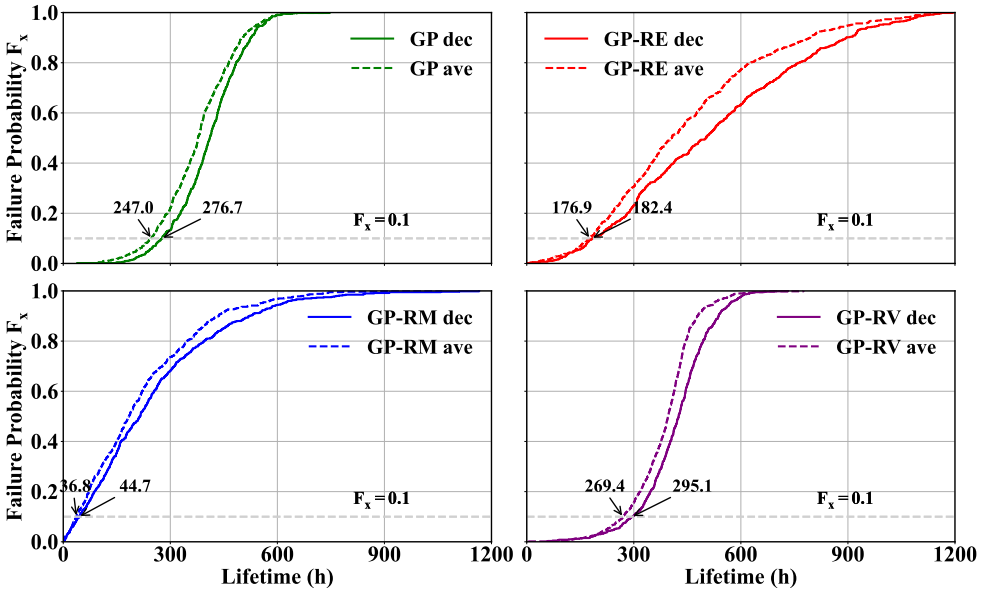

Figure 5.17: CDF results with $\ell = 30$.

Table 5.8: Lifetime indicator results for $\ell = 5$

	$\overline{T}_R$ (h)		$T_{R,med}$ (h)		$\Delta T_{R,pct}$ (%)	$T^{+}_{R,pct}$ (%)	$T^{ave}_{R,pct}$ (%)	$T^{dec}_{R,pct}$ (%)
	ave	dec	ave	dec				
GP	402	427	403	428	6.0	68	50.8	74.8
GP-RE	429	525	389	489	22.4	62.5	42.3	60.2
GP-RM	224	265	190	234	18.4	56.5	44.8	52.0
GP-RV	405	426	410	426	5.2	64.2	56.3	73.5

Table 5.9: Lifetime indicator results for $\ell = 10$

	$\overline{T}_R$ (h)		$T_{R,med}$ (h)		$\Delta T_{R,pct}$ (%)	$T^{+}_{R,pct}$ (%)	$T^{ave}_{R,pct}$ (%)	$T^{dec}_{R,pct}$ (%)
	ave	dec	ave	dec				
GP	397	420	399	421	5.8	64.0	51.5	68.7
GP-RE	421	525	368	492	24.6	63.5	40.3	64.5
GP-RM	225	266	199	234	18.5	55.5	44.2	50.7
GP-RV	399	426	410	426	6.1	61.3	58.2	73.0

Table 5.10: Lifetime indicator results for $\ell = 20$

	$\overline{T}_R$ (h)		$T_{R,med}$ (h)		$\Delta T_{R,pct}$ (%)	$T^{+}_{R,pct}$ (%)	$T^{ave}_{R,pct}$ (%)	$T^{dec}_{R,pct}$ (%)
	ave	dec	ave	dec				
GP	387	416	387	421	7.6	59	49.5	65.3
GP-RE	424	506	378	462	19.2	60.2	42.5	57.5
GP-RM	218	272	194	242	24.8	55.7	44.3	54.3
GP-RV	386	422	400	426	9.3	64.0	57.3	74.7

Table 5.11: Lifetime indicator results for $\ell = 30$

	$\overline{T}_R$ (h)		$T_{R,med}$ (h)		$\Delta T_{R,pct}$ (%)	$T^{+}_{R,pct}$ (%)	$T^{ave}_{R,pct}$ (%)	$T^{dec}_{R,pct}$ (%)
	ave	dec	ave	dec				
GP	375	406	378	411	8.1	59.8	52.0	65.2
GP-RE	446	519	406	503	16.4	56.8	43.2	56.7
GP-RM	218	252	184	215	15.7	56.8	41.3	48.5
GP-RV	385	418	396	426	8.7	60.7	56.3	67.3

5.4 Conclusion

The EMS development problem is formulated as a constrained nonlinear optimization problem. The SLSQP algorithm is suitable to solve formulated optimization problem in terms of speed and accuracy. The study of randomness in the dynamic loads showed that the proposed load allocation strategy is very dependent on the load demand information. Under the event-based decision-making, the performance of the proposed strategy can be improved by scheduling an extra decision before a load change event, achieving 9.46% improvement in the average system lifetime for GP-RE deterioration model. The simulation results proved that the proposed EMSs can be used in a wider range of operation scenarios as well as different deterioration models. Moreover, a relatively high improvements for random effects-based deterioration models can be achieved. The average system lifetime can be improved up to 24.8%. The EMSs studied in this chapter only consider the load and load varying deterioration factors. The start-stop operation mode is not considered in the proposed strategy. An EMS capable of optimizing start-stop operation in MFC systems will be developed in the following chapter.

Chapter 6

Multi-stack Fuel Cells Maintenance-based Energy Management Strategy Studies

In previous MFC EMS studies, we have proposed several deterioration-aware strategies to improve fuel cell system lifetime. The efficiency of those strategies has been illustrated on a range of deterioration models, including the GP model and the random effect models (GP-RE, GP-RM, GP-RV). On this basis, this chapter introduces an oversized MFC EMS problem. The operation task is to manage a three-stack system with two stacks only required to supply the power demand. A management strategy is proposed by taking into account the optimization of start-stop to decide the operating loads among different stacks. Eventually, this oversized operation problem in MFC can be extended to a maintenance problem. The replacement of deteriorated fuel cell stacks can be optimized by a maintenance scheduling policy. This is treated as a perspective problem of this thesis.

Contents

6.1 Three stacks operation problem formulation

6.1.1 General context

Current fuel cell technologies fail to meet the durability requirements in many practical applications. For example, in Fuel Cell Electrical Buses, the lifetime of MFC system is still below the DOE target of 8,000 hours. Thanks to the multi-stack architecture in MFC, one possible solution is to make use of the redundancy design in MFC, i.e., put together more stacks in the system to reach the operation durability requirements. This redundancy design enables MFC system to switch between different stacks according to their state of health. One practical example is addressed in DOE Durability-adjusted fuel cell system cost program [155]. The program proposed two types of analysis methods to estimate the durability-adjust cost of a fuel cell system. The first approach was to estimate the number of stack replacements to meet 8,000 hours durability requirement. The second approach was to extend system operating time through oversized stacks design. In both methods, proper durability analysis and lifetime estimation are required. The first approach is linked to the optimization of the maintenance schedule and replacement schedule. The concept of oversizing is found interesting and could be studied as a practice for reaching the DOE durability target. This oversizing is studied to enhance the durability of the studied fuel cell system.

However, the operation of such an MFC system needs to be properly managed by an efficient management strategy (i.e., EMS). A deterioration-aware EMS is needed to help improving fuel cell system durability by optimally allocating the operation load among different stacks. This section proposes a simplified study case for investigating such EMS via oversized MFC system.

6.1.2 Proposed decision-making problem

The studied case of this chapter consists in managing the operation of a three-stack fuel cell system, denoted as $\mathrm{M}_{fc,3}$= {FC1, FC2, FC3}. The power load supplied by three stacks FC1, FC2, and FC3 are noted as $\{L_i\}_{i=1,2,3}$. Assuming that the stacks of M_{fc} are identical, each stack operates with a production capacity ranging from L_{min} to L_{max} (detailed fuel cell parameters refer to Table 3.3).

A random dynamic load profile as introduced in Chapter 5 (Figure 5.3) is used to represent the demands for the studied MFC system. The same Markov Chain model is used to define the load cycle:

$$\mathbf{P_{tr}} = \begin{bmatrix} 0.1 & 0.35 & 0.35 & 0.2 \\ 0.35 & 0.1 & 0.35 & 0.2 \\ 0.2 & 0.35 & 0.1 & 0.35 \\ 0.2 & 0.35 & 0.35 & 0.1 \end{bmatrix} \tag{6.1}$$

and the four possible states are $L_{ds} = [2.9, 4.1, 5.8, 7.0]$.

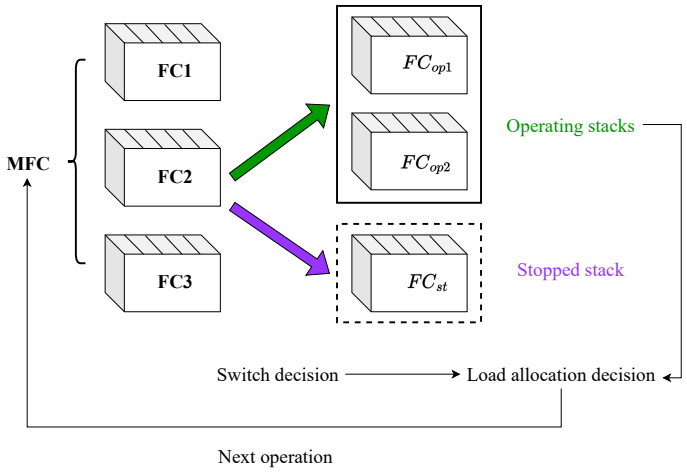

Figure 6.1: Proposed three stacks operation problem.

The overall three-stack fuel cell system operation problem is sketched in Figure 6.1. In this problem, at most two fuel cell stacks are necessary to supply the required power demands. The two operating stacks are denoted as $\mathrm{FC}_{op1}, \mathrm{FC}_{op2}$, and the one stopped stack is FC_{st}. The decision-making problem consists of two sub-problems. The first problem is to choose two stacks to operate at each decision, which requires a switch decision. Then the second problem is how to distribute the required power to working stacks. The proposed problem is formulated as a sequential decision-making problem. The overall deterioration model of the studied MFC is adopted from Chapter 3. The overall fuel cell stack resistance deterioration is modeled as a summation of load amplitude, load varying, and start-stop caused deterioration (Equation (3.13)).

6.2 Proposed decision-making strategy

In Chapter 5, we have built a load allocation strategy for optimizing the load allocation in a two-stack fuel cell system. The decision-making policy is optimized through a sequential event-based decision-making procedure. A new decision is made whenever there is a load change event. The load allocation decision-making strategy of this chapter is constructed based on this strategy by integrating the decision to switch on/off of fuel cell stacks.

Concerning the operation problem of this chapter (Section 6.1.2), limited by the special operation requirement, i.e., operating two stacks simultaneously within a three-stack fuel cells, an extra decision of choosing working stacks is required compare to the decision problems solved in Chapter 5. Thus, we propose a two-step decision-making strategy, where the load allocation decision and operating stacks decision are handle at each step. Then the final operation decision is decided by the operating stack combination with the load allocation that minimize the designed decision criterion which is linked to fuel cell system deterioration.

- Decision-making step 1: Optimizing load allocation for two operating stacks

For a multi-stack fuel cell system with three stacks, there are three possible operation combinations when all three stacks are available:

$$\begin{aligned} comb1 &= \{\mathrm{FC}_{op1} = \mathrm{FC1}, \mathrm{FC}_{op2} = \mathrm{FC2}, \mathrm{FC}_{st} = \mathrm{FC3}\} \\ comb2 &= \{\mathrm{FC}_{op1} = \mathrm{FC1}, \mathrm{FC}_{op2} = \mathrm{FC3}, \mathrm{FC}_{st} = \mathrm{FC2}\} \\ comb3 &= \{\mathrm{FC}_{op1} = \mathrm{FC2}, \mathrm{FC}_{op2} = \mathrm{FC3}, \mathrm{FC}_{st} = \mathrm{FC1}\} \end{aligned} \tag{6.2}$$

Then, for each operation combination, the load allocation decision is optimized by solving the optimization problem:

$$\begin{aligned} \underset{\{\gamma_i^j\}_{i=1,\cdots,n}}{\text{minimize}} \quad & J_{dec1}(\{\gamma_i^j\}_{i=1,\cdots,n}) = \sum_{i=1}^{n} \omega_i \{(\Delta R^0_{\Delta L,i})^2 + \Delta R^0_{L,i} + \sum_{j=1}^{m-1} (\Delta R^j_{L,i} + (\Delta R^j_{\Delta L,i})^2)\} \\ \text{subject to} \quad & L_{min} \leq \gamma_i^j L_d^j \leq L_{max}, \sum_{i=1}^{n} \gamma_i^j = 1 \\ & \Delta R^j_{L,i} = D(\gamma_i^j L_d^j) \cdot \tau_e^j \\ & \Delta R^0_{\Delta L,i} = K|\gamma_i^0 L_d^0 - \gamma_i^{ini,d} L_d^{ini,d}| \\ & \Delta R^j_{\Delta L,i} = \sum_{j=1}^{m-1} K|\gamma_i^{j+1} L_d^{j+1} - \gamma_i^j L_d^j|, \quad j = 1, \cdots, m-1 \end{aligned} \tag{6.3}$$

where τ_e^j is the time length of event j, m is the number of events taken into account during each decision, 0 stands for the current load change event; L_d^j defines the external dynamic load demands; γ_i^j is the load allocation ratio for FCi at decision time j, and $\gamma_i^{ini,d}$ is the initial load allocation ratio of stack i at each decision. ω_i is the corresponding weight of the overall FCi deterioration (R_{fci}) (Equation (5.9)). Note that the deterioration term due to load variation $\Delta R^j_{\Delta L,i}$ is expressed with a quadratic form for the optimization convenience. K is a constant term calculated by Equation (3.16). The problem of this chapter considers an MFC with three stacks, only two stacks are required to operate, thus, n equals to 2.

- Decision-making step 2: Optimizing (selecting) operating stacks

Then for each operation combination, estimating a second deterioration criterion J_{dec2} based on the optimized load allocation, which writes:

$$J_{dec2}(\gamma_i^0) = \sum_{i=1}^{n} \Delta R^0_{L,i} + K|\gamma_i^0 L_d^0 - \gamma_i^{ini,d} L_d^{ini,d}| + k_{ss}\Delta R_{ss} \tag{6.4}$$

It is seen from J_{dec2} that only the current load change event is considered when calculating the decision criterion. Then J_{dec2} estimates the weighted future overall system deterioration. ΔR_{ss} is the resistance deterioration by each start-stop cycle. A constant hyperparameter k_{ss} is defined to tune the weights of start-stop contribution to overall resistance deterioration. γ_{opt} is the optimal load allocation calculated from Equation (6.3). Then the allocation ratio for two operating stacks are $\gamma_1^0 = \gamma_{opt}$ for FC_{op1} and $\gamma_2^0 = 1 - \gamma_{opt}$ for FC_{op2}.

The final optimal operation combination is optimized by:

$$\underset{\{combi\}_{i=1,2,3}}{\text{minimize}} \ \{J_{dec2}(combi)\} \tag{6.5}$$

where $J_{dec2.}$ is the second deterioration criteria as defined in Equation (6.4). The optimized operation combination and its load allocation decision solved in decision step 1 give the final decision of the proposed decision-making strategy.

The hyperparameter k_{ss} is related to fuel cell failure threshold (FT):

$$k_{ss} = \begin{cases} k_1 & if\ 0.9FT \leq max(R_{fc1}, R_{fc2}, R_{fc3}) \\ k_2 & else \end{cases} \tag{6.6}$$

Here k_1 and k_2 are two parameters for fuel cell stack at different deterioration level. When the maximum resistance among three stacks reaches 90% of the failure threshold, the start-stop deterioration cost term is quantified by k_1. For maximum resistance level below this threshold ($0.9FT$), the start-stop deterioration cost term is quantified by k_2. These weights are linked with the optimization of switch decisions. When this weight is small, the cost of switching on/off stacks is relatively lower, thus increasing the frequency of start-stop actions. On the contrary, when the weight is large, the frequency of start-stop action will be decreased due to the high cost of switching stacks. Thus, here k_1, k_2 satisfy $k_2 < k_1$.

Figure 6.2 depicts the proposed operation strategy for the proposed three-stack operation problem. At the beginning of system operation, three stacks are available for operating (no stack failure occur). Then the above two-step optimization is applied to select the two operating stacks and optimal load allocation for these two stacks. In the diagram, this two steps optimization is represented by J_{dec1} for deciding the optimal load allocations, and the switch decision is optimized through J_{dec2}. When the system deteriorates to a certain level, stack failure may happen for the studied MFC system. When only one stack fails, the remaining two stacks keep running to provide the power demand. At this stage, there is no choice of switching stacks, the strategy only optimizes the load allocation between these two stacks. And finally, the system failure is triggered by the time when two stacks fail.

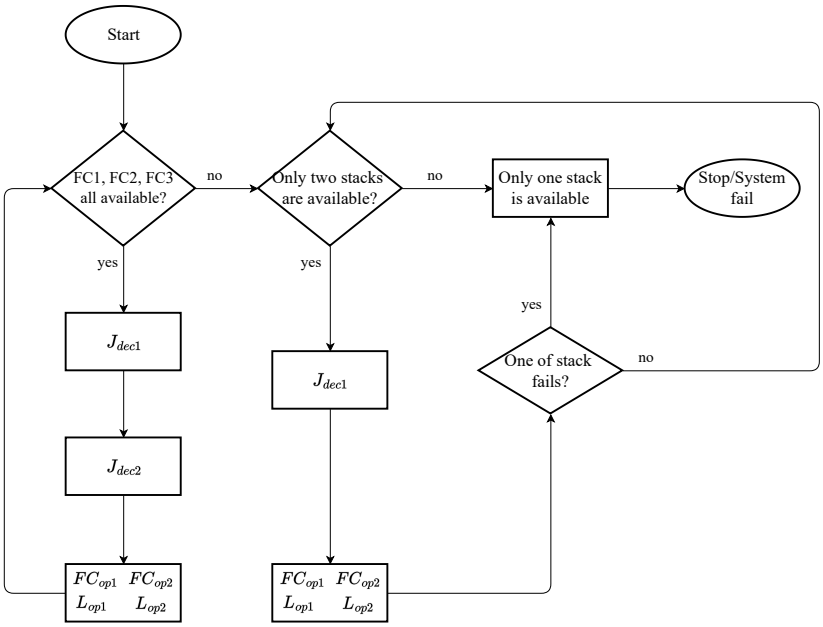

Figure 6.2: Proposed three stacks operation strategy.

6.3 Simulation results

To illustrate the simulation results, both the deterministic scenario and Monte Carlo simulations are conducted in this section. In deterministic scenario, both the load profile and fuel cell resistance deterioration are deterministically decided. Two Daisy chain-based decision-making strategy are then introduced, and their simulation results are compared with the proposed two-layer decision-making strategy. After setting simulation parameters, the simulation results of deterministic scenario and Monte Carlo simulation (with randomness) are presented and discussed.

6.3.1 Deterministic scenario settings

The deterministic scenario in this chapter refers to deterministic settings in terms of MFC system load profile and fuel cell stack deterioration. A deterministic load profile is set by draw a fixed realization of the Markov Chain model (Section 6.1.2, Equation (6.1)). Then the deterioration of fuel cell stacks are accumulated by the mean increment of the chosen Gamma process rather than a stochastic value. Deterministic scenario setting simplifies the deterioration behavior studies by removing the randomness exists within the load profile as well as fuel cell stack deterioration. Deterministic scenario simulation of the studied MFC system deterioration with different management strategies will be discussed in the results section (Section 6.3.4.1).

6.3.2 Daisy Chain average load and deterioration-aware Daisy Chain average load strategies

The classic daisy and average load strategy are adapted to design two comparison operation strategies, i.e., Daisy Chain-based Average Load Strategy, and Deterioration-aware Daisy Chain Average Load Strategy. The decision of operating stacks and their operating loads are two decisions to be made in these strategies.

- Daisy Chain-based Average Load (DC-ave). DC-ave strategy decides the operating stacks based on Daisy Chain strategy, i.e., sequentially switching the operating stacks. Then their operating loads are decided by Average Load method, namely, equally distributed the load demand by stacks.

- Deterioration-aware Daisy Chain-based Average Load (DDC-ave). DDC-ave also decides the operating loads by using the Average Load strategy. But the operating stacks are decided in a deterioration-aware manner rather than the totally sequential one as in DC-ave. This deterioration-aware strategy will stops the most deteriorated stack and replace it with the previously stopped stack. In this way, the overall system deterioration is considered to be balanced in the sense that the more deterioration stack is prevented from further deteriorating.

The basic procedure of these two comparison strategies is sketched in Figure 6.3. The switching on/off decisions are conducted every tau_sw hrs for both strategies. τ_{sw} is also known as the switch decision time interval. At initial time step fuel cell stack 1 (FC1) and fuel cell stack 2 (FC2) are in operating, and fuel cell stack 3 (FC3) is stopped. According to the deterioration levels shown in the figure, FC3 is currently most deteriorated stack. Then the next decision is performed at time τ_{sw}. It is observed that FC1 is now the most deteriorated stack, followed by FC2 and FCs. The pure Daisy Chain-based strategy sequentially switches on/off stacks without considering the current deterioration levels of each stack. That is, for decision at τ_{sw}, the DC-ave strategy switch off FC1, switch on FC3 (assuming the sequential operating order is (FC1, FC2), (FC2, FC3), (FC3, FC1)). The 'ave' represents that the average split method is applied to decide the operating load for each stack. Then at the next decision time $2\tau_{sw}$, FC2 is switched off, and FC1 is switched on.

By contrast, the DDC-ave is a deterioration-aware decision-making strategy in terms of the first decision on switching on/off stacks. For the same operation, at τ_{sw}, the DDC-ave strategy will switch off FC1, and switching on FC3 due to FC1 is the most deterioration stack. Then at $2\tau_{sw}$, considering FC1 is still the most deteriorated one, FC2 and FC3 will remain as the two operating stacks which are different from the decision of the DC-ave strategy.

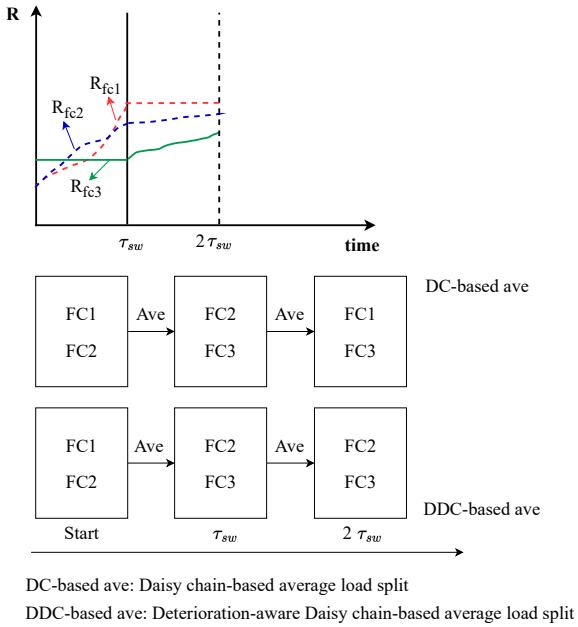

Figure 6.3: Basic decision process of DC-ave and DDC-ave strategies.

6.3.3 Parameters and simulation settings

The dynamic random load profile and main fuel cell parameters are taken from Chapter 5 Equation (5.7) and Table 5.4. The initial resistances for three stacks are:

$$R_{fc1}^{ini} = R_0 + \Delta R_0, R_{fc2}^{ini} = R_0, R_{fc3}^{ini} = R_0 \tag{6.7}$$

where $R_0 = 0.1803\ \Omega\ cm^2$ is the original initial value fitted from IEEE 2014 data challenge datasets. $\Delta R_0 = 0.01\ \Omega\ cm^2$ is the initial increment added to FC1 to simulate an aged stack.

The GP-RE model is chosen to model MFC system deterioration in order to take into account stack-to-stack deterioration variability of the studied MFC (Chapter 3, Section 3.2.3). The random dynamic load profile is generated based on the Markov Chain model as described in Section 6.1.2, Equation (6.1). The load profile of the deterministic scenario that draw based on the proposed Markov Chain model is shown in Figure 6.4.

Parameters for DC-ave and DDC-ave strategies The decision time interval τ_{sw} needs to be set for the DC-ave and DDC-ave strategies. These values are investigated and optimized under deterministic scenarios in order to compare the lifetimes of different parameter settings. The deterministic scenarios mean that the resistance deterioration is calculated by the expected value instead of random deteriorating values, and the random dynamic load cycle is kept the same for each simulation. Figure 6.5 shows the simulated lifetimes for a series of τ_{sw}. The DDC-ave is used as the EMS. It is seen that the overall number of start and stop times are decreasing with the increment of τ_{sw}. The maximum lifetime is observed at $\tau_{sw} = 45$ h, thus it is chosen for the following simulations.

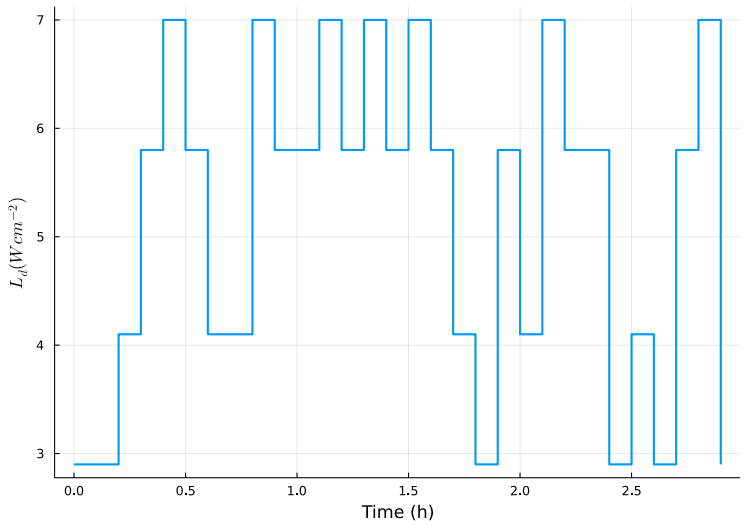

Figure 6.4: Simulation load demand profile (deterministic scenario)

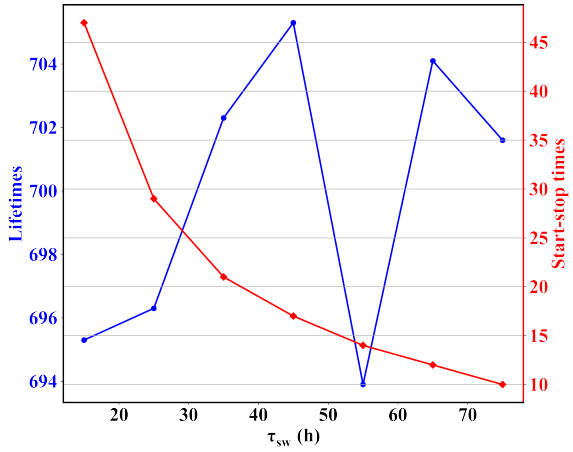

Figure 6.5: Simulated lifetimes and start-stop times under investigated τ_{sw}

Parameters for the proposed decision-making strategy The main parameters to be set for the proposed strategy are k_1, k_2 which are used to calculate the weight of start-stop deterioration as discussed in Section 6.2. Figure 6.6 shows the simulated lifetime (under deterministic scenario) with respect to different k_1 and k_2. The maximum lifetime is obtained by parameters of $k_1 = 15, k_2 = 88$.

6.3.4 Main simulation results

6.3.4.1 Results on deterministic one-run simulation

First, the behavior of the proposed load allocation strategy is analyzed under a deterministic scenario. This deterministic scenario is designed similar to the one used for optimizing

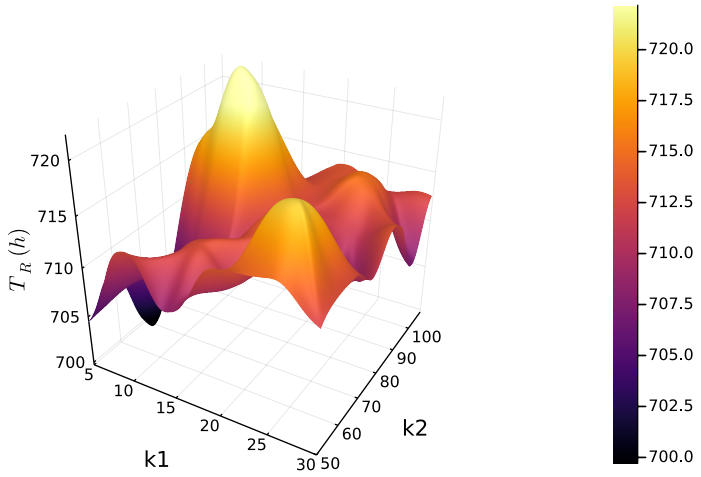

Figure 6.6: Selecting decision parameters k_1, k_2.

decision time interval τ_{sw}. The dynamic load profile is generated by the MC model defined in Equation (5.7). Figure 6.4 depicts part of the loads. This load is used as the demand for three studied strategies, i.e., DC-ave, DDC-ave, and our strategy (the proposed management strategy).

The constructed strategies are tested on the three stacks operation problem. Three independent simulations are performed from the beginning till system failure, obtaining three one-run trajectories. Figures 6.7, 6.8, and 6.9 show the detailed resistance deterioration level and load allocations information at each switching decision (here the switching decision specifically refers to switch on/off different stacks). For the studied MFC system, the deterioration variability is modeled by a GP-RE model as introduced in the parameter setting section. As a result, each stack is assigned with (sampled from a Gamma law) a different scale parameter β to simulate this random effects. For instance, in the trajectory results as shown in Figure 6.7, FC3 is assigned with the biggest scale parameter $\beta_{\mathrm{FC}_3} = 3.67 \times 10^{-3}$. This is why FC3 shows the highest deterioration rates. The scale parameters used in the simulation of DDC-ave and our strategies are specified in the figure captions (Figures 6.8, 6.9).

Our strategy obtained the highest lifetime for the studied system, 1731.2 h, followed by the DDC-ave strategy 1641 h, and the DC-ave strategy procedures the lowest lifetime 1467.8 h. DC-ave is a pure sequential switching strategy for deciding the operating stacks without considering stacks deterioration information. This can be observed from Figure 6.7, the three stacks are switched on/off in a sequential order: {FC2 off, FC1, FC3 on} $\rightarrow$ {FC1 off, FC2, FC3 on} $\rightarrow$ {FC3 off, FC1, FC2 on}$\cdots$. By contrast, the deterioration-aware strategies decide the switching actions by taking into account system deterioration states. This is beneficial for balancing the deterioration levels of all stacks so that the overall system life can be extended. It is observed that in DDC-ave and our strategy, they switch off FC1 in the first decision, then for the remaining decisions, they keep FC1 running, only switching between FC2 and FC3. This is due to FC1 being the most deteriorated stack at the beginning

Table 6.1: Resistance values of all stacks at the end of system life.

Stacks	Resistances ($\Omega\ cm^2$)		
	DC-ave	DDC-ave	Our strategy
FC1	0.25137	0.268716	0.277421
FC2	0.277488	0.27749	0.277491
FC3	0.277498	0.277498	0.2775

of life, thus it is beneficial to stop it in the first decision. In the following decisions, it will be restarted when the switch decision criterion is satisfied.

It is observed from the results figure that the three resistance trajectories are gradually grouped together from DC-ave strategy to DDC-ave strategy, and finally our strategy. This is verified from the resistance values at the end of the lifetime as listed in Table 6.1. For our strategy, the three values are very close to each other. While in DDC-ave, the FC1 is 0.268716 $\Omega\ cm^2$ which is lower than the value in our strategy. In DC-ave, the resistance value of FC1 is much smaller at the end of life. Besides, the resistance of FC2 is also slightly smaller than the other two strategies. These results prove that the proposed strategy can effectively control the deterioration variability among different stacks which helps to balance overall system deterioration levels, thus achieving an improved system life. Compared with the DDC-ave strategy, the efficiency of our strategy lies in the two aspects, which correspond to the two decisions:

- For the load allocation decisions. Our strategy decided the allocations by using the strategy proposed in Chapter 5, which is proved to be able to extend system life.
- For the switch decisions. Our strategy is relatively more flexible by designing two weights (k_1, k_2) for start-stop deterioration. While in DDC-ave, the switch decision is checked on a fixed time interval (τ_{sw}) which produces limited control effects for extending system life.

6.3.4.2 Monte Carlo simulation results

The system lifetime of the three strategies is now estimated with Monte Carlo simulations. The number of simulation runs is kept the same as in Chapter 5 ($N = 600$). The overall simulated lifetimes are summarized in Figure 6.10(a). The lifetime-related indicators are calculated based on this histogram and listed in Table 6.2. For the lifetime improvement percentage result, we have computed the values for our decision-making strategy with respect the DC-ave and DDC-ave strategies, respectively. Then the percentage values ($T_{R,pct}^{DC}$, $T_{R,pct}^{DDC}$, and $T_{R,pct}^{dec}$) of the Monte Carlo simulation lifetimes that are larger than the average lifetime of the DC-ave strategy for all studied strategies, namely, the DC-ave, DDC-ave, and proposed decision-making strategy. Among the three studied strategies, our strategy obtained the highest lifetime ($\overline{T}_R = 1268$ h, $T_{R,med} = 1229$ h). The mean and median lifetimes of the DDC-ave strategy

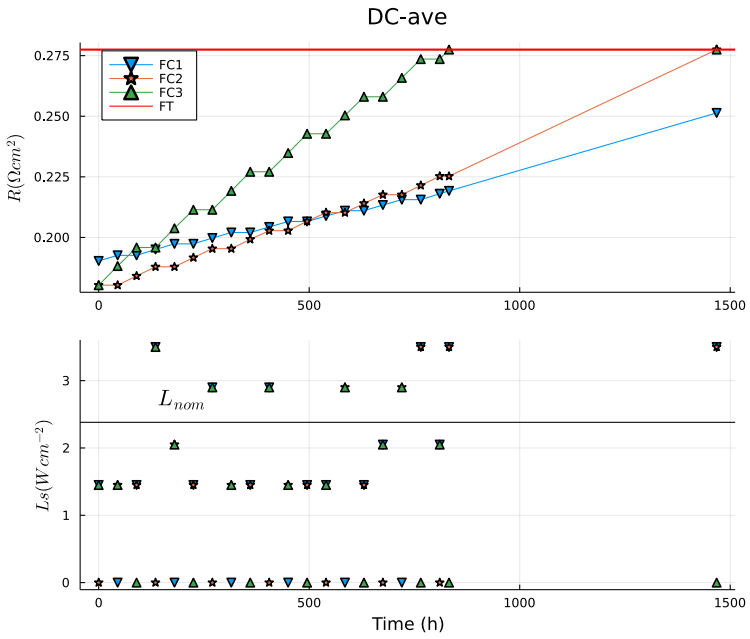

Figure 6.7: Switch decisions results for DC-ave strategy (deterministic scenario, $\beta_{FC1} = 1.067 \times 10^{-4}$, $\beta_{FC2} = 1.039 \times 10^{-3}, \beta_{FC3} = 3.67 \times 10^{-3}$).

Table 6.2: Overall lifetime indexes results.

	$\Delta T_{R,pct}(\%)$	$\Delta T_{R,pct}(\%)$	$T^{DC}_{R,pct}(\%)$	$T^{DDC}_{R,pct}(\%)$	$T^{dec}_{R,pct}(\%)$
	DC-ave Our strategy	DDC-ave Our strategy			
$\ell = 10$	21.7	8.1	45	51	61

are 1127 h and 1062 h, respectively. The DC-ave strategy only obtains an average lifetime of 1042 h and a median lifetime of 957 h. Compared with the DC-ave strategy, our approach obtains 21.7% of average lifetime improvement. In comparison to the deterioration-aware strategy (DDC-ave), our strategy helps to improve the average system lifetime by 8.1%. 45% of simulated lifetimes by DC-ave are larger than the average lifetime of the DC-ave strategy. For the deterioration-aware DC-ave strategy, this percentage increased to 51%. Our strategy further improves this value to 61 %. Thus, the proposed strategy outperforms both the basic daisy chain-based (deterioration-unaware) and deterioration-aware strategies.

Figure 6.10(b) plots the CDF curves based on the histogram results shown in Figure 6.10(a). The CDF results confirm the above conclusion. The proposed strategy greatly lowers the system failure probabilities in nearly all the time range shown in the figure. Thus obtaining the optimal system life.

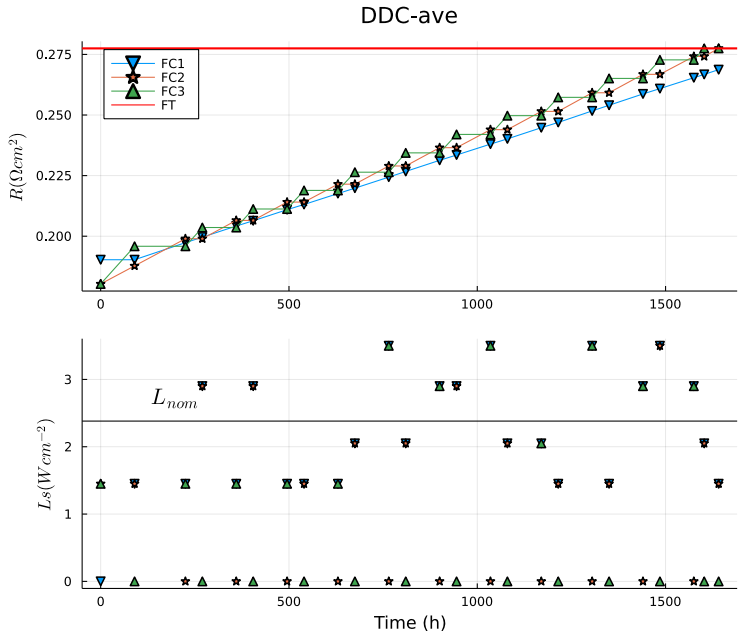

Figure 6.8: Switch decisions results for DDC-ave strategy (deterministic scenario, $\beta_{FC1} = 1.067 \times 10^{-4}$, $\beta_{FC2} = 1.039 \times 10^{-3}, \beta_{FC3} = 3.67 \times 10^{-3}$).

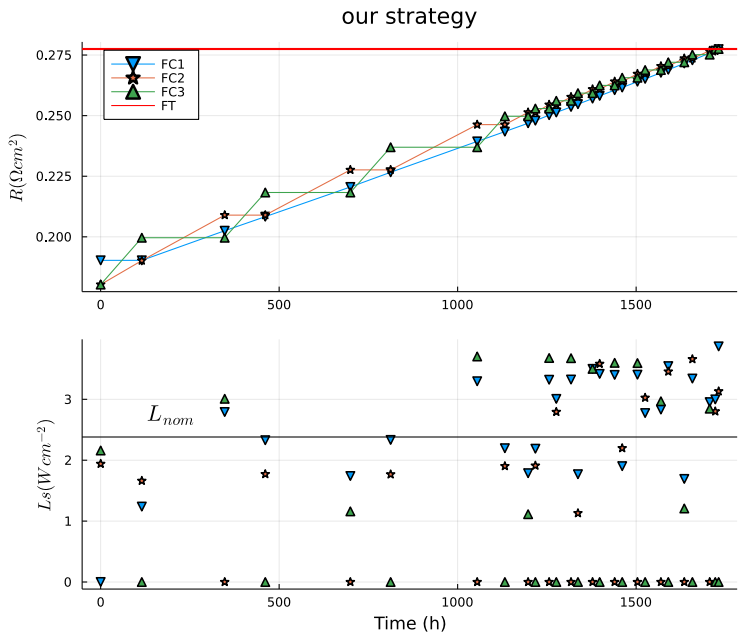

Figure 6.9: Switch decisions results for our strategy (deterministic scenario, $\beta_{FC1} = 1.067 \times 10^{-4}$, $\beta_{FC2} = 1.039 \times 10^{-3}, \beta_{FC3} = 3.67 \times 10^{-3}$).

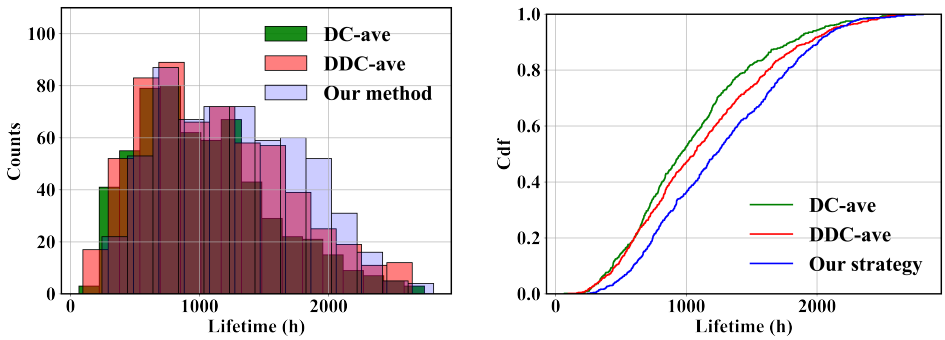

(a) Lifetime histograms.

(b) Lifetime CDF results.

Figure 6.10: Simulation results for random effects model under random load profile.

6.4 Proposal of maintenance-based management problem

6.4.1 Motivations

From the literature review, we have seen few works on investigating the reliability and maintenance scheduling for fuel cell-based energy systems. Indeed, developing a reliable energy system with lower operating costs is the goal of using these systems. For multi-stack fuel cell systems, the actual challenges include durability, cost and reliability. In previous studies, we have investigated the development of deterioration-aware EMS for improving MFC system durability and fuel economy under the static and dynamic load profiles. And in the three-stack problem proposed in this chapter, we have developed a new EMS for handling start-stop different stacks. Based on these studies, the following step is to incorporate the maintenance scheduling into previous deterioration-aware EMS, constructing a maintenance-based EMS for managing the operation of studied MFC system.

Different from previous problems, the maintenance-based EMS problem proposed here is dedicated to MFC long-term operation tasks. The maintenance scheduling strategy is responsible for optimizing stacks replacement, together with the deterioration-aware EMS to optimize MFC system long-term operation. In this way, the durability, reliability and operation cost of the MFC system can be optimized through the maintenance-based EMS thanks to the flexible modular architecture offered by MFC systems.

Therefore, we need a case study for multi-stack fuel cell systems to fulfill a long-term operation task under the supervision of a maintenance procedure. The aging awareness and stochasticity of the fuel cell stacks as well as the stochasticity in the dynamic loads are considered during system operation. The following problem formulation section will define a specific study case for the described maintenance-based EMS problem.

6.4.2 Problem formulation

6.4.2.1 System configuration

Consider a multi-stack fuel cell system with n identical parallel-connected stacks, $\mathrm{M}_{fc,n}$. Note here that even if the stacks within the MFC system are said to be initially fabricated identically, the deterioration state of a specific stack can be different as in the previous three-stack operation problem (Section 6.1). Each stack with a production capacity ranges from minimal load L_{min} to maximal load L_{max}. And the power load of the nominal condition is noted as L_{nom}.

A random dynamic type load profile generated by a MC model is used for modeling the power demands for the studied MFC system. The system is required to produce the power as defined in the load profile. The MC model is defined by the transition states $\mathbf{L_{ds}}$ and Markov transition matrix $\mathbf{P_{tr}}$. An example of the defined load profile is shown in Figure 6.4.

The overall fuel cell stack resistance deterioration is modeled as a summation of load, load varying, and start-stop caused deterioration (Equation (3.13)). The GP-RE model is used to model fuel cell resistance deterioration of load effect, i.e., ΔR_L. As addressed in Chapter 3, the individual stack deterioration heterogeneity is modeled by adding a random effect to the Gamma process model. The load varying ($\Delta R_{\Delta L}$) and start-stop (ΔR_{ss}) deterioration terms are modeled through deterministic model as presented in Chapter 3.

6.4.2.2 Maintenance-based EMS problem

The defined multi-stack fuel cell system is required to supply the random dynamic power demand for a fixed operation period (long duration e.g., 3000 hrs). The general problem is to construct a maintenance-based EMS for maintaining the long-term operation of the defined MFC system $M_{fc,n}$ while maximizing system durability and minimizing the maintenance cost. During the system operation, stack replacement is allowed. It is assumed that the failed stacks in the multi-stack system can be replaced without stopping the system.

The proposed maintenance-based EMS is sketched in Figure 6.11. Two key deterioration thresholds are required for the studied PEM fuel cell stack, i.e. the failure threshold FT and the preventive threshold P_{prev}. For a specific PEM stack FCi, when its deterioration level R_i reaches FT, the stack is said to be failed. When R_i reaches P_{prev}, a replacement maintenance is performed on FCi, and R_i recovers to initial level.

Then the decisions required by the joint maintenance problem include:

- Should we replace the stack? If replaced, which level of load to apply for the new stack?
- If no replacement, which loads to apply for the original stack?

The joint decision-making flowchart is given in Figure 6.12. For the maintenance scheduling problem, the optimal load decisions L_i^* are influenced by the replacement decision. The replacement action is conducted if $\mathbf{R}_i \geq P_{prev}$. The overall joint maintenance cost C is composed of three sources: the replacement cost C_{rep}, the waste of useful lifetime cost C_{rul}, and the system failure cost C_{fai}, which writes:

$$C = C_{rep} + C_{rul} + C_{fai} \tag{6.8}$$

where $C_{fai} > C_{rep}$.

The optimal load allocation decisions L_i^* are decided by minimizing the overall cost C. The objective of the joint maintenance problem is to find the optimal P_{prev} for minimizing the overall maintenance cost C.

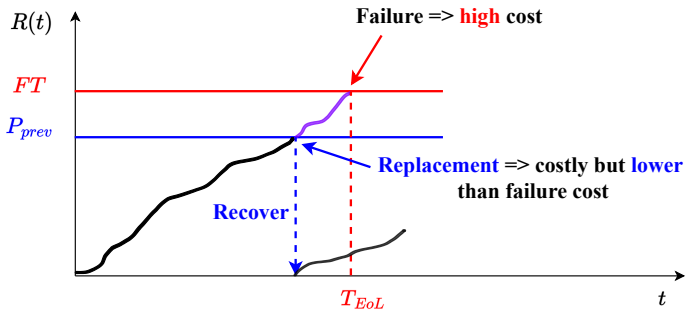

Figure 6.11: Proposed joint maintenance methodology.

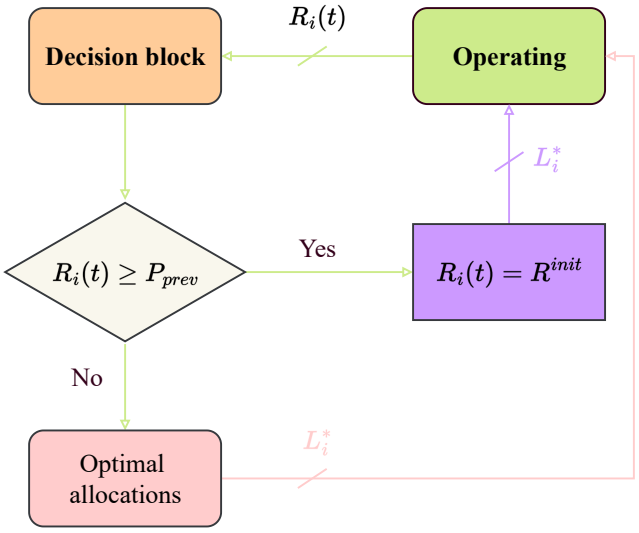

Figure 6.12: Joint maintenance decision flowchart.

6.5 Conclusion

The flexible modular architecture within an MFC system makes them easy to scale up for higher output power. The redundancy offered by MFC enables a flexible degradation mode operation. To put it another way, these advantages in the MFC system also make the EMS development relatively challenging concerning that the change in the operation requirements may require a different EMS. In the studied three-stack operation problem, the new strategy is designed by adding an extra decision layer for deciding the stack switching on/off actions. The proposed strategy is verified to improve system life by 21.7% compared to the classic DC-ave strategy. Moreover, the DC-ave strategy is improved by adding a deterioration-aware condition, i.e., the DDC-ave strategy. The lifetime simulation results confirmed that our strategy outperforms the DDC-ave strategy by 8.1%. Thus, in the three-stack operation problem, an EMS that is able to balance the deterioration over all stacks through the load allocation and stack switching decision is proven to be effective.

In fact, not only does the start and stop of the stacks need to be optimized for MFC

operation, but the replacement of failure stacks is also needed. This study opens the way to maintenance approaches to multi-stack systems. A perspective problem is defined to find the optimal maintenance-based EMS for minimizing maintenance costs as well as improving system durability and reliability.

General Conclusion

Main results

In this thesis, different deterioration-aware EMSs are developed for a stochastic deteriorating MFC systems under constant and dynamic load profiles, with the objective of enhancing MFC lifetime and efficiency. These strategies are responsible for optimally distributing the power demand among different stacks while considering their state of health thanks to the proposed deterioration model. A load-dependent stochastic deterioration model is built for the studied MFC by using a Gamma process model, taken its shape parameter as an empirical function of the fuel cell operation load according to fuel cell specificities. The above defined classic GP model fails to fit the stack-to-stack deterioration heterogeneity which turns out to be a critical deterioration feature within MFC systems. A random effect is added to the Gamma process on its scale parameter, taken as a random variable following a Gamma law. Three random-effect models, namely, the GP-RE, GP-RM, and GP-RV are specified to account for different configurations of the parameters of the GP model, which are used to simulate the cases where both the mean and variance are influenced by the random effects (GP-RE model), and the random effect only affect solely the mean (GP-RM model) or variance (GP-RV model) of the fuel cell degradation process.

In the first management strategy, the objectives of system deterioration and fuel consumption are estimated based on the conditional failure probability and the empirical fuel consumption function. In particular, the variance of stacks resistances are also added in the deterioration objective function, replying on the observation that reducing the resistance variances of all stacks will help to synchronize the degradation trajectories, to avoid early failure of a particular stack that would deteriorate much faster than the others. The optimal load allocation decisions of different stacks are decided based on the Pareto Front solved by the NSGA-II algorithm, and the ASF function-based decomposition method which use a user defined importance weight for the two objectives. The Monte Carlo simulation results showed that the proposed strategy achieves a higher average system life than those of the classic load allocation strategies under two constant loads. In the best case, our strategy can help to increase the system lifetime time by 25% compared with the Daisy Chain strategy.

As MFC systems are popular for vehicle applications, the energy management under the dynamic load profiles becomes a mandatory task. The deterioration objective function is estimated based on the prevision of the future system deterioration. A load demand change event-based decision-making strategy is built for the dynamic load demands to decide the optimal load allocations among stacks. A Markov Chain model is applied to generate the random dynamic loads. An illustrative study on the influence of the randomness loads on the proposed strategy shows that the average lifetime obtained with unknown event duration is close to that with known event duration, which proves the robustness of the proposed strategy. The event-based decision-making strategy is demonstrated to be improved by scheduling an

extra decision when the event duration is relatively long which shows the interests of possible work directions to obtain higher system life. Then, the above strategy is compared with the Average Load strategy on the four stochastic deterioration models (i.e., GP, GP-RE, GP-RM, and GP-RV) to justify the effectiveness of the proposed strategy. It is demonstrated that for our strategy obtains higher average lifetime for all cases. Besides, the GP-RE model is shown to gives the highest lifetime improvement which verifies that the proposed strategy can efficiently balance overall system deterioration to achieve an improved durability.

A possible extension of above discussed dynamic load energy management problem, a three-stack operation problem is proposed for optimizing system load allocation including start-stop operation mode. A two layers EMS is developed for the studied three-stack fuel cell system. The efficiency of the proposed strategy is verified by comparing it with the Daisy Chain-based average load and deterioration-aware Daisy Chain-based average load strategies. To enhance fuel cell system durability and reliability as well as minimize system maintenance cost, a maintenance-based EMS problem is formulated as a perspective problem.

Perspectives

This thesis focused on improving MFC system lifetime through an efficient EMS. Efforts have been made with respect to the deterioration modeling of MFC and the development of EMSs.

We have built a load-dependent stochastic deterioration model for MFC system. A random effect is added to the original GP model to model individual stack deterioration variability. The EMSs have been developed based on these deterioration models under constant and dynamic load profiles. In the last problem, we proposed an oversizing problem of optimizing start-stop operation in an MFC system which shows the possibilities of extending the current strategy to adapt to different operation scenarios. According to these results, further improvements are expected in terms of the deterioration model, intelligent management strategies, and EMS objectives.

The deterioration model proposed in this work only uses the resistance as HI. As fuel cell is a complex electrochemical device, it would be interesting to further develop a deterioration model by integrating several indicators. For instance, the Electrochemical Surface Area (ECSA) of a fuel cell is decreasing with the deterioration of the Pt electrocatalyst which could be used as an extra HI.

This thesis used the optimization-based approaches to produce the energy management strategy. However, more intelligent approaches like Reinforcement Learning (RL) based energy management can be considered. RL is suitable to solve sequential decision-making problems, either in a model-based or model-free manner. Moreover, the recently developed deep reinforcement learning techniques leverage the powerful representation advantages of neural network, which makes RL a promising technique in various applications, including the EMS of fuel cell systems.

Last but not least, EMS studies can be adapted to include more objectives, e.g., maintenance-based EMS to enhance fuel cell system lifetime and reliability as well as minimize maintenance costs. As indicated from the proposed perspective problem, fuel cell EMS studies can be combined with reliability and maintenance studies to optimize stack replacement for long-term operation.

Future research on the topic at all levels is envisaged to further enhance the scope of the proposal:

1. Deterioration model of MFC. Improve the health indicator, physical-based deterioration model.
2. Energy management approaches.
3. The combination of maintenance scheduling and load allocation decision-making strategy for optimizing system reliability and durability.

Bibliography

[1] J. Larminie *et al.*, *Fuel cell systems explained*. J. Wiley Chichester, UK, 2003, vol. 2 (cit. on p. 6).

[2] V. Cigolotti *et al.*, "Comprehensive review on fuel cell technology for stationary applications as sustainable and efficient poly-generation energy systems," *Energies*, vol. 14, no. 16, p. 4963, 2021 (cit. on pp. 6, 16).

[3] Y. Wang *et al.*, "Fundamentals, materials, and machine learning of Polymer Electrolyte Membrane Fuel Cell technology," *Energy and AI*, vol. 1, p. 100 014, 2020 (cit. on pp. 6, 16).

[4] N. Zamel, "The catalyst layer and its dimensionality–A look into its ingredients and how to characterize their effects," *Journal of Power Sources*, vol. 309, pp. 141–159, 2016 (cit. on p. 8).

[5] Q. Chen *et al.*, "Recent progress of gas diffusion layer in Proton Exchange Membrane Fuel Cell: Two-phase flow and material properties," *International Journal of Hydrogen Energy*, vol. 46, no. 12, pp. 8640–8671, 2021 (cit. on p. 9).

[6] P. Lin *et al.*, "A high efficient assembly technique for large PEMFC stacks: Part I. theory," *Journal of Power Sources*, vol. 194, no. 1, pp. 381–390, 2009, XIth Polish Conference on Fast Ionic Conductors 2008 (cit. on p. 9).

[7] A. L. Dicks *et al.*, *Fuel cell systems explained*. John Wiley & Sons, 2018 (cit. on pp. 10, 74).

[8] R. O'hayre *et al.*, *Fuel cell fundamentals*. John Wiley & Sons, 2016 (cit. on p. 10).

[9] X.-Z. Yuan *et al.*, "Electrochemical impedance spectroscopy in PEM fuel cells: Fundamentals and applications," 2010 (cit. on pp. 11, 13).

[10] J. Kim *et al.*, "Modeling of Proton Exchange Membrane Fuel Cell performance with an empirical equation," *Journal of the electrochemical society*, vol. 142, no. 8, p. 2670, 1995 (cit. on p. 12).

[11] F. Gao *et al.*, "A multiphysic dynamic 1-D model of a proton-exchange-membrane fuel-cell stack for real-time simulation," *IEEE transactions on industrial electronics*, vol. 57, no. 6, pp. 1853–1864, 2009 (cit. on p. 12).

[12] D. A. McKay *et al.*, "Parameterization and prediction of temporal fuel cell voltage behavior during flooding and drying conditions," *Journal of Power Sources*, vol. 178, no. 1, pp. 207–222, 2008 (cit. on p. 12).

[13] D. Gerteisen *et al.*, "Modeling the phenomena of dehydration and flooding of a Polymer Electrolyte Membrane Fuel Cell," *Journal of power sources*, vol. 187, no. 1, pp. 165–181, 2009 (cit. on p. 13).

[14] J. W. Plunkett, *Plunkett's Automobile Industry Almanac 2012: Automobile, Truck and Specialty Vehicle Industry Market Research, Statistics, Trends & Leading Companies*. Plunkett Research, Limited, 2011 (cit. on p. 13).

[15] G. Zhang *et al.*, "A solution to renewable hydrogen economy for fuel cell buses–A case study for zhangjiakou in north china," *International journal of hydrogen energy*, vol. 45, no. 29, pp. 14 603–14 613, 2020 (cit. on p. 14).

[16] IEA, *Global EV Outlook 2021*, https://www.iea.org/reports/global-ev-outlook-2021, Last accessed on 2022-03-24, 2021 (cit. on pp. 14, 15).

[17] Z. Li *et al.*, "A review of the applications of fuel cells in microgrids: Opportunities and challenges," *BMC Energy*, vol. 1, no. 1, pp. 1–23, 2019 (cit. on p. 15).

[18] U. Mitram *et al.*, "A comprehensive review on fuel cell technologies and its application in microgrids," in *2021 IEEE 2nd International Conference On Electrical Power and Energy Systems (ICEPES)*, IEEE, 2021, pp. 1–7 (cit. on p. 15).

[19] S. Campanari *et al.*, "Modeling, development and preliminary testing of a 2 MW PEM fuel cell plant fueled with hydrogen from a chlor-alkali industry," in *Energy Sustainability*, American Society of Mechanical Engineers, vol. 51418, 2018, V001T07A005 (cit. on p. 16).

[20] Japan LP Gas Association, *Japan LP Gas Association Home-use Fuel Cell(ENE-FARM)*, https://www.j-lpgas.gr.jp/en/appliances/, Last accessed on 2022-03-30, 2021 (cit. on p. 16).

[21] U.S. DOE Fuel Cell Technologies Office, *Fuel Cell Technologies Office Multi-Year Research, Development, and Demonstration Plan - Section 3.4 Fuel Cells*, https://www.energy.gov/sites/prod/files/2017/05/f34/fcto_myrdd_fuel_cells.pdf, Last accessed on 2022-03-30, 2017 (cit. on p. 16).

[22] P. Ahmadi *et al.*, "The effects of driving patterns and PEM fuel cell degradation on the lifecycle assessment of hydrogen fuel cell vehicles," *International Journal of Hydrogen Energy*, vol. 45, no. 5, pp. 3595–3608, 2020 (cit. on p. 16).

[23] US Department of Energy, *DOE Technical targets for fuel cell backup power systems*, https://www.energy.gov/eere/fuelcells/doe-technical-targets-fuel-cell-backup-power-systems, Last accessed on 2022-03-30, 2020 (cit. on p. 16).

[24] N. L. Garland, "US department of energy fuel cell technologies program," in *18th World Hydrogen Energy Conference 2010–WHEC 2010 Proceedings Speeches and Plenary Talks*, 2010 (cit. on p. 17).

[25] P. Pei *et al.*, "A quick evaluating method for automotive fuel cell lifetime," *International Journal of Hydrogen Energy*, vol. 33, no. 14, pp. 3829–3836, 2008 (cit. on pp. 17, 20, 22, 38, 40, 53, 60, 61).

[26] J. Wu *et al.*, "A review of PEM fuel cell durability: Degradation mechanisms and mitigation strategies," *Journal of Power Sources*, vol. 184, no. 1, pp. 104–119, 2008 (cit. on pp. 17, 18, 20).

[27] R Gouriveau *et al.*, "IEEE PHM 2014 data challenge: Outline, experiments, scoring of results, winners," *IEEE 2014 PHM Challenge, Tech. Rep*, 2014 (cit. on pp. 18, 19, 53, 64, 78, 93).

[28] D. Zhang, "Contribution to prognostics of PEM fuel cells: Approaches based on degradation information at multiple levels," PhD thesis, Communauté Université Grenoble Alpes, 2018 (cit. on p. 18).

[29] J. Zhao *et al.*, "A review of Polymer Electrolyte Membrane Fuel Cell durability for vehicular applications: Degradation modes and experimental techniques," *Energy Conversion and Management*, vol. 199, p. 112 022, 2019 (cit. on p. 18).

[30] L. Franck-Lacaze *et al.*, "Ageing of PEMFC's due to operation at low current density: Investigation of oxidative degradation," *international journal of hydrogen energy*, vol. 35, no. 19, pp. 10 472–10 481, 2010 (cit. on p. 20).

[31] Y. Nosaka *et al.*, "Detection of oh radicals generated in Polymer Electrolyte Membranes Fuel Cells," *Journal of the Electrochemical Society*, vol. 158, no. 4, B430, 2011 (cit. on p. 20).

[32] K. H. Wong *et al.*, "Mitigation of chemical membrane degradation in fuel cells: Understanding the effect of cell voltage and iron ion redox cycle," *ChemSusChem*, vol. 8, no. 6, pp. 1072–1082, 2015 (cit. on p. 20).

[33] C. G. Chung *et al.*, "Degradation mechanism of electrocatalyst during long-term operation of PEMFC," *International Journal of Hydrogen Energy*, vol. 34, no. 21, pp. 8974–8981, 2009 (cit. on p. 21).

[34] S. Zhang *et al.*, "Effects of open-circuit operation on membrane and catalyst layer degradation in Proton Exchange Membrane Fuel Cells," *Journal of Power Sources*, vol. 195, no. 4, pp. 1142–1148, 2010 (cit. on p. 21).

[35] S. Helmly *et al.*, "Microscopic investigation of platinum deposition in PEMFC cross-sections using afm and sem," *Journal of The Electrochemical Society*, vol. 160, no. 6, F687, 2013 (cit. on p. 21).

[36] A. Kawano *et al.*, "Influence of oxygen atmosphere on dissolution of platinum under potential cycling," *Journal of The Electrochemical Society*, vol. 161, no. 1, F67, 2013 (cit. on p. 21).

[37] P. Ren *et al.*, "Degradation mechanisms of Proton Exchange Membrane Fuel Cell under typical automotive operating conditions," *Progress in Energy and Combustion Science*, vol. 80, p. 100 859, 2020 (cit. on p. 21).

[38] G. Tsotridis *et al.*, "EU harmonised test protocols for PEMFC MEA testing in single cell configuration for automotive applications," *JRC Science for Policy report*, vol. 27632, 2015 (cit. on pp. 21–23, 54).

[39] J. Zuo *et al.*, "Long-term dynamic durability test datasets for single Proton Exchange Membrane Fuel Cell," *Data in Brief*, vol. 35, p. 106 775, 2021 (cit. on pp. 24, 31).

[40] M. Tutuianu *et al.*, "Development of the world-wide harmonized light duty test cycle (WLTC) and a possible pathway for its introduction in the european legislation," *Transportation research part D: transport and environment*, vol. 40, pp. 61–75, 2015 (cit. on p. 22).

[41] M. Mayur *et al.*, "Lifetime prediction of a Polymer Electrolyte Membrane Fuel Cell under automotive load cycling using a physically-based catalyst degradation model," *Energies*, vol. 11, no. 8, p. 2054, 2018 (cit. on p. 25).

[42] K. Meng *et al.*, "Dynamic current cycles effect on the degradation characteristic of a H2/O2 Proton Exchange Membrane Fuel Cell," *Energy*, vol. 224, p. 120 168, 2021. [Online]. Available: https://www.sciencedirect.com/science/article/pii/S0360544221004175 (cit. on p. 23).

[43] J. Liu *et al.*, "Mechanical degradation of catalyst layer under accelerated relative humidity cycling in a Polymer Electrolyte Membrane Fuel Cell," *Journal of Power Sources*, vol. 512, p. 230 487, 2021 (cit. on p. 23).

[44] T. Zhang *et al.*, "A review of automotive Proton Exchange Membrane Fuel Cell degradation under start-stop operating condition," *Applied energy*, vol. 223, pp. 249–262, 2018 (cit. on p. 23).

[45] J. Li *et al.*, "Degradation study of high temperature Proton Exchange Membrane Fuel Cell under start/stop and load cycling conditions," *International Journal of Hydrogen Energy*, vol. 46, no. 47, pp. 24 353–24 365, 2021 (cit. on p. 23).

[46] S. Thomas *et al.*, "New load cycling strategy for enhanced durability of high temperature Proton Exchange Membrane Fuel Cell," *International Journal of Hydrogen Energy*, vol. 42, no. 44, pp. 27 230–27 240, 2017 (cit. on p. 23).

[47] S. Hahn *et al.*, "Optimization of the efficiency and degradation rate of an automotive fuel cell system," *International Journal of Hydrogen Energy*, vol. 46, no. 57, pp. 29 459–29 477, 2021 (cit. on pp. 25, 38, 40).

[48] G. W. Vogl *et al.*, *Standards related to Prognostics and Health Management (PHM) for manufacturing*. US Department of Commerce, National Institute of Standards and Technology, 2014 (cit. on p. 25).

[49] E. Zio, "Prognostics and Health Management (PHM): Where are we and where do we (need to) go in theory and practice," *Reliability Engineering & System Safety*, vol. 218, p. 108 119, 2022 (cit. on p. 26).

[50] Z. Li *et al.*, "Online implementation of svm based fault diagnosis strategy for PEMFC systems," *Applied energy*, vol. 164, pp. 284–293, 2016 (cit. on p. 27).

[51] R.-H. Lin *et al.*, "Hydrogen fuel cell diagnostics using random forest and enhanced feature selection," *International Journal of Hydrogen Energy*, vol. 45, no. 17, pp. 10 523–10 535, 2020 (cit. on p. 27).

[52] S. Zhou *et al.*, "Machine learning as an online diagnostic tool for Proton Exchange Membrane Fuel Cells," *Current Opinion in Electrochemistry*, vol. 31, p. 100 867, 2022 (cit. on p. 27).

[53] X. Gu *et al.*, "Data-based flooding fault diagnosis of Proton Exchange Membrane Fuel Cell systems using lstm networks," *Energy and AI*, vol. 4, p. 100 056, 2021 (cit. on p. 27).

[54] Z. Zhang *et al.*, "Intelligent simultaneous fault diagnosis for solid oxide fuel cell system based on deep learning," *Applied Energy*, vol. 233, pp. 930–942, 2019 (cit. on p. 28).

[55] G. Jullian *et al.*, "Fault detection and isolation for Proton Exchange Membrane Fuel Cell using impedance measurements and multiphysics modeling," *Fuel Cells*, vol. 20, no. 5, pp. 558–569, 2020 (cit. on p. 28).

[56] M. Jouin *et al.*, "Prognostics of PEM fuel cell in a particle filtering framework," *International Journal of Hydrogen Energy*, vol. 39, no. 1, pp. 481–494, 2014 (cit. on pp. 28, 32, 37).

[57] M. Jouin *et al.*, "Degradations analysis and aging modeling for health assessment and prognostics of PEMFC," *Reliability Engineering & System Safety*, vol. 148, pp. 78–95, 2016 (cit. on pp. 28, 31).

[58] J. Zuo *et al.*, "Deep learning based prognostic framework towards Proton Exchange Membrane Fuel Cell for automotive application," *Applied Energy*, vol. 281, p. 115 937, 2021 (cit. on pp. 28, 29, 31).

[59] Z. Hua *et al.*, "Remaining useful life prediction of PEMFC systems under dynamic operating conditions," *Energy Conversion and Management*, vol. 231, p. 113 825, 2021 (cit. on pp. 28, 31).

[60] D. Zhou *et al.*, "Degradation prediction of PEM fuel cell using a moving window based hybrid prognostic approach," *Energy*, vol. 138, pp. 1175–1186, 2017 (cit. on p. 28).

[61] V. Atamuradov *et al.*, "Prognostics and Health Management for maintenance practitioners-review, implementation and tools evaluation," *International Journal of Prognostics and Health Management*, vol. 8, no. 060, pp. 1–31, 2017 (cit. on p. 29).

[62] M. Jouin *et al.*, "Prognostics and Health Management of PEMFC–State-of-the-art and remaining challenges," *International Journal of Hydrogen Energy*, vol. 38, no. 35, pp. 15 307–15 317, 2013 (cit. on p. 29).

[63] K. Chen *et al.*, "Performance analysis of PEM fuel cell in mobile application under real traffic and environmental conditions," *Energy Conversion and Management*, vol. 227, p. 113 602, 2021 (cit. on p. 29).

[64] S. Morando *et al.*, "Anova method applied to Proton Exchange Membrane Fuel Cell ageing forecasting using an Echo State Network," *Mathematics and Computers in Simulation*, vol. 131, pp. 283–294, 2017 (cit. on p. 29).

[65] Z. Hua *et al.*, "Lifespan prediction for Proton Exchange Membrane Fuel Cells based on Wavelet Transform and Echo State Network," *IEEE Transactions on Transportation Electrification*, 2021 (cit. on pp. 29, 30).

[66] Z. Hua *et al.*, "Health indicators for PEMFC systems life prediction under both static and dynamic operating conditions," in *IECON 2020 The 46th Annual Conference of the IEEE Industrial Electronics Society*, IEEE, 2020, pp. 3963–3968 (cit. on pp. 29, 30).

[67] D. Zhang *et al.*, "PHM-oriented degradation indicators for batteries and fuel cells," *Fuel cells*, vol. 17, no. 2, pp. 268–276, 2017 (cit. on p. 29).

[68] J. Chen *et al.*, "A novel health indicator for PEMFC state of health estimation and remaining useful life prediction," *International Journal of Hydrogen Energy*, vol. 42, no. 31, pp. 20 230–20 238, 2017 (cit. on p. 29).

[69] D. Liu *et al.*, "Investigation of the effect of cathode stoichiometry of Proton Exchange Membrane Fuel Cell using localized electrochemical impedance spectroscopy based on print circuit board," *International Journal of Hydrogen Energy*, vol. 44, no. 14, pp. 7564–7573, 2019 (cit. on pp. 29, 30).

[70] Z. Li *et al.*, "Adaptive prognostic of fuel cells by implementing ensemble Echo State Networks in time-varying model space," *IEEE Transactions on Industrial Electronics*, vol. 67, no. 1, pp. 379–389, 2019 (cit. on p. 30).

[71] M. Bressel *et al.*, "Remaining useful life prediction and uncertainty quantification of Proton Exchange Membrane Fuel Cell under variable load," *IEEE Transactions on Industrial Electronics*, vol. 63, no. 4, pp. 2569–2577, 2016 (cit. on p. 30).

[72] H. Liu *et al.*, "Prognostics methods and degradation indexes of Proton Exchange Membrane Fuel Cells: A review," *Renewable and Sustainable Energy Reviews*, vol. 123, p. 109 721, 2020 (cit. on p. 30).

[73] F Chen *et al.*, "An algorithm for on-line measurement of the internal resistance of Proton Exchange Membrane Fuel Cell," *Fuel Cells*, vol. 15, no. 2, pp. 337–343, 2015 (cit. on p. 30).

[74] T. Ma *et al.*, "Impedance prediction model based on Convolutional Neural Networks methodology for Proton Exchange Membrane Fuel Cell," *International Journal of Hydrogen Energy*, 2021 (cit. on p. 30).

[75] O. Z. Sharaf *et al.*, "An overview of fuel cell technology: Fundamentals and applications," *Renewable and sustainable energy reviews*, vol. 32, pp. 810–853, 2014 (cit. on pp. 31, 74).

[76] M. Bressel *et al.*, "Extended kalman filter for prognostic of Proton Exchange Membrane Fuel Cell," *Applied Energy*, vol. 164, pp. 220–227, 2016 (cit. on pp. 31, 37, 44).

[77] D. Zhang *et al.*, "An ensemble of models for integrating dependent sources of information for the prognosis of the remaining useful life of Proton Exchange Membrane Fuel Cells," *Mechanical Systems and Signal Processing*, vol. 124, pp. 479–501, 2019 (cit. on p. 31).

[78] S. Hochreiter *et al.*, "Long Short-term Memory," *Neural computation*, vol. 9, no. 8, pp. 1735–1780, 1997 (cit. on p. 31).

[79] Y. LeCun *et al.*, "Convolutional Networks for images, speech, and time series," *The handbook of brain theory and neural networks*, vol. 3361, no. 10, p. 1995, 1995 (cit. on p. 31).

[80] R. Ma *et al.*, "Data-driven Proton Exchange Membrane Fuel Cell degradation prediction through deep learning method," *Applied energy*, vol. 231, pp. 102–115, 2018 (cit. on p. 31).

[81] D. Zhou *et al.*, "Online remaining useful lifetime prediction of Proton Exchange Membrane Fuel Cells using a novel robust methodology," *Journal of Power Sources*, vol. 399, pp. 314–328, 2018 (cit. on p. 32).

[82] N Marx *et al.*, "A review of multi-stack and modular fuel cell systems: Interests, application areas and on-going research activities," *International Journal of Hydrogen Energy*, vol. 39, no. 23, pp. 12 101–12 111, 2014 (cit. on pp. 34, 35).

[83] A. De Bernardinis *et al.*, "Fuel cells multi-stack power architectures and experimental validation of 1 kW parallel twin stack pefc generator based on high frequency magnetic coupling dedicated to on board power unit," *Energy Conversion and Management*, vol. 49, no. 8, pp. 2367–2383, 2008 (cit. on pp. 34, 35).

[84] J. Cardozo *et al.*, "Comparison of multi-stack fuel cell system architectures for residential power generation applications including electrical vehicle charging," in *2015 IEEE Vehicle Power and Propulsion Conference (VPPC)*, IEEE, 2015, pp. 1–6 (cit. on p. 34).

[85] N. Marx *et al.*, "On the sizing and energy management of an hybrid multistack fuel cell–battery system for automotive applications," *International Journal of Hydrogen Energy*, vol. 42, no. 2, pp. 1518–1526, 2017 (cit. on p. 35).

[86] N. Marx *et al.*, "Degraded mode operation of multi-stack fuel cell systems," *IET Electrical Systems in Transportation*, vol. 6, no. 1, pp. 3–11, 2016 (cit. on pp. 35, 54).

[87] A. J. Calderón *et al.*, "Integration of a multi-stack fuel cell system in microgrids: A solution based on Model Predictive Control," *Energies*, vol. 13, no. 18, p. 4924, 2020 (cit. on p. 35).

[88] M. Becherif *et al.*, "Multi-stack fuel cells powering a vehicle," *Energy procedia*, vol. 74, pp. 308–319, 2015 (cit. on p. 35).

[89] S. Zhou *et al.*, "A review on proton exchange membrane multi-stack fuel cell systems: Architecture, performance, and power management," *Applied Energy*, vol. 310, p. 118 555, 2022 (cit. on p. 35).

[90] M. Radovanovic, *Sustainable Energy Management: Planning, Implementation, Control, and Security*. Elsevier Science, 2022. [Online]. Available: https://books.google.fr/books?id=sifLyAEACAAJ (cit. on p. 36).

[91] Y. Zhou, "Predictive energy management for fuel cell hybrid electric vehicle," Theses, Université Bourgogne Franche-Comté, Nov. 2020. [Online]. Available: https://tel.archives-ouvertes.fr/tel-03080574 (cit. on p. 36).

[92] D.-D. Tran *et al.*, "Thorough state-of-the-art analysis of electric and hybrid vehicle powertrains: Topologies and integrated energy management strategies," *Renewable and Sustainable Energy Reviews*, vol. 119, p. 109 596, 2020 (cit. on p. 36).

[93] A. L. Bukar *et al.*, "A review on stand-alone photovoltaic-wind energy system with fuel cell: System optimization and energy management strategy," *Journal of cleaner production*, vol. 221, pp. 73–88, 2019 (cit. on p. 36).

[94] C. Zheng *et al.*, "Fuel economy evaluation of fuel cell hybrid vehicles based on equivalent fuel consumption," *International Journal of Hydrogen Energy*, vol. 37, no. 2, pp. 1790–1796, 2012, 10th International Conference on Clean Energy 2010 (cit. on p. 36).

[95] C. A. Ramos-Paja *et al.*, "Minimum fuel consumption strategy for PEM fuel cells," *IEEE transactions on industrial electronics*, vol. 56, no. 3, pp. 685–696, 2008 (cit. on pp. 36, 40).

[96] M.-J. Kim *et al.*, "Power management and design optimization of fuel cell/battery hybrid vehicles," *Journal of power sources*, vol. 165, no. 2, pp. 819–832, 2007 (cit. on pp. 36, 40).

[97] W. Zhang *et al.*, "Optimization for a fuel cell/battery/capacity tram with equivalent consumption minimization strategy," *Energy Conversion and Management*, vol. 134, pp. 59–69, 2017 (cit. on pp. 36, 40).

[98] P. König. *et al.*, "Increase of the fuel cell system efficiency - modular testing, analysis and development environment," *Journal of Power Sources*, vol. 190, no. 1, 121 – 132, 2009, Cited by: 8 (cit. on pp. 37, 40).

[99] S. Kelouwani *et al.*, "Online system identification and adaptive control for PEM fuel cell maximum efficiency tracking," *IEEE Transactions on Energy Conversion*, vol. 27, no. 3, pp. 580–592, 2012 (cit. on p. 37).

[100] M. Kandidayeni *et al.*, "Efficiency upgrade of hybrid fuel cell vehicles' energy management strategies by online systemic management of fuel cell," *IEEE Transactions on Industrial Electronics*, vol. 68, no. 6, pp. 4941–4953, 2020 (cit. on p. 37).

[101] M Kandidayeni *et al.*, "Towards health-aware energy management strategies in fuel cell hybrid electric vehicles: A review," *International Journal of Hydrogen Energy*, 2022 (cit. on p. 37).

[102] C. Zheng *et al.*, "Prolonging fuel cell stack lifetime based on Pontryagin's Minimum Principle in fuel cell hybrid vehicles and its economic influence evaluation," *Journal of Power Sources*, vol. 248, pp. 533–544, 2014 (cit. on pp. 38, 40).

[103] C. Zheng *et al.*, "Real-time application of pontryagin's minimum principle to fuel cell hybrid buses based on driving characteristics of buses," *International Journal of Precision Engineering and Manufacturing-Green Technology*, vol. 4, no. 2, pp. 199–209, 2017 (cit. on pp. 38, 40).

[104] H. Chen *et al.*, "Lifetime prediction and the economic lifetime of Proton Exchange Membrane Fuel Cells," *Applied Energy*, vol. 142, pp. 154–163, 2015 (cit. on pp. 38, 61).

[105] B. Geng *et al.*, "Two-stage energy management control of fuel cell plug-in hybrid electric vehicles considering fuel cell longevity," *IEEE Transactions on vehicular technology*, vol. 61, no. 2, pp. 498–508, 2011 (cit. on pp. 38, 40).

[106] L. De Pascali *et al.*, "Aging-aware optimal energy management control for a parallel hybrid vehicle based on electrochemical-degradation dynamics," *IEEE Transactions on Vehicular Technology*, vol. 69, no. 10, pp. 10 868–10 878, 2020 (cit. on pp. 38, 40).

[107] Z. Hu *et al.*, "Multi-objective energy management optimization and parameter sizing for proton exchange membrane hybrid fuel cell vehicles," *Energy Conversion and Management*, vol. 129, pp. 108–121, 2016 (cit. on pp. 38, 40).

[108] C. Zhang *et al.*, "Real-time optimization of energy management strategy for fuel cell vehicles using inflated 3D Inception Long Short-term Memory Network-based speed prediction," *IEEE Transactions on Vehicular Technology*, vol. 70, no. 2, pp. 1190–1199, 2021 (cit. on pp. 38, 40).

[109] K. Song *et al.*, "Degradation adaptive energy management strategy using fuel cell state-of-health for fuel economy improvement of hybrid electric vehicle," *Applied Energy*, vol. 285, p. 116 413, 2021 (cit. on pp. 38, 40).

[110] M. Yue *et al.*, "Health-conscious energy management for fuel cell hybrid electric vehicles based on prognostics-enabled decision-making," *IEEE Transactions on Vehicular Technology*, vol. 68, no. 12, pp. 11 483–11 491, 2019 (cit. on pp. 38, 40).

[111] M. Rausand *et al.*, *System reliability theory: models, statistical methods, and applications*. John Wiley & Sons, 2003, vol. 396 (cit. on pp. 39, 58).

[112] M Tanrioven *et al.*, "Reliability modeling and analysis of stand-alone PEM fuel cell power plants," *Renewable Energy*, vol. 31, no. 7, pp. 915–933, 2006 (cit. on p. 39).

[113] V Mangoni *et al.*, "Fuel cell reliability model based on uncertain data," in *2007 International Conference on Clean Electrical Power*, IEEE, 2007, pp. 730–735 (cit. on p. 39).

[114] M. Z. Gargari *et al.*, "Preventive maintenance scheduling of multi energy microgrid to enhance the resiliency of system," *Energy*, vol. 221, p. 119 782, 2021 (cit. on pp. 39, 40).

[115] L. Guedes *et al.*, "A continuous compact model for cascaded hydro-power generation and preventive maintenance scheduling," *International Journal of Electrical Power & Energy Systems*, vol. 73, pp. 702–710, 2015 (cit. on pp. 39, 40).

[116] Q. de Bortoli *et al.*, "Thermal management for efficiency enhancement for multi-stack fuel cell electric vehicle," in *2015 IEEE Vehicle Power and Propulsion Conference (VPPC)*, IEEE, 2015, pp. 1–6 (cit. on pp. 40, 43).

[117] T. Wang *et al.*, "Hydrogen consumption minimization method based on the online identification for multi-stack PEMFCs system," *International Journal of Hydrogen Energy*, vol. 44, no. 11, pp. 5074–5081, 2019 (cit. on pp. 40, 43, 74).

[118] M. Moghadari *et al.*, "Hydrogen minimization of a hybrid multi-stack fuel cell vehicle using an optimization-based strategy," in *2021 IEEE Vehicle Power and Propulsion Conference (VPPC)*, IEEE, 2021, pp. 1–5 (cit. on pp. 41, 43).

[119] Y. Wang *et al.*, "Two-level energy management strategy for a hybrid power system based multi-stack fuel cell," in *ICRT 2021*, American Society of Civil Engineers Reston, VA, 2022, pp. 545–556 (cit. on pp. 41, 43).

[120] R. Ghaderi *et al.*, "Quadratic programming based energy management in a multi-stack fuel cell hybrid electric vehicle," in *2021 IEEE Vehicle Power and Propulsion Conference (VPPC)*, IEEE, 2021, pp. 1–6 (cit. on pp. 41, 43).

[121] A. M. Fernandez *et al.*, "An adaptive state machine based energy management strategy for a multi-stack fuel cell hybrid electric vehicle," *IEEE Transactions on Vehicular Technology*, vol. 69, no. 1, pp. 220–234, 2019 (cit. on pp. 41, 43).

[122] N. Herr *et al.*, "Decision process to manage useful life of multi-stacks fuel cell systems under service constraint," *Renewable energy*, vol. 105, pp. 590–600, 2017 (cit. on pp. 41, 43).

[123] S. Zhou *et al.*, "Scenario-oriented stacks allocation optimization for multi-stack fuel cell systems," *Applied Energy*, vol. 308, p. 118 328, 2022 (cit. on pp. 41, 43).

[124] T. Fletcher *et al.*, "An energy management strategy to concurrently optimise fuel consumption & PEM fuel cell lifetime in a hybrid vehicle," *international journal of hydrogen energy*, vol. 41, no. 46, pp. 21 503–21 515, 2016 (cit. on p. 42).

[125] Q. Jiang *et al.*, "A comparison of real-time energy management strategies of FC/SC hybrid power source: Statistical analysis using random cycles," *International Journal of Hydrogen Energy*, vol. 46, no. 63, pp. 32 192–32 205, 2021 (cit. on p. 42).

[126] A. J. Ritchie *et al.*, "Design of fuel cell powered data centers for sufficient reliability and availability," *Journal of Power Sources*, vol. 384, pp. 196–206, 2018 (cit. on p. 42).

[127] G. Cardoso *et al.*, "Microgrid reliability modeling and battery scheduling using stochastic linear programming," *Electric power systems research*, vol. 103, pp. 61–69, 2013 (cit. on pp. 42, 43).

[128] K. W. E. Colombo *et al.*, "Reliability analysis for a multi-stack solid oxide fuel cell system subject to operation condition-dependent degradation," *Journal of Quality in Maintenance Engineering*, 2020 (cit. on pp. 42, 43).

[129] K. W. E. Colombo *et al.*, "Reliability analysis of a multi-stack solid oxide fuel cell from a systems engineering perspective," *Chemical Engineering Science*, vol. 238, p. 116 571, 2021 (cit. on pp. 42, 43).

[130] S. Phommixay *et al.*, "Real time power sharing of fuel cells microgrid considering short term preventive maintenance outage," in *2019 IEEE 2nd International Conference on Renewable Energy and Power Engineering (REPE)*, IEEE, 2019, pp. 83–89 (cit. on pp. 42, 43).

[131] D. Flammia *et al.*, "Enhanced Kalman Filter-based identification of a fuel cell circuit model in Impedance Spectroscopy tests," in *ELECTRIMACS 2019*, Springer, 2020, pp. 117–128 (cit. on p. 44).

[132] Y. Chatillon *et al.*, "Heterogeneous aging within PEMFC stacks," *Fuel Cells*, vol. 14, no. 4, pp. 581–589, 2014 (cit. on p. 53).

[133] A. Macias *et al.*, "A novel online energy management strategy for multi fuel cell systems," in *2018 IEEE International Conference on Industrial Technology (ICIT)*, IEEE, 2018, pp. 2043–2048 (cit. on p. 53).

[134] J. M. van Noortwijk, "A survey of the application of Gamma processes in maintenance," *Reliability Engineering & System Safety*, vol. 94, no. 1, pp. 2–21, 2009 (cit. on pp. 56, 58, 75).

[135] M. E. Cholette *et al.*, "Degradation modeling and condition-based maintenance of boiler heat exchangers using Gamma processes," *Reliability Engineering & System Safety*, vol. 183, pp. 184–196, 2019 (cit. on p. 56).

[136] S.-H. Park *et al.*, "Application of Gamma process model to estimate the lifetime of photovoltaic modules," *Solar Energy*, vol. 147, pp. 390–398, 2017 (cit. on p. 57).

[137] C. P. Lin *et al.*, "Prognostics for lithium-ion batteries using a two-phase Gamma degradation process model," *Reliability Engineering & System Safety*, vol. 214, p. 107 797, 2021 (cit. on p. 57).

[138] M. Laguna-Bercero *et al.*, "Electrolyte degradation in anode supported microtubular yttria stabilized zirconia-based solid oxide steam electrolysis cells at high voltages of operation," *Journal of Power Sources*, vol. 196, no. 21, pp. 8942–8947, 2011 (cit. on p. 61).

[139] S. Takao *et al.*, "Observation of degradation of pt and carbon support in Polymer Electrolyte Fuel Cell using combined nano-X-ray absorption fine structure and transmission electron microscopy techniques," *ACS applied materials & interfaces*, vol. 10, no. 33, pp. 27 734–27 744, 2018 (cit. on p. 61).

[140] S. Yang *et al.*, "Improvement of fuel cell durability performance by avoiding high voltage," *International Journal of Automotive Technology*, vol. 20, no. 6, pp. 1113–1121, 2019 (cit. on p. 61).

[141] L. A. Rodríguez-Picón *et al.*, "Degradation modeling based on Gamma process models with random effects," *Communications in Statistics-Simulation and Computation*, vol. 47, no. 6, pp. 1796–1810, 2018 (cit. on p. 63).

[142] E. Cinlar *et al.*, "Stochastic process for extrapolating concrete creep," *Journal of the Engineering Mechanics Division*, vol. 103, no. 6, pp. 1069–1088, 1977 (cit. on p. 64).

[143] J. Zuo *et al.*, "Post-prognostics decision making for a two-stacks fuel cell system based on a load-dependent deterioration model," in *PHME 2020-European Conference of the Prognostics and Health management (PHM) Society*, vol. 5, 2020, p. 9 (cit. on pp. 73, 88).

[144] J. Zuo *et al.*, "Post-prognostics decision making strategy to manage the economic lifetime of a two-stack PEMFC system," in *2021 Annual Reliability and Maintainability Symposium (RAMS)*, IEEE, 2021, pp. 1–7 (cit. on p. 73).

[145] J. Zuo *et al.*, "Post-prognostics decision-making strategy for load allocation on a stochastically deteriorating multi-stack fuel cell system," *Proceedings of the Institution of Mechanical Engineers, Part O: Journal of Risk and Reliability*, p. 1748006X221086381, 2022 (cit. on p. 73).

[146] Y. Yan *et al.*, "Online control and power coordination method for multistack fuel cells system based on optimal power allocation," *IEEE Transactions on Industrial Electronics*, vol. 68, no. 9, pp. 8158–8168, 2020 (cit. on p. 74).

[147] C. Depature *et al.*, "IEEE VTS motor vehicles challenge 2017-energy management of a fuel cell/battery vehicle," in *2016 IEEE Vehicle Power and Propulsion Conference (VPPC)*, IEEE, 2016, pp. 1–6 (cit. on p. 74).

[148] W. Xu *et al.*, "An adaptive Gamma process based model for residual useful life prediction," in *Proceedings of the IEEE 2012 Prognostics and System Health Management Conference (PHM-2012 Beijing)*, IEEE, 2012, pp. 1–4 (cit. on p. 76).

[149] N. Marx *et al.*, "Comparison of the series and parallel architectures for hybrid multi-stack fuel cell-battery systems," in *2015 IEEE Vehicle Power and Propulsion Conference (VPPC)*, IEEE, 2015, pp. 1–6 (cit. on p. 77).

[150] K. Deb *et al.*, "A fast and elitist multiobjective genetic algorithm: NSGA-II," *IEEE transactions on evolutionary computation*, vol. 6, no. 2, pp. 182–197, 2002 (cit. on p. 90).

[151] A. P. Wierzbicki, "The use of reference objectives in multiobjective optimization," in *Multiple criteria decision making theory and application*, Springer, 1980, pp. 468–486 (cit. on p. 90).

[152] J. Blank *et al.*, "Pymoo: Multi-objective optimization in python," *IEEE Access*, vol. 8, pp. 89 497–89 509, 2020 (cit. on pp. 91, 94).

[153] J. Blank *et al.*, "Investigating the normalization procedure of NSGA-III," in *International Conference on Evolutionary Multi-Criterion Optimization*, Springer, 2019, pp. 229–240 (cit. on p. 91).

[154] J. Blank *et al.*, "A running performance metric and termination criterion for evaluating evolutionary multi-and many-objective optimization algorithms," in *2020 IEEE Congress on Evolutionary Computation (CEC)*, IEEE, 2020, pp. 1–8 (cit. on p. 94).

[155] DOE, *DOE Hydrogen Program Record*, https://www.hydrogen.energy.gov/program_records.html, Last accessed on 2022-06-14, 2021 (cit. on p. 128).